

**ELECTRICAL TRANSPORT AND MAGNETIC PROPERTIES
OF Co, (Ni, Mo) SUBSTITUTED
IRON-RICH METAL-METALLOID GLASSES**

**A THESIS
SUBMITTED FOR THE DEGREE OF
DOCTOR OF PHILOSOPHY**

**By
N. R. MUNIRATHNAM**



**SCHOOL OF PHYSICS
UNIVERSITY OF HYDERABAD
HYDERABAD - 500 134.
INDIA**

JANUARY 1989

..... TO MY PARENTS

LIST OF THE CONTENTS

Page No.


CERTIFICATE.....	(I)
ACKNOWLEDGEMENTS.....	(II)
PREFACE.....	(III)
1 INTRODUCTION :	1
1.1 1.1 Glass formation	3
1.2 Preparation techniques	6
1.3 Classification of metallic glasses	11
1.4 Disorder in glasses	11
1.5 Electronic structure and transport	13
1.6 Magnetic properties	18
1.7 Crystallization	20
1.8 Applications	21
1.9 Research in this work	22
2 SAMPLES AND EXPERIMENTAL TECHNIQUES :	25
2.1 Samples	26
2.2 Characterization	27
2.3 Experimental techniques:	29
2.3.1 Resistance measurements from 1.5 to 300 K	29
2.3.2 Resistance measurements from 80 to 900 K	32
2.3.3 Thermoelectric power measurements from 80 to 400 K : Integral technique	34
2.3.4 Mössbauer measurements	38
2.3.5 Differential Scanning Calorimetry (DSC)	41

3	RESISTIVITY MEASUREMENTS :	Page No. 46
3.1	Introduction	47
3.2	Temperature dependence of resistivity	49
3.3	Theoretical models	50
3.3.1	Diffraction model	50
3.3.2	Mott s-d scattering model	54
3.3.3	Two-level tunneling model	56
3.2.4	The theory of localization	56
3.4	Experimental results	58
3.4.1	Resistivity measurements of Fe-Co-Si-B alloys	59
3.4.2	Resistivity measurements of Fe-Ni-Mo-B-Si alloys	65
3.5	Discussion	75
3.5.1	Resistivity minimum	75
3.5.2	Temperature dependence of electrical resistivity : evidence of magnetic contribution to resistivity	84
3.5.3	Moolj correlation	88
3.5.4	Curie temperature and crystallization studies	89
3.6	Summary	96
4	THERMOELECTRIC POWER MEASUREMENTS :	98
4.1	Introduction	99
4.2	Experimental results	100
4.3	Discussion	106
4.4	Summary	113
5	MÖSSBAUER SPECTROSCOPY MEASUREMENTS :	114
5.1	Introduction	115
5.2	Theoretical discussions	118
5.2.1	Isomershift	118
5.2.2	Quadrupole interaction	119
5.2.3	Magnetic hyperfine interactions	121

	Page No.
5.3 Analysis of the Mössbauer spectra	127
5.3.1 Least square fitting (LSF)	127
5.3.2 Evaluation of hyperfine field, P(H)	129
5.4 Results and discussion	134
5.4.1 Mössbauer spectra of metallic glasses	134
5.4.2 Room temperature spectra of Fe-Co-B-Si alloys	135
5.4.3 Room temperature spectra of Fe-Ni-Mo-B-Si alloys	142
5.4.4 Magnetization axis	147
5.4.5 Thermal scan method	153
5.4.6 Temperature dependence studies of Mössbauer spectra of Fe-Ni-Mo-B-Si alloys	158
5.4.6a Magnetic hyperfine interactions	163
5.4.6b Temperature dependence of isomer shift	174
5.4.6c Temperature dependence of line widths	178
5.5 Summary	182
6 CRYSTALLIZATION STUDIES OF AMORPHOUS Fe₄₀Ni₃₈Mo₄B₁₈ ALLOY :	183
6.1 Introduction	184
6.2 Isothermal transformation	185
6.3 Nonisothermal transformation	187
6.4 Experimental results and discussion	188
6.5 Summary	203
7 CONCLUSIONS :	204
7.1 Overall conclusions of the present work	205
7.2 Suggestions for future work	211
REFERENCES :	216

CERTIFICATE

This is to certify that the research work compiled in this thesis entitled **Electrical Transport and Magnetic Properties of Co, (Ni,Mo) Substituted Iron-Rich Metal-Metalloid Glasses** has been carried out by **Mr. N. R. Munirathnam** under my supervision and the same has not been submitted elsewhere for a Ph. D. degree to the best of my knowledge.


Anil K. Bhatnagar

PROF. ANIL K. BHATNAGAR
SCHOOL OF PHYSICS
UNIVERSITY OF HYDERABAD
HYDERABAD-500 134,
INDIA.


Dean

School of Physics

University of Hyderabad

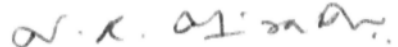
Hyderabad 500134, India

DEAN
SCHOOL OF PHYSICS
University of Hyderabad
P.O. Central University
Hyderabad-500 134 (INDIA)

CERTIFICATE

This is to certify that I, N. R. MUNIRATHNAM, have carried out the research embodied in the present thesis for the full period prescribed under Ph.D. ordinances of the University of Hyderabad under the supervision of Prof. Anil K. Bhatnagar.

I declare to the best of my knowledge that no part of the thesis was earlier submitted for the award of Ph.D. research degree of any university.


N. R. Munirathnam


Thesis supervisor

PROF. ANIL K. BHATNAGAR
SCHOOL OF PHYSICS
UNIVERSITY OF HYDERABAD,
HYDERABAD-500 134.
INDIA.


~~Dean, School of Physics~~

DEAN
SCHOOL OF PHYSICS
University of Hyderabad
P.O. Central University
Hyderabad-500 134 (INDIA)

ACKNOWLEDGEMENTS

I express my deepest gratitude to my research supervisor Prof. Anil K. Bhatnagar for introducing me to this research field and for the freedom given to me through out the research career.

It is with great pleasure I thank Prof. V. Srinivasan, Dean, School of Physics, for providing me the facilities in persuing this work.

My sincere thanks to Prof. R. Jagannathan, Prof. S.N. Kaul, Dr. V.S.S. Sastry, Dr. C.G. Sunandana and Dr. G. Rajaram for their help and numerous enlightening discussions.

I would like to thank Prof. O.V. Nielsen (Technical University of Denmark) and Dr. V.R.V. Ramanan (Allied Corporation, USA) for their timely help in sending the samples of our interest.

I take this opportunity to thank Prof. Girish Chandra and Dr. S. Ramakrishnan (TIFR, Bombay) for providing the facilities for low temperature resistivity measurements.

The help of Prof. P. Rama Rao and Dr. T. Rajasekharan (DMRL, Hyderabad) in providing x-ray and atomic absorption spectroscopy facilities are greatly acknowledged.

My special thanks to my colleague Mr. G. Venugopal Rao and Mr. Bharatam V. Prasad in bringing out the thesis in this shape.


I would like to thank my colleagues Dr. B. Bhanu prasad, Dr. S. Venkataraman, Dr. K. V. Reddy and Mr. Uno N. V. Swaroop and other friends for their cooperation during my research work.

I express my sincere thanks to Mr. A. Subbarami Reddy and Mr. K. Veera Raju and other staff of school of physics, C.I.L and C.W.S. for their technical assistance. I would like to thank Mr. K. Srinivas for typing the thesis.

I greatly acknowledge the financial support from University Grants Comission (UGC) in the form a research scheme (Grant No. F.10-18/82, SR III) and Council of Scientific and Industrial Research (CSIR) in the form of a Pre-doctoral fellowship.

I thank Mr. Vinay Roy (Managing Director) and Mr. Jagdish Chandra (Director), Usha Amorphous Metals Ltd., New Delhi for their encouragement.

Lastly, I wish to acknowledge all the people, who directly or indirectly involved in bringing up this piece of work.


(N.R.M. Rathnam)

PREFACE

The thesis presents the transport, magnetic and thermal stability of the magnetic metallic glasses based on iron-silicon-boron alloy systems. In particular, Fe-B-Si alloys in which cobalt/molybdenum/molybdenum and nickel have been partially substituted for iron have been studied. These metallic glasses have become important materials for scientific investigations as well as for technological applications. The thesis is divided in to seven chapters.

Chapter 1 gives a brief introduction to the subject of metallic glasses and a review of their important physical and chemical properties. This also contains the current status of research in the area of the work undertaken.

Chapter 2 deals with the experimental techniques used for the present investigations. A description of procedure adopted for various measurements and error analysis are discussed.

Chapter 3 describes low temperature (1.5 to 300 K) and high temperature (up to 900 K) electrical resistivity measurements of $(\text{Fe}_{1-x}\text{Co}_x)_{75}\text{B}_{10}\text{Si}_{15}$ ($0.00 \leq x \leq 0.12$) and $\text{Fe}_{70}\text{Ni}_{12-x}\text{Mo}_x\text{B}_{16}\text{Si}_2$ ($0 \leq x \leq 3$) metallic glasses although the whole range has not been necessarily used for all sample measurements. A detailed discussion on data analysis, magnetic contribution to resistivity and Debye temperature calculations have also been presented. Theoretical models related to the present investigations are

given and the experimental results are discussed in the light of these models.

Chapter 4 presents thermopower measurements of $(\text{Fe}_{1-x}\text{Co}_x)_{75}\text{B}_{10}\text{Si}_{15}$ ($0.00 \leq x \leq 0.12$) alloys in the temperature range 80 to 400 K. The results are discussed in the light of present theoretical models.

Chapter 5 deals with the Mössbauer measurements of $(\text{Fe}_{1-x}\text{Co}_x)_{75}\text{B}_{10}\text{Si}_{15}$ ($0.00 \leq x \leq 0.12$) and $\text{Fe}_{70}\text{Ni}_{12-x}\text{Mo}_x\text{B}_{16}\text{Si}_2$ ($0 \leq x \leq 3$) alloys. A brief review of various Mössbauer parameters and their physical interpretation are discussed. It deals with thermal scan method, isomershift, temperature dependence of line widths and hyperfine fields of the above mentioned metallic glasses.

Chapter 6 presents the results of thermal and crystallization studies of $\text{Fe}_{40}\text{Ni}_{38}\text{Mo}_4\text{B}_{18}$ glass by differential scanning calorimetry. It deals mainly with the extent of validity of the isothermal and nonisothermal analysis for the investigation of activation energies and Avrami exponents in $\text{Fe}_{40}\text{Ni}_{38}\text{Mo}_4\text{B}_{18}$ metallic glass. The results are compared and discussed with the existing literature.

Chapter 7 presents overall conclusions of this study and certain unresolved problems. It concludes with the suggestion made for further work, which could not be carried out due to the experimental facility limitations.

CHAPTER I

INTRODUCTION

CHAPTER I

1.1 INTRODUCTION :

Until very recently when one thought of a solid one meant a crystalline solid having a long range translational order in its atomic arrangement. Disordered solids were the solids showing departures from this ordered structure. Although insulating silicate glasses have been known since ancient times and have been extensively used for diverse applications, yet it is only in this century that they have been studied systematically. Glassy solids now include semiconducting and metallic glasses exhibiting absence of long range crystalline periodicity in their atomic arrangements. Semiconducting glasses were discovered quite early and have been exploited since then for practical applications. Although amorphous metals were prepared earlier by depositing metal vapours on liquid helium cooled substrates, these were stable only at very low temperatures, i.e., below 30 K, metallic glasses prepared by rapid quenching of an alloy melt and stable at room temperature have been discovered only recently in 1960. Klement, Willens and Duwez (Klement et al 1960), while trying to prepare metallic alloys by rapid quenching to study metastable phases, they found that melt of the alloy $\text{Au}_{80}\text{Si}_{20}$, when rapidly quenched at the rate of 10^6 K/sec, was amorphous and showed glassy or liquid-like structure when examined by X-ray diffraction and it was stable at room temperature. This discovery, that certain alloys can be rapidly quenched to produce

glassy solids which remain stable at room temperature, started a new era of research and development in this area. During last three decades new techniques have been developed to produce metallic glasses, in small as well as bulk quantities. Variation in composition of metallic glasses is used as a mean to vary their physical and chemical properties of interests to physicists, chemists and technologists. Metallic glasses have not only been exploited for potential applications but have also contributed a great deal in enhancing our knowledge of the solid state. A great deal of research and development literature has appeared on these materials since 1960. Some of important books and references in this area have been listed in the beginning of references under the heading "General References". Some of these will be referred as (GR) at the appropriate places in this thesis again. In this chapter we provide a brief introduction to preparation and some of important properties of metallic glasses. In the last, our motivation to take up this work is given.

1.2 GLASS FORMATION :

The basic criterion for the preparation of glasses is that the cooling process be so fast that the crystallization is bypassed quickly. This is illustrated in the Time-Temperature-Transformation (TTT) diagram, as shown in Fig. 1-1, in which the time for the onset of crystallization in an undercooled melt (T_m) is plotted against the temperature. As T_m is lowered, the free energy difference between the liquid and the crystalline

phases increases, hence the time for crystallization decreases. At T_g , the glass transition temperature, usually defined as the temperature at which the viscosity becomes larger than 10^{13} poise, the crystal growth becomes impossible and the liquid remains frozen in a single configuration. It is then called a glass. At sufficiently large cooling rates even the nucleation is eliminated. When a liquid is cooled from a high temperature, its specific volume (V) changes discontinuously at or below melting temperature T_m . This is illustrated in Fig. 1-2. If the growth of the nuclei is low or absent, then the volume of the supercooled liquid continues to decrease till T_g , where the remarkable change in the slope of V vs. T plot occurs. The glass transition depends upon the cooling rate as shown in Fig. 1-2. T_g increases with the cooling rate and so does the specific volume of the glass formed. Differences in volume are typically only a few percent but these have enormous effect on the properties of the material. A sample in the glassy state is in a thermodynamically metastable state, and therefore, its configuration tends to change with time towards the equilibrium structure of lowest free energy. Therefore, the structure of a glass is dependent on its thermal history.

Marcus and Turnbull (1976) have proposed an empirical criterion for the formation of metallic glasses. They have suggested that the glass forming ability may be related to the depression of the melt temperature T_m below certain average temperature T_a of ideal solution liquidus. The criterion for the

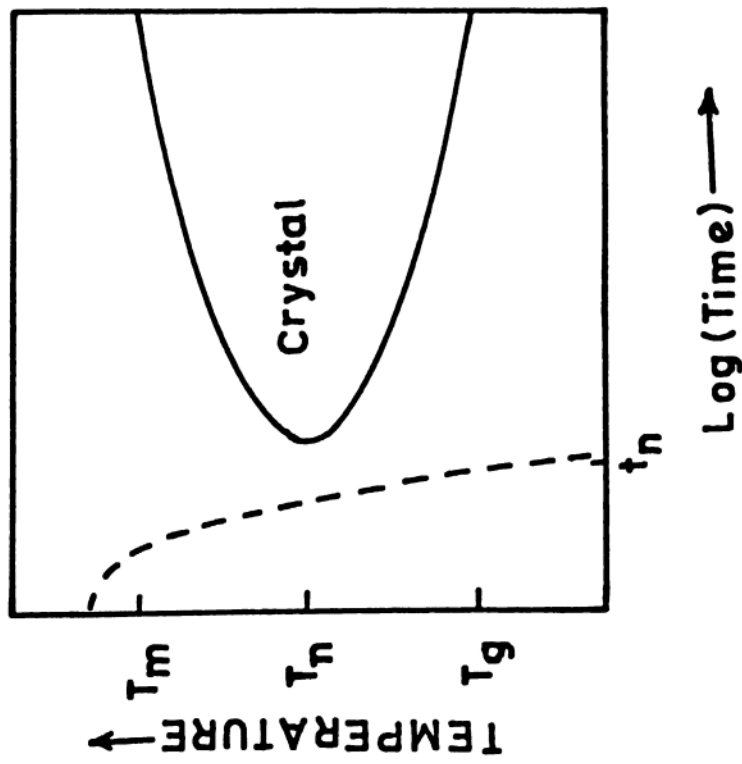


Fig. 1-1 : Schematic time-temperature-transformation diagram (TTT) for the onset of crystal growth in an under cooled melt.

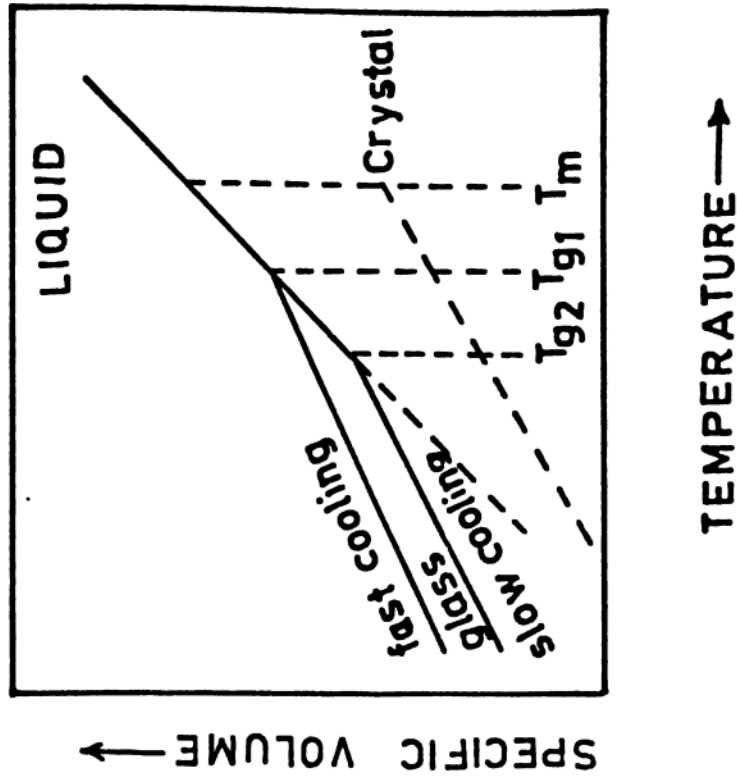


Fig. 1-2 : Schematic illustration of the changes of specific volume of a liquid with temperature by fast and slow cooling.

glass formation is that $(T_g - T_m)/T_g \geq 0.15$ to 0.2, metallic glasses can be formed using cooling rates of the order of 10^6 K/sec. A typical example of alloy Fe-B is shown in Fig. 1-3 where dotted line represents temperature T_g . Another criterion for ease of metallic glass formation is that if a liquid has $T_g/T_m \geq 0.7$ then the liquid can be rapidly cooled (cooling rate = 10^6 K/s) to produce glass without much difficulty (Davies 1983). On the other hand, if $T_g/T_m < 0.5$, then it is very difficult to cool liquid in a glassy state. This criterion is related to the one previously given by Rawson (1967) based on the ratio of bond strength to T_m . Glass formation is easier in multicomponent systems in comparison with a single component system, since the ratio of the bond strength to liquidus temperature will be greater for intermediate compositions, and largest of all at the eutectic composition.

1.3 PREPARATION TECHNIQUES :

During the last twenty five years, a number of methods have been developed for the production of metallic glasses. The basic procedure is to rapidly quench a metallic system either from its vapour phase or liquid phase on a heat sink so as to bypass the crystallization quickly to produce noncrystalline structure akin to frozen liquid. Generally, preparation of noncrystalline solids by quenching of vapour phase is referred as "amorphous" while the one prepared by liquid quenching is called "glass" (In this thesis we shall use both of these words interchangeably).

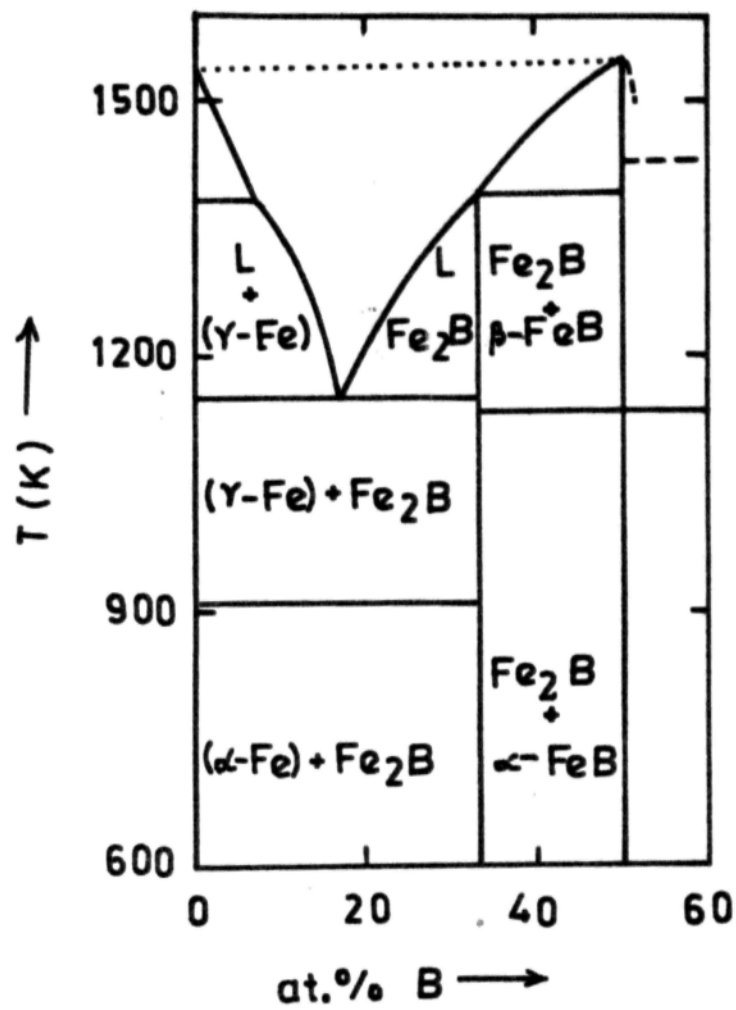


Fig. 1-3 : Phase diagram of the $\text{Fe}_{100-x}\text{B}_x$ alloy.

There are numerous variations of these two methods details of which can be found in most of general references (GR 1978a, GR 1982, GR 1983d, GR 1984a and GR 1987a). Most widely used current methods to produce metallic glasses for small scale research purposes are (1) Single roller chill-block melt spinning (CBMS), (2) Splat cooling, and (3) sputtering. In the research work reported here, samples were produced by the first method, therefore, a short description of this method is given below.

The chill-block melt spinning technique was originally developed by Pond (1969). The equipment consists of a rotating copper or stainless steel wheel as shown in Fig. 1-4. Master of alloy is prepared separately first by melting constituent elements in an arc furnace having inert gas atmosphere. A small amount of this master alloy is placed in a quartz crucible with a small hole (usually less than 1 mm). The alloy is melted either using a resistive heater or an induction heater and then forced out onto the rotating wheel, having surface speed of 25 to 50 m/s, by applying pressure inside the crucible. The melt quickly solidifies on contact with the surface of the copper wheel and a ribbon of approximately 1 to 5 mm width and 10 to 40 μm thick is produced depending upon various initial conditions. Ribbons of few cm to km lengths can be produced depending upon the amount of the alloy charge placed in the crucible and the hole size of the crucible. To avoid oxidation the whole apparatus can be placed either in a vacuum chamber or an inert atmosphere. Usually the side of the ribbon which remains

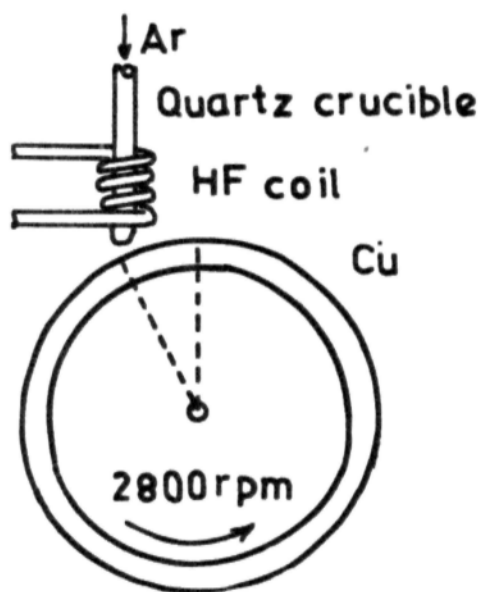


Fig. 1-4 : Schematic diagram of single roller quenching technique.

in contact with the wheel is dull in appearance while the other side has metallic shine. Most of iron based metallic glasses, as well as many others, can be bent by almost 180 degrees. Hence a quick way of finding out whether the ribbon is glassy or not is to apply this bend test. The real test, of course, has to be done by measuring X-ray diffraction.

Most of metallic glasses prepared earlier were binary or ternary alloys. Later, metallic glasses having four to six constituents have been produced for commercial usage, as well as for research purposes to investigate the effects of additional components in the alloy to improve thermal stability and other properties.

The melt quench method can usually produce glasses in a limited alloy composition range near eutectic point although some exceptions exist. Sputtering and vapour quenching technique can produce amorphous thick layers over a large composition range. For example, Chien and Unruh (1982) were able to obtain $\text{Fe}_{100-x}\text{B}_x$ for $x = 30$ to 90 by sputtering while one can prepare the same alloys only for $x = 15$ to 30. One should note that all the present methods to produce metallic glasses only produce forms which are thin, a severe drawback for many practical applications. A new technique of solid state diffusion by Johnson et al (1985) to produce metallic glasses is found to be very promising towards the production of thicker metallic glasses.

1.4 CLASSIFICATION OF METALLIC GLASSES :

The classification of metallic glasses can be done by either their composition or some chosen property, for example, magnetic properties of these glasses. In the first kind of classification (Davies 1983) there are four categories: (1) Transition metal-metalloid (TM-M) glasses. A typical and important example of this group is $\text{Fe}_{80}\text{B}_{20}$. (2) Metallic glasses combining an early transition metal with a late transition metal (TE-TL), like $\text{Nb}_{40}\text{Ni}_{60}$. (3) Metallic glasses made up of simple metals like Ca-Al. (4) Metallic glasses having rare earth-transition metal composition (RE-TM). Mizutani (1983) has proposed another classification for metallic glasses in five categories based on their magnetic state, on which the electronic state and electron transport property heavily depend. These classifications are : (1) ferromagnetic (e.g., $\text{Fe}_{80}\text{B}_{20}$), (2) weak ferromagnetic (e.g., Ni-Y and Fe-Zr), (3) spin glass (e.g., $\text{Fe}_x\text{Ni}_{80-x}\text{P}_{16}\text{B}_4$), (4) paramagnetic (e.g., Cu-Zr, Nb-Ni), and (5) weak paramagnetic or diamagnetic (e.g., Mg-Zn, Pd-Si). This classification is more useful when one is interested in physical and chemical properties of these materials.

1.5 DISORDER IN GLASSES :

In a perfect crystalline solid atoms occupy definite positions with lattice periodicity, hence, there is a long-range order present in the structure. However, no such perfect solid

exists in practice. Even the highest quality crystals have some impurities and defects besides lattice vibrations at finite temperatures. One can introduce disorder in an otherwise almost perfect crystal by various means which includes radiation damage.

Glasses, which have structure akin to frozen liquid, lack long range order in their atomic arrangement although some short-range order may exist. Glasses show three types of disorder in their structure. These are: (1) bond disorder, i.e., bonds between atoms are of different lengths making different lengths with each other, (2) topological disorder, i.e., random distribution of atoms instead of fixed locations as required by the lattice periodicity in crystals, and (3) chemical disorder, i.e., distribution of atoms A in a system like $A_{1-x}B_x$ becomes random. Generally a glass is characterized by the presence of all the three disorders.

The commonly used technique to probe structure of solids is the diffraction using X-rays, neutrons and electrons. In the diffraction experiment the structure factor $S(q)$ vs. q is measured, where q is the diffraction wave vector. Fig. 1-5 shows the difference in behaviour of $S(q)$ for a crystalline solid, a glass and a liquid. The sharp peaks exhibited by a crystalline solid are absent in the glass and liquid which are replaced by a broad peak followed by smaller broad peaks. The broad peaks in the $S(q)$ behaviour of a glass are similar to that of a liquid. It clearly brings out similarities between glassy and liquid structures at the atomic level although there are subtle

differences present. From $S(q)$ vs. q it is clear that the glassy structure has no long range order in atomic arrangement characteristic of crystalline solids. The atomic order in glasses seem to extend only for two or three nearest neighbour distances and is classified as short range order. One can differentiate between two types of short range orders in glassy alloys. The topological short range order (TSRO) characterizes the atomic arrangement of atoms with respect to a reference atom regardless of the type of atoms. The chemical short range order (CSRO) characterizes strongly correlated atomic positions in the nearest neighbour shells and uncorrelated beyond a few atomic spacings. Since metallic glasses prepared by liquid quenching are multicomponent alloys, these show both TSRO and CSRO.

1.6 ELECTRONIC STRUCTURE AND TRANSPORT :

To understand physics and chemistry of metallic glasses, it is necessary to obtain information on their electronic band structure and transport properties (electrical resistivity, etc.). The ideas of Bloch's theorem and reciprocal space, break down for glasses since there is no long range lattice periodicity. Hence it is of interest to study the effect of the lack of crystalline periodicity on the band structure of these materials. Since a number of physical properties of solids like electronic specific heat, superconductivity, magnetic susceptibility, ferromagnetism etc., are directly related to their electronic structure, the usual experimental methods, viz.,

ultraviolet and X-ray photoemission spectroscopy, Auger electron spectroscopy, soft X-ray spectroscopy, and optical reflectivity, to study band structure of crystalline solids have been applied to glasses. These studies have shown that the valence bands show distinct bonding effects which are directly observable in the valence band spectra. Besides the information on the valence bands in many metallic glasses, information on the density of states near Fermi energy (E_F) has also been obtained. It may be noted that the density of states at E_F is a very important parameter for solids to understand many of their electronic properties including specific heat. Detailed survey on the electronic spectroscopy on metallic glasses has been given by Oelhafen (GR 1981b).

Electronic transport properties, namely, electrical resistivity (ρ), Hall effect (Hall coefficient R_H) and thermoelectric power (S) provide valuable information on electronic transport and electronic scattering mechanisms in solids and particularly metallic systems. Electrical resistivity has been the most investigated electrical property of metallic glasses since their discovery in 1960 (GR 1981b, GR 1983a and GR 1983b). Data on Hall effect and thermoelectric power on metallic glasses is not of the same magnitude as it is for ρ .

Electrical resistivity of metallic glasses is typically of the order of 100-250 $\mu\Omega\text{-cm}$ at room temperature which is quite high in comparison with that of pure metals. Temperature coefficient of resistivity (TCR), defined as $1/\rho (d\rho/dT)$, is

typically of the order of 10^{-4} K^{-1} and it can be positive, zero or negative depending upon the glass composition and the temperature interval. It has been possible to change the sign of TCR by continuously changing the composition of many metallic glasses (Altounian et al 1983 and Carini et al 1983). The magnitude and composition dependence of ρ of metallic glasses and its temperature dependence above θ_D have been found comparable to liquid metal data (Guntherodt et al 1978). Therefore, theoretical models which have been earlier used to explain liquid metal data on electronic transport properties have also been applied to metallic glasses with reasonable success.

One of important features of $\rho(T)$ behaviour in metallic glasses is that many of these show a resistivity minimum at low temperatures ($T \leq 25 \text{ K}$) and some even at higher temperatures. Attempts to explain this widely observed effect have been made either by invoking Kondo effect mechanism (Hasegawa et al 1970 and Grest et al 1979) or the existence of two level system (TLS) (Cochrane et al 1975) or spin fluctuations (Asomoza et al 1977). However, there are difficulties associated with these theoretical models which have been discussed in detail by Harris and Strom-Olsen (1983).

Thermoelectric power (S), which is essentially the entropy per unit charge transported is another important property of metals and metallic glasses. Measurements of ρ along with S have resulted in testing theoretical models for transport properties of these materials (Babic et al 1980, Bhanuprasad et al 1982 and

Kettler et al 1984). The magnitude and temperature dependence of S for a simple and pure metal can be calculated considering it as a degenerate electron gas; S should be of the order of a few $\mu\text{V}/\text{K}$ and should vary linearly with absolute temperature T . However, in practice, there are other effects present in metals which lead to departures from this simple behaviour of S . One of these is the phonon drag effect which gives rise to nonlinear behaviour of $S(T)$ and large magnitudes at low temperatures. Due to large disorder in metallic glasses resulting in high resistivity, phonon drag effect is reduced considerably, and therefore, one would expect S to behave more ideally, i.e., S must be proportional to T and its magnitude should be a few $\mu\text{V}/\text{K}$. This has been generally observed for $\theta_D \geq T \leq 300 \text{ K}$, for many metallic glasses. However, magnetic as well as nonmagnetic glasses show nonlinear behaviour at low temperatures, which for the later type of metallic glasses has been interpreted in terms of enhancement due to electron-phonon interaction (Gallagher 1981). Nonlinear behaviour of $S(T)$ of magnetic metallic glasses still remains to be understood although some suggestions have been made (Harris et al 1983).

For nonmagnetic metallic glasses it has been found that there is correlation between the sign of TCR and the sign of S (GR 1978a). If TCR of a nonmagnetic metallic glass is negative then S is positive and vice versa. The magnitude of S also seem to scale with the magnitude of TCR (GR 1978a). On the other hand magnetic glasses show positive TCR near room temperature and

mostly negative thermopower. $S(T)$ for these glasses shows nonlinear temperature dependence between $0 < T < 300 \text{ K}$ (Kettler et al 1982 and Bhanuprasad et al 1982).

Hall coefficient (R_H) is another important parameter as it provides information on the sign and density of current carriers. For metallic glasses consisting of simple metals R_H is found to be negative, whereas it is positive for many metallic glasses containing transition metals (GR 1984e). Of course, for magnetic glasses one has to take account of extra-ordinary Hall coefficient also (GR 1984e). Observation of positive R_H in semiconductors is always associated with the hole conduction, while the same observation in some crystalline metals is associated with the unusual dynamics of electrons and their band structure. Positive R_H in magnetic metallic glasses with no hole conduction has been a challenge to theoreticians. Morgan et al (1987) and Grieg (1987) have now firmly established that positive R_H in metallic glasses arises due to the anomalous dispersion of s-like states due to s-d hybridization which result in negative slope of E vs. k dispersion curve. Further theoretical support for this idea has been provided by Nguyen-Manh et al (1987).

In summary, the electron transport phenomena in metallic glasses has many interesting features which makes experimentalists and theoreticians to continue their vigorous research effort in this area, and to further our knowledge of glassy state in metals.

1.7 MAGNETIC PROPERTIES :

Originally it was thought that it is unlikely that magnetic order could exist in amorphous solids. Gubanov (1960a) showed theoretically that the crystalline periodicity was not necessary for solids to exhibit ferromagnetic order. This prediction was experimentally confirmed by the works of Mader et al (1965) on vapour quenched Co-Au films, Tsuei et al (1960) on splat quenched $\text{Pd}_{80}\text{Si}_{20}$ alloy containing ferromagnetic impurities, and on amorphous $\text{Fe}_{75}\text{P}_{15}\text{C}_{10}$ alloy by Duwez et al (1967). The discovery of ferromagnetism in amorphous solids lead to the large scale scientific and engineering investigations. Most of early metallic glasses based on the Fe-B alloy system were found to have excellent soft magnetic properties, e.g., low coercivity and hysteresis losses and high saturation magnetic induction etc. which seem to be very good for a large number of applications in the electromagnetic industry. Magnetic metallic glasses are already being used now for a number of applications, a brief description of which is given in a later section.

Magnetic properties of amorphous solids and particularly metallic glasses have been investigated in great detail to understand magnetism in these materials (GR 1984b). For magnetic order to exist in a solid there must be magnetic moments associated with unpaired electrons on the atoms and an interaction to couple them together. Except for so called weak itinerant ferromagnets, the above conditions remain valid for

magnetic order to exist in a vast majority of metallic and nonmetallic solids. For ferromagnetic order to exist the exchange interaction to couple the moments together must be positive and, in principle, there are no fundamental differences between glassy and crystalline ferromagnets. However, disorder in amorphous solids leads to smearing effects in some of properties, and magnetic and nonmagnetic atoms can coexist in the ferromagnetic state. Besides this, the chemical and bond disorder in amorphous solids leads to a distribution both in magnetic moments and the exchange interaction in contrast to the crystalline solids which show unique values for these parameters. Differences in Curie temperature etc., are also there even when one considers the same composition alloy in crystalline, and glassy state. On the other hand, antiferromagnetic interactions on a disorder lattice produces quite a different and novel result and it has lead to discovery on non-collinear magnetic structures classified as speromagnetic, sperimagnetic and asperomagnetic structure (GR 1984b).

The structure of glasses is normally considered to be isotropic on a long range scale, therefore, the magnetization vector in ferromagnetic glasses should, in general, be free from special magnetic anisotropy. However, in practice, most amorphous ferromagnets behave anisotropically (GR 1983d). Certain mechanical treaments like cold rolling, magnetic field cooling and stress annealing can induce additional anisotropy. Similarly relaxation due to annealing or by some other method as well as

crystallization result in changes of magnetic properties and therefore one has to be careful and certain about the thermal history of magnetic glasses before interpreting results or considering applications.

1.8 CRYSTALLIZATION :

The amorphous/glassy state is thermodynamically metastable phase and is stable only at low temperatures. The approximate value of "low temperature" will be different for different glasses but for most metallic glasses produced by rapid quenching the glassy state remains stable against crystallization below approximately 600 K although relaxation, that is, transition to a lower energy glassy state, may take place. The glassy state is never the true equilibrium state and the ultimate stable state for glasses is the crystallized state. Therefore, depending upon the external conditions like temperature, glasses would tend to crystallize irreversibly over a time period. This imposes a strict boundary on the operating times for these materials at elevated temperatures.

It has been well established that the metallic glasses lose most of their excellent mechanical and magnetic properties on crystallization and become useless for many practical applications as well as for research purpose. Therefore, impeding and controlling crystallization of metallic glasses has been an important area of research in this field (Uwe Koster 1987). The

work on crystallization behaviour of metallic glasses has contributed in enhancing our understanding of glass formation, factors affecting thermal stability, and nucleation and growth processes during crystallization. Excellent reviews have appeared in this area which cover a wide variety of research topics and results obtained (Scott 1983 and Uwe Koster 1981 and 1987).

1.9 APPLICATIONS :

Metallic glasses have found many applications in electromagnetic industry due to their excellent mechanical, and magnetic properties (GR 1983d, GR 1984b and GR 1987a). These applications include power distribution transformers, magnetic sensors, magnetic heads for audio, video and data recording, magnetic shielding, transducers, and electronics (delay lines, inductive electronic components like choke coils, spike killers, amorphous beads etc., magnetic amplifiers, magnetic modulator, etc.). The possibility that Nd-Fe-B metallic glasses may eventually replace high energy density but costly Sm-Co₅ permanent magnets is being exploited recently (Dugdale et al 1985). Their mechanical properties are being utilized in applications for brazing filler materials, strengthening fibers in composite materials etc. (Beck 1981). Some of Cr containing metallic glasses show excellent resistance to corrosion and therefore their applications in this area are being exploited. As new materials are being prepared more and more applications for these materials are being considered and implemented.

2.0 RESEARCH IN THIS WORK :

This thesis presents experimental research work on the magnetic metallic glasses based on the Fe-Si-B alloy system as part of the ongoing research and development in the area of metallic glasses at University of Hyderabad. The alloys investigated are $(\text{Fe}_{1-x}\text{Co}_x)_{75}\text{B}_{10}\text{Si}_{15}$, where $0 \leq x \leq 0.12$; $\text{Fe}_{70}\text{Ni}_{12-x}\text{Mo}_x\text{B}_{16}\text{Si}_2$, where $0 \leq x \leq 3$, and $\text{Fe}_{40}\text{Ni}_{38}\text{Mo}_4\text{B}_{18}$. The first two glasses will be referred in the thesis as Fe-Co-B-Si and Fe-Ni-Mo-B-Si alloys, respectively. The properties measured in this investigations are electrical resistivity, thermopower, magnetic interaction by Mössbauer effect and crystallization behaviour. Some of these properties of Fe-Co-B glasses have been investigated and reported by other workers since this work was started (Dey et al 1981, Kettler et al 1982 and Kheirn et al 1982). However, the substitution of Co was 15% or higher. In this work the substitution of Co is kept below 15% to see subtle changes in the Fe-Si-B glasses due to small addition of Co in this glassy alloy.

Fe-Ni-B, Fe-Ni-B-Si, Fe-Mo-B and Fe-Mo-B-Si alloys have also been investigated by other workers since this work was started. The effect of Ni or Mo substitution on the magnetic properties of Fe-B or Fe-B-Si glasses is found to be quite drastic in the sense that the Curie temperature shows a large change. It, therefore, was considered of interest to see the effect of both Ni and Mo substitution in the Fe-B-Si glasses and we do find a different behaviour as discussed in later chapters.

The experimental techniques used are electrical resistivity, thermoelectric power, Mössbauer spectroscopy and differential scanning calorimetry (DSC) and the temperature range used is 1.5 to 900 K although the same temperature range has not been used for all the measurements. The results on electrical resistivity measurements have been discussed in terms of widely used theoretical models and data has been analyzed to obtain (1) absolute resistivity at room temperature, $\rho(RT)$, (2) temperature coefficient of resistivity (TCR), α , (3) resistivity minimum temperature, T_{min} , (4) Debye temperature, θ_D , (5) Curie temperature, T_c , (6) crystallization temperature, T_x and (7) magnetic contribution to resistivity, ρ_{mag} .

Mössbauer studies have been done to obtain information on hyperfine fields, isomershift, magnetization axis, hyperfine field distribution and Curie temperature as a function of composition. Differential scanning calorimetry has been used to study crystallization process to obtain crystallization temperatures, Curie temperature, activation energy and Avrami exponent as a function of composition for various glasses studied. Thermoelectric power (S) measurements have only been done on Fe-Co-B-Si samples and a discussion of changes of S as a function of temperature and composition is given.

The thesis presents the details of experimental arrangements and related details wherever necessary. Each chapter presents in the beginning a brief discussion of theoretical background and important models used widely to interpret data. Last chapter

contains the summary of results of this work, our conclusions and some suggestion for further work.

CHAPTER II

SAMPLES AND EXPERIMENTAL TECHNIQUES

CHAPTER II

This chapter presents description of samples and experimental methods used.

2.1 SAMPLES :

The metallic glass system Fe-B-Si is chosen as the basic system to study its electrical resistivity, thermoelectric power, magnetic interactions using Mössbauer spectroscopy and thermal stability. The aim of the work is to study the effect of the substitution of other elements in the Fe-B-Si system. The list of samples studied is given below.

1. $(\text{Fe}_{1-x}\text{Co}_x)_{75}\text{B}_{10}\text{Si}_{15}$ ($0.00 \leq x \leq 0.12$),
2. $\text{Fe}_{70}\text{Ni}_{12-x}\text{Mo}_x\text{B}_{16}\text{Si}_2$ ($0 \leq x \leq 3$) and
3. $\text{Fe}_{40}\text{Ni}_{38}\text{Mo}_4\text{B}_{18}$ metallic glasses.

Some effort is made to prepare Fe-B-Si samples in our laboratory using the chill-block melt spinning method, but most of other samples are prepared elsewhere. Fe-Co-B-Si samples are prepared at the Technical University, Denmark and Fe-Ni-Mo-B-Si and $\text{Fe}_{40}\text{Ni}_{38}\text{Mo}_4\text{B}_{18}$ samples are prepared at Allied Signal Corp., USA. The starting materials had 99.9% purity while the composition of Fe-Co-B-Si samples is checked by the atomic absorption spectroscopy. No similar composition check is done for Fe-Ni-Mo-B-Si alloys.

2.2 CHARACTERIZATION :

Samples are checked by X-ray diffraction at the place of production and are found to be amorphous. A similar check has been done on the samples after receiving them and while studying their crystallization. All samples have shiny appearance, uniform thickness and can be bent by almost 180 degrees without breaking. Further characterization is done using differential scanning calorimetry (DSC) as described in chapter VI.

The chemical composition is studied using the atomic absorption spectroscopy which is a destructive method. It ignites the sample dissolved in aqua regia (25% conc. HNO_3 and 75% conc. HCl) to be analyzed in presence of a mixture of air or N_2O with acetylene or hydrogen flame to attain high enough temperatures ($T > 2500 \text{ K}$) to dissociate the material into its atomic constituents. They can be identified by their characteristic optical absorption by measuring the attenuation of intensity of a beam of light traversing the flame.

Figure 2-1 shows the graph between atomic weight of the standard solution (cobalt dissolved in aqua regia in this case) and the absorption in counts. Usually the linear portion is selected for further calculations. Actually the composition of the unknown sample is estimated by the corresponding absorption counts. The accuracy of the results are about 0.1 at. wt.% .

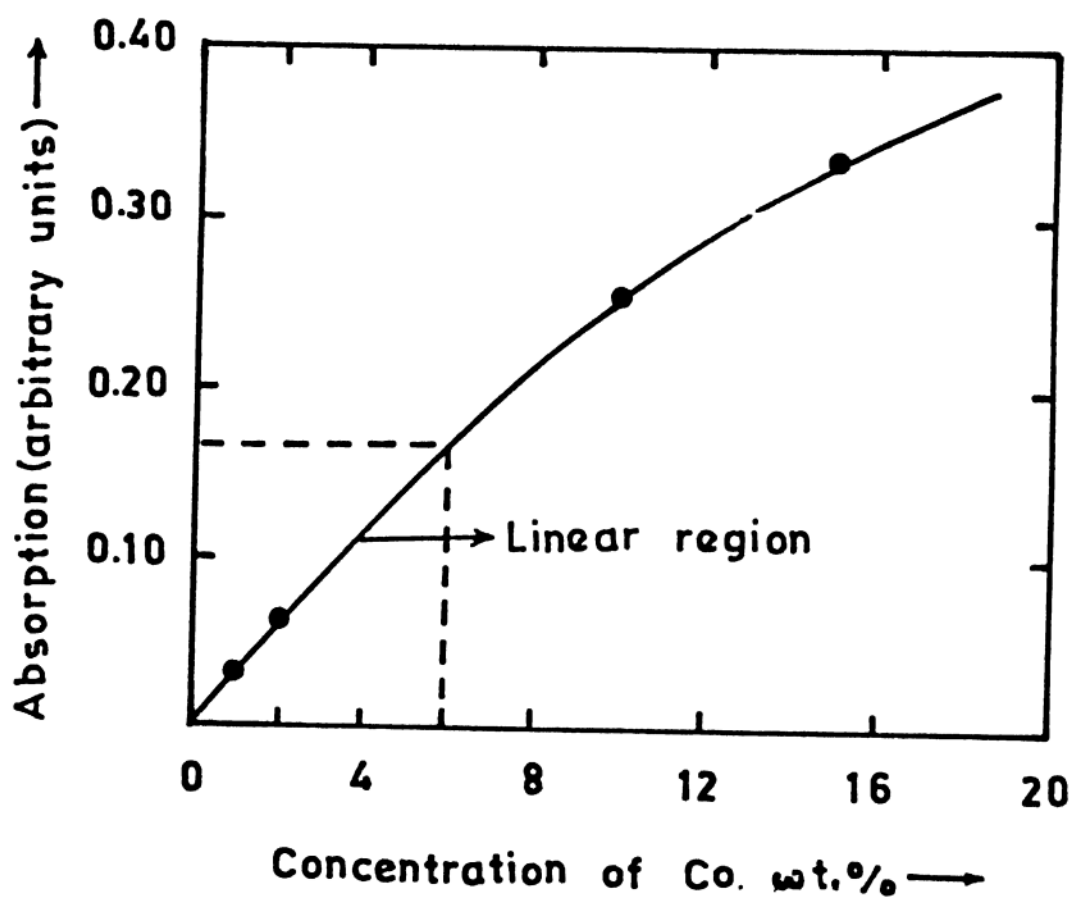


Fig. 2-1 : Atomic absorption (counts) vs. cobalt wt.% of amorphous $(\text{Fe}_{1-x}\text{Co}_x)_{75}\text{B}_{10}\text{Si}_{15}$ alloys.

2.3 EXPERIMENTAL TECHNIQUES :

Four techniques viz., electrical resistivity (ρ), thermoelectric power (TEP), Mössbauer spectroscopy (MS) and Differential Scanning Calorimetry (DSC) have been used to study the electrical transport, magnetic properties and crystallization of metallic glasses listed in section 2.1. The details of the experimental setups are as follows.

2.3.1 Resistance measurements from 1.5 to 300 K :

The block diagram of the experimental setup for low temperature resistance measurements from 1.5 to 300 K is as shown in Figure 2-2. Four probe DC method is used in both low and high temperature resistance measurements. The low temperature liquid helium cryostat used for our measurements is described in detail by Ramakrishnan et al (1985). It consists of a fibre glass Dewar (SHE Corp. Model LHD5) and a double walled system comprising an outer stainless steel tube and an inner quartz tube. The high-purity copper sample holder is connected to a stainless tube which goes inside the quartz tube. Germanium and platinum sensors are used to measure temperature from 1.5 to 300 K. A heater is attached near top of the sample holder to control the temperature of the sample. The temperature 1.5 K is achieved by pumping on liquid He from 4.2 K. A constant current source (Keithley 225) is used to heat the mantle heater (surrounding the sample holder) for uniform heat flux around the sample. A LAKE

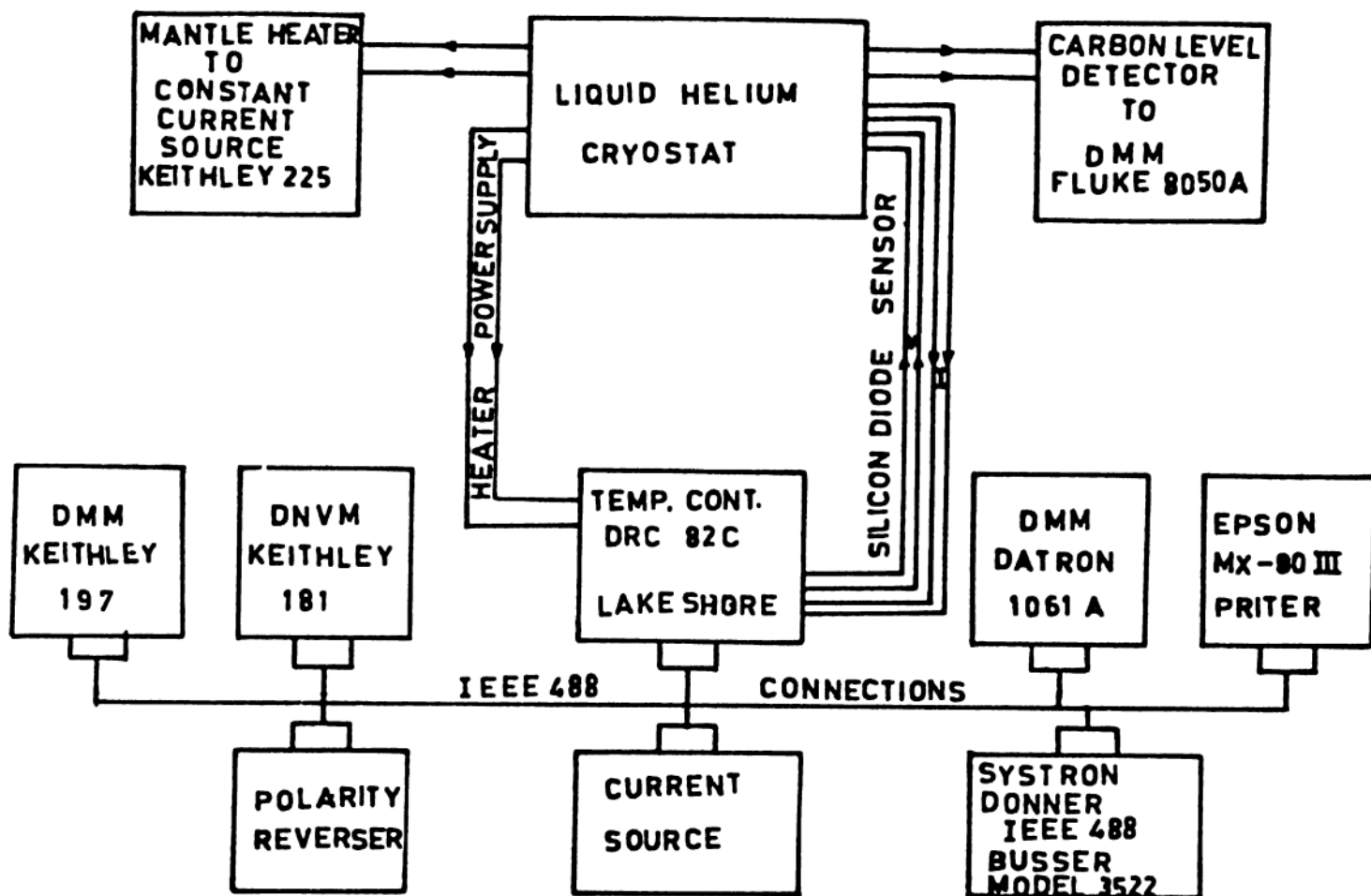


Fig. 2-2 : Schematic diagram of low temperature electrical resistivity measurements.

SHORE (DRC 82C model) temperature controller is used to monitor the temperature in a vacuum of about 10^{-4} torr. The whole setup is controlled by a microprocessor for automatic data collection.

Heating rates used for the measurements varies from 0.1 K/min at lower temperatures (< 80 K) to 1 K/min at higher temperatures (> 80 K). The accuracy of the resistance measurements is about a few parts per million.

Amorphous ribbons of ~ 3 cms length are cut and four contacts are made using 42 guage super enameled copper wires. The ends of the copper wires are dipped in conc. formic acid to remove the enameled coating and cleaned immediately with ethanol to prevent further decay of the coating. The wires are spot-welded to the sample with non-superconducting soft solder ($\text{Pb}_{40}\text{Sn}_{60}$) using a UNITEK spot-welding machine. The sample is fixed to the sample holder using a thin coating of Apelzone-N grease, which provides a good thermal contact and does not introduce any stress-induced effects. A resistor is connected in series with the sample in the current path to monitor current in the sample. The current during measurements is kept constant upto one part in 10^4 , and the parasitic thermoelectric voltages are eliminated either by reversing the current polarity or by noting the zero-current voltage for each reading.

Samples used for measurements are cut from 'as quenched' ribbons. The width of the samples is ~ 0.5 mm and the thickness is ~ 20 μm for Fe-Co-B-Si alloys, where as the width and

thickness of Fe-Ni-Mo-B-Si alloys are ~ 0.5 cms and ~ 25 μm respectively. The width and length (between voltage leads) are measured using a travelling microscope with an accuracy of 0.01 mm. A number of readings are taken over the whole dimensions of the sample to get a good accuracy. The measurement of thickness posed a problem because of thin samples. We used a sensitive screwgauge to measure thickness at various positions over the whole length in order to get a reasonably accurate average value of the thickness. A better method would have been to measure the density and then find the thickness. However, since we are more interested in the temperature variations of resistivity, we did not follow the density method to determine thickness.

2.3.2 Resistance measurements in the temperature range 80 to 900 K :

The schematic diagram of the measuring setup is as shown in Figure 2-3. Here the spot-welding is made directly on to the sample with the copper leads. A high current transformer with a dimmerstat controlling facility is used for this purpose. A copper rod with a sharp edge is used for welding. Spot-welding is done by passing minimum possible current to localize heating of the sample only at its contact with the copper wire.

The measurements procedure is almost similar to that of low temperature measurements (section 2.3.1 of this thesis). However,

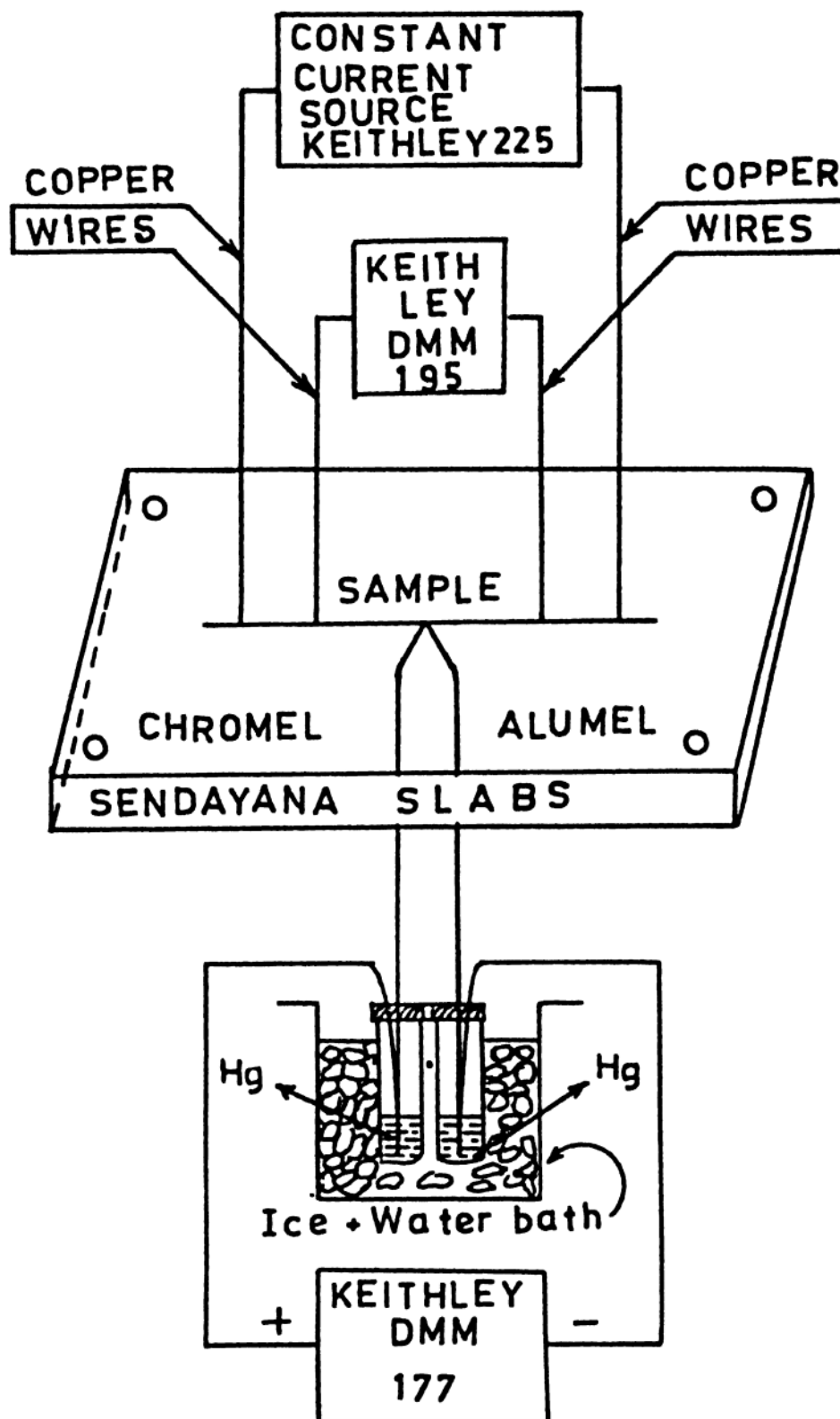


Fig. 2-3 : Schematic diagram of the experimental setup for the electrical resistivity measurements in the temperature range 80 to 900 K.

there are a few differences. The sample holder is designed so as to enable to take measurements from low to high temperatures. The temperature of the sample is measured in the middle of its length using chromel-alumel thermocouple obtained from Omega Inc., USA. The voltage between the leads can be measured here with an accuracy of $0.1 \mu\text{V}$ and a relative accuracy of 1 to 5 parts in 10^4 . The heating rate used is $\sim 5 \text{ K/min}$ through out the experiment.

The error in the measurement of the absolute values of the resistivity is mainly determined by the error in the thickness measurement. The estimated error in the absolute values of resistivity is approximately $\sim 10\%$. However, the relative resistivity ratios are much more accurate and the error in these measurements is better than 1% neglecting any effects due to thermal expansion or contraction. The accuracy in the absolute temperature measured is about 0.5 K or better.

2.3.3 Thermoelectric power measurements from 80 to 400 K :

The potential difference developed between two points a and b maintained at different temperatures T_1 and T_2 is given by

$$\Delta V = - \int_a^b \vec{E} \cdot d\vec{l} = - \int_a^b S \nabla T \cdot d\vec{l} = - \int_{T_a}^{T_b} S dT \quad 2-1$$

where \vec{E} is the effective electric field, ∇T is the temperature

gradient and S is the absolute thermopower of the material.

The Junction between two dissimilar matters are maintained at temperatures T_1 and T_2 where $T_2 = T_1 + \Delta T$. The potential difference developed between the terminals (1) and (2) is given by

$$\Delta V = \left\{ \int_{T_0}^{T_1} S_a dT + \int_{T_1}^{T_1+\Delta T} S_b dT + \int_{T_1+\Delta T}^{T_0} S_a dT \right\} = \int_{T_1}^{T_1+\Delta T} (S_b - S_a) dT \quad 2-2$$

The thermopower of the thermocouple S_{ab} is given by

$$S_{ab} = (S_b - S_a) = \lim_{\Delta T \rightarrow 0} \left(\frac{\Delta V}{\Delta T} \right) \quad 2-3$$

The usual procedure to determine the absolute thermopower of an unknown material, a material with known absolute thermopower (Blatt et al 1976) is used as a reference. The schematic representation of this is shown in Figure 2-4a.

Integral method: In this method, one junction is maintained at constant temperature, the other is at variable temperature to measure thermo e.m.f. developed between the junctions. The instrument used for these measurements is as shown in Fig. 2-4.

A grooved (to reduce thermal conduction) brass tube of about 1 cm diameter and 1 m length is brazed to the sample holder at one end. The upper junction in the figure is a Copper slab which is in good thermal contact with the base. This also acts as

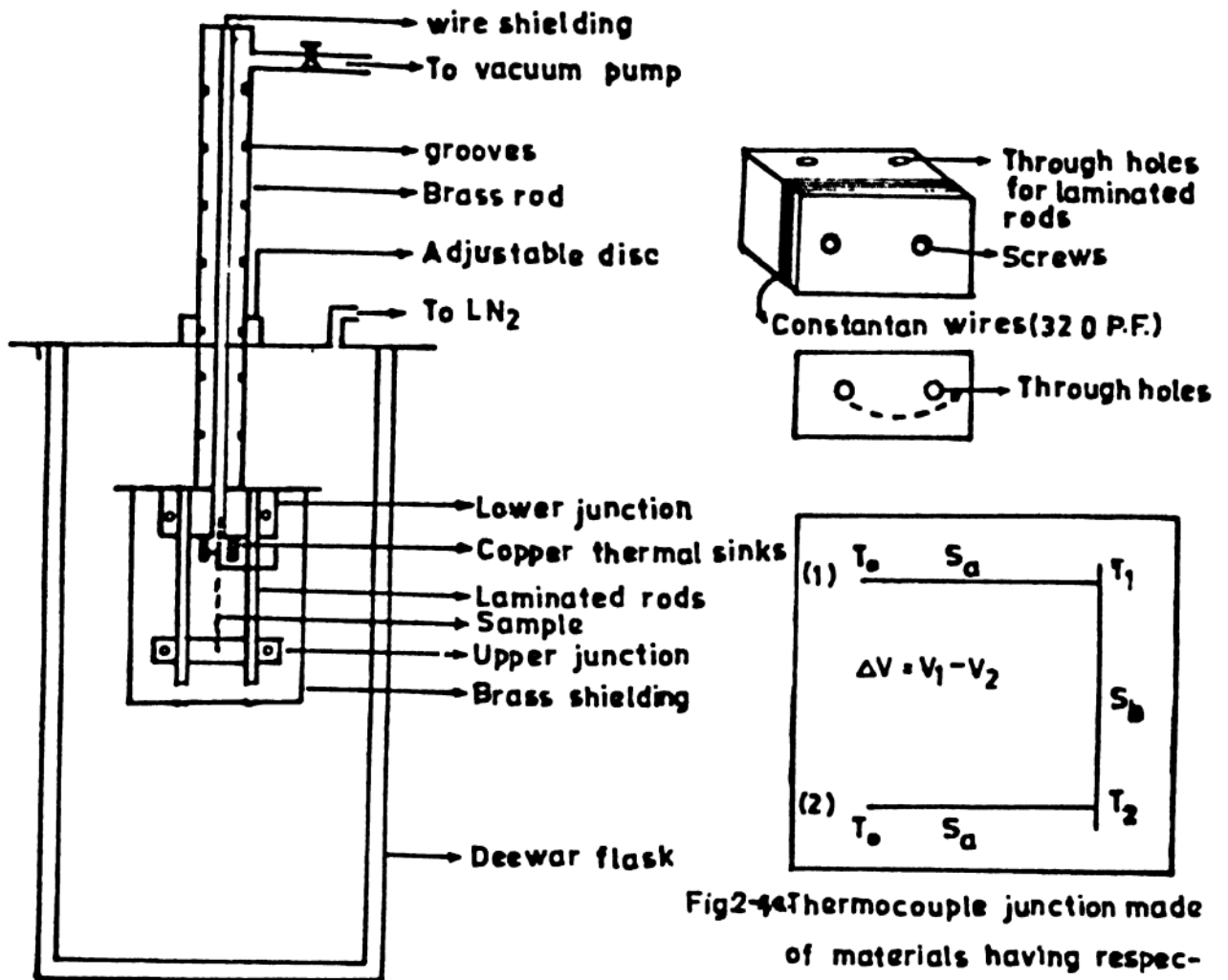


Fig2-4 Thermocouple junction made of materials having respective absolute thermopower S_a and S_b

Fig. 2-4 : Thermoelectric power measurements apparatus.

a thermal sink. Two laminated rods of about 8 cms length and 5 mm diameter are connected to the base through the upper copper slab as shown in Figure 2-4. To the other end of the laminated rods a second slab (lower junction) of copper is attached. The complete sample holder is shielded with a brass tin and fixed to the base with an indium O'ring.

The sample is connected between the lower and upper copper slabs. The reference wires (well annealed copper wires) and thermocouples (chromel-alumel) are taken out through brass pipe. An outlet is made for vacuum on the top of the brass tube. A heater is attached on the lower slab to create thermal gradient. The whole setup is immersed in a LN_2 flask of about 15 liters capacity. Initially the setup is allowed to cool to LN_2 temperature and then the lower junction is heated to measure thermo e.m.f. developed between the sample junctions. The measurements are carried out from 80 to 400 K in the vacuum of about 10^{-4} torr and the heating rate of about 1 K/min is maintained through out the experiment.

Each time a thermocouple is made using sample and a well annealed copper wire of 0.010 inches diameter (Omega Inc., USA). The connections are either spot-welded or soldered using non-superconducting lead, although there is no difference in the absolute values of TEP between these two contacts. Thermoelectric voltages are measured using a Keithley multimeter (model 195) with an accuracy of 0.1 μV or better. The thermoelectric power of the sample with respect to copper is obtained by differentiating

point by point thermoelectric voltage vs. temperature data and by fitting 5 data points to a straight line and determining the slope of the line. Absolute value of the thermoelectric power, S is then obtained using the TEP data of copper as published by Cusack et al (1958) and fitting it to a polynomial to get the integrated values of S_{Cu} vs. T . The relative resolution of the experimental setup is $0.05 \mu V/K$, whereas relative accuracy of the experimental data is nearly 3%. Measurements are repeated at least two times on each composition using fresh samples every time. The readings are found to be reproducible within the experimental error.

2.3.4 Mössbauer measurements :

The phenomena of recoilless emission and resonant absorption of gamma rays by a nucleus was discovered by Rodolf L. Mössbauer in 1958 and is known as the Mössbauer effect. Since then this effect has been extensively used to study a variety of phenomena of science and technology (Gonser 1975). The Mössbauer effect has been used to investigate solids, especially magnetic materials, since ^{57}Fe happens to be a common Mössbauer isotope suitable for such studies. Since many of magnetic glasses, useful for practical applications as well as for basic studies of magnetism in amorphous metals, have iron as one of the elements in the composition, Mössbauer effect has been used to study magnetic interactions in these glasses (Chien 1981 and Bhatnagar 1985a). In addition, Mössbauer absorption is a sensitive probe of the

local atomic structure around the Mössbauer isotope/probe, hence one can also expect to obtain information from these measurements on the structure of magnetic glasses.

General information on the Mössbauer measurements using ^{57}Fe isotope is given in a number of references (Bhide 1973, Gonser 1975, Cohen 1976 and Bhatnagar 1984).

A block layout of the Mössbauer spectrometer used is shown in Figure 2-5. We used a transmission configuration. The gamma ray energy sweep is obtained by the Doppler effect. The Doppler effect shifted gamma ray energy by $E_D = (V/c)E_\gamma$, where E_γ is the gamma ray energy when the source is at rest. The source is operated in a constant acceleration mode. The spectra obtained are measured using the gamma ray counts as a function of source velocity.

The γ -ray source used in this work is ^{57}Co embedded in rhodium-matrix. The gamma rays are detected by a proportional counter. The amplitude of the output voltage pulses generated by this detector is proportional to the incident gamma ray energy. An amplifier is used to amplify the signal and then 14.4 keV signal radiation is separated by fixing upper and lower window voltages in a single channel analyzer. The data are collected and stored in a multichannel analyzer (MCA) in 520 channels (First 256 channels are due to the first half of triangular wave and the next 256 are due to the next half). The linear ramp signal produced by function generator synchronized with the source

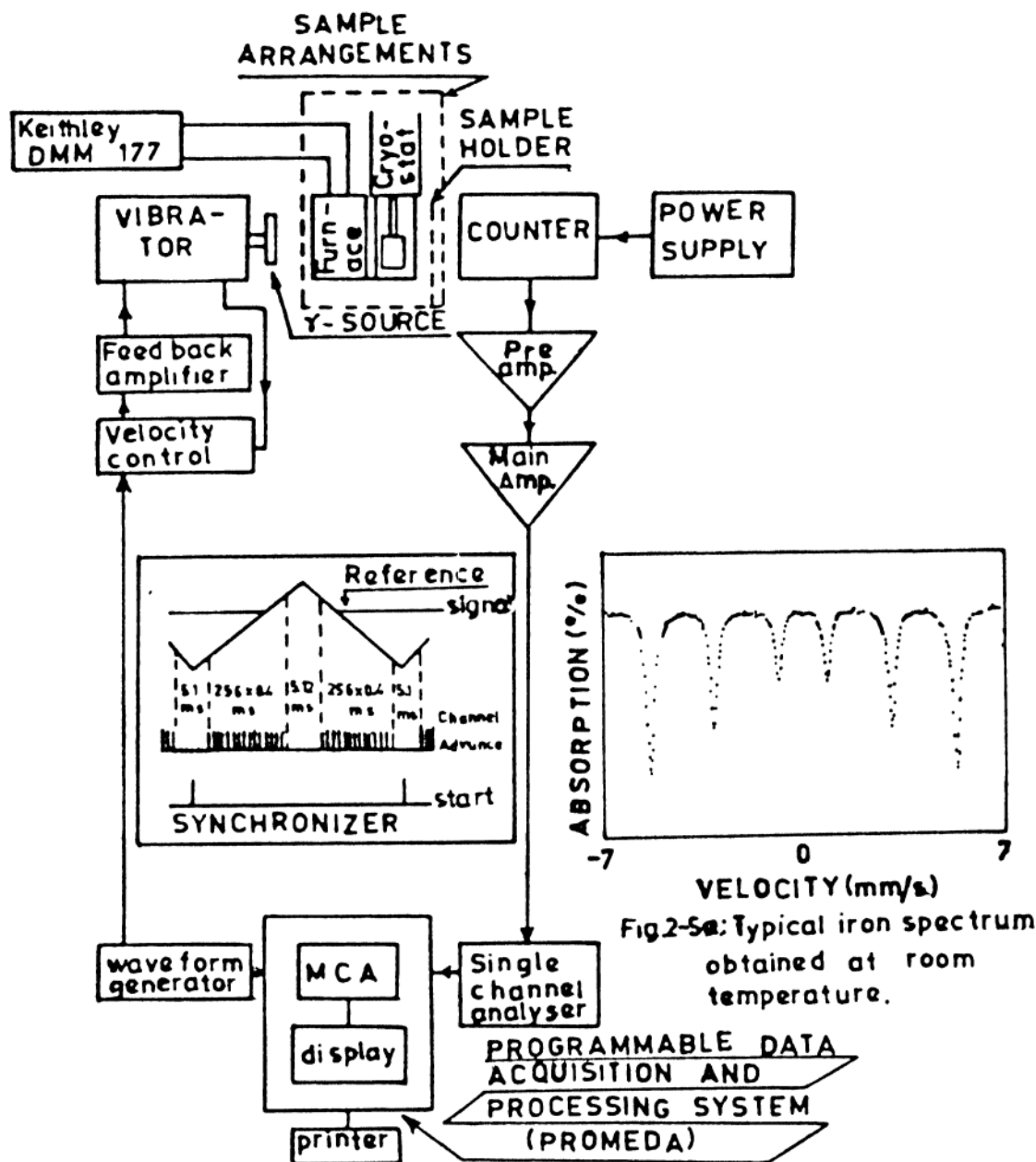


Fig2-5a: Typical iron spectrum obtained at room temperature.

Fig. 2-5 : Block diagram of Mossbauer spectrometer (elscint).

motion to control the channel sweep which gives the velocity interval same to the each channel.

For room temperature Mössbauer measurements the sample is sandwiched between two copper rings of about 2 cms outer diameter. The effective diameter of the absorber is limited to only 1.5 to 1 cm. A cryostat equipped with a cold finger copper sample holder is used for measurements below room temperature. The schematic diagram of the low temperature cryostat is as shown in Figure 2-6.

The velocity scale is calibrated using α -Fe spectra (foil $\sim 10 \mu\text{m}$ thick) collected at room temperature. A typical room temperature spectrum of α -Fe is shown in Fig. 2-4a. Ideally the full width at half maximum (FWHM) of the six overlapping lorentzian lines of the iron spectrum is given by sum of the absorber Γ_a and emitter Γ_e line widths ($\Gamma_a + \Gamma_e \sim 0.19 \text{ mm/sec}$). The observed average line width of the two inner absorption lines of the six line iron spectrum at room temperature, in our experimental setup is 0.28 mm/sec . Although these conditions are not ideal, they are adequate for the interpretation of the spectra at different temperatures. The parabolic distortion of the spectrum was taken care of by a spectrum folding procedure (Bhanuprasad 1985).

2.3.5 Differential scanning calorimetry (DSC) :

The crystallization studies of all the samples are done using differential scanning calorimetry (DSC). The calorimetric

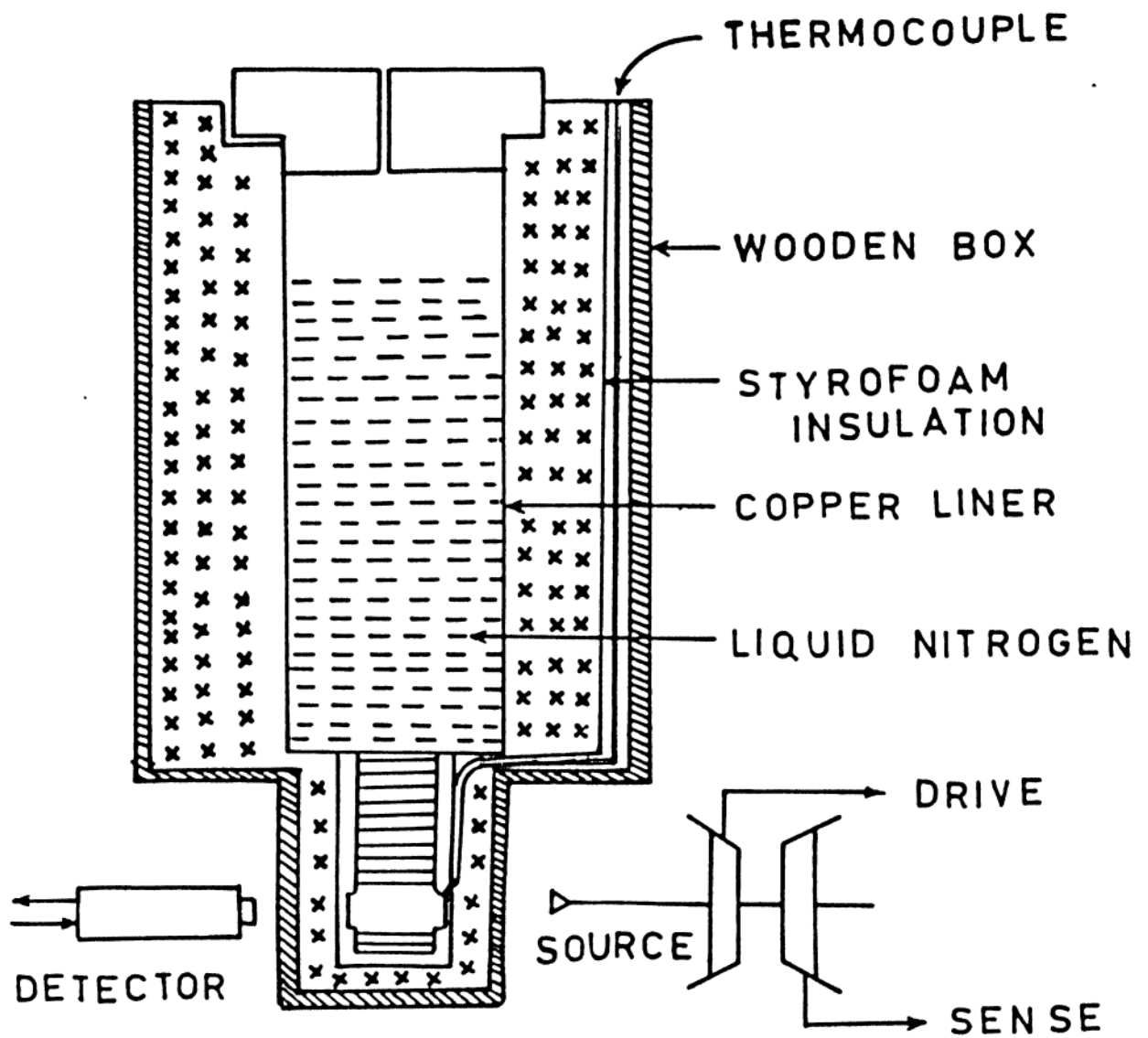


Fig. 2-6 : Styrofoam dewar for low temperature measurements.

measurements are performed using a DUPONT 910 model DSC instrument. A schematic diagram of the instrument is shown in Figure 2-7. The DSC cell employs a constantan disc as its primary means of transforming heat to the sample and reference positions, and as one of the element of the temperature measuring thermoelectric junctions. The sample of interest and a reference are placed in pans which sit on raised platforms on the constantan disc. Heat is transferred through the disc into the sample and reference. The differential heat flow to the sample and reference is monitored by chromel/constantan area thermocouples formed by the junction of the constantan disc and the chromel wafer which covers the underside of each platform. Chromel and alumel wires are connected to the underside of the chromel wafers, and the resultant chromel/alumel thermocouple is used to directly monitor the sample temperature. Constant calorimetric sensitivity is maintained by electronic linearization of the cell-calibration coefficient.

Ideally the heat flow rate in the sample is given by

$$dH/dt = mC_p(dT/dt) \quad 2-4$$

where m is the sample mass, C_p is the sample specific heat per unit mass and dT/dt is the program rate (K/s).

In practice some complications arise mostly because the sample holders are not identical and also because a temperature gradient can develop across the finite thermal resistance between the sample and sample holder. Even then, the physics

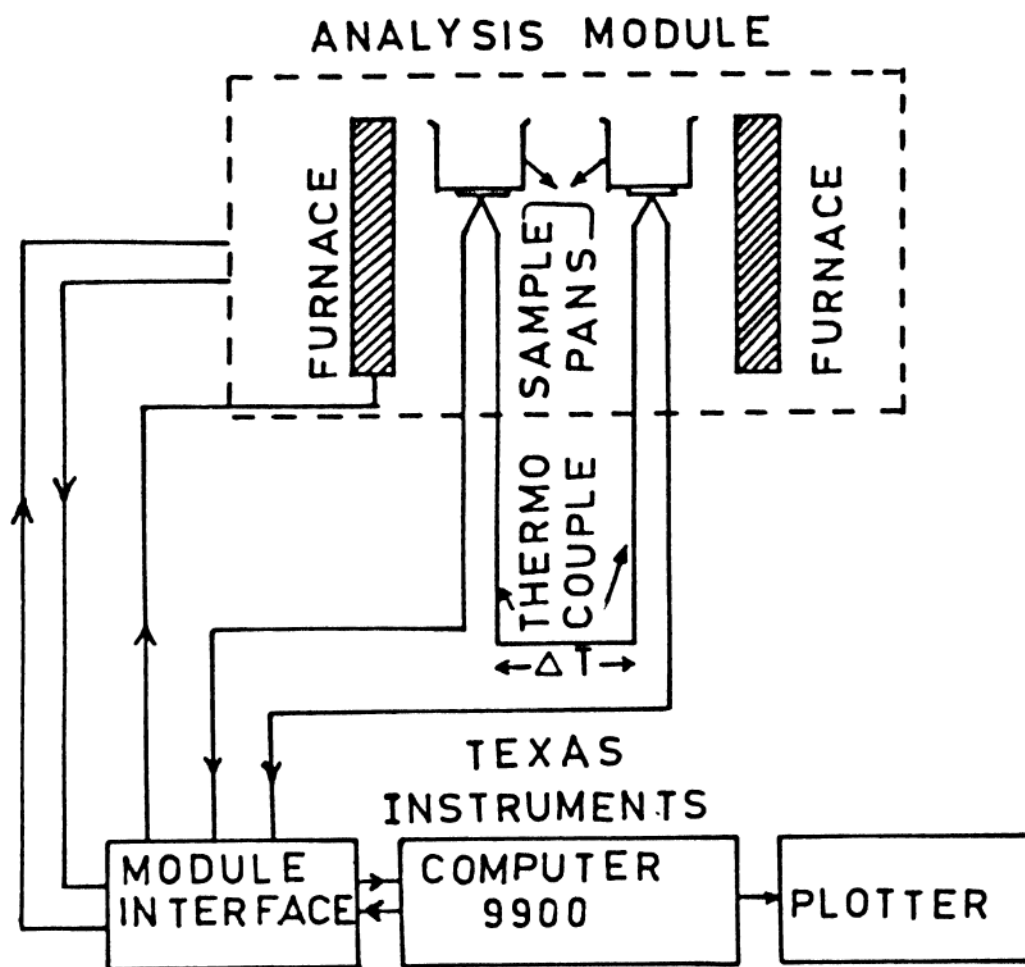


Fig. 2-7 : Schematic diagram of differential scanning calorimetry instrument.

Involved is adequately summarized by the Equation 2-4.

In all the DSC experiments ~ 6 mg of the metallic glass was weighed in aluminium pans using digital balance and empty pans were used as references. Continuous flow of dry argon gas is used throughout the experiment. The measurements were carried out in the temperature range 300 to 925 K with a resolution of ± 0.1 K.

In case of nonisothermal runs the sample usually heated with one of the heating rates ranging from 1 to 100 K/min. In isothermal runs, the sample is heated upto the desired temperature with the maximum heating rate (250 K/min) and data is collected with time. The most important factor here is that the trial runs have to be performed carefully while selecting the starting temperature for isothermal annealing.

CHAPTER III

RESISTIVITY MEASUREMENTS

CHAPTER III

In this chapter, resistivity measurements of Fe-Co-B-Si and Fe-Ni-Mo-B-Si metallic glasses have been presented and discussed in the temperature ranges 1.5 to 900 K and 4.2 to 900 K, respectively. The presentation of the results are as follows.

Section 3.1 introduces the motivation for studying electrical resistivity, ρ in the present alloys. The general features of temperature dependence of ρ of metallic glasses are listed in section 3.2. Theoretical models such as diffraction model, Mott s-d scattering model, two-level tunneling model, theory of localization etc. are presented in sec. 3.3. Section 3.4 presents the experimental results of amorphous Fe-Co-B-Si and Fe-Ni-Mo-B-Si alloys. The discussion of all the experimental results in the frame work of some theoretical models are presented in section 3.5. This section mainly discusses resistivity minimum temperature, T_{min} , magnetic contribution to electrical resistivity, ρ_{min} , Moolj correlation and Curie and crystallization temperatures. A brief summary of the results is given in section 3.6.

3.1 INTRODUCTION :

Temperature dependence of electrical resistivity, $\rho(T)$ of metallic glasses has been the subject of interest for both theoreticians and experimentalists over the years. Many important physical mechanisms such as low temperature resistivity anomaly,

magnetic contribution to electrical resistivity etc. are yet to be generalized using suitable theoretical models. Efforts have been made to explain ρ_{min} by invoking Kondo effect, amorphous structure and quantum corrections to the resistivity in disordered materials (Hasegawa and Tsuei 1970, Cochrane et al 1975, Grest and Nagel 1979, Abrahams et al 1979 and Al'tshuler et al 1979). However, no theory seems to explain the general behaviour of low temperature resistivity anomaly in metallic glasses.

In general, ρ of metallic glasses is dominated by structural relaxation (100-300 $\mu\Omega$ -cms). It has been a common practice to neglect the significant magnetic contribution to ρ in magnetically concentrated metallic glasses. Recently, Kaul et al (1986) have suggested that the magnetic contribution to ρ should not be neglected in case of ferromagnetic metallic glasses. This can be confirmed by separating a small magnetic contribution from a dominant structural contribution to electrical resistivity and evaluating its effect on any physical parameter like Debye temperature by including or avoiding the magnetic term in the calculations. Such a situation, therefore, calls for an elaborate data analysis, which we have studied in amorphous Fe-Co-B-Si and Fe-Ni-Mo-B-Si alloys.

Although main emphasis is placed on the T_{min} and ρ_{mag} , considerable effort is also made to explain the other physical parameters such as Moolj correlation and Curie and crystallization temperatures.

3.2 TEMPERATURE DEPENDENCE OF ELECTRICAL RESISTIVITY :

A typical temperature dependence of resistivity of an amorphous alloy has the following common features:

(i) Metallic glasses have much more higher residual resistivities than those of their crystalline counter parts since the scattering from structural disorder is the dominant mechanism.

(ii) Resistivity for amorphous glasses containing ferromagnetic or antiferromagnetic elements (Nagel et al 1982) does not vary monotonically but has a minimum value at a temperature T_{min} in the temperature range 4 to 300 K. Below T_{min} , ρ increases approximately logarithmically with decreasing temperature, a behaviour akin to the Kondo effect (Cochrane et al 1975 and 1977, Tsuei et al 1977 and 1978a).

(iii) The temperature coefficient of resistivity (TCR) of metallic glasses is numerically smaller than that of crystalline metallic systems, and it can be negative, positive or even zero over a wide range of temperatures (Naugle 1984, Mizutani 1983 and 1987).

(iv) The most surprising features are the negative TCR and the resistance minimum in some metallic glasses. Mooij (1973) is the first man to find out the correlation between TCR and ρ . Based on a thorough examination of ρ and TCR of a large number of disordered alloys (mostly crystalline samples with chemical disorder), he found that as the magnitude of ρ increases, TCR

decreases, and becomes negative for samples with $\rho > 150 \mu\Omega\text{-cm}$. This seems to be universal and did not depend upon the constituents (Naugle 1984) of the alloy, or whether the alloy is amorphous/glassy or a disordered crystalline material.

3.3 THEORETICAL MODELS :

A large number of models for the electrical resistivity of metallic glasses have been proposed over the years. The most important among them are diffraction model, Mott s-d scattering model, tunneling model and the theory of localization.

3.3.1 Diffraction model :

The electron transport properties of the amorphous metals are similar to the corresponding liquid metals (Guntherodt et al 1978) have led various workers to use a theoretical model, originally proposed by Ziman (1961) and subsequently developed by Evans et al (1971) to explain a number of peculiarities observed and to include liquid transition metals in the transport properties of metallic glasses. This theory takes in to account the scattering of conduction electrons from the potential of the disordered lattice of a transition-metal system and gives the following expression (Evans et al 1971) for resistivity.

$$\rho \approx (30\pi^3\hbar^3/me^2k_F^2E_F\Omega) \sin^2[\eta_2(E_F)]S_T(2k_F) \quad 3-1$$

where k_F is the Fermi wave vector, E_F is the Fermi energy, Ω is the atomic volume, $\eta_2(E_F)$ is the d-partial-wave phase shift describing the scattering of the conduction electrons by the ion cores which carry a muffin-tin potential centered on each ion position, and $S(2k_F)$ is the structure factor at $k = 2k_F$. The temperature dependence of ρ is mainly determined by $S(2k_F)$, which for a glass made up of Einstein oscillators, behaves as (Sinha 1970, Nagel 1977 and Cote 1977)

$$S_T(k) \approx 1 + [S_E(k) - 1] e^{-2W_k(T)} \quad 3-2$$

where $S_E(k)$ is the equilibrium structure factor and $e^{-2W_k(T)}$ is the Debye-Waller factor with $W_k(T)$, in the Debye approximation, given by (Ziman 1972)

$$W_k(T) = W_k(0) + 4W_k(0) [T/\theta_D]^2 \int_0^{\theta_D/T} \left(\frac{z}{e^z - 1} \right) dz \quad 3-3a$$

where

$$W_k(0) = 3\hbar^2 k^2 / 8Mk_B\theta_D \quad 3-3b$$

M is the atomic mass, k is the wave vector, and k_B is the Boltzmann constant. With the aid of Equations 3-1 and 3-2 the ρ as a function of T can be written as (Nagel 1977)

$$\rho_{str}(T) = [30\pi^3 \hbar^3 / m e^2 k_F^2 E_F \Omega] \sin^2[\eta_2(E_F)] \cdot [1 + (S_0(2k_F) - 1)] e^{-2[W_{2k_F}(T) - W_{2k_F}(0)]} \quad 3-4$$

ρ_{str} is the structural contribution to ρ and the parameters $W_{2k}(T)$ and $W_{2k}(0)$ appearing in Equation 3-4 denote the $W_k(T)$ and $W_k(0)$ at $k = 2k_F$, i.e.,

$$W_k(0) = W_{2k_F}(0) = [3\hbar^2 k_F^2 / 2Mk_B \theta_D] \quad 3-5$$

substituting $W_k(0)$ in Equations 3-3a and 3-3b and dropping the subscripts for the sake of simplicity, the temperature coefficient of resistivity (TCR) can be calculated from Eq. 3-4

$$\begin{aligned} \alpha &= (1/\rho)[d\rho/dT] = 2[(1-S_T(2k_F))/S_T(2k_F)] dW(T)/dT \\ &= 8[(1-S_T(2k_F))/S_T(2k_F)] W(0)/T \end{aligned}$$

$$[2(\frac{T}{\theta_D})^2 \int_0^{\theta_D/T} (\frac{z}{e^z - 1}) dz - (\frac{1}{e^{\theta_D/T} - 1})] \quad 3-6$$

Equation 3-6 demonstrates that $dW(T)/dT > 0$ at all temperatures and as such α is negative if $S_T(2k_F) > 1$ and positive if $S_T(2k_F) < 1$. Alternatively, a negative TCR is expected only when $2k_F$ lies in the vicinity of k_p , the k value corresponding to the first peak of $S(k)$; otherwise a positive TCR is expected. In low and high temperature limits, Eqn. 3-3a reduces to

$$W(T) \simeq W(0) + 4W(0) (\pi^2/6) [T/\theta_D]^2, \quad T \ll \theta_D \quad 3-7a$$

$$W(T) \simeq 4W(0) [T/\theta_D], \quad T \geq \theta_D \quad 3-7b$$

Bearing in mind that $W(0) \ll 1$, Eqs. 3-4 and 3-7 can be combined and the exponential function in the modified version of Equation 3-4 expanded in power series to yield the asymptotic temperature dependence of ρ . Also, in order to facilitate the direct comparison between theory and experiment, a different form of Eqn. 3-4 has been used as

$$r(T) = \rho(T)/\rho(T_0) = a_1 + a_2 e^{-2[W(T) - W(0)]} \quad 3-8a$$

$$r(T) = a_1 + a_2 \{-8W(0) [T/\theta_D]^2 \int_0^{\theta_D/T} \frac{z}{(e^z - 1)} dz\} \quad 3-8b$$

where

$$a_1 = \{1 + [S_0(2k_F) - 1] e^{-2(W(T) - W(0))}\}^{-1} \quad 3-9a$$

$$a_2 = a_1 [S_0(2k_F) - 1] \quad 3-9b$$

or

$$S_0(2k_F) = 1 + a_2/a_1 \quad 3-10$$

T_0 is 273.15 K is the ice temperature. From the Equations 3-7a and 3-7b one can also see that

$$\rho(T) \propto T^2, \quad T \ll \theta_D$$

$$\rho(T) \propto T, \quad T \geq \theta_D$$

One can also estimate θ_D for a given glass from the above relations, since

$$\alpha = (1/\rho_{RT})(d\rho/dT) = L/\theta_D, \quad T \geq \theta_D \quad 3-11$$

$$s = (1/\rho_{RT})(d\rho/dT^2) = \pi^2/6(L/\theta_D), \quad T \ll \theta_D \quad 3-12$$

Where L is a constant. From the above two equations one can obtain

$$\theta_D = (\pi^2/6)(\alpha/s) \quad 3-13$$

Thus the Ziman theory is able to predict the following :

$$\begin{aligned} (i) \quad \rho &\propto T^2, & T &\ll \theta_D \\ \rho &\propto T, & T &\geq \theta_D \end{aligned}$$

(ii) negative or positive TCR depending upon the relative positions of $2k_F$ and k_p

(iii) numerical values of ρ and TCR of some alloys where partial structure factors are available (Waseda 1978)

(iv) the change in $\rho(RT)$ but not in TCR due to relaxation (Lin 1979).

3.3.2 The Mott s-d scattering model :

In case of transition metal alloys the electrical resistivity, ρ is composed of two parts ($\rho = \rho_s + \rho_d$), where ρ_s is the contribution from the sp-band and ρ_d is from the d-band. General assumption is that the effective mass of the d-electrons is too large for them to contribute significantly to the conduction process (Naugle 1984).

Mott s-d scattering assumes that the more mobile s or p carriers are strongly scattered into less mobile d-holes at the Fermi surface (Mott 1972). Since the number of d-holes is proportional to the density of states at the Fermi energy, the electrical resistivity will be given by $\rho \propto \{N_d(E_F)/N_0(E_F)\}$. Brown et al (1979) used a muffin-tin model to obtain the following approximate expression.

$$\rho_{\text{mott}} \propto N_d(E_F)$$

3-14

Brouers et al (1975) have suggested that $N_d(E)$ does depend on temperature and there exist a significant smearing out of $N_d(E)$ with increasing temperature. When E_F is close to a maximum in $N_d(E)$, the ρ is high and thermal smearing causes $N_d(E_F)$ and ρ to decrease with increasing temperature. When E_F is far from a maximum in $N_d(E_F)$ the resistivity is low and the smearing causes $N_d(E_F)$ and ρ to increase with increasing temperature. Both these effects produce negative TCR when E_F is close to maximum in $N_d(E)$ and TCR becomes positive as $[\partial(\ln N_d)/\partial E]^2_{E_F}$ and $N_d(E_F)$ are decreased.

Mott has stressed that this model is valid only when there is a significant difference in mobilities of s and d electrons. This model may break down for very-high-resistivity materials where all mobilities are very low.

3.3.3 Two-level tunneling model:

This theory proposes the existence of quantum mechanical two level tunneling states for some of the atoms in a disordered solid. This model is similar to the model proposed by Anderson et al (1972) and Phillips (1972) in insulating glasses. Cochrane et al (1975) used this model to explain low-temperature minimum found in some metallic glasses, which resembles the minimum seen in the crystalline Kondo systems. They calculated a term in ρ of the form $-C \ln(T^2 + \Delta^2)$, where $2k_B \Delta$ is the energy splitting between the tunneling states. The one half of the energy difference between the two levels is ≈ 1 K. Thus the effect is more pronounced at low temperatures.

Tsuei (1978) has suggested that the Hamiltonian for electrons scattering from the localized excitations arising from these tunneling states is assumed to be identical with the Kondo Hamiltonian which can give rise to a resistivity minimum and a negative TCR over a wide temperature range in high resistivity metals. He found a better fit to $\rho(T) = \rho(0) - C \ln(T^2 + \Delta^2)$ than with Ziman theory's linear decrease in resistivity with temperature at higher temperatures.

3.3.4 The theory of localization :

Jonson et al (1979) have used the theory of localization to explain the Moolj correlation of TCR to ρ on very general

grounds. They assumed the short electronic mean free path (strong scattering) as it is in the metallic glasses. At low temperatures phonons scatter electrons and thereby ρ increases with increasing T . In high-resistivity materials the adiabatic approximation breaks down and the phonon dynamics must be included in any picture of the conduction. The effect of phonons when the electron mean free path is very short is to increase the mobility of the conduction electrons. The Moolj correlation follows directly from this model. It is produced by the competition of two effects of phonons: increased scattering due to increased disorder and the increase in mobilities of electrons due to inelastic processes.

Imry (1980) has reached similar conclusions based on the scaling theory of localization. He finds that when the inelastic mean free path is smaller than the coherence length in the extended phase, the resistivity decreases with temperature and is proportional to the inelastic mean free path. The higher the resistivity, the shorter should be the mean free path, so that phonons should become more effective at increasing conduction. Thus a high value of ρ should be associated with a negative value of TCR.

In addition to these models there are several other theories of magnetic origin. The important among them are Kondo approach predicted by Kondo (1967) using perturbation approach, in the second Born-approximation and coherent-exchange scattering model. The Kondo effect is associated with the scattering of

conduction electrons from a local magnetic impurity in an otherwise non-magnetic matrix. This gives rise to a spin-dependent increase in ρ at low temperatures which, coupled with the usual increased scattering by phonons at higher temperatures produces a minimum in the total resistivity of these alloys. The striking resistance rise at low temperatures and its sensitivity to the nature and concentration of the impurity in dilute transition metal-metalloid based amorphous alloys has been associated with the Kondo effect. The coherent-exchange scattering model is proposed by Asomoza et al (1977) in order to explain the unusual resistivity behaviour of rare-earth based amorphous alloys. This model is based on the temperature dependence of spin-spin correlation.

3.4 EXPERIMENTAL RESULTS :

The experimental studies of the electrical resistivity, ρ measurements of $(\text{Fe}_{1-x}\text{Co}_x)_{75}\text{B}_{10}\text{Si}_{15}$ ($0.00 \leq x \leq 0.12$) alloys in the temperature range 1.5 to 900 K and $\text{Fe}_{70}\text{Ni}_{12-x}\text{Mo}_x\text{B}_{16}\text{Si}_2$ ($0 \leq x \leq 3$) alloys in the temperature range 4.2 to 900 K have been carried out, although the whole temperature range has not been necessarily used for all sample measurements. The results have been discussed in the light of diffraction model discussed in section 3.3.1.

3.4.1 Resistivity measurements of Fe-Co-B-Si alloys :

The $(\text{Fe}_{1-x}\text{Co}_x)_{75}\text{B}_{10}\text{Si}_{15}$ alloys have been studied in the temperature range 1.5 to 300 K for compositions $0.00 \leq x \leq 0.08$. Figure 3-1 shows the temperature dependence of $\rho/\rho(300)$ of these glasses. The high temperature studies in the temperature range 80 to 900 K have been performed for the compositions $0.00 \leq x \leq 0.12$. The results are plotted in Figure 3-4 with $\rho/\rho(300)$ on the y-axis and temperature, T on the x-axis. The following observations are made during the measurements.

(i) All the samples show a broad minimum around 20 K. This has been observed by plotting $\Delta\rho/\Delta T$ vs. T in the low temperature region from 1.5 to 300 K ($\Delta\rho$ between the points 1 and 3 in the resistivity vs. temperature plot is given by $\rho_3 - \rho_1$ and ΔT is the corresponding temperature difference between them). The point where the slope in the above mentioned plot becomes zero or nearly zero is taken as the minimum in resistivity, ρ_{\min} and the corresponding temperature as T_{\min} .

(ii) The minimum does not seem to be affected by the addition of Co in small quantities at least till 9 at.% of Co in $\text{Fe}_{75}\text{B}_{10}\text{Si}_{15}$ metallic glass.

(iii) Below T_{\min} a logarithmic behaviour is observed between 3 to 15 K and below 3 K the ρ seems to saturate towards a constant value. The region between 3 to 15 K has been fitted to an equation of the type $Y = A + B \ln T$ where $Y = \rho/\rho(300)$ and the

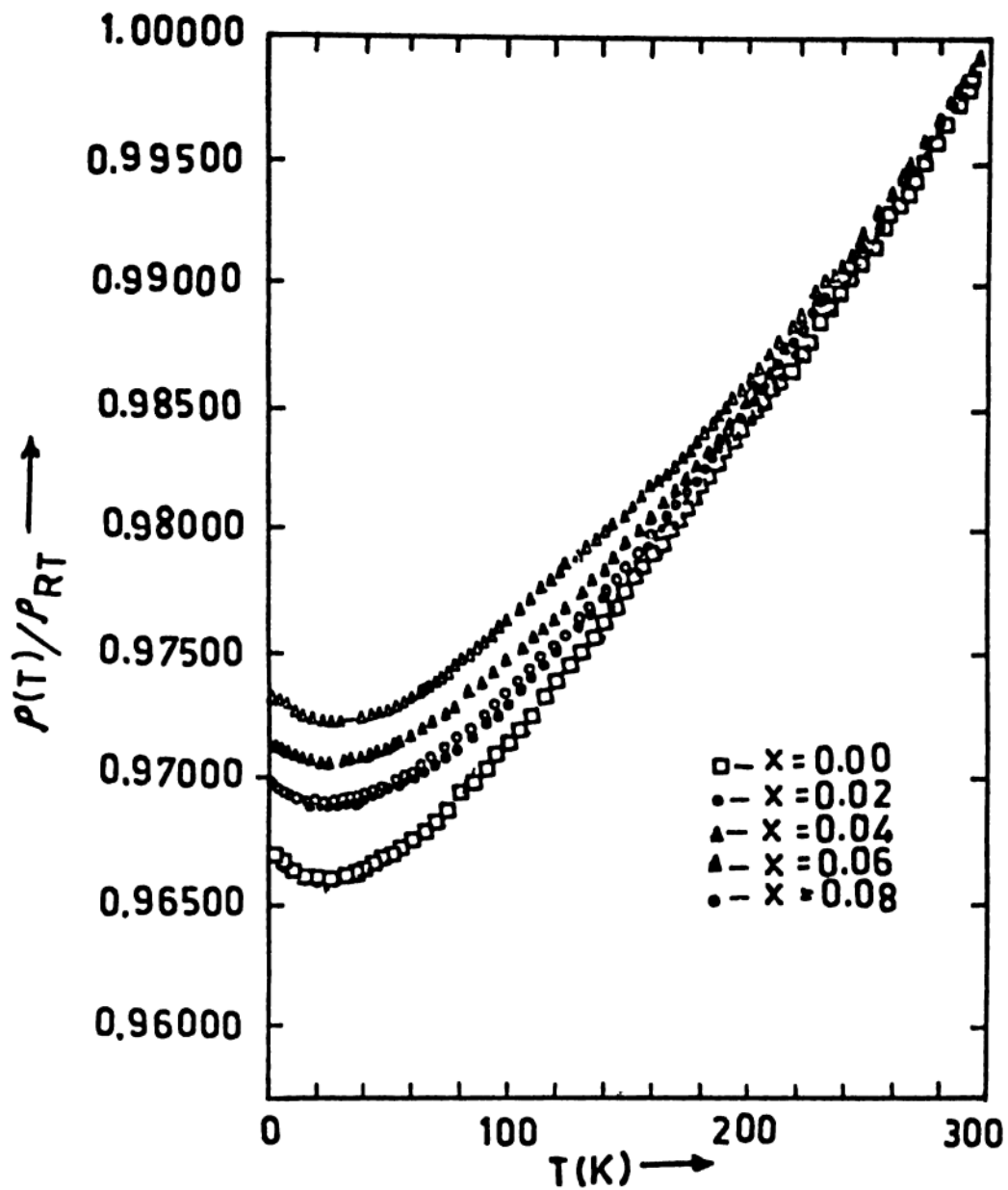


Fig. 3-1 : Temperature dependence of reduced electrical resistivity ratio, $\rho(T)/\rho(RT)$ of amorphous $(\text{Fe}_{1-x}\text{Co}_x)_{75}\text{B}_{10}\text{Si}_{15}$ alloys.

results are tabulated in Table 3-1. The graphs between $\ln T$ and $[(\rho(T) - \rho_{\min})/\rho_{\min}]$ are shown in Figures 3-3a and 3-3b.

(iv) The T^2 behaviour is observed above T_{\min} and upto 100 K. The data in this region is fitted to $Y = C + DT^2$ and the values are tabulated in Table 3-1. Figure 3-2 clearly shows the existence of T^2 dependence. Here $[(\rho(T) - \rho_{\min})/\rho_{\min}]$ is plotted against T^2 .

(v) Above 100 K a parabolic behaviour is observed with a small but not negligible quantity of T^2 term. This region has been fitted to $Y = E + FT + GT^2$ and the values are given in Table 3-1.

(vi) The Debye temperature, θ_D calculated by subtracting an extra T^2 term due to coherent electron-magnon scattering are in very good agreement with the θ_D values of other similar ferromagnetic amorphous alloys. The values of θ_D obtained without neglecting T^2 term due to magnetic contribution yielded much higher values as listed in Table 3-2.

(vii) In the high temperature resistivity measurements and in the temperature region 80 to 400 K, a slight parabolic behaviour is observed. However, the region from 400 to 500 K shows a linear temperature dependence of resistivity. This region has been fitted to an equation $Y = J + KT$ and the values of J and K can be seen in Table 3-1.

(viii) All the samples show double crystallization and the intensity of the second crystallization peak diminishes with the addition of Co. This can be seen clearly in the Figure 3-5b. The

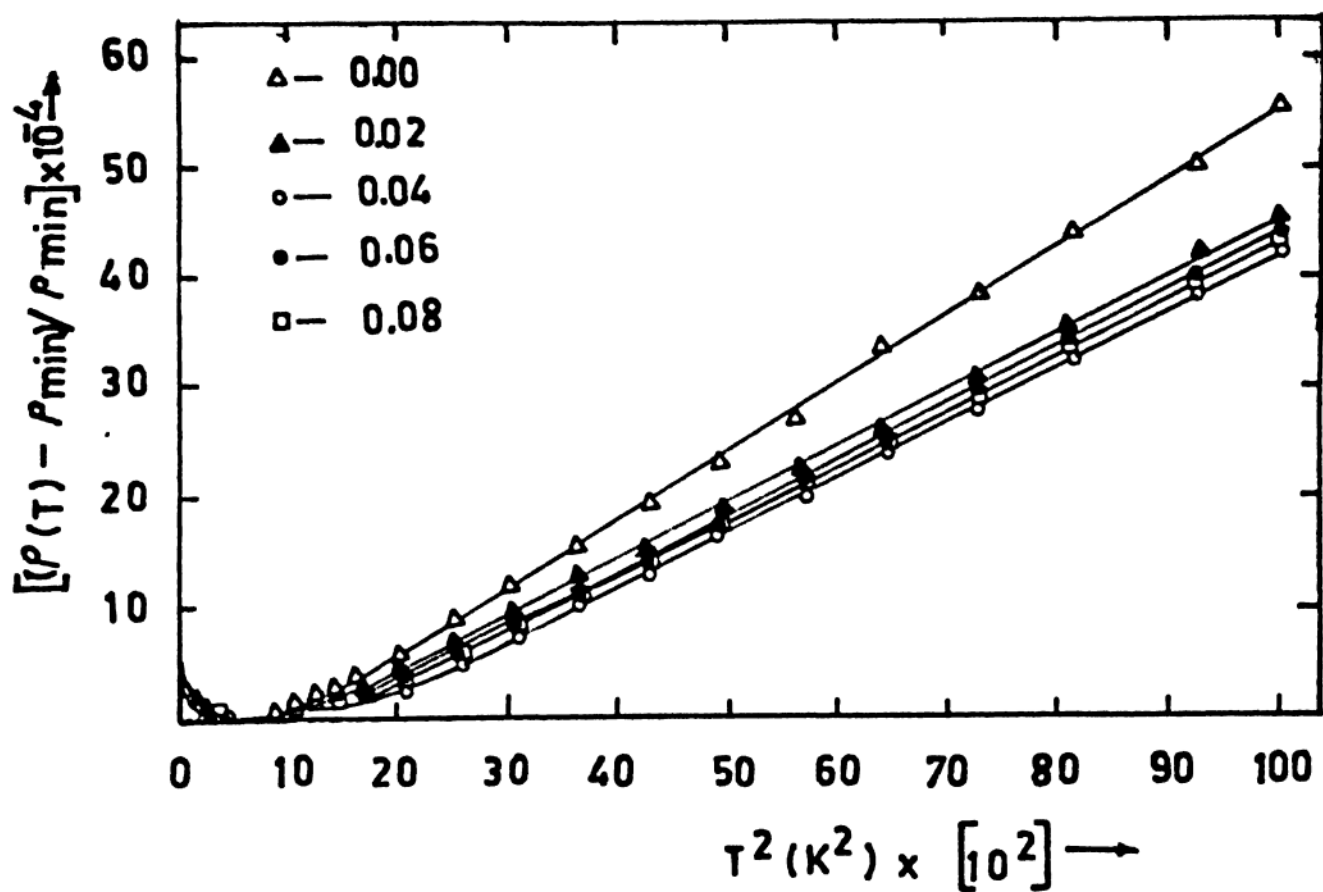


Fig. 3-2 : $[(\rho(T) - \rho_{\min})/\rho_{\min}]$ vs. T^2 of amorphous $(Fe_{1-x}Co_x)_{75}B_{10}Si_{15}$ alloys.

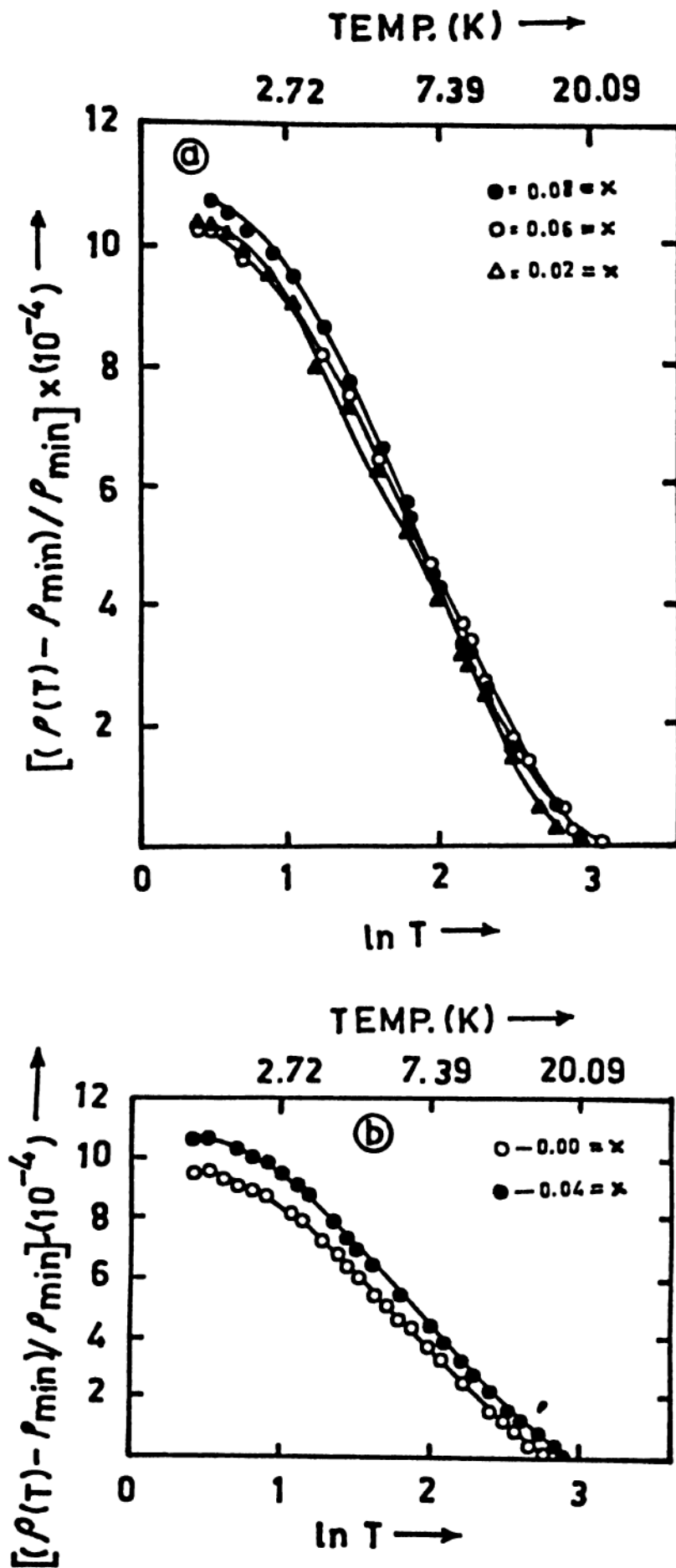


Fig. 3-3 : $[\rho(T) - \rho_{\min}] / \rho_{\min}$ vs. $\ln T$ of amorphous $(\text{Fe}_{1-x}\text{Co}_x)_{75}\text{B}_{10}\text{Si}_{15}$ alloys.

Table 3-1: Details of the low temperature least square fits, based on the equations $Y = A + B \ln T$, $Y = C + DT^2$ and $Y = E + FT + GT^2$ ($Y = \rho(T)/\rho(300)$) of amorphous $(Fe_{1-x}Co_x)_{75}Si_{15}B_{10}$ alloys. The values of the high temperature fits in the region 400 to 500 K is also given from the Eqn. $Y = J + KT$ of these alloys.

x	A	B (10 ⁻⁶) ln K	fit range ΔT(K)	sigma (10 ⁻⁵)	C	D (10 ⁻⁷) (K ⁻²)	fit range ΔT(K)	sigma (10 ⁻⁵)	E (K ⁻¹) (10 ⁻⁵)	F (K ⁻¹) (10 ⁻⁵)	G (K ⁻²) (10 ⁻⁷)	fit range ΔT(K)	sigma (10 ⁻⁶)	J (K ⁻¹) (10 ⁻⁶)	fit range T(K)	sigma (10 ⁻⁶)	
0.00	0.967	-4.68	3-15	1.26	0.965	6.10	45-100	6.51	0.962	8.61	1.40	100-300	1.61	0.933	2.15	400-500	1.26
0.02	0.971	-5.03	3-15	1.76	0.969	5.08	45-100	3.56	0.965	6.22	1.78	100-300	0.46	0.945	2.49	400-500	1.44
0.04	0.974	-5.24	3-15	1.78	0.972	3.75	45-100	5.34	0.971	3.38	2.06	100-300	1.20	0.944	1.86	400-500	1.96
0.06	0.972	-4.94	3-15	1.89	0.970	4.35	45-100	5.14	0.968	4.97	1.93	100-300	0.37	0.929	2.28	400-500	1.96
0.08	0.970	-5.20	3-15	0.95	0.968	4.75	45-100	4.57	0.965	6.12	1.83	100-300	0.63	0.929	2.26	400-500	1.49

DSC thermogram (Fig. 3-5a) shows initially a small peak followed by a bigger peak for the crystallization processes in Fe-Co-B-Si glass for $x = 0.02$.

(ix) At T_c , a slight slope change in $\rho/\rho(300)$ vs. T is observed. The values of T_c and crystallization temperatures, T_x s increases with 1.5 at.% of Co to $Fe_{75}B_{10}Si_{15}$ alloy. Further addition in small quantities of cobalt at the steps of 1.5 at.% does not show much increase in these temperatures. All these values are once again conformed by DSC studies and are listed in Table 3-3.

(x) The room temperature coefficient of resistivity, $\alpha(300)$ are positive for all the alloys. The absolute room temperature resistivity, $\rho(300)$ values lie below $150 \mu\Omega\text{-cm}$ s, which is a requisite condition for Moolj correlation. This is described in the forthcoming section.

(xi) The percentage of drop in resistivity during amorphous to crystalline transformation increases with Co addition. For example, for $x = 0$, the percentage of drop in resistivity is 2.3% and it is nearly 7% for $x = 0.12$ in Fe-Co-B-Si alloys.

3.4.2 Resistivity measurements on Fe-Ni-Mo-B-Si alloys :

The resistivity measurements of $Fe_{70}Ni_{12-x}Mo_xB_{16}Si_2$ ($0 \leq x \leq 3$) alloys have been carried out from 4.2 to 900 K. The plot of $\rho/\rho(300)$ vs. T for these alloys is shown in Figure 3-6 in the temperature range 4.2 to 80 K. Figures 3-7 and 3-8 shows the

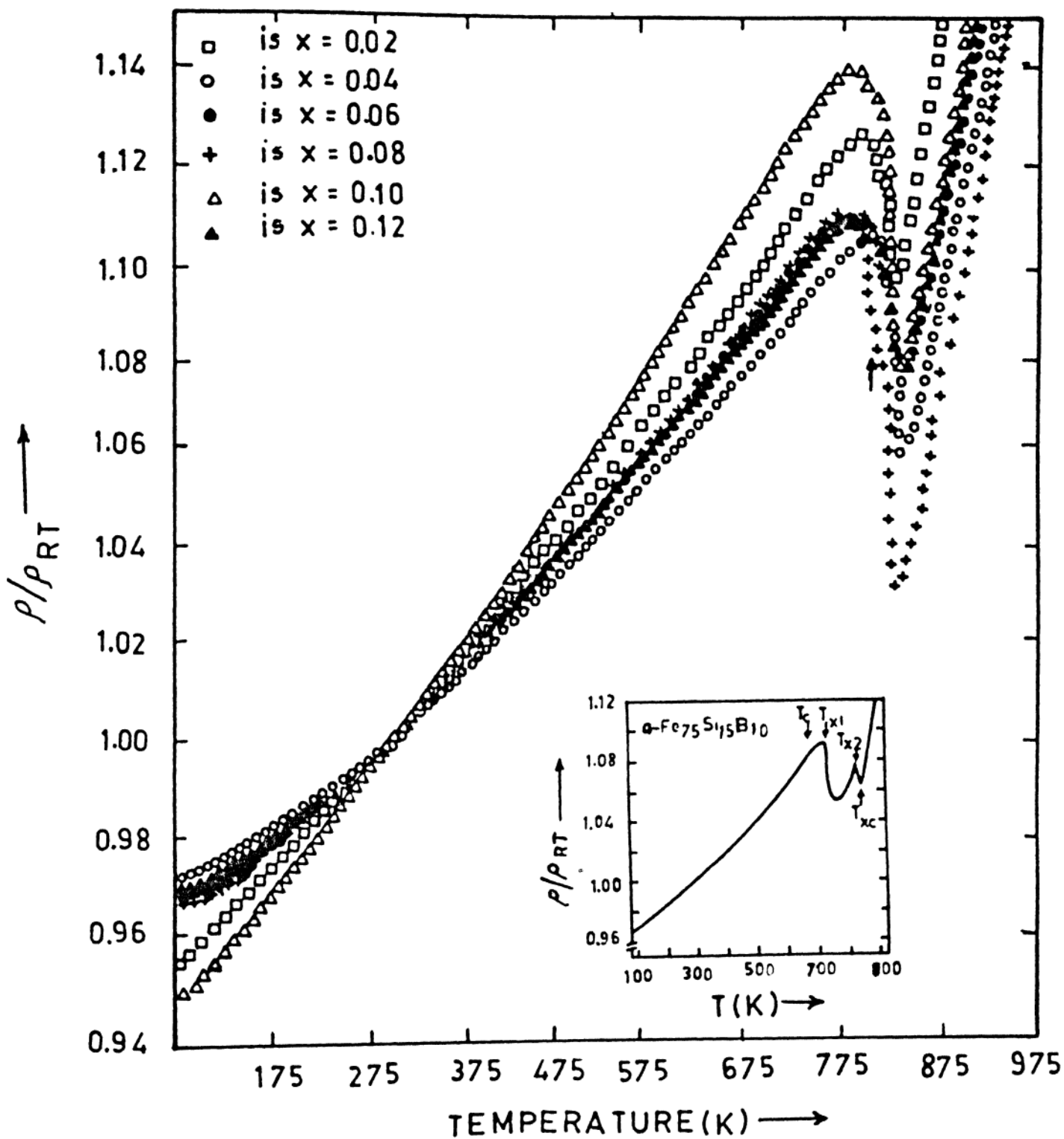


Fig. 3-4 : Resistivity ratio vs. temperature of amorphous $(Fe_{1-x}Co_x)_{75}B_{10}Si_{15}$ alloys.

Table 3-2 : Debye temperature, θ_D calculations in the various temperature ranges of $(\text{Fe}_{1-x}\text{Co}_x)_{75}\text{B}_{10}\text{Si}_{15}$ amorphous alloys and the θ_D values of $\text{Fe}_{80}\text{B}_{20-x}\text{C}_x$ (Kaul et al 1986), $\text{Fe}_x\text{Co}_{80-x}\text{B}_{20}$ alloys (Kettler et al 1982) and $\text{Fe}_{78-x}\text{Co}_x\text{Si}_{10}\text{B}_{12}$ (Kuentzler et al 1985). First three are from resistivity measurements and the last one is from specific heat measurements.

$(\text{Fe}_{1-x}\text{Co}_x)_{75}\text{Si}_{15}\text{B}_{10}$ $\text{Fe}_{80}\text{B}_{20-x}\text{C}_x$ $\text{Fe}_x\text{Co}_{80-x}\text{B}_{20}$ $\text{Fe}_{78}\text{Co}_x\text{Si}_{10}\text{B}_{12}$
(specific heat data)

x	$^*\theta_D(\text{K})$	$^{**}\theta_D(\text{K})$	x	$\theta_D(\text{K})$	x	$\theta_D(\text{K})$	x	$\theta_D(\text{K})$
at. %			at. %		at. %		at. %	
0.00	580	301	0	328	0	284	00.0	288
0.02	806	310	2	331	20	310	15.6	316
0.04	815	329	4	301	40	362	54.6	320
0.06	862	338	10	310	60	371	73.2	202
0.08	783	345	--	---	80	342	78.0	299

$^*\theta_D \simeq (\pi^2/6)(K/D)$ and $^{**}\theta_D \simeq (\pi^2/6)(F/D-G)$

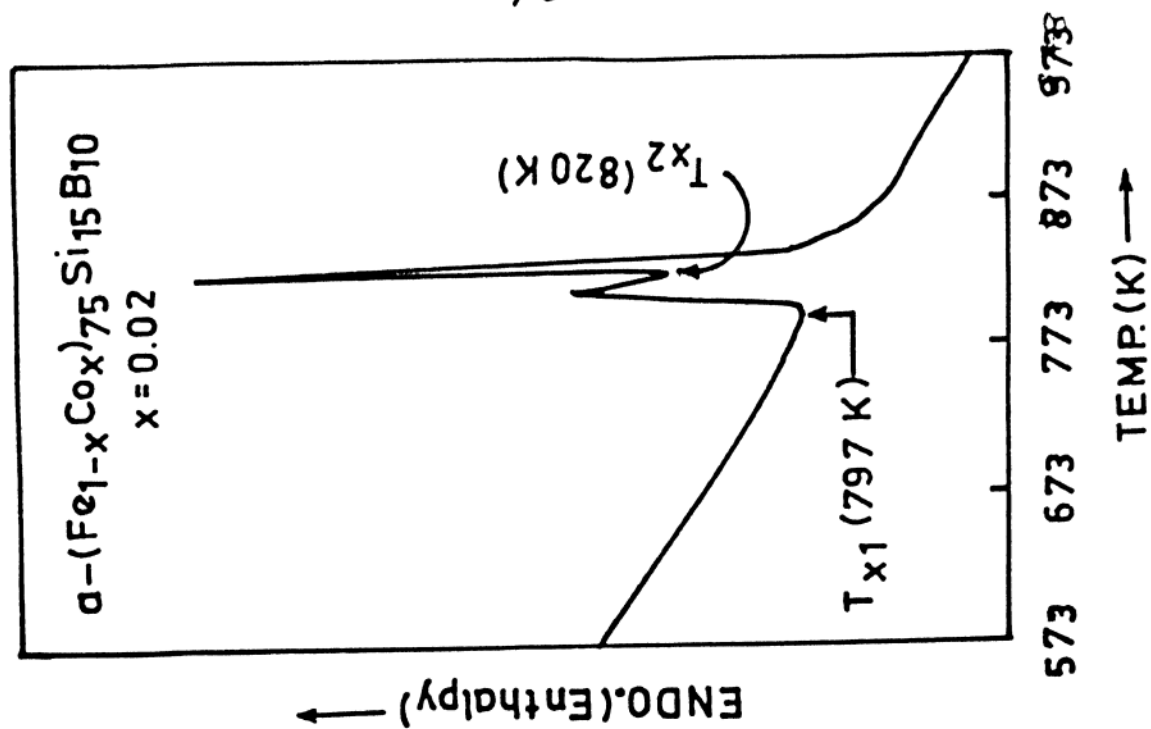


Fig. 3-5a : DSC thermogram of amorphous $\text{Fe}_{73.5}\text{Co}_{1.5}\text{B}_{10}\text{Si}_{15}$ alloy with the heating rate of 10 K/min.

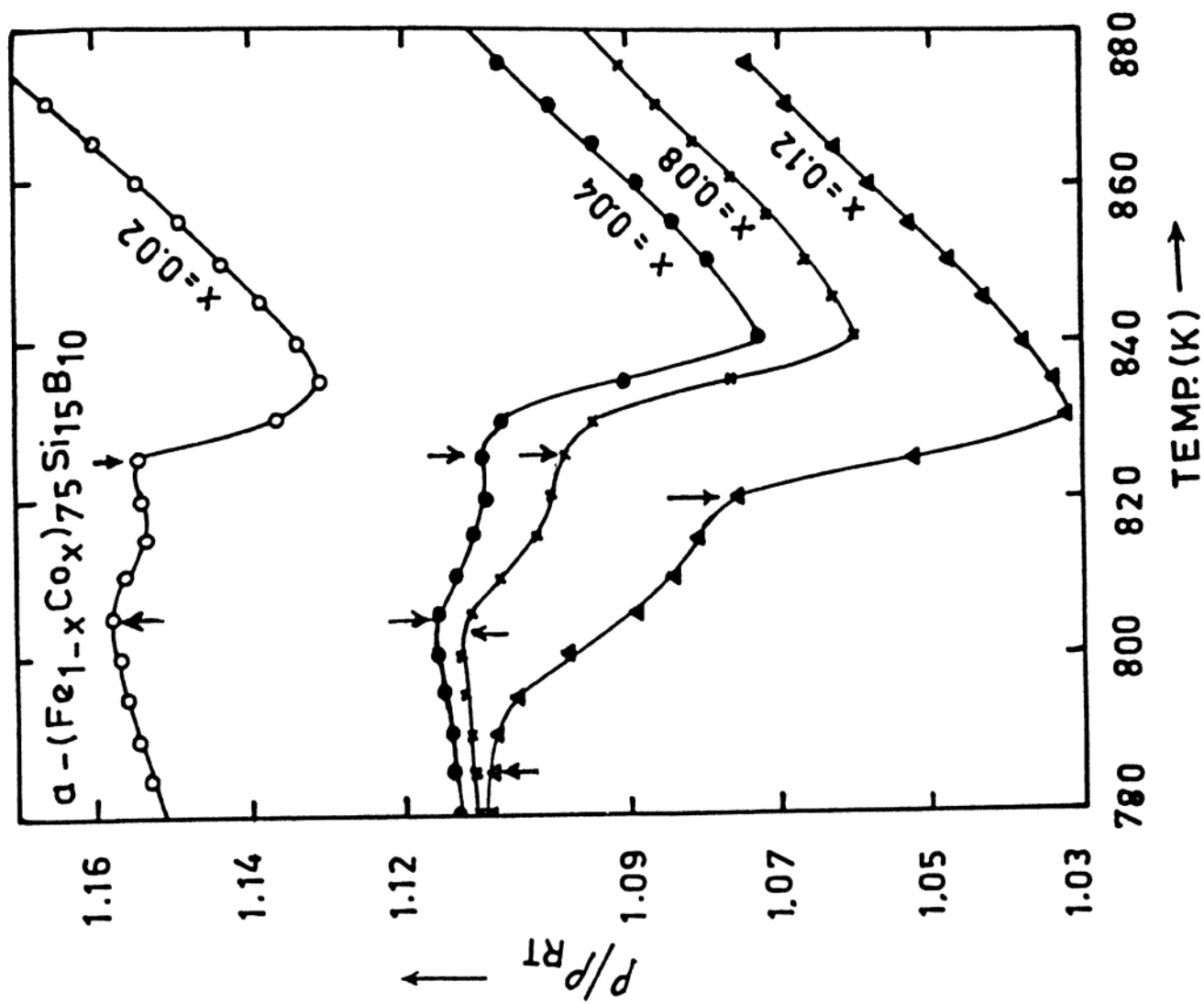


Fig. 3-5b : Resistivity ratio. $\rho(T)/\rho(300)$ vs. T of $\alpha-(\text{Fe}_{1-x}\text{Co}_x)_{75}\text{B}_{10}\text{Si}_{15}$ alloys.

Table 3-3 : Details of high-temperature measurements values of resistivity of $(\text{Fe}_{1-x}\text{Co}_x)_{75}\text{B}_{10}\text{Si}_{15}$ amorphous alloys. T_c = Curie temperature, T_{x1} = Starting point of first crystallization peak, T_{x2} = Starting point of second crystallization peak, T_{xc} = Complete crystallization point, $\alpha(300)$ = Temperature coefficient of resistivity and $\rho(300)$ = Room temperature resistivity. The T_c and T_x values in the brackets are taken from DSC data. The $\rho(300)$ values in brackets are calculated by pressure contacts using platinum wires.

x at.%	T_c (K)	T_{x1} (K)	T_{x2} (K)	T_{xc} (K)	% of drop in ρ	$\rho(300)$ (± 5) $\mu\Omega\text{-cms}$	$\alpha(300)$ ($10^{-4} \times \text{K}^{-1}$)
0.00	690 (683)	715 (712)	825 (820)	840 (835)	2.3	102 (-)	1.3
0.02	760 (712)	795 (797)	815 (820)	830 (835)	2.7	107 (113)	2.2
0.04	750 (717)	813 (802)	833 (814)	848 (838)	2.8	125 (132)	1.8
0.06	760 (723)	805 (800)	825 (822)	840 (838)	3.8	108 (120)	1.9
0.08	755 (729)	800 (800)	815 (817)	830 (841)	4.8	84 (88)	2.0
0.10	755 (738)	785 (791)	815 (821)	830 (838)	5.4	86 (88)	2.6
0.12	760 (739)	785 (791)	815 (820)	830 (832)	7.0	--	1.9

-- data is not sufficient to calculate.

plots of resistivity ratio vs. T of these alloys in the temperature ranges 80 to 300 K and 80 to 900 K, respectively. The experimental observations are listed below.

(i) A broad minimum in resistivity is observed around 11 K for $\text{Fe}_{70}\text{Ni}_{12}\text{B}_{16}\text{Si}_2$ alloy and it increases drastically to 60 K with 3 at.% of Mo addition in this glass.

(ii) Below T_{\min} a logarithmic behaviour of resistivity with temperature is observed as shown in Fig. 3-6a. The data in this region has been fitted to an empirical relation of the form $Y = A + B \ln T$. The values are tabulated in Table 3-4.

(iii) A quadratic temperature dependence of resistivity is observed above T_{\min} and the data in this region has been fitted to an equation of the form $Y = C + DT^2$ and the values are tabulated in Table 3-4.

(iv) The temperature dependence of resistivity ratio shows a slightly parabolic behaviour above 80 K. This region has been fitted to an equation of the form $Y = E + FT + GT^2$ and the values are tabulated in Table 3-4.

(v) At higher temperatures the temperature dependence of resistivity is found to be linear and follows an equation of the type $Y = J + KT$. The values of J and K are presented Table 3-5.

(vi) All the samples show double crystallization indicating a two stage crystallization process.

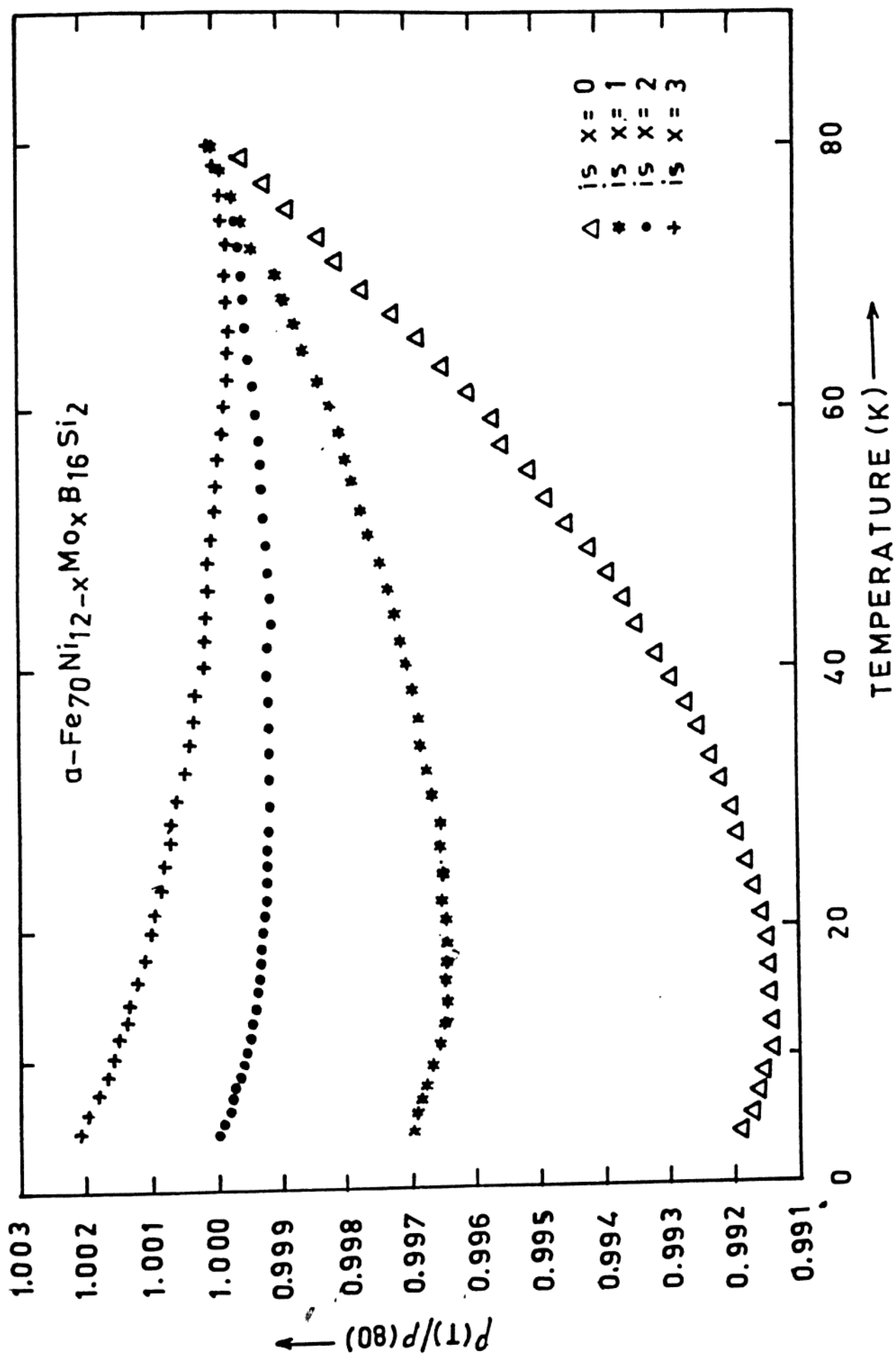


Fig. 3-6 : Resistivity ratio, $\rho(T)/\rho(80)$ vs. T of amorphous $\text{Fe}_{70}\text{Ni}_{12-x}\text{Mo}_x\text{B}_{16}\text{Si}_2$ alloys from 4.2 to 80 K.

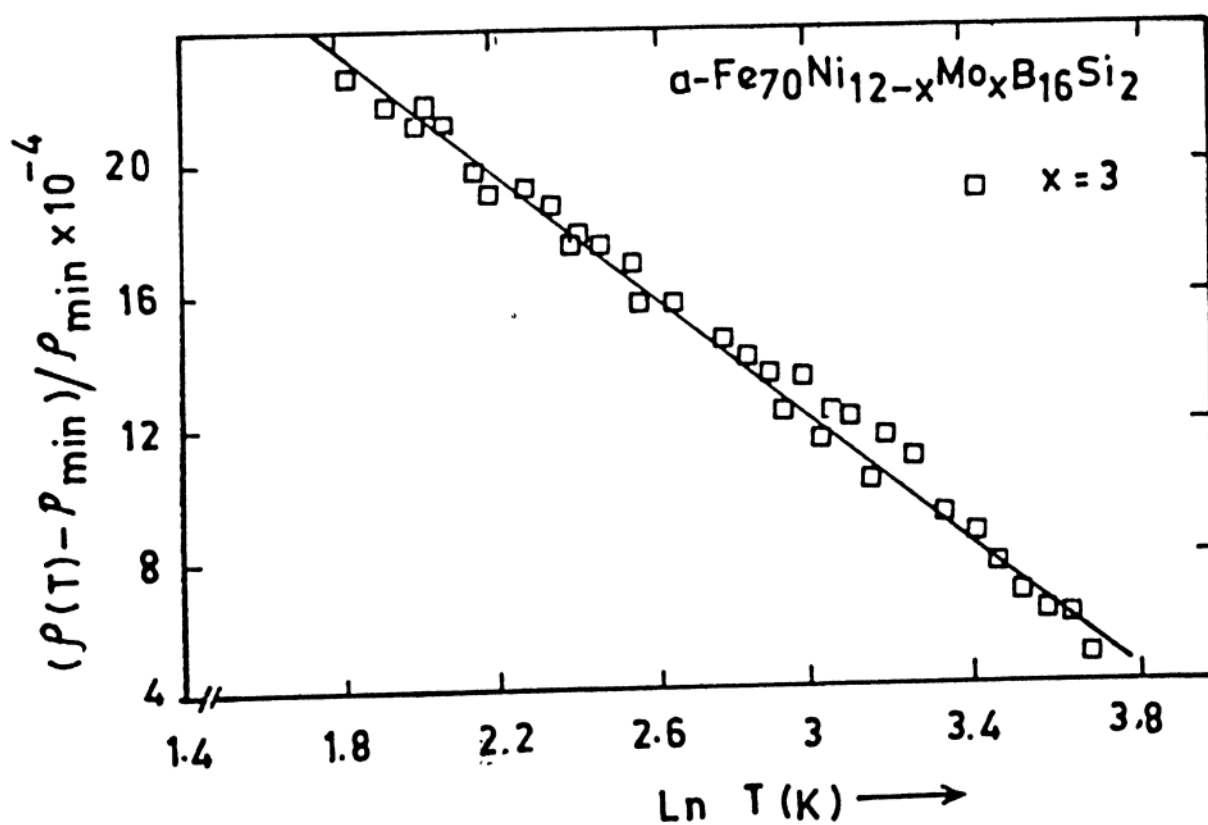
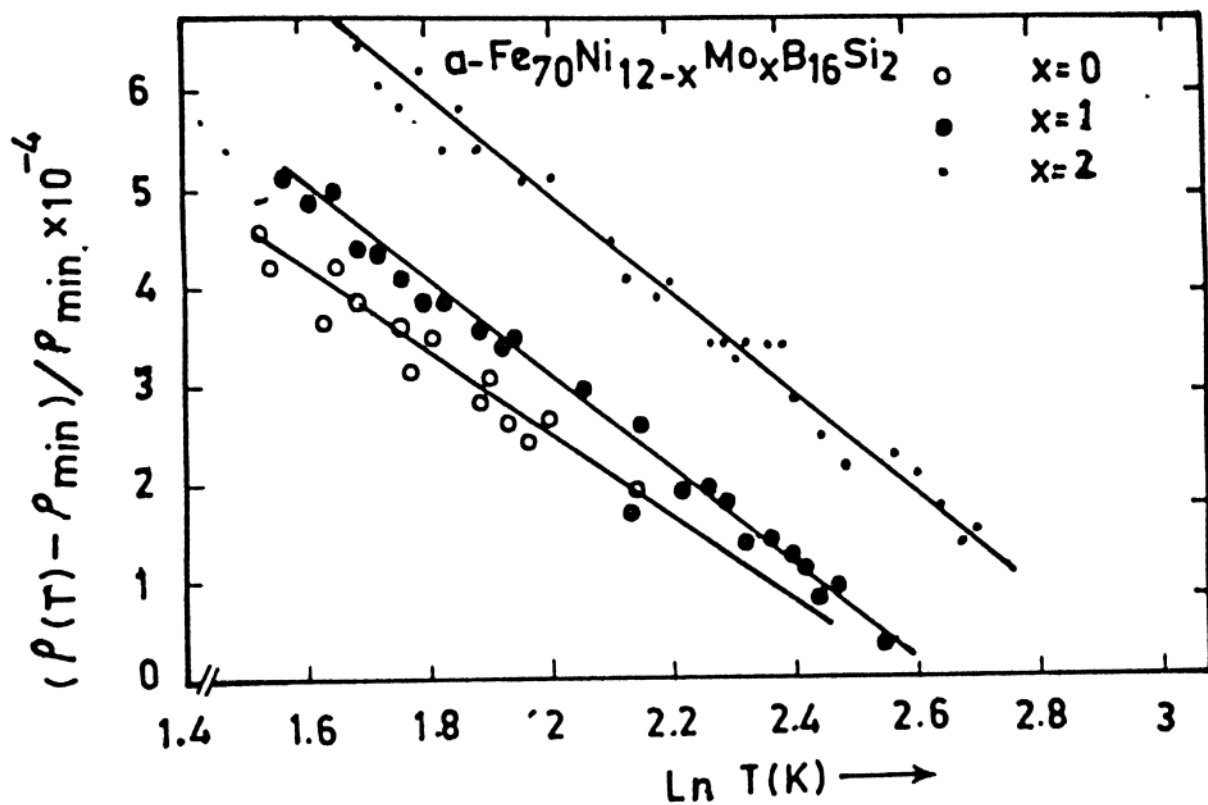


Fig. 3-6a : $[(\rho(T) - \rho_{\min}) / \rho_{\min}]$ vs. $\ln T$ of amorphous $\text{Fe}_{70}\text{Ni}_{12-x}\text{Mo}_x\text{B}_{16}\text{Si}_2$ alloys.

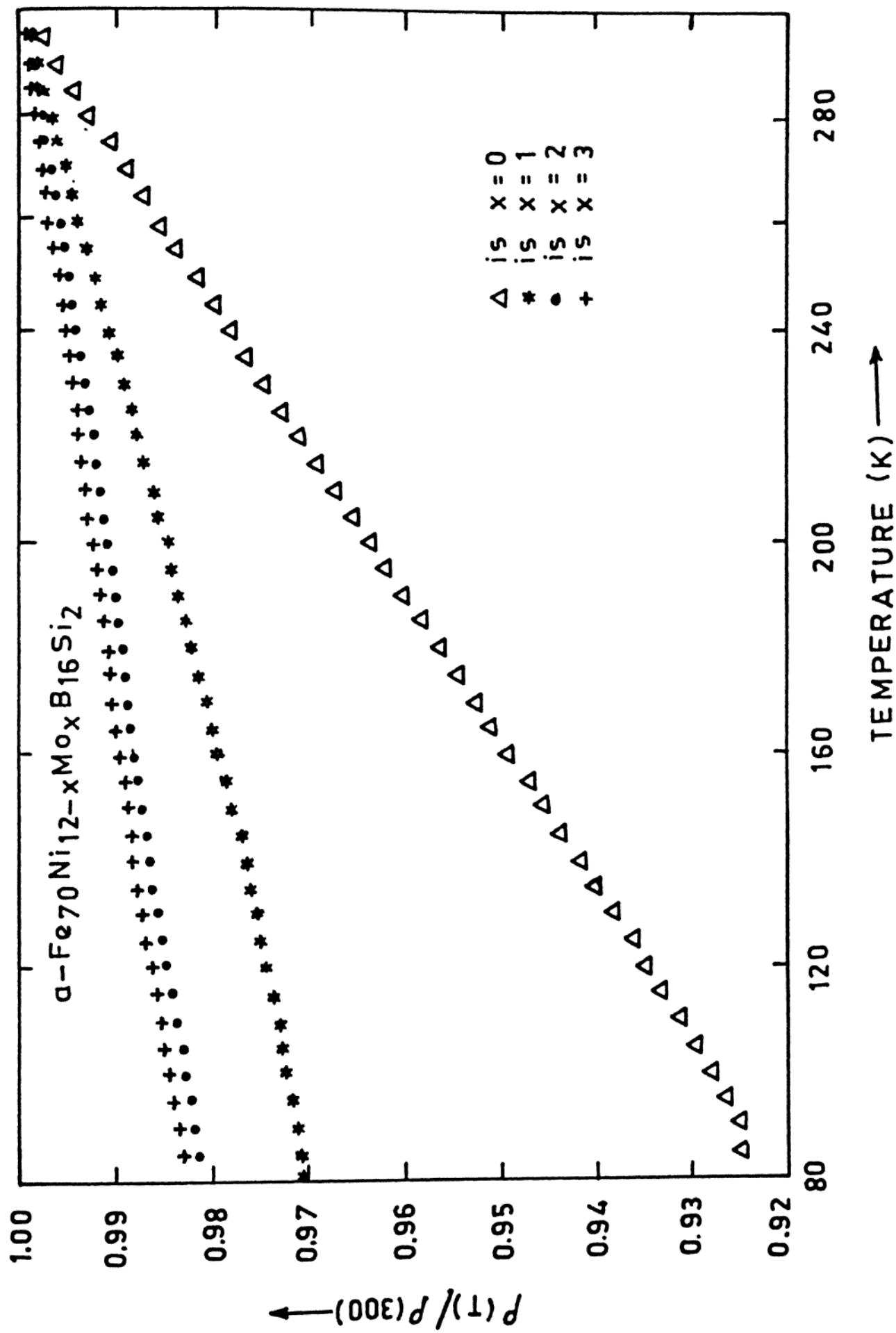


Fig. 3-7 : Resistivity ratio, $\rho(T)/\rho(300)$ vs. T of amorphous $\text{Fe}_{70}\text{Ni}_{12-x}\text{Mo}_x\text{B}_{16}\text{Si}_2$ alloys from 80 to 300 K.

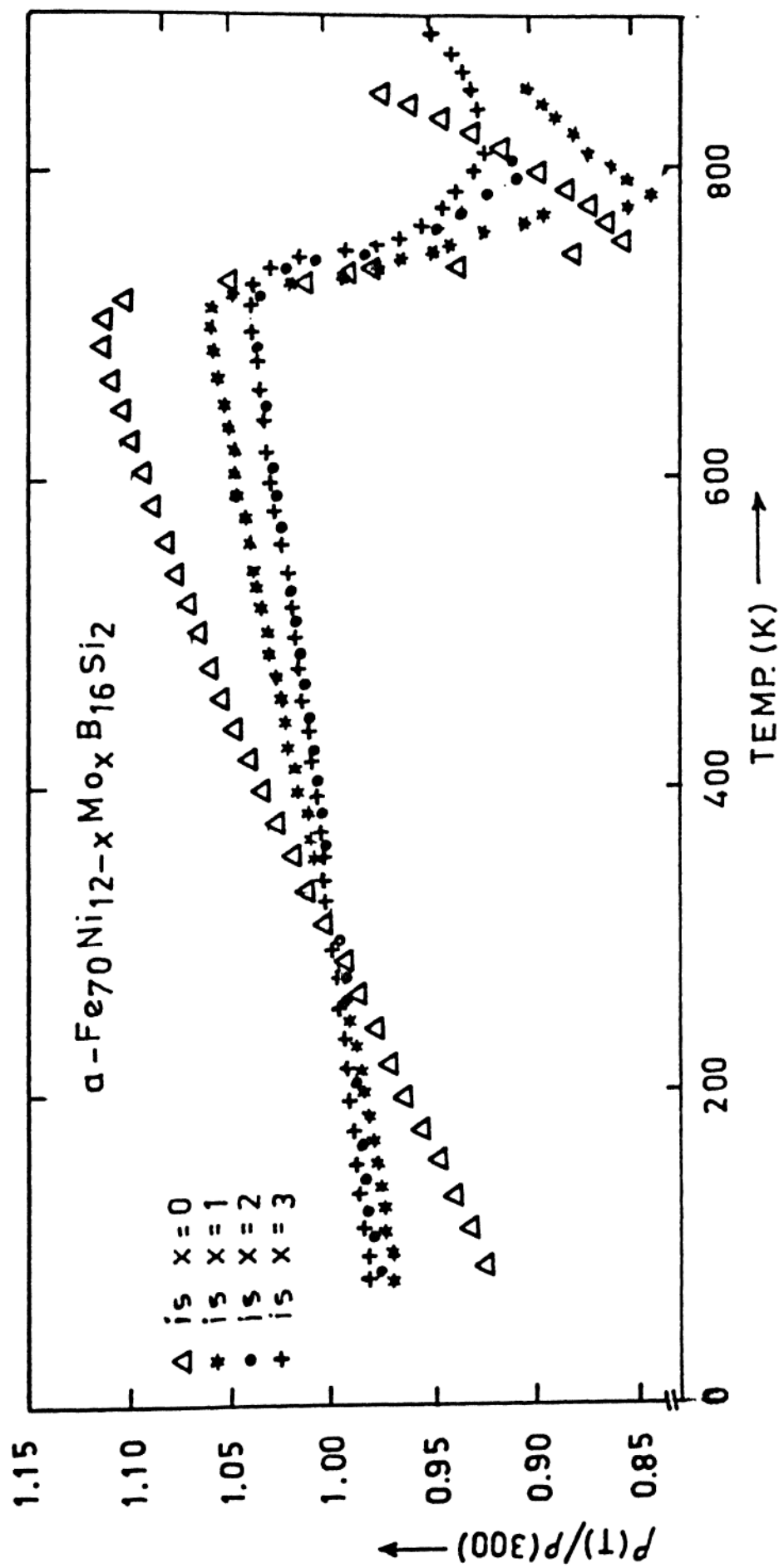


Fig. 3-8 : Resistivity ratio, $\rho(T)/\rho(300)$ vs. T of amorphous $\text{Fe}_{70}\text{Ni}_{12-x}\text{Mo}_x\text{B}_{16}\text{Si}_2$ alloys from 80 to 900 K.

(vii) The percentage of drop in resistivity during amorphous to crystalline transformation decreases with Mo concentration in contrast to Fe-Co-B-Si amorphous alloys where it increases with Co addition. In addition, the percentage of drop in resistivity in these alloys is about one order more than the Fe-Co-B-Si alloys. For example, the drop in resistivity for $\text{Fe}_{70}\text{Ni}_{12}\text{B}_{16}\text{Si}_2$ glass is around 23% and for 3 at.% of Mo addition the drop in resistivity comes down to 11% in Fe-Ni-Mo-B-Si alloys.

(viii) The T_c and T_x s decreases with increase in Mo atomic percent and these values are lower than Fe-Co-B-Si alloys as listed in Table 3-5.

(ix) As $\rho(300)$ increases $\alpha(300)$ decreases. The presence of Mo seems to increase $\rho(300)$ monotonically and the values are given in Table 3-5.

(x) The θ_D values lie between 130 to 255 K and these values are lower than the θ_D values of Fe-Co-B-Si alloys by about 100 K or more.

3.5 DISCUSSION :

3.5.1 Resistivity minimum :

The behaviour of T_{min} varies with the type of the elements that constitute the alloy, their composition and thermal treatment. For instance, in $\text{Fe}_{80}\text{B}_{20-x}\text{C}_x$ alloys (Kaul et al 1986)

Table 3-4: Details of low and high temperature resistivity data fittings for the equations $Y = A + B \ln T$, $Y = C + DT^2$ and $Y = E + DT + FT^2$ of $Fe_{70}Ni_{12-x}Mo_xB_{16}Si_2$ alloys.

x at. %	A	B (10^{-4}) ln K	fit range $\nabla T(K)$	sigma (10^{-5})	C	D (10^{-7}) (K^{-2})	fit range $\nabla T(K)$	sigma (10^{-5})	E	F (10^{-4}) (K^{-1})	G (10^{-8}) (K^{-2})	sigma (10^{-4})
0	0.993	-4.4	4.2-11	5.9	0.991	0.14	20.80	8.6	0.893	3.6	0.29	3.7
1	0.998	-4.6	4.2-16	3.6	0.996	6.25	30-80	5.9	0.961	1.1	7.56	2.8
2.	1.001	-4.5	4.2-25	4.1	0.999	1.60	52-80	3.0	0.981	0.3	9.77	1.9
3	1.000	-8.0	4.2-40	9.7	0.980	4.47	85-130	1.8	0.979	0.5	5.57	5.8

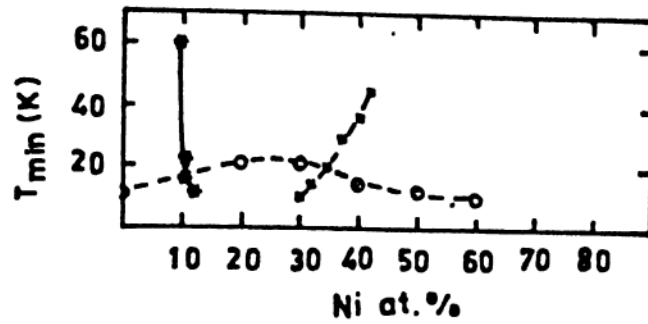
Table 3-5 : Details of high temperature data fit to $Y = J + KT$ (400 to 500 K), Debye temperatures, θ_D , Curie temperatures, T_C , Crystallization temperatures, T_x s, room temperature resistivity, $\rho(300)$ and room temperature coefficient of resistivity, $\alpha(300)$ of $Fe_{70}Ni_{12-x}Mo_xB_{16}Si_2$ alloys. The values in brackets are taken from DSC studies.

x at. %	J	K (10^{-4}) (K^{-1})	sigma (10^{-4})	* θ_D (K)	** θ_D (K)	T_C (K)	T_{x1} (K)	T_{xc} (K)	$\rho(300)$ (K)	$\alpha(300)$ (10^{-4}) (K^{-1})
0	0.910	3.11	3.85	366	255	697	700 (736)	750 (768)	96	3.57
1	0.950	1.65	0.95	437	195	668	705 (745)	780 (786)	138	1.31
2	0.963	1.16	1.58	---	---	627	730 (754)	800 (799)	142	0.60
3	0.960	1.20	2.31	444	130	587	725 (753)	815 (816)	145	0.50

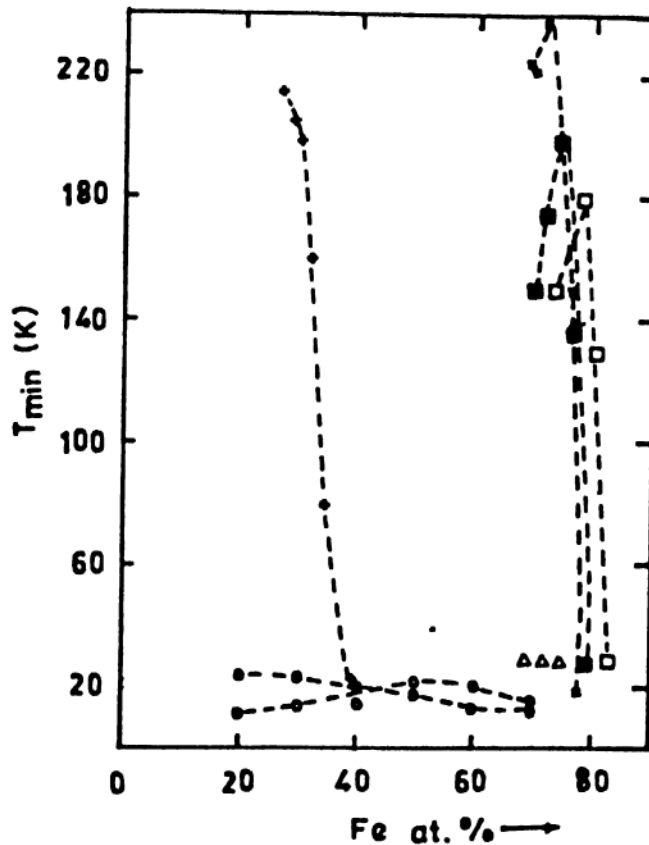
$$*\theta_D \simeq (\pi^2/6)(K/D) \text{ and } **\theta_D \simeq (\pi^2/6)[E/(D-G)]$$

--- data is not sufficient to calculate θ_D value.

T_{min} increases with increasing carbon content. Fig. 3-8a shows the T_{min} vs. Fe at.% and Ni at.% of various metallic glasses. The T_{min} of $Fe_xT_{80-x}B_{20}$ ($T = Co, Ni$) alloys are lying between 10 to 25 K, whereas in Fe-(Cr/W)-B alloys the T_{min} is increasing drastically with increase in Cr or W concentration. Similar observation can be seen in $Fe_{40-x}Ni_{40}Cr_xB_{20}$ alloys (Piotr Czernecki et al 1985). In $Fe_xNi_{80-x}B_{20}$ alloys (Kaul et al 1987) it increases with iron composition till 55 at.% and decreases thereafter. In $Fe_8Ni_{72}P_{10}B_{10}$ (Kadlecova et al 1986) alloys, T_{min} increases by annealing near to crystallization temperature but as the crystallization starts (below T_x) T_{min} decreases which is not an usual behaviour indeed. In $Au_{1-x}Ni_x$ alloys (Yu Mei et al 1986) the minimum in temperature increases with Ni concentration. In $Fe_xCo_{80-x}B_{20}$ alloys (Kettler et al, 1982) the T_{min} decreases with increase in Fe content. However, for $Fe_{80}B_{20}$ ($x = 80$ in the above system) T_{min} increases slightly from 12.5 to 12.8 K where the later is for $Fe_{70}Co_{10}B_{20}$ alloy. This implies that 10 at.% of cobalt does not seem to affect T_{min} much in $Fe_xCo_{80-x}B_{20}$ alloys. In the present study and in $(Fe_{1-x}Co_x)_{75}B_{10}Si_{15}$ alloys, the minimum is around 20 K for all the samples. The changes in T_{min} with Co addition is feeble, if there is any, atleast till 9 at.% of Co substitution. In $Fe_{70}Ni_{12-x}Mo_xB_{16}Si_2$ alloys, T_{min} increases drastically from 11 to 60 K for $x = 0$ to $x = 3$, respectively. In case of the alloy $Fe_{72}Ni_4Mo_6B_{16}Si_2$, where 6 at.% of Mo is added and Fe concentration is increased by 2 at.% at the cost of Ni (when compared to Fe-Ni-Mo-B-Si alloys studied here), the T_{min} is



- $Fe_{70}Ni_{12-x}Mo_xB_{16}Si_2$ (present work)
- $Au_{1-x}Ni_x$ (Yu Mei et al, 1986)
- $Fe_xNi_{80-x}B_{20}$ (Kaul et al, 1987)



- $Fe_{40-x}Ni_{40}Cr_xB_{20}$ (Piotr Czerneck et al, 1985)
- $Fe_xNi_{80-x}B_{20}$ (Kaul et al, 1987)
- $Fe_xCo_{80-x}B_{20}$ (Kettler et al, 1982)
- $(Fe_{1-x}Co_x)_{75}Si_{15}B_{10}$ (Present work)
- $Fe_{80-x}Cr_xB_{12}Si_8$ (Srinivas et al, 1987)
- $(Fe_{1-x}Cr_x)_{84}B_{16}$ and
- $(Fe_{1-x}W_x)_{80}B_{20}$ (Toth et al, 1985)

Fig. 3-8a : T_{min} vs. Fe and Ni at.% for different amorphous alloys.

drastically changing to around 100 K. This minimum could not be accurately determined as the ρ vs. T curve is showing a broad minimum and the resistivity experiment was done only from 80 K due to some experimental limitations. However, it is understood from the overall results that even in the presence of higher concentration of magnetic atoms, a small non magnetic impurity (Mo in the present case) will shift the T_{min} to higher temperatures. The resistivity ratio, $\rho(T)/\rho(300)$ vs. temperature for this alloy is as shown in Fig. 3-8b. The dotted lines in the figure shows the reproducibility of the experimental results. It may be noted here that Mo falls in VIB group of elements of the periodic table where Cr and W are there.

Sas et al (1987) have shown that in case of $Fe_{80}T_3B_{17}$ alloys (where $T = Pd, Pt, Fe, Ni, Rh, Co$ and Cu) the T_{min} does not shift significantly, whereas, for $T = Ir, Mn, Ta, W, Ru, V, Cr, Os$ and Nb , T_{min} is shifted towards higher temperatures. It may be noted by observing the overall results in these alloys that for the elements of the groups VB, VIB and VIIB, that is, for the elements which are located to the left of Iron in the periodic table, T_{min} is shifted towards higher temperatures, whereas for the elements in groups VIII and IB, that is to the right side of Fe, T_{min} do not change significantly. These results agree with the measurements of average magnetic moment and hyperfine field for similar amorphous alloys $(Fe_{1-x}T_x)_{78}B_{12}Si_{10}$ (Kemeny et al 1981). In these works a strong decrease of average hyperfine

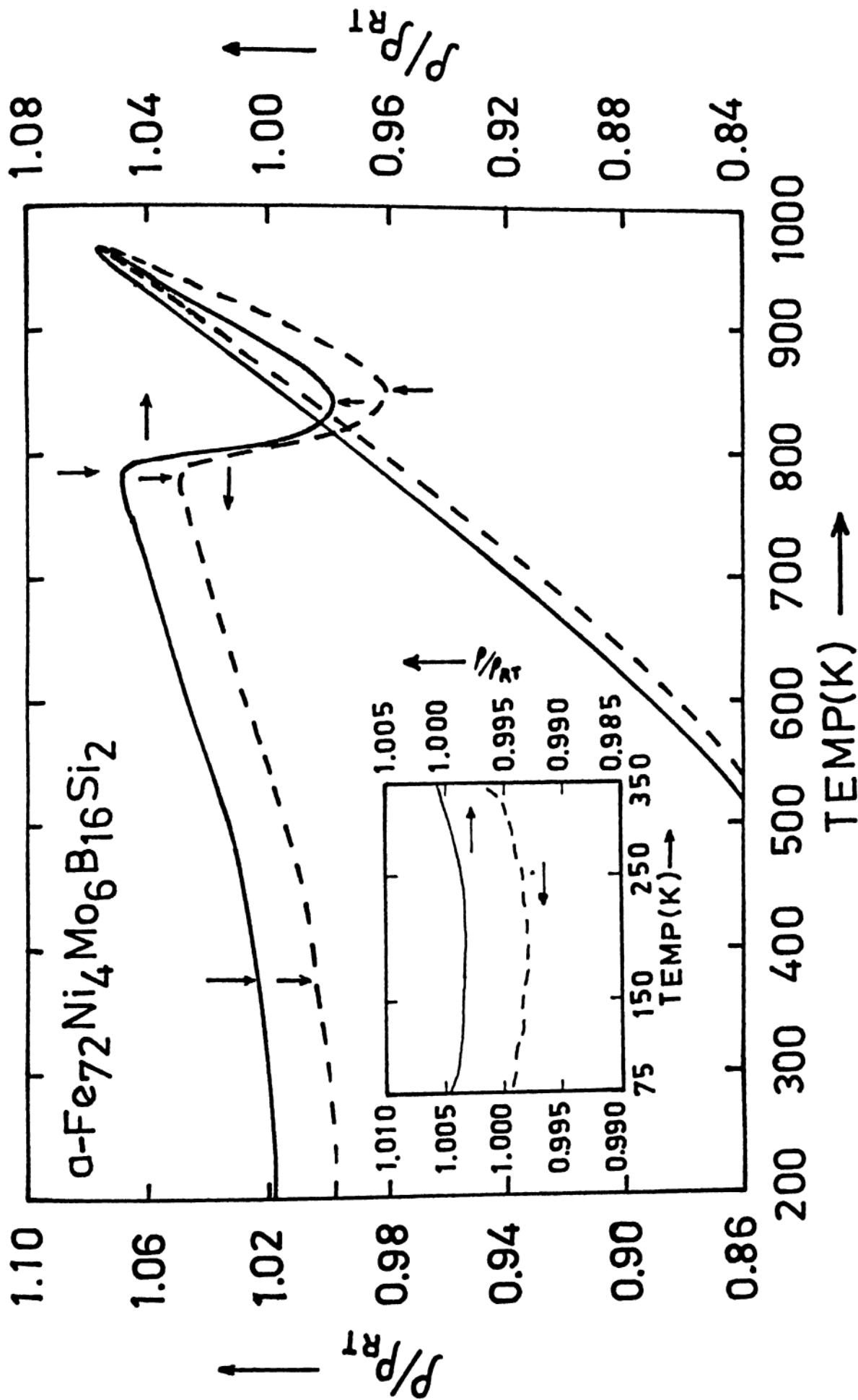


Fig. 3-8b : Resistivity ratio, $\rho/\rho(300)$ vs. temperature of

Fe₇₂Ni₄Mo₆B₁₆Si₂ alloy.

The dotted lines in the figure represents the reproducibility of the results. The insert in the figure shows the low temperature variation of resistivity ratio.

field is observed for the materials where the T_{min} is increasing drastically. In our studies also, it is quite interesting to note that the hyperfine fields of Fe-Co-B-Si alloys are not changing much (Table 5-2), and also the T_{min} . On the other hand in case of Fe-Ni-Mo-B-Si alloys the T_{min} is increasing and hyperfine field is decreasing systematically (Table 5-3) with increase in Mo addition.

It is quite interesting to note that no ρ_{min} is observed in high purity Pd-Si and Pd-Cu-Si glasses (Suryanarayana 1984). However, by the addition of controlled quantities of Co, Fe, Cr and Mn to amorphous $Pd_{80}Si_{20}$ resulted in a ρ_{min} and the T_{min} increased with the magnetic impurity (Tsuei et al 1969 and Hasegawa et al 1970). Thus, the ρ_{min} has been explained on the basis of Kondo type s-d exchange scattering (Tsuei et al 1969). Lin (1969) has showed that there is a connection between the resistivity minimum and the degree of amorphousness of the glass.

Cochrane et al (1975) has observed that $\ln T$ dependence of resistivity is unaltered by an applied magnetic field of 45 KOe and they suggested that the resistivity minimum may not have its origin in the Kondo effect. It may not be due to magnetic impurities alone. They explained the resistivity minimum using two-level tunneling model described in section 3.3.

Philippe Meltreplierre (1970) observed that in pure $Ni_{63}Pd_{17}P_{20}$ alloy where the over all Iron impurity in Pd is about

5 ppm or less, the resistivity minimum is still observed and did not differ much with the observed minimum of less pure alloys. He attributed this puzzling result may be due to the difference in the concentrations of the actual localized moments contributing to the ρ_{\min} and over all Fe concentration. It is likely that the electron transfer occurs between phosphorous and d-band of the magnetic iron atoms. Most iron atoms would then have no localized moments except for a few isolated ones shielded from the electron transfer process. This implies that the Kondo type phenomenon in resistivity does not seem to be directly related to concentration of iron but to localized moments on the iron impurities.

The T_{\min} is not observed in case of non-magnetic alloys like $\text{Ca}_{70}\text{Mg}_{30-x}\text{Al}_x$ (Mizutani 1987) and $\text{Ca}_{1-x}\text{Al}_x$ (Naugle 1984) alloys. The $\ln T$ behaviour at low-temperatures ($< T_{\min}$) and existence of T_{\min} in only the alloys where the magnetic atoms are present can only say that the resistivity minimum is of magnetic origin.

Thus, although a few models can explain the minimum in resistivity in a few samples, no particular model seems to explain the low-temperature resistivity minimum as a general phenomena in amorphous ferromagnets.

3.5.2 Temperature dependence of electrical resistivity :

Evidence of magnetic contribution to the resistivity.

It has been stated that the magnetic contribution to electrical resistivity exist in case of $\text{Fe}_{80}\text{B}_{20-x}\text{C}_x$ alloys (Kaul et al 1986). We made an effort to check the presence of this contribution in case of Fe-Co-B-Si and Fe-Ni-Mo-B-Si alloys for the first time.

Usually, the temperature dependence of resistivity is analyzed using diffraction model (Nagel et al 1977) by taking into consideration the intermediate and high temperature resistivity data and by completely neglecting the magnetic state of the alloy. The reasons for this are two fold. Firstly, in the intermediate and high temperature regions ρ exhibits the same temperature dependence in several magnetic as well as non magnetic glasses. Secondly, the diffraction model yields both quadratic ($T \ll \theta_D$) and linear ($T \geq \theta_D$) temperature dependence of ρ . There are several works where the simple T^2 dependence of resistivity is contradicted for the ferromagnetic alloys at intermediate temperatures (Babic et al 1980 and Kaul et al 1986). A sharp anomaly in the temperature derivative of electrical resistivity at the Curie point reminiscent of critical resistivity behaviour normally found in crystalline ferromagnets has been observed (Bohnke et al 1983) in ferromagnetic glasses. These observations shows that the contribution due to the scattering of conduction electrons from electron-magnon

scattering (which at low temperatures gives rise to a quadratic temperature dependence for crystalline ferromagnetic 3d-transition metals) gives a significant contribution to ρ in magnetic metallic glasses and hence the approach of neglecting the magnetic contribution to resistivity, $\rho_{\text{mag}}(T)$ while analyzing the resistivity data on ferromagnetic alloys may not be correct. Theoretical investigations of Bergmann et al (1978) and Richter et al (1979) which realise the magnetic contribution to the resistivity used spin-wave approximation to calculate $\rho_{\text{mag}}(T)$ for amorphous ferromagnets. This approximation reveal that $\rho_{\text{mag}}(T)$ comprises of two positive contributions; one varying as T^2 , as in crystalline ferromagnets and the other as $T^{3/2}$. The contribution to $\rho_{\text{mag}}(T)$ from $T^{3/2}$ term (which appear only in amorphous alloys) is atleast 2 orders of magnitude greater than the one arising from the T^2 term. Hence, these theories predict a $T^{3/2}$ power law for $\rho(T)$ at low temperatures in amorphous ferromagnets has contrasted with the T^2 dependence found in these materials.

The resistivity exhibits the variation with temperature in both the Fe-Co-B-Si and Fe-Ni-Mo-B-Si systems studied by the following relations.

$$Y(T) = A + B \ln T, \quad T < T_{\text{min}} \quad 3-15$$

$$Y(T) = C + DT^2, \quad T > T_{\text{min}} \quad 3-16$$

$$Y(T) = E + FT + GT^2 \quad 100 \leq T \leq 300 \text{ K} \quad 3-17$$

In view of theoretical results (Ritcher et al 1979) upto the second order in the scattering potential, the Matthiessen's

rule is

$$\rho(T) = \rho_{\text{str}}(T) + \rho_{\text{mag}}(T) \quad 3-18$$

where $\rho_{\text{str}}(T)$ is the structural contribution and $\rho_{\text{mag}}(T)$ is the magnetic contribution to the electrical resistivity. At low temperatures, both $\rho_{\text{mag}}(T)$ and $\rho_{\text{str}}(T)$ follow T^2 power law (Kaul et al 1986). Keeping in view that the structural contribution to electrical resistivity which goes as T^2 at low temperatures and which turns as T dependent at higher temperatures ($T \geq \theta_D$), the extra T^2 term at high temperature fits (i.e., GT^2) can be attributed to the electron-magnon scattering. Comparing the values of D, F and G in the Tables 3-1 and 3-4, it is clear that ρ_{str} dominates ρ_{mag} in the entire temperature range 60 to 300 K and hence the magnetic contribution to resistivity can be missed easily while analyzing the results. Following this argument the terms DT^2 , FT and GT^2 in Equations 3-16 and 3-17 are identified as $[\rho_{\text{str}}(T) + \rho_{\text{mag}}(T)]$, $\rho_{\text{str}}(T)$ and $\rho_{\text{mag}}(T)$ respectively. Now the equation for Debye temperature can be obtained as

$$\theta_D = (\pi^2/6) [F/(D-G)] \quad 3-19$$

The θ_D values calculated from the equation 3-19 of amorphous $(\text{Fe}_{1-x}\text{Co}_x)_{75}\text{B}_{10}\text{Si}_{15}$ ($0.00 \leq x \leq 0.08$) alloys and $\text{Fe}_{70}\text{Ni}_{12-x}\text{Mo}_x\text{B}_{16}\text{Si}_2$ ($0 \leq x \leq 3$) alloys are listed in Tables 3-2 and 3-5 respectively. The θ_D values of Fe-Co-B-Si alloys are compared with the Debye temperature values of $\text{Fe}_{78-x}\text{Co}_x\text{Si}_{10}\text{B}_{12}$ ($0.00 \leq x \leq 78.0$) alloys (Kuentzler et al 1985) and $\text{Fe}_{80}\text{Co}_{20-x}\text{C}_x$ ($0 \leq x \leq 80$) alloys (Kettler et al 1982). The

θ_D values of Fe-Co-B-Si alloys are in reasonably good agreement with the θ_D values of the above mentioned iron-rich metallic glasses as listed in Table 3-4. For further clarification the following exercise has been taken up.

According to diffraction model, linear temperature dependence of resistivity is expected for $T \geq \theta_D$. We have selected the temperature region from 400 to 500 K and the data has been fitted to a linear relation

$$Y(T) = J + KT \quad 3-20$$

which gave rise to a minimum x^2 value and the θ_D values are calculated using the Equation 3-13. The values from this equation yielded much higher θ_D values in both Fe-Co-B-Si and Fe-Ni-Mo-B-Si alloys and the values are listed in Tables 3-2 and 3-5 respectively. The reason for this is that in eqn. 3-13, though the linear temperature dependence for α is satisfied by considering the temperature region $T \geq \theta_D$ (400 to 500 K). In the s term, it is not purely structural contribution as expected by diffraction model, but a mixture of structural contribution to resistivity which goes as T^2 and an extra T^2 contribution due to magnetic scattering. This term was subtracted to calculate θ_D values using eqn. 3-19.

The θ_D values are around 300 to 330 K for the Co containing glasses and 130 to 255 K for Mo containing glasses depending on the alloy composition. The presence of Mo decreases θ_D drastically. The region above θ_D has been tried for a linear

fitting. We found a linear temperature dependence above θ_D for Mo containing samples. However, these values have to be justified either by fitting the data to the theoretical equation or by comparing the θ_D values with the θ_D values obtained from specific heat data.

The θ_D values obtained by subtracting the magnetic term (i.e., GT^2) which eventually gave rise to reasonably good values. The θ_D values of Fe-Co-B-Si alloys are very well agreeing with the θ_D values of other ferromagnetic alloys shown in Table 3-2. These observations supports the magnetic contribution to electrical resistivity in Fe-Co-B-Si and Fe-Ni-Mo-B-Si metallic glasses.

3.5.3 Moolj correlation :

Moolj (1973) found a remarkable correlation between the temperature coefficient of resistivity, α , and the magnitude of electrical resistivity, ρ . He observed a large number of magnetic as well as nonmagnetic glasses including crystalline samples with chemical disorder and found that as ρ increases α decreases and becomes negative for $\rho > 150 \mu\Omega\text{-cm}$. He also concluded that this universal behaviour does not depend on the constituents of the alloy or the amorphous nature. Naugle (1984) listed the ρ and α values of many nonmagnetic glasses and observed a similar behaviour in almost all the glasses.

In $(\text{Fe}_{1-x}\text{Co}_x)_{75}\text{B}_{10}\text{Si}_{15}$ ($0.00 \leq x \leq 0.12$) metallic glasses the resistivity values lie below $150 \mu\Omega\text{-cm}$ and α values are positive. A systematic change in these values with composition is not observed for the following reasons. Firstly, the difference in composition of the constituents of the alloys is very low and any change in physical parameters during preparation of these samples may change the structural disorder which in turn affects the absolute values of ρ . Secondly, the error in the measurements of thickness, breadth and length between voltage leads also influence the absolute resistivity values. The absolute resistivity values of Fe-Ni-Mo-B-Si alloys at room temperature lies between 96 and 145 $\mu\Omega\text{-cm}$ and the $\alpha(300)$ values are between $0.5 \times 10^{-4} \text{ K}^{-1}$ to $3.57 \times 10^{-4} \text{ K}^{-1}$ as given in Table 3-5. The absolute resistivity values of Fe-Ni-Mo-B-Si alloys are greater than the Fe-Co-B-Si alloys. The ρ values of Fe-Ni-Mo-B-Si alloys systematically increase with the addition of molybdenum. For example, the $\rho(300)$ and $\alpha(300)$ values of $\text{Fe}_{70}\text{Ni}_{12}\text{B}_{16}\text{Si}_2$ alloy are 96 K and $3.57 \times 10^{-4} \text{ K}^{-1}$, respectively. Whereas, for the alloy $\text{Fe}_{70}\text{Ni}_9\text{Mo}_3\text{B}_{16}\text{Si}_2$ alloy, they are 145 K and $0.5 \times 10^{-4} \text{ K}^{-1}$. This implies that as ρ increases α decreases systematically and hence seems to follow the Mooij correlation.

3.5.4 Curie temperature and crystallization studies :

Crystallization studies of metallic glasses are very important while studying the stability. Amongst all the available methods to measure, the simplest is electrical

resistivity. Of course, the DSC thermograms originally developed for polymer studies also acts as a method to elucidate crystallization due to the large enthalpy, H of metallic glasses. The Curie temperature, T_c can be seen in DSC with a cusp in the H vs. T graph. In resistivity, a slope change in ρ vs T occurs at T_c . The crystallization temperatures are observed by a sudden drop in enthalpy and ρ in DSC and resistivity measurements, respectively. Usually one or more number of crystallization stages occur depending on the crystallization products.

Measurements show that Fe-Co-B-Si metallic glasses crystallizes in a two stage process. The values of T_c , the starting point of first crystallization, T_{x1} , the starting point of second crystallization or decomposition, T_{x2} and the complete crystallization temperatures, T_{xc} for these alloys are listed in Table 3-3. The T_c is 690 K for $Fe_{75}B_{10}Si_{15}$ alloy and increases to 760 K by the addition of 1.5 at.% of Co. Further addition at the steps of 1.5 at.% of Co shows a slight increase in T_c in these samples. A double crystallization is observed in all the alloys similar to the crystallization observed by Baro et al (1984) in $Fe_{78}B_9Si_{13}$ metallic glass. They attributed first crystallization due to α -(Fe,Si) and the second crystallization due to the (Fe_3B) products. In $Fe_{75}B_{10}Si_{15}$ glass (i.e., $x = 0.00$ in Fe-Co-B-Si alloys) T_{x1} is observed at 715 K, T_{x2} at 825 K and T_{xc} at 848 K. Further addition of Co to this alloy increases the crystallization temperatures slightly, although the crystallization temperatures for $x = 0.10$ and 0.12 seems to be

decreasing slightly. The effect of Co addition on crystallization is shown in Figs. 3-9a by resistivity measurements and 3-9b by DSC studies.

In Co rich alloys like $\text{Fe}_{74}\text{Co}_{10}\text{B}_{16}$ and $\text{Fe}_{67}\text{Co}_{18}\text{B}_4\text{Si}_1$ it was shown that T_{x1} is higher by 40 K for the later compound (Bhanu Prasad et al 1983). However, this may have been due to Si in the second sample which is known to increase thermal stability and T_x of transition metal-metalloid glasses. The other interesting observation is that the second but small peak appears in the first crystallization region moves to higher temperatures with lesser intensity. This has been observed previously also for Fe-Co amorphous alloys (Bhanu Prasad et al 1983). This indicates that the crystallization is taking place in two stages. It is suggested that the first crystallization results in the precipitation of (Fe-Co) alloy within (Fe-Co)B-Si amorphous matrix, which then crystallize further with higher concentration of Co. More (Fe-Co) alloy precipitates leading to a sharper drop in the resistivity which is seen in Figure 3-5b. The percentage of drop in resistivity during amorphous to crystalline transformation increases monotonically with increase in cobalt content from 2.3% to 7.0% for $x = 0.00$ to 0.12, respectively.

The T_c for these alloys increases with increase in Co concentration. These temperatures are plotted with Co at.% in Fig. 3-10a. Figure 3-10b shows that by heating the same material second time (below T_x) increases T_c by nearly 7 K which means some structural changes are occurring with thermal treatment.

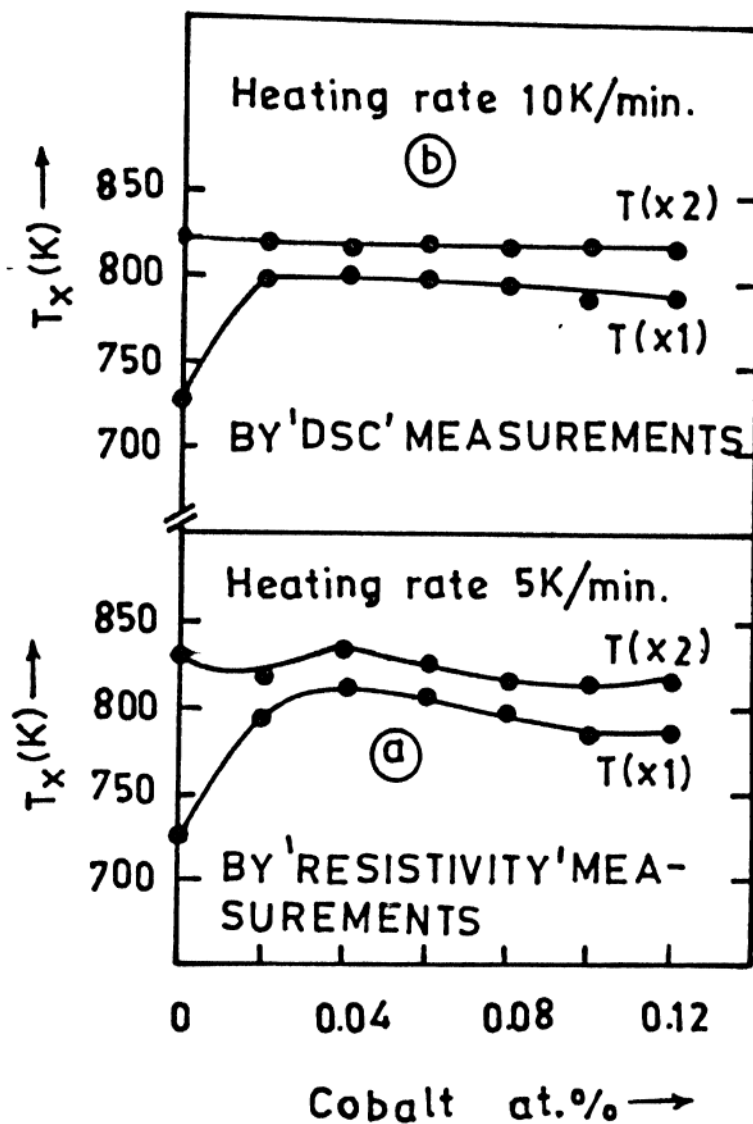


Fig. 3-9 : Crystallization temperatures of Fe-Co-B-Si alloys for the first and second peaks.

- (a) By resistivity measurements.
- (b) By DSC measurements.

However, no change in T_c is observed at least for the heating rates 10 to 100 K/min as shown in Fig. 3-11a for $x = 0.02$ in Fe-Co-B-Si alloys. This implies that the structural changes are occurring somewhere in between the starting temperature and T_c . The isochronal annealing studies for 15 minutes annealing at different temperatures showed a sudden jump in T_c somewhere in between 573 K to 773 K as shown in Fig. 3-11b indicating structural relaxation related effect, as these temperatures are close to T_x . Figure 3-11c shows the effect of isothermal annealing at 773 K (below 25 K to T_x) for different times for $x = 0.02$ alloy. It is interesting to see that the T_c rises initially which is interpreted due to structural relaxation. Heating for longer times at this temperature changes T_c only slightly and eventually leading to almost a saturated value of 727 K. Thus one must be careful in making measurements at higher temperatures without taking care of relaxation effects.

In Fe-Ni-Mo-B-Si alloys also, a double crystallization is observed. Here, the T_c and T_x s decreases systematically with Mo addition (as shown in Table 3-5) and they are less than that of Fe-Co-B-Si alloys. Also the second crystallization peak is not as prominent as that of Fe-Co-B-Si alloys.

Babu et al (1984) have showed the presence of $\alpha(\text{Fe,Mo})$, Fe_2B and Fe_2Mo phases apart from $\alpha\text{-Fe}$ in similar alloy of composition $\text{Fe}_{72}\text{Ni}_4\text{Mo}_6\text{B}_{16}\text{Si}_2$ by crystallizing the sample at 912 K using Mossbauer spectroscopy. This sample when it is heated to 1273 K and then cooled to room temperature showed additional features

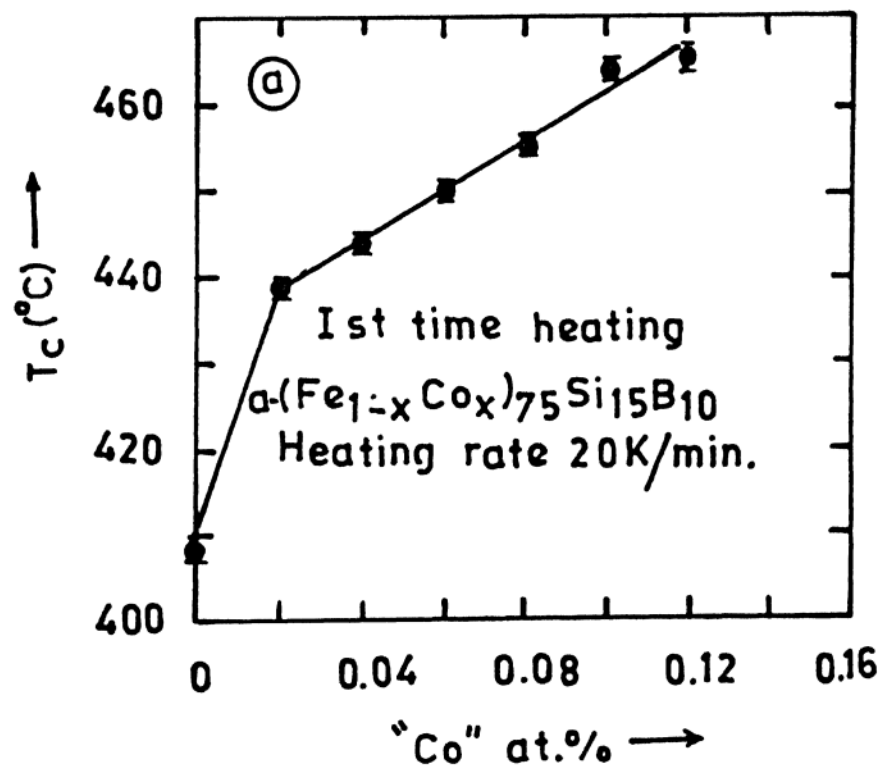
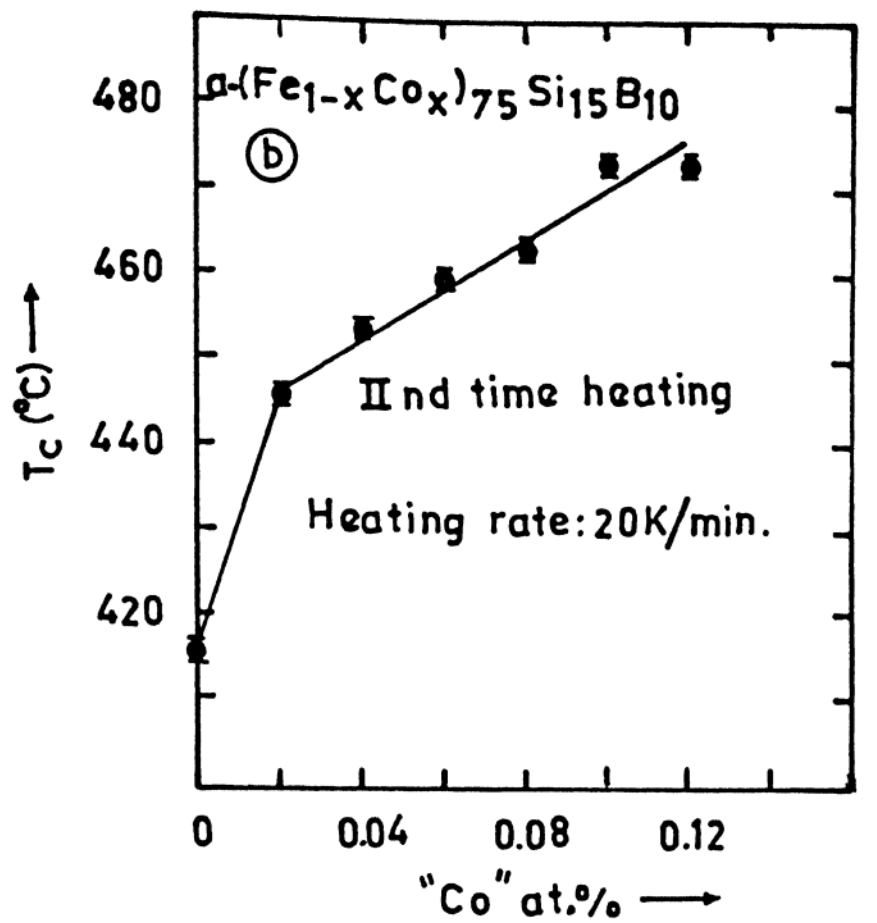


Fig. 3-10 : Variation of T_c with Co at.% in amorphous Fe-Co-B-Si alloys.

- (a) Heating 'as quenched' sample.
 (b) Heating the sample second time.

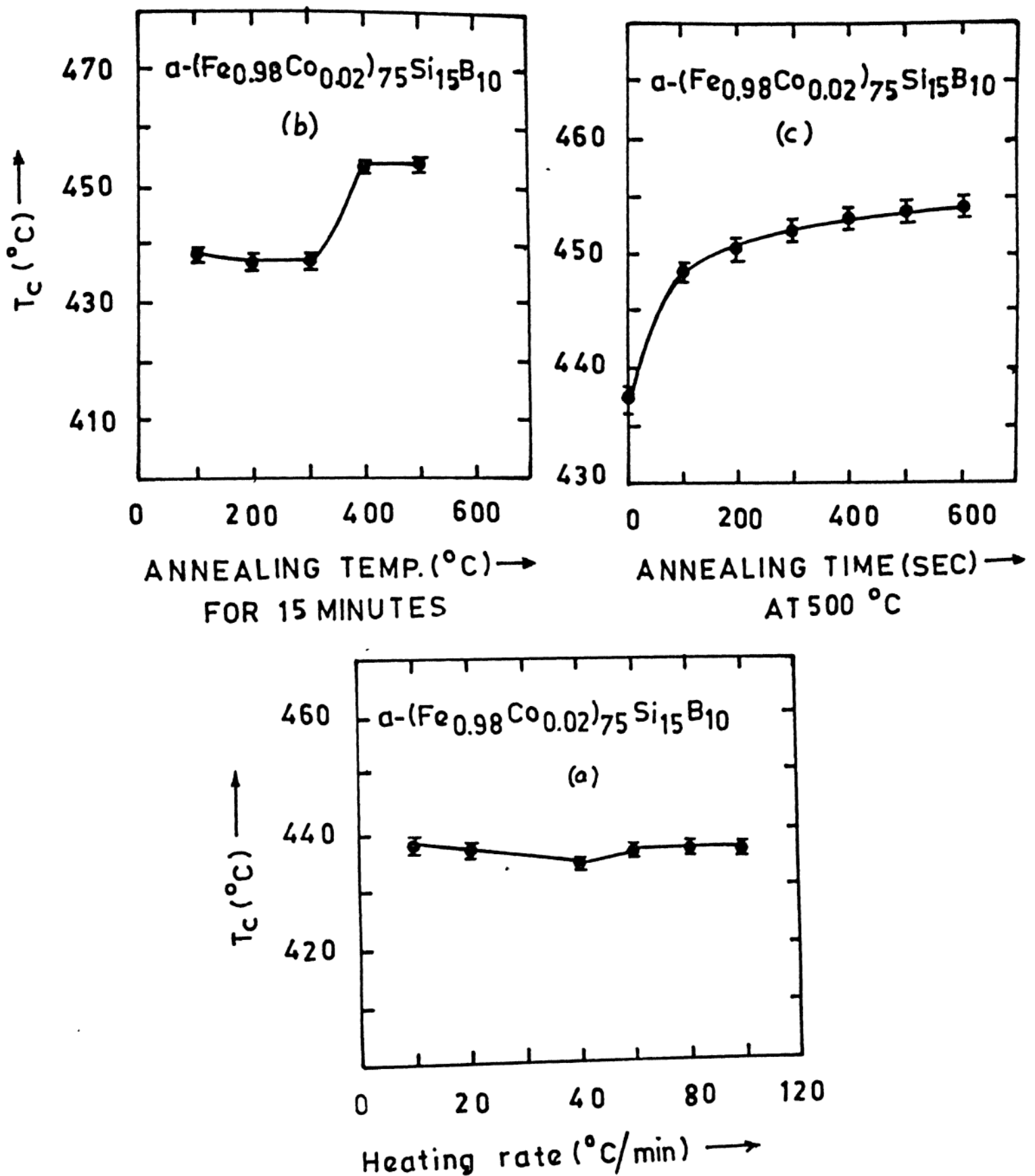


Fig. 3-11 : Variation of T_c with different heat treatments of $a\text{-Fe}_{73.5}\text{Co}_{1.5}\text{B}_{10}\text{Si}_{15}$ alloy.

- (a) Effect of heating rates.
- (b) Isochronal annealing for 15 minutes.
- (c) Isothermal annealing at 773 K.

such as an Invar alloy with a composition of $\text{Fe}_{1-x}\text{Ni}_x$. Interestingly, the alloy like $\text{Fe}_{40}\text{Ni}_{38}\text{Mo}_4\text{B}_{18}$ has showed a γ -FeNiMo phase followed by a fcc- $(\text{FeNi})_{23}\text{B}_6$ (Raja et al 1987). Also the $\text{Fe}_{40}\text{Ni}_{40}\text{B}_{20}$ glass crystallized into four types of crystals (Raja, 1986). The first two of them are eutectic mixtures of γ -FeNi + orthorombic $(\text{FeNi})_3\text{B}$ and γ -FeNi + fcc $(\text{FeNi})_{23}\text{B}_6$ and a third and the fourth are a single phase γ -FeNi solid solution and an unknown Fe-rich phase. He claims that the Mo enhances the formation of a fcc- $(\text{FeNi})_{23}\text{B}_6$ phase.

In case of Fe-Ni-Mo-B-Si alloys, we expect the initial formation of (FeNiMo) and (FeNiB) phases similar to the work of Raja et al (1987). Probably, these phases are dissociated to the multiphases as observed by Babu et al (1984) in $\text{Fe}_{72}\text{Ni}_4\text{Mo}_6\text{B}_{16}\text{Si}_2$ glass. Hence the transformation of amorphous to crystalline phases in $\text{Fe}_{70}\text{Ni}_{12-x}\text{Mo}_x\text{B}_{16}\text{Si}_2$ alloys is multiphase oriented. The percentage of drop in resistivity during amorphous to crystalline transformation in Fe-Ni-Mo-B-Si alloys is more than Fe-Co-B-Si alloys and decreases with Mo addition in contrast to Fe-Co-B-Si alloys where it increases with increase in Co content.

3.6 SUMMARY :

The electrical resistivity minimum, ρ_{\min} does not seem to be affected by the addition of small quantities of cobalt to $\text{Fe}_{75}\text{B}_{10}\text{Si}_{15}$ metallic glass at least till 9 at.% of cobalt content. The T_{\min} in Fe-Co-B-Si alloys studied is around 20 K. In contrast

to this Mo addition in Fe-Ni-Mo-B-Si system increases the T_{min} drastically from 11 K for $x = 0$ to 60 K for $x = 3$. All the metallic glasses studied showed logarithmic T dependence of ρ below T_{min} . Presence of magnetic contribution to ρ is suggested in both Co and Mo containing metallic glasses and it is a dominant T^2 dependence. The Debye temperatures calculated by subtracting the magnetic contribution to ρ gave rise to reasonably good values which are in agreement with the θ_D values of other similar ferromagnetic metallic glasses. The θ_D , T_C s and T_X s increases with the addition of Co to Fe-Co-B-Si alloys and decreases with the addition of Mo in Fe-(Ni-Mo)-B-Si alloys. The percentage of drop in resistivity (while transforming from amorphous to crystalline phase) increases even with the addition of small quantity Co to Fe-Co-B-Si alloys. On the otherhand, it decreases in Fe-(Ni-Mo)-B-Si metallic glasses with the addition of Mo content. As α increases, ρ decreases in all metallic glasses studied and hence seems to follow Moolj correlation.

CHAPTER IV

THERMOELECTRIC POWER MEASUREMENTS

CHAPTER IV

This chapter presents thermoelectric power measurements of Fe-Co-B-Si alloys in the temperature range 80 to 400 K and discusses the results.

4.1 INTRODUCTION :

Thermoelectric power (TEP) is very sensitive to the scattering process present in the material. TEP of amorphous alloys is particularly valuable to test theories put forward to explain the behaviour of electrical resistance since it is proportional to the energy derivative of electrical resistivity at E_F . Various models described in section 3.3 are able to reproduce the observed features of ρ of metallic glasses reasonably well within some range of temperatures for certain sets of parameters of the model. However, the same models predict entirely different behaviour of the thermoelectric power (S). Therefore, measurements of S can provide a way to distinguish among various theories, the theories which describe the electronic transport in metallic glasses adequately. However, it requires a systematic study of S with parameters like composition, full temperature range. i.e., low temperatures to the crystallization temperatures etc.

In this section we present the TEP of $(\text{Fe}_{1-x}\text{Co}_x)_{75}\text{B}_{10}\text{Si}_{15}$ ($0.00 \leq x \leq 0.12$) amorphous alloys in the temperature range 80 to 400 K. Due to experimental limitations on low temperature

available, we could not go to low (< 80 K) and high (> 400 K) temperatures. TEP of nonmagnetic metallic glasses has been extensively studied by Nagel (1978), Basak et al (1980), Gallagher (1981), Gallagher et al (1982), Matsuda et al (1982), Balbich et al (1982), Rao (1983), Delgado et al (1986) and Mizutani (1987). The experimental results in general are in good agreement with the Mott s-d scattering and Ziman models (Ziman 1961 and 1969, Mott 1972 and Nagel 1978). Certain features of TEP of these glasses can be explained in terms of the electron-phonon mass enhancement (Gallagher 1981 and Gallagher et al 1982). However, the TEP of ferromagnetic metallic glasses have not yet been well explained.

Recently, a number of papers have been reported on the thermopower of ferromagnetic metallic glasses (Babic et al 1980, Pekala et al 1981, Kettler et al 1982, Bhanu Prasad et al 1982 and 1983, Kettler et al 1984, Pekala et al 1984 and Fritsch et al 1985). Kettler et al have shown that for $T < T_c$, the temperature dependence of TEP is mainly decided by the magnetic scattering from the moment bearing atoms.

4.2 EXPERIMENTAL RESULTS :

The temperature dependence of the absolute TEP of amorphous $(\text{Fe}_{1-x}\text{Co}_x)_{75}\text{B}_{10}\text{Si}_{15}$ ($0.00 \leq x \leq 0.12$) alloys in the temperature range 80 to 400 K is as shown in Figure 4-1. All samples studied show some common and general features of ferromagnetic metallic glasses as given below.

- (I) S is negative throughout the temperature range 80 to 400 K and is a non-linear function of T .
- (II) S vs. T varies approximately linearly at lower temperatures ($T < T_{\max}$).
- (III) $|S|$ shows a broad peak around 300 to 400 K depending upon the sample composition. The peak value $|dS/dT|_{\max}$ at $T = T_{\max}$ varies from 3.8 $\mu\text{V/K}$ for $x = 0.0$ to 2.4 $\mu\text{V/K}$ for $x = 0.02$. Further addition of cobalt in small quantities (1.5 at.% at a time) does not seem to affect $|dS/dT|_{\max}$ but has a very small effect. For instance, $|dS/dT|_{\max}$ varies from 2.4 $\mu\text{V/K}$ for $x = 0.02$ to 2.1 $\mu\text{V/K}$ for $x = 0.12$.
- (IV) For $T > T_{\max}$, S again is expected to vary linearly with temperature but with dS/dT being positive. This can be seen in the Figure 4-1a for $\text{Fe}_{72}\text{Co}_3\text{B}_{10}\text{Si}_{15}$ alloy. Thermoelectric power of the alloy ($x = 0.04$ in the present study) falls to -13.0 $\mu\text{V/K}$ during crystallization and then increases with temperature after crystallization. TEP is negative throughout the temperature interval 80 to 800 K and shows parabolic behaviour with a maximum negative $S = -6.1 \mu\text{V/K}$ at approximately 350 K. Slight structures are observed in the data below 800 K. A steep linear drop in S is also observed at 800 K which is close to the crystallization temperature, 815 K (agreeing very well with the value from resistivity measurements. See Table 3-3), which reaches a minimum value of -13 $\mu\text{V/K}$ at 850 K, the temperature at which the crystallization process gets completed. Beyond 850 K the TEP

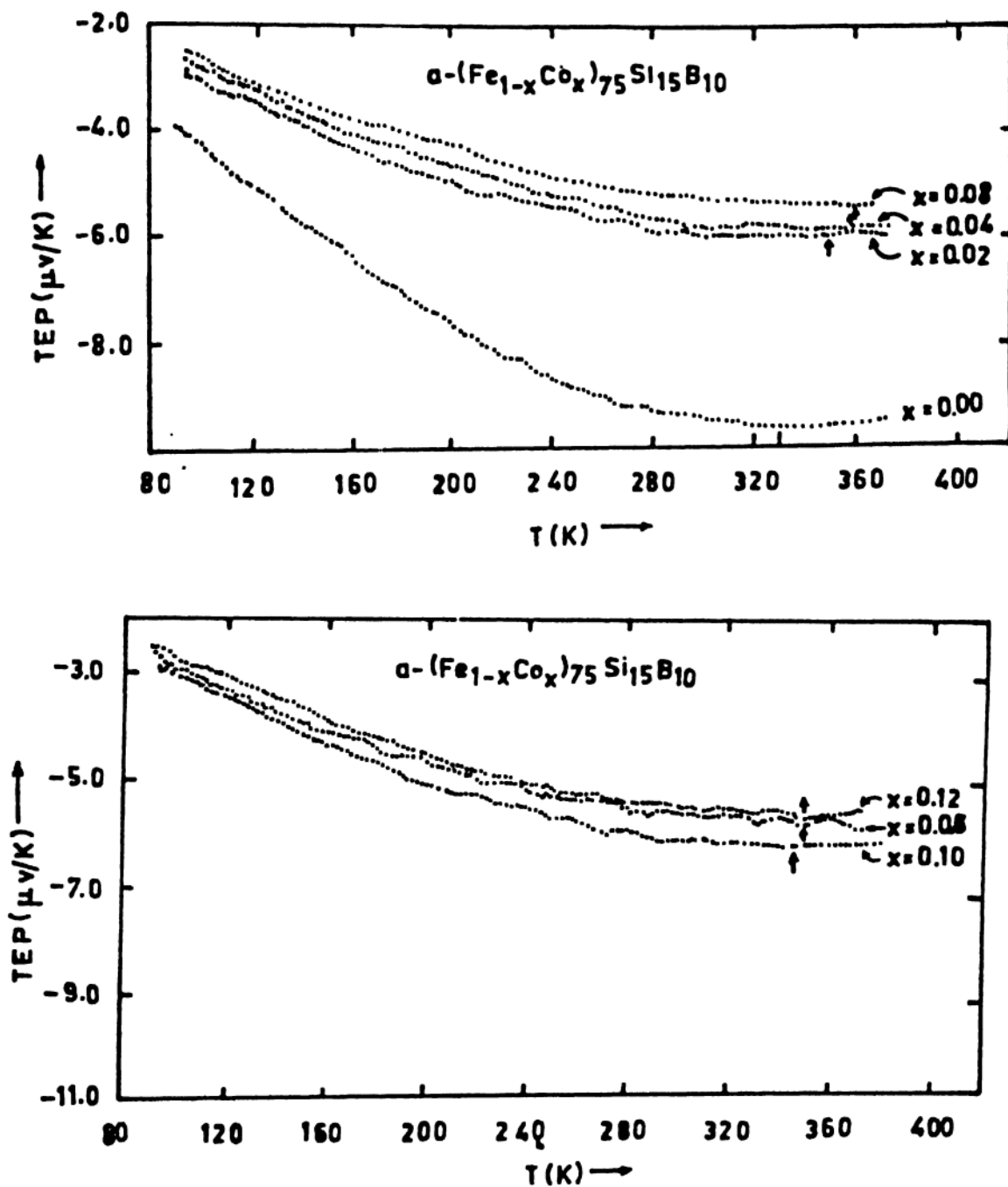


Fig. 4-1 : Thermoelectric power of $a-(\text{Fe}_{1-x}\text{Co}_x)_{75}\text{B}_{10}\text{Si}_{15}$ alloys in the temperature range 80 to 400 K.

Increases linearly with rise in temperature. The negative value of S of the sample over the entire temperature range 80 to 800 K indicate that it is of magnetic origin and has been observed in various iron-rich metallic glasses (Bhanu prasad et al 1982).

Table 4-1 gives the values of T_c , S_{max} , T_{max} , $(dS/dT)_{T<T_{max}}$, T_{max}/T_c and $|S_{max}/T_c|$. The table infers the following observations.

(I) Addition of 1.5 at.% of Co to $Fe_{75}B_{10}Si_{15}$ alloy decreases $|S_{max}|$ and Co seems to have a stronger effect on S even in small quantity. However further addition of Co in small quantities does not seem to effect $|S_{max}|$.

(II) T_{max} increases whereas S_{max} decreases with 1.5 at.% of Co addition. Also, with the addition of Co, T_{max}/T_c seems to increase whereas $|S_{max}/T_c|$ decreases. However further addition of Co seems to reverse the above behaviour with a slight variation in ratios. The values of T_{max}/T_c are 0.483 and 0.492 corresponding to 14.06×10^{-3} and $8.43 \times 10^{-3} \mu V/K^2$ of $|S_{max}/T_c|$ for $x = 0.00$ and 0.02 respectively.

(III) The slope $(dS/dT)_{T<T_{max}}$ decreases with the addition of Co. For $x = 0.0$, the slope is $-3.8 \times 10^{-2} \mu V/K^2$ and for $x = 0.02$, it is $-2.4 \times 10^{-2} \mu V/K^2$. This implies that the parabolic behaviour of the TEP decreases drastically with the presence of small quantity Co.

(IV) The T_c of $Fe_{72}Co_3B_{10}Si_{15}$ is around 717 K whereas the

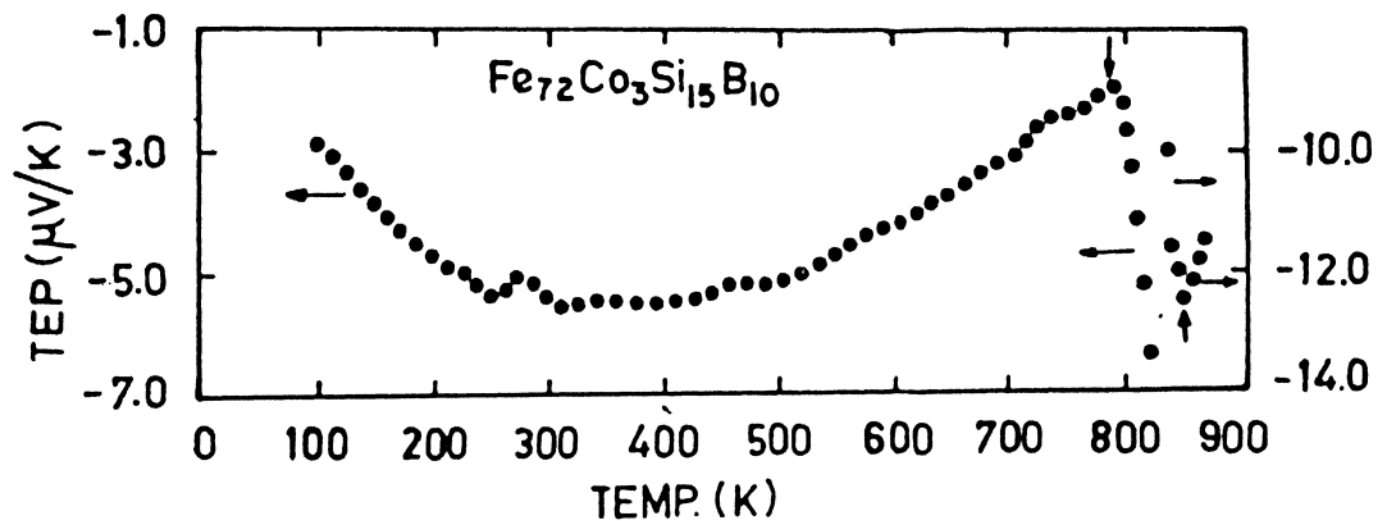


Fig. 4-1a : Thermoelectric power of $\alpha\text{-Fe}_{72}\text{Co}_3\text{B}_{10}\text{Si}_{15}$ alloy in the temperature range 80 to 900 K.

Table 4-1 : Curie temperature and various parameters of TEP of $(\text{Fe}_{1-x}\text{Co}_x)_{75}\text{B}_{10}\text{Si}_{15}$ ($0.00 \leq x \leq 0.12$) amorphous alloys.

x at. %	T_c (K)	S_{\max} μVK^{-1}	T_{\max} (K)	(dS/dT) $10^{-2} \mu\text{VK}^{-2}$	Temp. (K)	T_{\max}/T_c	$ S_{\max} /T_c$ $10^{-3} \mu\text{VK}^{-2}$
0.00	683	-9.6	330	-3.8	90-140	0.483	14.06
0.02	712	-6.0	350	-2.4	90-140	0.492	8.43
0.04	717	-6.1	352	-2.3	90-140	0.491	8.51
0.06	723	-6.2	354	-2.2	90-140	0.490	8.58
0.08	729	-6.3	356	-2.2	90-140	0.488	8.64
0.10	738	-6.3	358	-2.2	90-140	0.485	8.54
0.12	739	-6.4	360	-2.1	90-140	0.487	8.66

T_c values are taken from DSC studies of these glasses.

crystallization temperature is around 815 K which means the critical temperature is near to crystallization temperature. This may be the reason why the change in shape of the TEP curve at T_c is not clearly shown up like as observed by Pekala et al (1983). However, close observation of the Figure 4-1a reveals that there is a slope change at around 720 K which is the phase transition region.

4.3 DISCUSSION :

In this section the common observed features of ferromagnetic metallic glasses mentioned in the section 4.2 will be discussed in the light of existing theoretical models. In the resistivity of the metallic glasses discussed in chapter 3 we have already enumerated a few theoretical models which have been proposed to explain the transport properties of amorphous systems. Most of these models can produce TCR greater than or less than zero depending upon the theoretical parameters. These models predict different behaviours for the TEP. The ferromagnetic glasses produce a further complication due to an additional contribution from the magnetic scattering to the total value of S .

The system studied here and most of the other ferromagnetic metallic glasses (Babic et al 1980, Kettler et al 1982 and Kaul et al 1987) have the resistivity minimum around 20 K. Therefore one may apply Kondo type theory (Rao 1983) based on tunneling

levels for transport in these glasses. Since the tunneling levels in these glasses are supposed to be a consequence of the extreme disorder, the observed different S vs. T behaviour in magnetic and nonmagnetic glasses indicated the inability of this model to explain the transport behaviour.

Using Boltzmann transport equations the TEP can be written as

$$S = [\pi^2 k_B T / 3 |e|] [\partial \ln \rho(E) / \partial E]_{E=E_F} \quad 4-1$$

where $\rho(E)$ is the electrical resistivity as a function of energy. The above expression is generally rewritten as

$$S(T) = [-\pi^2 k_B / 3 |e| E_F] \zeta \tau \quad 4-2$$

where $\zeta = -E_F [\partial \ln \rho / \partial E]_{E=E_F}$

which is called as the thermoelectric parameter. In the Ziman's theory one can write ζ in the following form

$$\zeta = 3 - 2q - r/2$$

where

$$q = [|U(2k_F)|^2 S(2k_F)] / \langle |U(Q)|^2 S(Q) \rangle,$$

and

$$r = k_F \langle (\partial |U(Q)| / \partial k)_V S(Q) \rangle / \langle |U(Q)|^2 S(Q) \rangle$$

The brackets indicates an average of the form

$$F(Q) = (1 - k_F^2)^{-1} \int_0^{2k_F} F(Q) Q^3 dQ \quad 4-3$$

The term r appears only if the pseudopotential U depends upon Q , $S(Q)$ is the static structure factor of the material for the scattering wave vector Q , parameters q and r are generally constants with $r \ll q$. Sign of S is mainly determined by the magnitude of q while the temperature dependence of S is determined by the proportionality to T in Equation 4.2. Near $2k_F \approx Q = k_p$, q becomes large which leads to a $TCR < 0$ and a positive S . In the alloys investigated here $2k_F$ is definitely far away from k_p which will make q small (Chapter III). Hence in these samples $\alpha > 0$ and $S < 0$ is expected as observed. Thus, although the Ziman theory predicts the correct sign of S in these samples it lags in the prediction of nonlinearity of S with T .

Nagel (1977, 1978) has given the possible explanation of the observed behaviour of $S(T)$ in ferromagnetic glasses based on the work of Grest et al (1979). They observed a tail in the distribution of effective field, $P(H)$ at zero effective field in glassy ferromagnets which implies that a fraction of magnetic atoms would be sitting in the region of zero effective field. Nagel (1978) and Basak et al (1980) have argued that the Kondo scattering of electron from such magnetic atoms not only account for the coexistence of the Kondo-type resistivity minimum and ferromagnetism in these metallic glasses but also for the non-linear behaviour of their TEP, and hence, for the difference

between TEP of magnetic and nonmagnetic glasses. Kettler et al (1984) have argued that their results of $\text{Fe}_x\text{Ni}_{80-x}\text{B}_{19}\text{Si}_1$ alloys can not be explained using this theoretical model since (i) peak in $P(H)$ of these nickel-rich alloys is near $H = 0$ and (ii) ρ_{\min} in these alloys occur at temperatures much lower than the temperatures at which S_{\max} is observed. The first argument does not apply to our samples since a peak in $P(H)$ curves appears at higher effective fields, but the second argument does hold in our samples also. So, it is not possible to say whether the quantitative arguments of Nagel et al (1978) does apply to our samples or not.

Mott s-d scattering model has also been used to explain some of the features of TEP of metallic glasses. According to Mott, the s-p electrons, having longer mean free path than the d-electrons, exclusively carry the current and are scattered into the d-band holes. Hence, the relaxation time is inversely proportional to the density of d-states at $E = E_F$, i.e., $N_d(E_F)$. The thermoelectric parameter ξ in Equation 4-2 is then defined by

$$\xi = -3/2 + E_F [\partial \ln N_d(E) / \partial E]_{E=E_F} \quad 4-3$$

for s-p electrons with the free electron band. According to the theory, TEP of elements with less than half filled d-bands should be opposite in sign to the TEP of the elements having more than half filled bands.

If one takes the account of the splitting of the d-band into the spin-up ($d\uparrow$) and spin-down ($d\downarrow$) d sub-bands, then from

equation 4-3

$$S = \left(\frac{3}{2}\right) - \frac{N'_{d\uparrow}(E_F) + N'_{d\downarrow}(E_F)}{N_{d\uparrow}(E_F) + N_{d\downarrow}(E_F)} E_F \quad 4-4$$

where $N'_{d\uparrow,\downarrow} = dN_{d\uparrow,\downarrow}/dE$, and $N_{d\uparrow}$ and $N_{d\downarrow}$ are the density of states in the spin-up and spin-down d sub-bands, respectively. It is possible to explain qualitatively $S(T)$ behaviour in the Fe-Co-B-Si alloys using Kettler et al (1984) and the argument is as follows.

The first term in equation 4-4 is too small to account for the observed values of S at low temperatures, hence the second term must be important. The magnetic values of TEP can be explained only if the d sub-bands are almost full, only then $N_{d\uparrow}$ and $N_{d\downarrow}$ possess large negative values. As the temperature is increased from low temperature the d-band splitting decreases in magnitude. As T increases the numerator (N) in eqn. 4-4 increases much more rapidly than does denominator, hence S increases rapidly with T . On further increase in T the rate at which the numerator increases progressively slows down till $N'_{d\downarrow}(E_F)$, N and hence S attain their maximum value at a temperature T_{\max} . For $T > T_{\max}$, the second term in Equation 4-4 starts decreasing and so does S , as observed. Above T_c , the position of the Fermi level relative to the d-band edge changes only slightly and as such S should vary linearly with T , a variation which we do not seem to observe. Thus the Mott s-d scattering model is capable of explaining S vs. T behaviour of amorphous ferromagnetic alloys at $T \ll T_c$.

Korenblit (1982) has proposed that the unusual behaviour of TEP in ferromagnetic metallic glasses is due to the simultaneous presence of two scattering processes in these materials, namely, the inelastic electron-magnon scattering at the host-atoms, and the elastic scattering of electrons at the solute atoms that depends on the electron spin direction. The expression for TEP obtained by Korenblit is

$$S(T) = (k_B/e) (\tau_{\uparrow} - \tau_{\downarrow})/t \quad 4-5$$

where τ is the elastic relaxation time of the electrons with spin-up (\uparrow) and spin-down (\downarrow) and t is the mean relaxation time. This relaxation predicts a non-linear behaviour of S vs. T at $T \ll T_c$. Mean inelastic relaxation time t decreases with increasing T so that S increases with T , whereas $(\tau_{\uparrow} - \tau_{\downarrow})$ tends to zero and so does S , as T tends to T_c . Sign of S depends on the spin of $(\tau_{\uparrow} - \tau_{\downarrow})$. Our results show that S does not go through zero as T tends to T_c , although the nonlinear behaviour of S vs. T is observed at low temperatures.

Recently, Herzer (1984) carried out independent calculations on the TEP of amorphous ferromagnets, which essentially confirmed the Korenblit's results. He also discussed the TEP at and around T_c by taking the mean field approach into account. Following Kasuya's work, Herzer has derived an equation for the magnetic contribution to TEP by assuming that the conduction electrons are scattered locally at statistically independent spin-moments of d-electrons, which are subject to an effective local exchange field $H_{ex}(R_i)$.

He has derived an equation for $H_{ex}(R_i)$ within the frame work of Helsenberg model by the mean field approach (Fahnle et al 1983) which is as follows.

$$H_{ex}(R_i) = \left(\frac{1}{2\mu_B} \right) \sum_{j=1}^z J_{ij} \langle S_j^z \rangle_{eff} \quad 4-6$$

Here, J_{ij} is the exchange integral between neighbouring spins, $\langle S_j^z \rangle_{eff}$ is the effective mean field value of the z-component of the spin S_j . This has not necessarily to be identified with the thermal averages, which would imply that H_{ex} vanishes above T_c . Fahnle et al (1983) and Bohnke et al (1983) have shown that the smearing out of the critical region occurs in amorphous ferromagnets which extends to temperatures as high as 50% above T_c . This suggests a non-vanishing distribution of local exchange fields even from above T_c . In recent times there is again much more evidence for the local moments above T_c (Holden et al 1984).

More recently, Kettler et al (1989) have studied the TEP of $Fe_xNi_{80-x}B_{20}$ alloys. They suggested that the nonlinear TEP behaviour is due to dominant magnetic scattering of conduction electrons from magnetic atoms for $T \leq T_c$. Qualitatively, the Mott s-d scattering model (Mott 1972) and Herzer models (Herzer 1984) provided an explanation for certain observed features of TEP and no clear quantitative agreement between theory and experiment could be achieved without using unphysical values to electronic and magnetic properties in the theoretical expression of Herzer model (Herzer 1984 and Kettler 1989).

Thus, although a few models can explain the low temperature behaviour of the temperature dependence of TEP of amorphous ferromagnetic alloys, no theory seems to be capable of explaining their S versus T behaviour over the whole temperature range. i.e. $T \ll T_c$ to $T \gg T_c$.

4.3 SUMMARY :

Temperature dependence of thermoelectric power of ferromagnetic metallic glasses exhibit nonlinear behaviour. Addition of 1.5 at.% of Co seems to have a stronger effect on S even in small quantities and further addition of Co in small quantities does not seem to affect S_{\max} significantly. For $T \ll T_c$ Mott s-d scattering model seems to explain S vs. T behaviour in these alloys. No theoretical model seems to explain the temperature dependence of TEP of amorphous ferromagnetic alloys in the whole temperature range, although an attempt is being made to explain the nonlinear TEP by taking Herzer models into account (Kettler et al 1989).

CHAPTER V
MOSSBAUER SPECTROSCOPY MEASUREMENTS

CHAPTER V

This chapter presents the results of room temperature Mössbauer studies of Fe-Co-B-Si metallic glasses and temperature variation (80 to 700 K) Mössbauer studies of Fe-Ni-Mo-B-Si metallic glasses.

5.1 INTRODUCTION :

Mössbauer Spectroscopy (MS) is a phenomenon of recoilless emission and resonance absorption of gamma rays by the nuclei of atoms. Since its discovery in 1957 by Rudolf L. Mössbauer, the technique has been widely used to study hyperfine interactions and many other properties of solids, such as bonding, valency, charge distribution, etc. (Wertheim 1964, Cohen 1976, Luborsky 1983 and Bhatnagar 1985a). The structure of amorphous alloys in general and metallic glasses in particular has the random distribution function similar to each other among themselves but definitely different from that of liquid state, has allowed various experimentalists (Gonser et al 1978) to concentrate on the physical properties like mechanical strength, phase stability, resistance to chemical reactions, magnetic behaviour etc. of amorphous alloys. MS acts as a very good experimental tool to investigate all the above mentioned properties. It can also be used in finding out the structure, oxidation, diffusion, dislocation and point defects in physical metallurgy. The importance of this technique lies in the sharpness of the

Mössbauer line in conjunction with the possibility of determining the energies of the emitted gamma rays from a source relative to the absorber with a very high degree of accuracy. There are a number of Mössbauer isotopes available now but the ^{57}Fe isotope is the most widely used one since, Fe forms one of the important constituents in most of the magnetic materials. The work presented here has also utilized ^{57}Fe to investigate magnetic and other hyperfine interactions in iron-rich metallic glasses. However, we present only a brief discussion of the Mössbauer effect and its related parameters in iron-rich metallic glasses.

The decay of ^{57}Fe nuclei from the excited state ($I=3/2$) to the ground state ($I=1/2$) emits gamma rays of 14.4 KeV energy. The energy of this gamma ray changes slightly due to the presence of one or more effects like isomer shift (IS), electric quadrupole interaction (ΔE_Q) and magnetic dipole interaction which will be discussed in the forthcoming sections. The effect of these parameters on the transition from excited to ground state in ^{57}Fe nucleus is illustrated in Figure 5-1. If an absorber were same as the source then the recoilless absorption would consist of a single line of exactly the same energy as the emitted gamma rays from the source. However, if an absorber were different than the source, then this may not be the case due to the perturbation of the nuclear energy levels as a result of the difference between hyperfine interactions as experienced by the Mössbauer isotopes in the source and in the absorber.

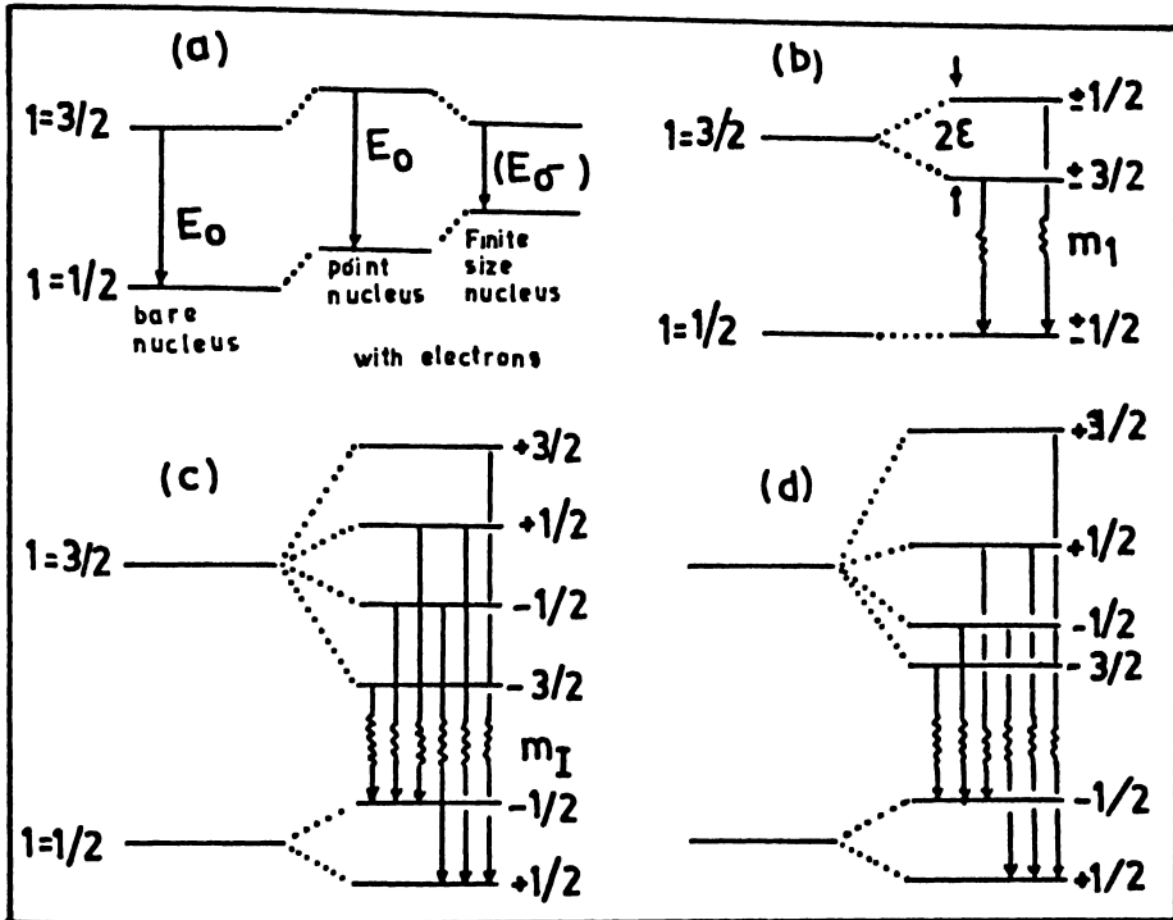


Fig. 5-1 : Schematic energy level diagram of the ground state ($I = 1/2$) and first excited state ($I = 3/2$) of ^{57}Fe nucleus :

- (a) isomer shift,
- (b) electric quadrupole interaction,
- (c) magnetic dipole interaction and
- (d) mixed magnetic dipole and electric quadrupole interactions.

The arrows correspond with the usually observable Mossbauer transitions.

5.2 THEORETICAL DISCUSSIONS :

5.2.1 Isomer shift (IS) :

The interaction between the nuclear charge distributed over a finite radius R and the s-electron density at the position of the nucleus will generally not be the same for the source and the absorber. This energy difference is called isomer shift, as shown in Fig.5-1.. This shift can be expressed as

$$IS = (2\pi/3)(Ze^2/R) [|\Psi_A(0)|^2 - |\Psi_S(0)|^2](\langle R_e^2 \rangle - \langle R_g^2 \rangle) \quad 5-1$$

where $|\Psi_A|^2$ and $|\Psi_S|^2$ are the densities of penetration electrons (s-electrons) at the nuclear site for the absorber and source, Z is the atomic number of the Mossbauer atom, e is the charge of the proton and $\langle R_e^2 \rangle$, $\langle R_g^2 \rangle$ are the mean square radius of the nucleus in the excited and ground state respectively. $|\Psi(0)|^2$ depends on several factors. In the case of ^{57}Fe nucleus the 3d-electrons affect $|\Psi(0)|^2$ mainly through partial screening of s-electrons from the nuclear charge. The nature of the chemical bonding (ionic, covalent, metallic) thus influence $|\Psi(0)|^2$.

Usually the isomer shift (IS) of a given absorber is defined relative to the shift of a standard absorber. In our case we always use natural α -Fe thin foil ($\sim 10 \mu\text{m}$) at room temperature as a reference, i.e., arbitrarily we set the isomer shift of metallic iron equal to zero. As $R_e < R_g$ the isomer shift tends towards smaller values with increasing $|\Psi(0)|^2$.

The effect of the vibrating atoms in a solid does not make any perturbation on the gamma rays emitted since the atoms make $\sim 10^{13}$ /sec oscillations during the life time (10^{-6} to 10^{-10} sec) of the excited state of the nucleus. The average velocity $\langle v \rangle$ of the atoms is therefore, zero and hence a first-order Doppler effect can not change the Mossbauer spectrum of a solid. However, $\langle v \rangle^2$ is non-zero which causes a shift of the resonance line by a second order Doppler effect (Blide 1973).

$$\Delta E = - \frac{3kT}{2Mc^2} \left[1 + \frac{1}{12} \left(\frac{\theta_D}{T} \right)^2 - \frac{1}{1680} \left(\frac{\theta_D}{T} \right)^4 + \dots \right] E_\gamma \quad 5-2$$

$$\Delta E = \frac{\langle v^2 \rangle}{2c^2} E_\gamma \quad 5-3$$

where C , k , θ_D , M and E_γ are the velocity of light, Boltzmann constant, Debye temperature, mass of ^{57}Fe and energy of 14.4 KeV gamma ray respectively. At high temperatures Equation 5-2 reduces to

$$\Delta E = - \left(\frac{3}{2} \right) \frac{kT}{Mc^2} E_\gamma \quad 5-4$$

Equation 5-4 gives $d(\Delta E/E_\gamma)/dT \simeq 7 \times 10^{-4}$ mm/sec-K. Equation 5-2 can be applied to estimate θ_D of a solid by Mössbauer spectroscopy.

5.2.2 Quadrupole Interaction :

Quadrupole interaction, ΔE_Q , is an anisotropic interaction since it depends on the local symmetry of the central Fe-atom.

$\Delta E_Q = 0$, only for cubic symmetry. Therefore in metallic glasses this anisotropy will be present.

The interaction of the nuclear electric quadrupole moment eQ with the principal component of the diagonalized electric field gradient (EFG) tensor $V_{zz} = \partial^2 V / \partial z^2$ at the site of the nucleus splits the nuclear state into sublevels with the eigen values

$$E_Q = \frac{eQV_{zz}}{4I(2I-1)} + \left[\frac{3m_I^2}{I(I+1)} - I(I+1) \right] \left[1 + \frac{\eta^2}{3} \right] \quad 5-5$$

The assymetry parameters η is given by

$$\eta = \frac{V_{xx} - V_{yy}}{V_{zz}} \quad 5-6$$

with $|V_{zz}| \geq |V_{yy}| \geq |V_{xx}|$; $V_{zz} + V_{yy} + V_{xx} = 0$ thus, $0 \leq \eta \leq 1$.

The electric quadrupole interaction splits the first excited state of ^{57}Fe ($I=3/2$) into sublevels with eigen values which can be seen in Figure 5-1.

$$E_Q = \pm \frac{1}{4} eQV_{zz} \left(1 + \frac{1}{3} \eta^2 \right)^{1/2} \quad 5-7$$

It should be noted that the inaccuracy of the absolute value of the derived EFG is rather high. The reverse situation applies to the magnetic hyperfine interaction where the excited and ground state magnetic nuclear moment of ^{57}Fe are known very precisely.

Quadrupole Interaction for $T > T_c$ in metallic glasses is almost a common observation (Le Caer et al 1984). A first attempt to include the effect of quadrupole interaction below T_c in the evaluation of Mössbauer spectra of metallic glasses was proposed by Le Caer et al (1979). We are not going to discuss about this parameter in this thesis. Further details on ferromagnetic glasses can be found elsewhere in Trammell et al (1969), Czjzek (1982) and Le Caer et al (1984).

5.2.3 Magnetic Hyperfine Interactions :

The Zeeman interaction of the nuclear magnetic dipole moment with an effective magnetic field (H_{eff}) at the nucleus is defined by the Hamiltonian

$$\hat{H}_Z = - \vec{\mu} \cdot \vec{H}_{eff} = - g_N \beta_N \hat{I} \cdot \vec{H}_{eff} \quad 5-8$$

Where g_N is the gyromagnetic factor of the nuclear state, μ is the nuclear magnetic moment, \hat{I} is the nuclear spin and β_N is the nuclear Bohr magneton ($e\hbar/2Mc$). For the observation of Zeeman splitting the following condition is required.

$$|g_N| \beta_N H_{eff} \geq \Gamma \quad \text{or} \quad \omega_L \tau_N \geq 1 \quad 5-9$$

where Γ is the natural line width, ω_L is the nuclear Larmor frequency ($|g_N| \beta_N H_{eff} / \hbar$) in the field H_{eff} and τ_N is the mean life time. For ^{57}Fe , the Eq. 5-9 is fulfilled, if $H_{eff} \geq 10$ KOe. Hanna et al (1960a) are the first to measure H_{eff} in metallic iron. In another experiment Hanna et al (1960b) determined the

direction of the effective magnetic field. At room temperature, $H_{\text{eff}} = -331$ KOe. The negative sign indicates that H_{eff} is antiparallel to the magnetic moment of the ^{57}Fe -atom. The isotope ^{57}Fe has $I = 1/2$ for the ground state and $I = 3/2$ for the 14.4 KeV first excited state. A magnetic field at the site of the nucleus (no quadrupole interaction) causes the splitting of the nuclear states into $(2I + 1)$ sublevels with the eigen values $E_m = -g_N \beta_N H_{\text{eff}} m_I$, where $m_I = I, I-1, \dots, -I$, as shown in Fig. 5-1. The ordering of the sublevels m_I indicates the fact that the ground state magnetic moment is positive, while the excited state has negative magnetic moment. The multipolarity of the 14.4 KeV gamma ray transition is almost exclusively a magnetic dipole in nature. Thus for the nuclear Zeeman effect, we have only $\Delta m_I = 0, \pm 1$ allowed transitions. Therefore, we have six transitions observed in the normal Mössbauer emission spectrum of iron-isotope.

In the magnetic dipole interaction the lines from the centre of the Mössbauer spectrum has to be symmetrically placed on both the sides. Due to the electric quadrupole interaction, isomershift etc., the lines are asymmetrically placed from the centre. The H_{eff} may be split into several contributions (Schaafsma 1981 and Marc Oliver 1984)

$$\vec{H}_{\text{eff}} = \vec{H}_F + \vec{H}_{\text{CON,P}} + \vec{H}_{\text{CON,N}} + \vec{H}_{\text{OR}} + \vec{H}_D \quad 5-10$$

where H_F is the Fermi contact hyperfine field caused by the spin polarized 1s, 2s and 3s core electrons (by the unpaired 3d electrons via the so called exchange polarization mechanism).

This field is proportional to the difference in the spin density at the nucleus $|\Psi_{\uparrow}(0)|^2 - |\Psi_{\downarrow}(0)|^2$ for up (1) and for down (1) spins.

$$\vec{H}_F = - \left(-\frac{8\pi}{3} \right) [g_N \beta_N \vec{S}_e(0)] \quad 5-11$$

where $S_e(0)$ is the total electron spin density at the center of the nucleus. $H_{CON,P}$ is the field from the contact interaction produced by the spin polarized 4s conduction electrons. If the 3d electrons are localized (so that we can define a moment per atom), this term may be split into local contribution arising from the polarization and hybridization effects due to unpaired 3d - electrons centered on the Mössbauer atom and a non-local contribution due to the spin polarization by surrounding atoms. $H_{CON,N}$ is a non-local contribution produced by neighbouring atoms via the overlap distortion of the core s orbitals, or by the dipole fields produced by localized moments on neighbouring atoms. Finally H_{OR} and H_D are the orbital and the dipolar contributions due to the Mössbauer atom electrons.

$$\vec{H}_{OR} = - 2\beta_N \langle -r^{-3} \rangle \langle \vec{L} \rangle \quad 5-11$$

where $\langle L \rangle$ is the quantum mechanical expectation value of the orbital angular momentum of the iron-ion. $\langle r^3 \rangle$ is the expectation value for the radius cubed of a 3d-orbital. A magneto-mechanical factor of $g = 2$ has been assumed for the electron spin.

$$\vec{H}_D = - 2\beta_N \left\langle \sum_i 3(\vec{r}_i - \vec{s}_i)\vec{r}_i - r_i^2 \cdot \vec{s}_i \right\rangle / r_i^5 \quad 5-12$$

here, r_l is the position and S_l is the spin angular momentum of the electron l

Approximate magnitude for these contributions for pure iron are $H_D = 0$, $H_F \simeq -200$ to -400 KeV, $H_{CON,P} \simeq 180$ KeV, $H_{CON,N} \simeq -200$ KeV and $H_{OR} \simeq 50$ KeV (Van der Woude 1966). Since $H_{CON,P}$ and $H_{CON,N}$ are usually of the same order of magnitude and opposite in direction, the H_{eff} value mainly depends on H_F contribution. In a random alloy, the following simple phenomenological relation for the average hyperfine field $\langle H_{eff} \rangle$ is often used (Campbell et al 1970 and 1974).

$$\langle \vec{H}_{eff} \rangle = A \vec{\mu}_{Fe} + B \langle \vec{\mu}_{Fe} \rangle \quad 5-13$$

where A and B are constants and μ is the average moment per transition metal atom. The first term represents the local contribution which is proportional to the local moment on Fe (μ_{Fe}) while the second term represents the contribution from the surroundings.

In the angular dependence of (^{57}Fe isotope) the allowed transitions in the nuclear Zeeman pattern are as follows:

Intensities		Transitions	Δm_I	Angular dependence
$I_{1,6}$	\Leftrightarrow	$(\pm 3/2 \text{ to } \pm 1/2)$	$\Leftrightarrow \pm 1$	$\Leftrightarrow 3/4(1+\cos^2\theta_m)$
$I_{2,5}$	\Leftrightarrow	$(\pm 1/2 \text{ to } \pm 1/2)$	$\Leftrightarrow 0$	$\Leftrightarrow \sin^2\theta_m$
$I_{3,4}$	\Leftrightarrow	$(+1/2 \text{ to } \pm 1/2)$	$\Leftrightarrow +1$	$\Leftrightarrow 1/4(1+\cos^2\theta_m)$

Here θ_m represents the angle between the direction of the magnetic field at the nucleus and the propagation direction of the gamma ray. From this angular dependence one can find the relative line intensities of a Zeeman hyperfine pattern in the thin absorber approximation, assuming isotropy of the lattice vibrations. The relative line intensities for $\theta_m = 0$ degrees are 3:0:1 :: 1:0:3 and for $\theta_m = 90$ degrees, 3:4:1 :: 1:4:3. Because the total radiation pattern is isotropic, it follows by integration over all directions that the relative line intensities for a randomly oriented magnetic material is 3:2:1 :: 1:2:3. For amorphous materials the relative intensities are given by

$$I_{1,6} : I_{2,5} : I_{3,4} = 3:b:1; \quad b = \frac{4\sin^2\theta}{(1 + \cos^2\theta)} \quad 5-14$$

where θ is the angle between the gamma ray direction and the magnetic moment. b is determined by the distribution of the magnetic moment directions in the sample which in general is not a priori.

Since the nuclear energy level of the ^{57}Fe nucleus in the absorber get perturbed due to hyperfine interactions, it is possible to observe resonant absorption only if the energy of the gamma ray emitted from the source is modulated. This energy modulation is accomplished by moving the source back and forth with respect to the absorber which causes a Doppler shift of the gamma ray energy proportional to the source velocity, v . The Mössbauer velocity scale is defined from the IS and H_{eff} values

of α -Fe at room temperature (isomer shift = 0, $H_{eff} = 330 \text{ KOe} = 10.625 \text{ mm/sec}$).

Mössbauer spectrum can be obtained in two modes. One is the transmission mode and other is the scattering mode. First one needs very thin samples and the second one can make use of thick samples also. The measurements in these two modes as a function of Doppler velocity, V , gives the Mössbauer spectrum. Scattering permits the study of only thin layers ($\sim 1000 \text{ \AA}$) due to the penetration depth of conversion and / or Auger electron after a Mössbauer absorption. In the investigation reported here, we have used transmission geometry to get Mössbauer spectrum.

The Mössbauer spectroscopy (MS) has a high resolution, since the width, Γ of the observed absorption lines is nearly the same as the natural line width. The natural line width of ^{57}Fe is nearly 10^{-8} eV , which is much smaller than the gamma ray energy E_0 of 14.4 KeV . This gives the resonance quality factor $Q = E_0/\Gamma \simeq 10^{12}$, a very high value. The energies involved in IS and ΔE_Q are of the same order as Γ , and in the case of magnetic interaction, the energies involved are one order of magnitude larger. While the line width of Mössbauer line of natural iron is approximately 0.20 mm/sec (Bhide 1973), the observed average line width of the two inner absorption lines of the 6 line Mössbauer spectrum of a thin iron foil at room temperature in our experimental set up is 0.28 mm/sec . This essentially determines the resolution of the Mössbauer spectrometer.

The MS has emerged as a good technique to study the atomic structure of solids. Each non-equivalent site of the probe atom in a solid give rise to its own characteristic hyperfine field spectrum which can be easily analyzed to obtain the structural information of the solid if there are not too many inequivalent sites. However, if there are a large number of non-equivalent sites, as is the case for the amorphous materials, overlapping of hyperfine field patterns for various inequivalent sites gives rise to a complex spectrum or a spectrum having rather broad lines. The analysis of such spectrum becomes difficult but it can still be done although the resolution of the technique becomes relatively poor.

5.3 ANALYSIS OF THE MÖSSBAUER SPECTRA :

The salient features of the methods employed to extract the hyperfine parameters from the Mössbauer spectra are as follows.

5.3.1 Least square fitting (LSF) :

The six line Mössbauer spectra of metallic glasses have been least square fitted to an equation to obtain corrected line positions, area under each curve, line widths and amplitude. Actually the spectrum is assumed to be of six independent lorentzian line shapes with a parabolic background. The equation used for one or more lorentzians plus a parabola (May et al 1968)

$$Y = \sum_{i=1}^n \frac{A_i}{\left[\frac{X - P_i}{(\Gamma_i/2)} \right]^2} + E + FX + GX^2 \quad 5-15$$

where A_i is the amplitude of the i^{th} peak, X is the number in the i^{th} channel, P_i is the position of the i^{th} peak, Γ_i is the half width of the i^{th} peak at half maximum amplitude and E, F and G are constants of parabola.

Initially, the programme uses the estimated values of the parameters to solve the equation of the curve for each X to obtain a calculated value for each Y . This calculated Y is substituted from the observed Y for the corresponding X to give the residual, ΔY . The residual for each X is squared and summed over all values and it is this sum of squared residuals that is minimized. Those observed Y s that lie sufficiently below the other Y values to be rejected and set equal to zero. These values are ignored in fitting the curve by giving them a weight (W) of zero. Each other Y value has a weight of 1.

The glassy nature of the samples investigated produces Mössbauer lines which are not strictly lorentzians. A few methods have been developed to take this effect into account. These are Fourier analysis of the spectra (Window 1971) and overlapping six-line patterns with lorentzian line shapes and the use of non-lorentzian line shapes (Schurer et al 1978, Gonser et al 1978, OK et al 1980 and Prince et al 1980). The LSF is improved a

little bit by using the non-lorentzian line shapes but it is not significantly different from the one obtained using the lorentzian line shapes. Hence we have used the lorentzian line shapes to fit our spectra.

For a Mössbauer spectrum of a sample the parameters obtained from the output using Equation 5-15 are amplitude, position, half width at half maximum (HWHM), peak area of each peak and the parabolic constants E, F and G from which H_{eff} , IS and ΔE_Q can be calculated. These calculated values are essentially the average values.

5.3.2 Evaluation of the hyperfine field, P(H) :

The Window's method is used for the deconvolution of the broad Mössbauer spectra to evaluate the hyperfine field, P(H). The choice IS = \overline{IS} and $\Delta E_Q = 0$ are taken as good approximations. There are mainly two ways to calculate P(H) in broad Mossbauer spectra. Firstly, fixed shape is assumed before calculating P(H). The assumption could be a simple Gaussian (Sharon et al 1971), modified lorentzian (Sharon et al 1972) or split gaussian (Logan et al 1976). However, the accuracy of the result depends on the assumed shape of the spectral lines and hence this has no general applicability. Secondly, evolution of the P(H) by expanded Fourier-series (FS), which is the recent method. Hesse et al (1974) have proposed a more direct deconvolution procedure to evaluate P(H) and showed that the results are almost same as

far as the Window method is concerned. Recently, Le Caer et al (1979) have proposed an improved version of the Hesse and Rubartsch method (1974).

There is one more binomial distribution (BD) method (Vincze et al 1974) in which the assymetry of the line pattern can be fitted by releasing the conditions that $IS = \overline{IS}$ and $\Delta E_Q = 0$. However, the $P(H)$ distributions obtained with FS and BD methods were the same within the error limits (Schaafsma 1981).

Fourier series method :

In this method the $P(H)$ is expanded in a cosine-series. We know that

$$P(H) = \sum_{l=1}^m a_l f_l[X(H)] \quad 5-16$$

where $f_l(X) = \cos(lX) - (-1)^l$ and $X = \pi [(H-H_{min})/(H_{max}-H_{min})]$; ($H_{min} \leq H \leq H_{max}$). The Mössbauer spectrum is calculated by convolution of $P(H)$, given by Eqn. 5-16 with a sextuplet of lorentzian lines $L_6(H,V)$:

$$Y_{cal}(V) = a_0 + \int_{H_{min}}^{H_{max}} P(H) L_6(H,V) dH \quad 5-17$$

where a_0 is the free parameter for the constant background. There are $(M+1)$ unknown parameters of $a_l = (l=0,1,2,\dots,M)$. Suppose, the measured spectrum has been collected in N channels

where the number of counts in channel i is given by $Y_{\text{mean}}(V_i)$. Then, the $(M+1)$ unknown parameters can be solved directly from the usual condition that the sum of squares of the deviations $\Delta Y = [Y_{\text{cal}}(V_i) - Y_{\text{meas}}(V_i)]^2$ is minimal, with the additional condition that $P(H)$ should be normalized. The $P(H)$ obtained depends on the choices for the following parameters, viz., IS , ΔE_Q , Γ_0 , b , H_{min} , H_{max} and the number of terms in the expansion M . The first 4 parameters appear in the well known expression for $L_6(H, V)$. The choices $IS = \overline{IS}$ and $\Delta E_Q = 0$ are good approximations. Γ_0 is the line width of the lorentzian lines for which we choose the value equal to 0.28 mm/sec (average inner line width of the natural iron at room temperature(RT)).

The parameter b represents the priori unknown intensity ratio of lines 2 and 5 to 3 and 4. The correct choice for b is only problematic. The correct value of b corresponds to (not at low fields) value of b to a sharp minimum of the goodness of fit parameter χ^2 , defined by

$$\chi^2 = \frac{1}{[N-(M+1)]} \sum_{i=1}^N \frac{[Y_{\text{cal}}(V_i) - Y_{\text{meas}}(V_i)]^2}{Y_{\text{meas}}(V_i)} \quad 5-18$$

optimal choices for the remaining parameters H_{min} , H_{max} and M are strongly correlated. $H_{\text{min}} = 0$ and H_{max} sufficiently high so that $P(H_{\text{max}}) = 0$, for instance, $H_{\text{max}} = 400$ to 500 KOe (450 KOe in our case) for a typical Mossbauer spectrum for transition metal-metalloid glass are the optimal choices. These choices imply

rather high value of M ($M = 9$ to 25 and $M = 9$ in our case) in order to obtain a satisfactory fit.

A Mössbauer spectrum of $\text{Fe}_{70}\text{Ni}_{12}\text{B}_{16}\text{Si}_2$ amorphous alloy at 80 K is tried for different choices of fitting using Window's programme. The average field, \bar{H} and the mean square deviation, x^2 is plotted against the M values and the number of Fourier coefficients as shown in Figure 5-2. It has been observed that as M value increases the x^2 decreases and \bar{H} increases. For $M > 12$ the \bar{H} seems to saturate towards a constant value and change in x^2 reduces to smaller values. It is also observed that for $M = 12$ the oscillations are more in the $P(H)$ vs. \bar{H} graph when compared to $M = 9$ and also the difference in \bar{H} between $M=9$ and 12 is only 2 KOe (Fig. 5-2b). Hence, $M = 9$ is selected for the evaluation of $P(H)$ during all of our measurements. The values of a, b and c , the relative intensities of the three types of transitions (section 5.2.3) are varied (keeping a and c as constants and varying b value alone) to get good correlation between theoretical and observed Mössbauer spectrum.

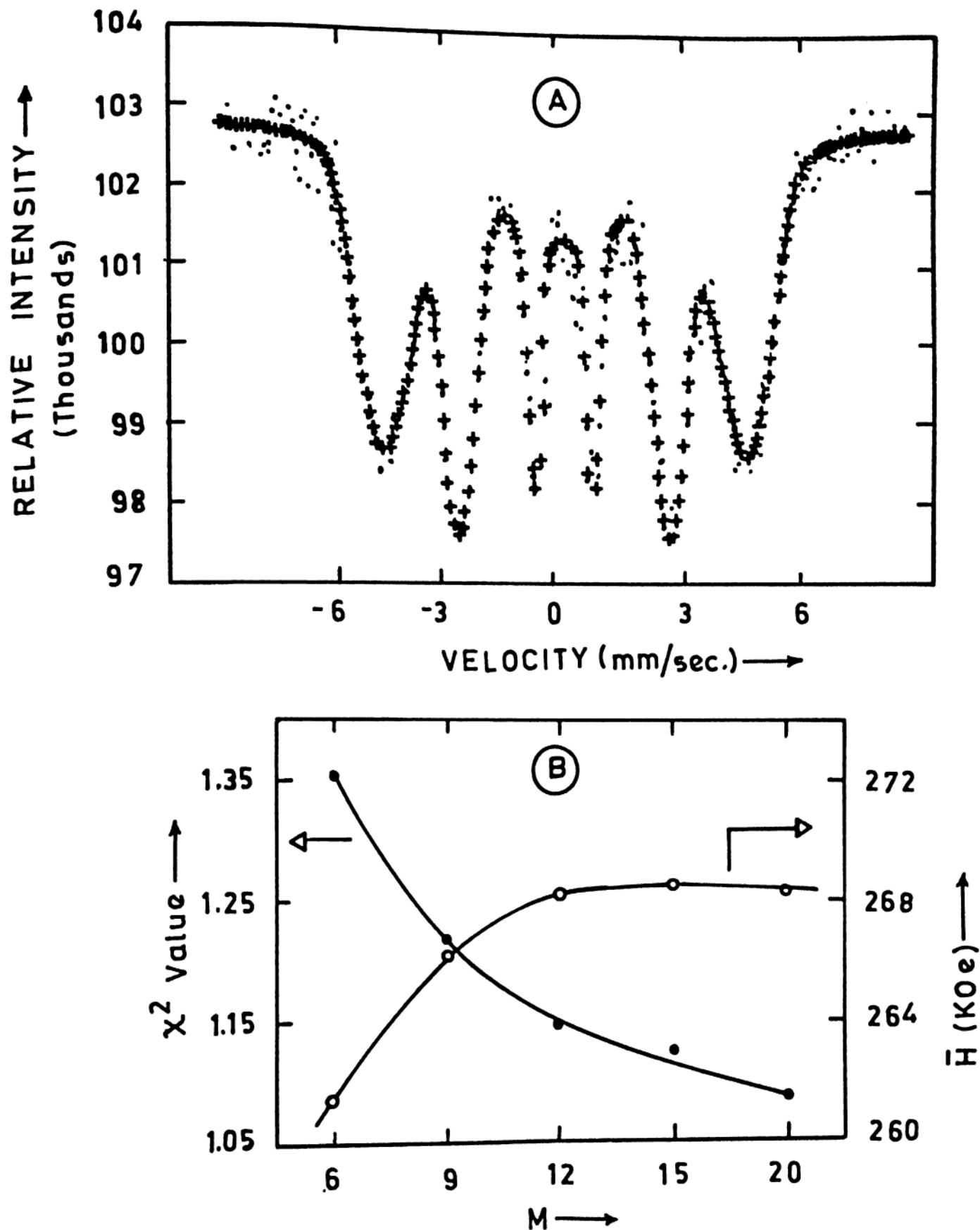


Fig. 5-2 : (A) Mossbauer spectrum of amorphous $\text{Fe}_{70}\text{Ni}_{12}\text{B}_{16}\text{Si}_2$ alloy at 80 K.

(.) represents experimental plot

(+) represents theoretical plot from P(H) analysis

(B) (o) represents mean field, \bar{H} and

(.) represents χ^2 obtained from P(H) analysis as a function of M.

5.4 RESULTS AND DISCUSSION :

5.4.1 Mössbauer spectra of metallic glasses :

All the spectra of iron-rich ferromagnetic metallic glasses consist of six overlapping broad lines indicative of the ferromagnetic state of each sample. The absorption lines have rather large line widths (0.5 to 1.9 mm/sec) which are about five to six times the width of the absorption lines in the Mössbauer spectrum of a thin Fe-foil. This is a characteristic feature observed in the Mössbauer spectra of all metallic glasses. In pure crystalline iron all the iron atoms occupy crystallographically equivalent positions, and therefore, a single set of the hyperfine parameters H_{eff} , IS and ΔE_Q characterize the iron Mössbauer spectrum. The mean isomer shift is determined from the centroid of either the doublet or sextuplet spectrum. In crystalline compounds and dilute iron alloy each Mössbauer spectrum consists of reasonably sharp absorption peaks. Since the number of different neighbourhoods is small in such cases, it is usually not difficult to establish a correspondence between the different sets of H_{eff} , IS and ΔE_Q and compound. However, the situation is quite different in metallic glasses.

The large line widths in six-line Mössbauer spectra of metallic glasses are usually explained by invoking the existence of a distribution of values of magnetic hyperfine fields, effective field gradients at Mössbauer probe atom, and isomer shift which are consequences of amorphous nature of the

solid which is responsible for a wide distribution in the neighbours of any of iron atom in the solid, i.e., all iron atoms sites are crystallographically inequivalent in an amorphous solid. However, it is observed that the line width increases from the central to the outermost lines of the spectrum, i.e., $\Gamma_{1,6} > \Gamma_{2,5} > \Gamma_{3,4}$. This shows that the major broadening is caused by the magnetic hyperfine field distribution and the effect of the distribution of other hyperfine parameters is comparatively less (Eibschutz et al 1973). It is not easy to extract information about the local surroundings of the iron atom from the observed Mössbauer spectrum since the difference between the various neighbourhoods of the iron atom are too small to be resolved separately in the spectrum. However, since the Mössbauer spectrum still shows a well resolved six lines below T_c , it is possible to get information about the average magnetic behaviour of the sample directly from the spectrum. The characteristic features of the Mössbauer spectrum of particular metallic glasses like Fe-Co-B-Si and Fe-Ni-Mo-B-Si glasses and their results will be discussed in the following sections.

5.4.2 Room temperature Mössbauer spectra of Fe-Co-B-Si alloys :

The room temperature (RT) Mössbauer measurements of $(\text{Fe}_{1-x}\text{Co}_x)_{75}\text{B}_{10}\text{Si}_{15}$ ($0.00 \leq x \leq 0.12$) alloys have been carried out and shown in Figure 5-3. The right hand side of the figure contains the $P(H)$ analysis of the respective samples from 0 to 450 KOe. All samples show similar six broad line spectra at RT.

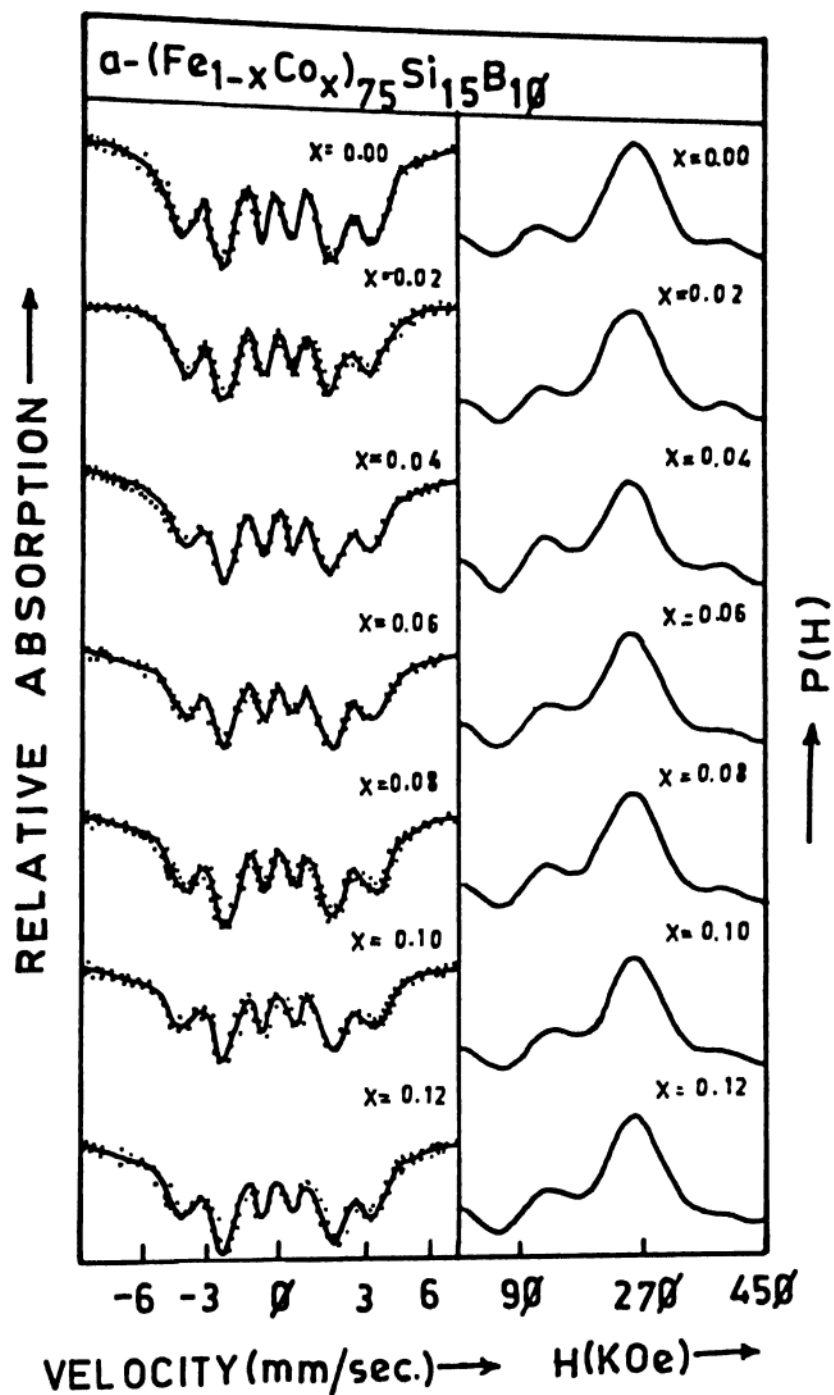


Fig. 5-3 : Room temperature Mössbauer spectra of $a-(\text{Fe}_{1-x}\text{Co}_x)_{75}\text{Si}_{15}\text{B}_{10}$ alloys.

It may be noted that the assymetry in line widths and line intensities exists in the spectra, i.e., the intensities and the widths of lines J and (7-J) (J = 1,2,3) are different. At RT, the line widths of these samples are $\Gamma_1 < \Gamma_6$, $\Gamma_2 < \Gamma_5$, $\Gamma_3 < \Gamma_4$, where Γ_J is the line width of the line J. The values of these line widths are listed in Table 5-1.

Various explanations have been proposed to explain this assymetry. Some of them are (i) linear relationship between IS and H_{eff} (Takacs 1980), (ii) linear relationship between H_{eff} and $IS + \Delta E_Q$ (Vincze 1978). Le Caer et al (1981) have shown that it is possible to account for this assymetry in the Mössbauer spectra by assuming the anisotropic hyperfine fields (H_a) observed in related crystalline systems such as iron borides (Weisman et al 1969 and Takacs et al 1975). In addition to the variation of H_{eff} with IS, major contribution coming from the former. They found that the best fit to the Mössbauer spectrum of $\alpha\text{-Fe}_{75}\text{B}_{25}$ was given for $H_a \simeq 14$ KOe (Le Caer et al 1981) a value approximately $(1/20)^{th}$ of H_{eff} . In our analysis, we have not included this effect which is expected to improve the fit.

Figure 5-3 shows the room temperature Mössbauer spectra of $(\text{Fe}_{1-x}\text{Co}_x)_{75}\text{B}_{10}\text{Si}_{15}$ ($0.00 \leq x \leq 0.12$) alloys and their hyperfine field distribution. It is quite interesting to note that all the spectra look alike including the cobaltless sample. The assymetries in amplitude and areas are observed similar to other ferromagnetic metallic glasses (Chappert 1982 and Bhatnagar 1985a). The hyperfine field is 254 ± 3 Koe for $\text{Fe}_{75}\text{B}_{10}\text{Si}_{15}$ alloy,

Table 5-1: The Mössbauer line widths of $(\text{Fe}_{1-x}\text{Co}_x)_{75}\text{B}_{10}\text{Si}_{15}$ ($0.00 \leq x \leq 0.12$) alloys at room temperature.

x	Γ_1	Γ_2	Γ_3	Γ_4	Γ_5	Γ_6
at. %	mm/s	mm/s	mm/s	mm/s	mm/s	mm/s
0.00	1.580	0.991	0.626	0.655	1.255	1.690
0.02	1.524	1.041	0.580	0.618	1.225	1.540
0.04	1.427	1.039	0.356	0.511	1.244	1.443
0.06	1.464	0.987	0.499	0.631	1.201	1.615
0.08	1.550	1.001	0.511	0.593	1.203	1.550
0.10	1.507	0.970	0.552	0.554	1.189	1.557
0.12	1.525	0.995	0.542	0.614	1.206	1.559

whereas it is 237 ± 3 KOe for the alloy with 1.5 at.% of Co in the above glass. Further addition of Co at the steps of 1.5 at.% increases the hyperfine field but not linearly. Similar observation can be found in case of isomer shift, mean field, H , peak field (H_p), and in half width at half maximum (HWHM), the results of which are tabulated in Table 5-2. Here H_p and HWHM are the peak field and half width at half maximum of the prominent peak. However, if we look into the results of the samples for $x = 0.00, 0.04, 0.08$ and 0.12 carefully, an increase in trend in all the above mentioned properties is observed. This unexpected and slightly nonlinear trend may be attributed to the changes in physical conditions while forming the glass, which can lead to the magnetic structure different from the expected one. If we compare the hyperfine fields of these alloys to the alloy without Si and with 10 at.% of Co (Bhatnagar et al 1985) with composition $Fe_{74}Co_{10}B_{16}$, it is well understood that the hyperfine field is less by about 20 KOe. This is not unusual as it has been suggested that $P(H)$ is sensitive to s-p atoms around Fe-sites than Fe nearest neighbours (Durand 1983). The small peak in probability analysis, which has been attributed to be due to the fitting procedure, has the maximum at around 122 KOe and it shifts slightly towards the positive side by about 4 KOe and for all other cobalt containing alloys it is almost at the same place. The physical parameters like IS, $H_{eff}(RT)$, H , H_p and HWHM (ΔH) are plotted against Co at.% in Figure 5-4.

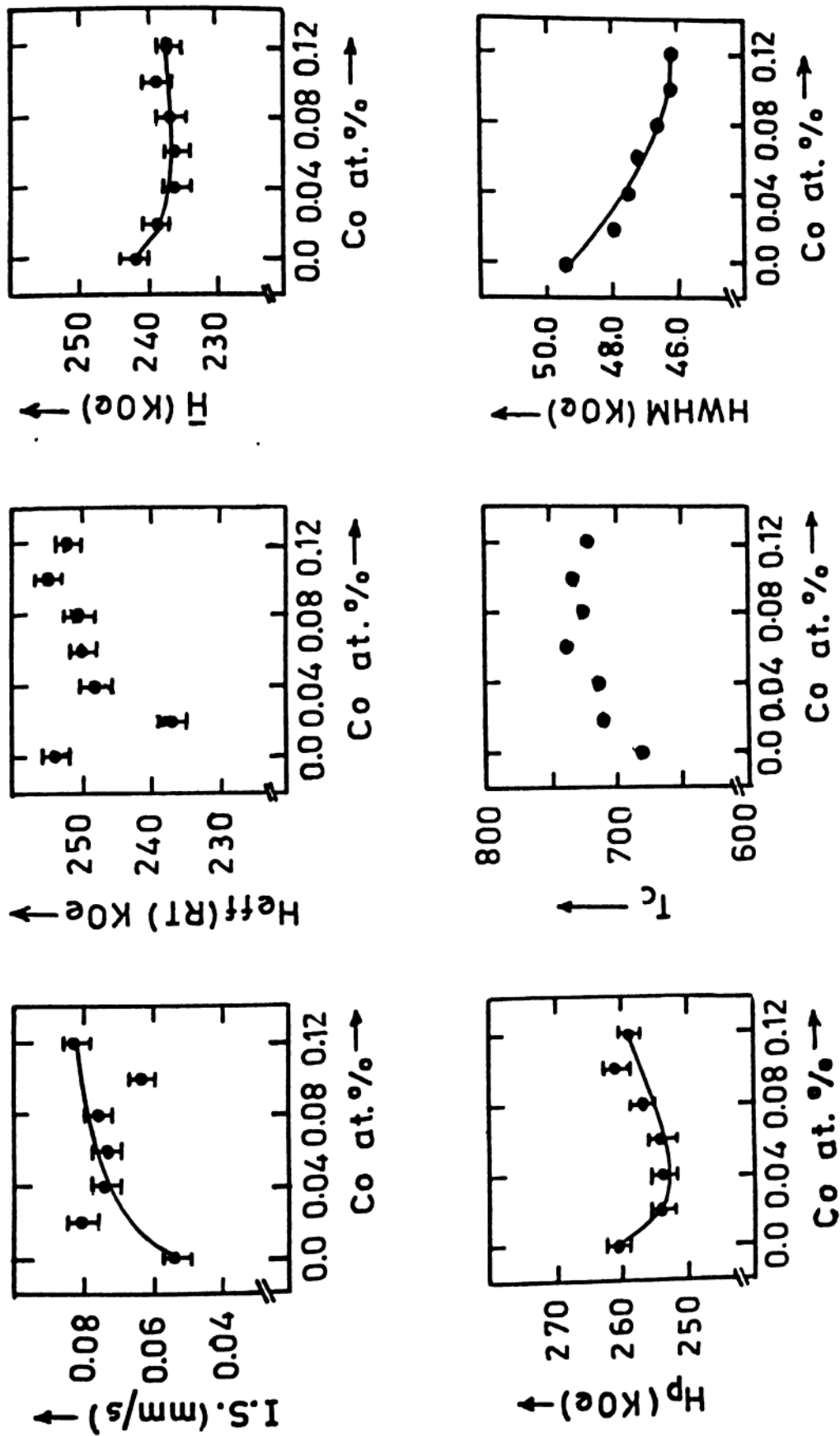


Fig. 5-4 : Isomer shift (IS), hyperfine field, $H_{\text{eff}}(\text{RT})$, mean field, H , peak field, H_p , Curie temperature, T_c and half width at half maximum (HWHM) vs. Co at.% of amorphous $(\text{Fe}_{1-x}\text{Co}_x)_{75}\text{B}_{10}\text{Si}_{15}$ alloys.

Table 5-2: Isomershift (IS), effective field (H_{eff}), Mean field (H), peak field (H_p), Curie temperature (T_c) and Half width at half maximum (HWHM) of $(\text{Fe}_{1-x}\text{Co}_x)_{75}\text{B}_{10}\text{Si}_{15}$ ($0.00 \leq x \leq 0.12$) metallic glasses.

x at. %	IS (± 0.02) (mm/sec)	H_{eff} (RT) (± 3 KOe)	H (± 3 KOe)	H_p (± 3 KOe)	T_c^* (± 2 K)	HWHM (± 3 KOe)
0.00	0.054	254	242	262	682	49.5
0.02	0.082	237	239	254	712	48.0
0.04	0.075	248	236	254	717	47.5
0.06	0.074	250	236	254	737	47.3
0.08	0.077	251	237	257	728	46.7
0.10	0.064	255	239	261	739	46.2
0.12	0.083	252	237	259	723	46.2

* Values taken from DSC studies

5.4.3 Room temperature Mössbauer spectra of Fe-Ni-Mo-B-Si alloys :

The room temperature Mössbauer spectra of $\text{Fe}_{70}\text{Ni}_{12-x}\text{Mo}_x\text{B}_{16}\text{Si}_2$ ($0 \leq x \leq 4$) alloys are shown in Figure 5-5. As usual all the samples show broad peaks which is a characteristic feature of amorphous alloys due to random distribution of atoms. The asymmetries in the lines is evident from the figure which is also an observed feature in Fe-Co-B-Si alloys and other ferromagnetic metallic glasses (Bhatnagar et al, 1985). The average IS obtained by least square fitted peak positions of Fe-Ni-Mo-B-Si alloys are given in Table 5-3. These values lie between 0.10 to 0.26 ± 0.02 mm/sec. This coulombic shift in molybdenumless alloy ($x = 0$) is nearly half of that of Mo containing alloys.

Figure 5-5 also shows the distribution of hyperfine fields of $\text{Fe}_{70}\text{Ni}_{12-x}\text{Mo}_x\text{B}_{16}\text{Si}_2$ ($0 \leq x \leq 4$) alloys obtained for the RT Mössbauer spectra. The results have been reproduced after optimising the parameters required for the analysis, which gave rise to a minimum χ^2 value. The hyperfine field distribution shows a prominent peak at 272 KOe for $x = 0$ and the peak shifts slightly towards lower fields with the addition of Mo. Similar shift in hyperfine field distribution is observed in case of amorphous $\text{Fe}_{72}\text{Ni}_{10-x}\text{Mo}_x\text{B}_{16}\text{Si}_2$ alloys (Narendra Babu et al 1986). A relatively weak peak at ~150 KOe is observed for all the alloys and this peak does not increase with increase in Mo content. The

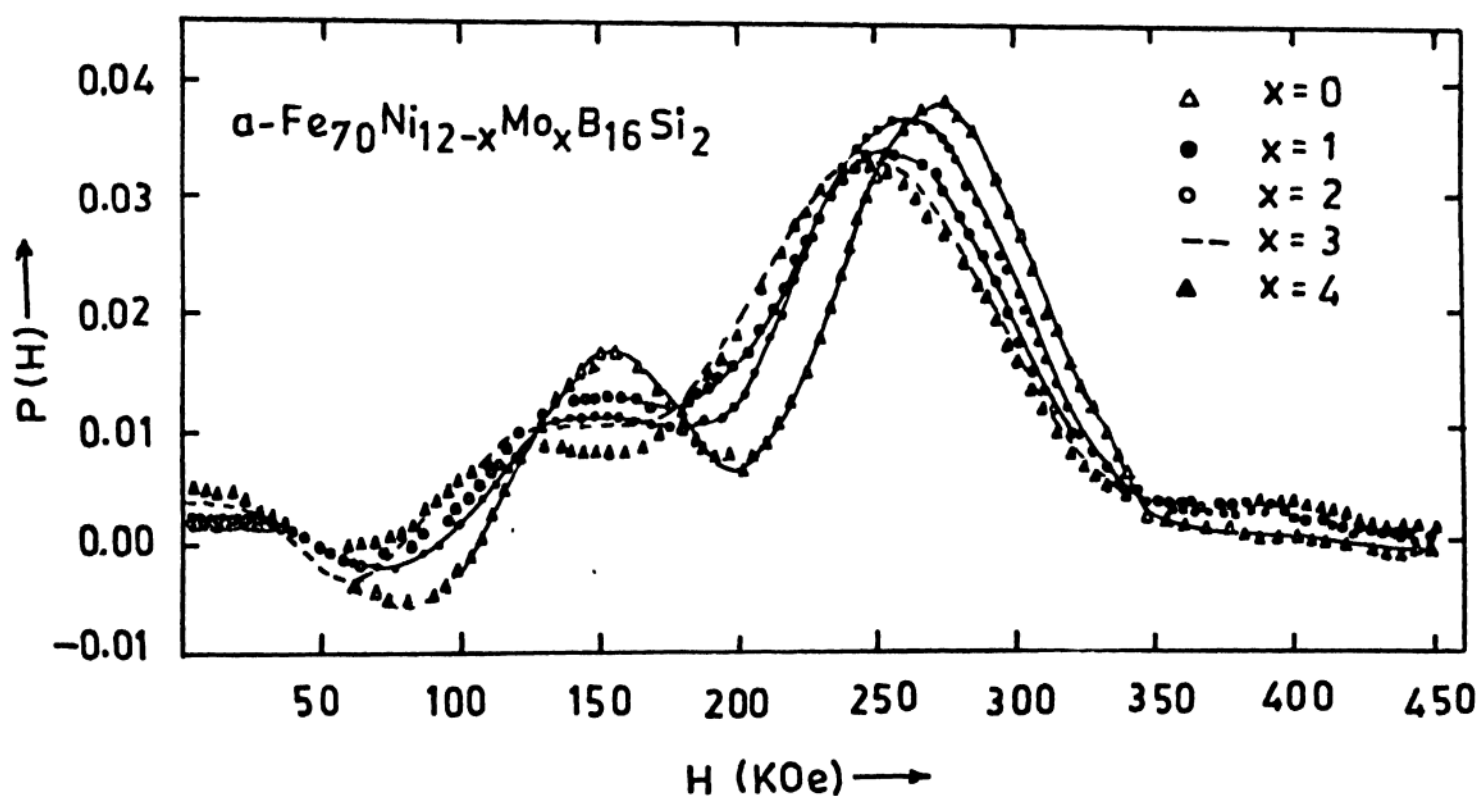
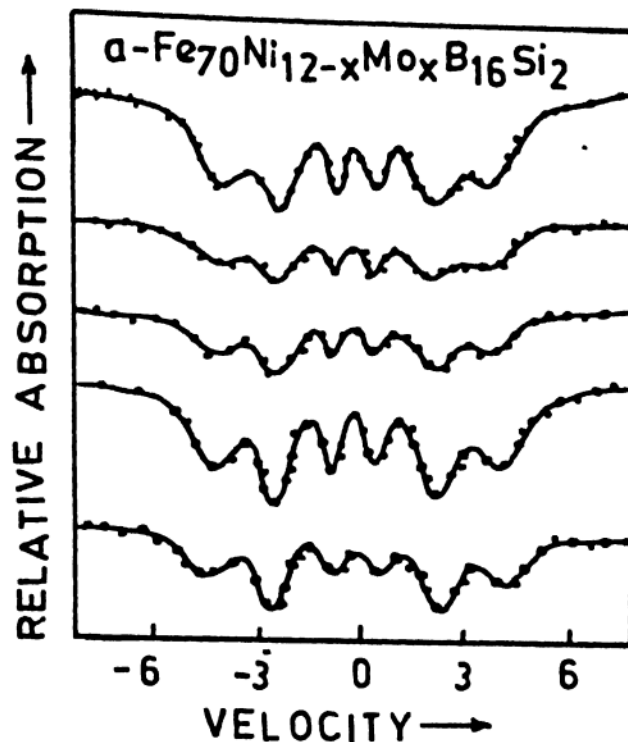


Fig. 5-5 : (a) Room temperature Mössbauer spectra of amorphous $\text{Fe}_{70}\text{Ni}_{12-x}\text{B}_{16}\text{Si}_2$ alloys.

(b) Distribution of hyperfine field of amorphous $\text{Fe}_{70}\text{Ni}_{12-x}\text{Mo}_x\text{B}_{16}\text{Si}_2$ alloys.

Table 5-3: Isomershift (IS), Curie temperature (T_c), $H_{eff}(RT)$, average hyperfine field (\bar{H}), most probable field (H_p), full width at half maximum (ΔH) and the ratio of average hyperfine field to the average magnetic moment, $\bar{H}/\bar{\mu}$ of amorphous $Fe_{70}Ni_{12-x}Mo_xB_{16}Si_2$ ($0 \leq x \leq 4$) alloys at room temperature.

Sample	IS (± 0.02) (mm/sec)	T_c (± 2) (K)	$H_{eff}(RT)$ (± 3) (KOe)	H_p (± 3) (KOe)	\bar{H} (± 3) (KOe)	ΔH (± 3) (KOe)	$\bar{H}/\bar{\mu}$ (± 0.1) KOe-gm/emu
$x = 0$	0.10	697	267	272	252	87.8	1.53
$x = 1$	0.18	668	256	260	241	94.0	1.52
$x = 2$	0.26	627	251	254	234	101.3	1.62
$x = 3$	0.20	587	245	250	227	108.0	1.60
$x = 4$	0.21	590	243	248	227	105.0	1.70

weak peak at the lower fields is a common observation for many metallic glasses and it depends on the fitting procedure (Chien et al 1979a and Dunlap et al 1985). The shift in the major peak position arises due to the change in the internal magnetic field with Mo content. A change in the peak width (ΔH) is observed with Mo addition. The ΔH increases by ~ 10 KOe per one Mo at.% up to $x = 3$. For $x = 4$ there is no significant change in ΔH from that of $x = 3$. At room temperature the effective hyperfine field is 267 ± 3 KOe for Mo less sample and H_{eff} decreases with the addition of Mo content as shown in Table 5-3. This is in contrast to the alloys $(\text{Fe}_x\text{Mo}_{1-x})_{75}\text{P}_{16}\text{B}_6\text{Al}_3$ (Chien et al 1979a) in which there is a drastic decrease with x .

The ratio of hyperfine field to saturation magnetization at room temperature is found to be $\sim 1.6 \pm 0.1$ KOe-gm/emu for these glasses. It has been previously reported (Chien 1981) that the measured values of the average hyperfine field H_{eff} and the average magnetic moment $\bar{\mu}_{\text{Fe}}$ of the iron-atoms are proportional to a good approximation, in iron-metalloid crystalline compounds, that is $\vec{H}_{\text{eff}} = a \vec{\mu}_{\text{Fe}}$, where $a \sim 130$ KOe/ μ_B and μ_B is the Bohr magneton. This is clearly shown in Fig.5-6. The data in the Figure are collected from Lischer et al (1974). Vincze et al (1974) and Raj et al (1978). Data on crystalline ferromagnetic compound Fe_3P (Lischer et al 1974) suggests that (i) the iron magnetic moment is determined mainly by the number of metalloid first neighbours, and (ii) H_{eff} at the ^{57}Fe nucleus is determined mainly by the magnetic moment of the parent Fe-atom. Figure 5-6

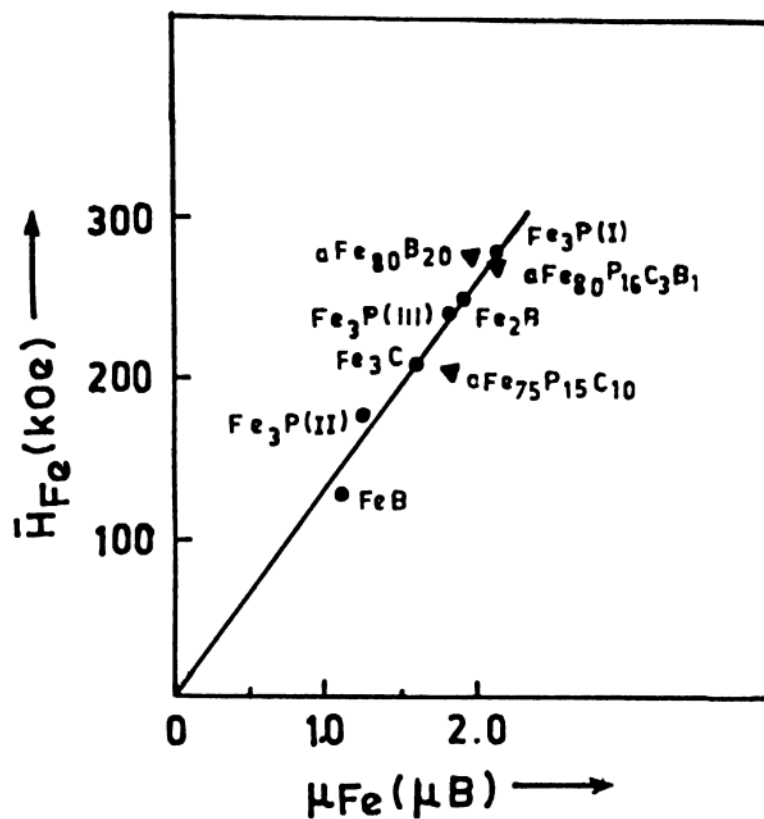


Fig. 5-6 : Average iron hyperfine field vs. average iron moment in some iron-metallloid crystalline compounds and amorphous alloys (a) for measurements at $T \leq RT$ (room temperature).

also shows that in iron-rich metallic glasses the average hyperfine fields are approximately proportional to the average magnetic moments with constant proportionality being approximately the same. The comparison may be regarded as semi-quantitative and suggested as a trend in view of the fact that it would be more appropriate to plot the data at very low temperatures to avoid any errors due to temperature dependence of the moments and the fields and different materials having different T_c .

Addition of 1.5 at.% of Co does not seem to change much the hyperfine field of $\text{Fe}_{75}\text{B}_{10}\text{Si}_{15}$ glass. Whereas, even 1 at.% of Mo addition shifts H_p towards lower fields side in $\text{Fe}_{70}\text{Ni}_{12-x}\text{Mo}_x\text{B}_{16}\text{Si}_2$ metallic glasses. This invokes that the Fe-magnetic moment is reducing by the addition of a non-magnetic atom.

5.4.4 Magnetization axis :

The direction of saturation magnetization, M_s of an iron-rich ferromagnetic alloy can be inferred from the ratio of intensities of the second (fifth) line to the first (sixth) line in the ^{57}Fe Mossbauer spectrum. The ratio is given by

$$\frac{A_{2,5}}{A_{1,6}} = \frac{4 \sin^2\theta}{3(1 + \cos^2\theta)} \quad 5-20$$

where θ is the angle between the 14.4 KeV gamma rays and the

direction of the magnetization. The values of $A_{2,5}/A_{1,6}$ vary from 0 to $4/3$ as θ changes from 0 to 90 degrees. If a sample contains more than one magnetization direction then the values of $A_{2,5}/A_{1,6}$ has to be averaged suitably. It is, therefore, possible to derive information about the magnetization axis from the Mössbauer spectrum. For a glassy sample since the six Mössbauer lines do not have the same line width, because of a hyperfine field distribution, one compares area ratios instead of line intensity ratios. For the same reason we have chosen to compare area ratios $(A_2+A_5)/(A_1+A_6)$ rather than A_2/A_1 or A_5/A_6 . These ratios are plotted in Figure 5-7, for $x = 0, 1, 2$ and 3 in case of $Fe_{70}Ni_{12-x}Mo_xB_{16}Si_2$ alloys as a function of temperature. It may be pointed out that all of our samples were clamped between two copper rings. Due to some unavoidable experimental difficulties, measurements could not be taken on the unclamped samples. Therefore, the area ratios as a function of temperature as shown in Figure 5-7 may not be true representatives of the behaviour of the magnetization axis, since the difference in thermal expansions of copper and a glassy sample would induce a stress in the sample which would change the magnetization axis in the sample. However, for the sake of completeness, we present and discuss these results. The area ratios for each glassy sample studied at the room temperature (RT) for Fe-Ni-Mo-B-Si alloys are listed in Table 5-4.

It has been previously reported by Chien (1978) that magnetization axis of glassy $Fe_{80}B_{20}$ and $Fe_{40}Ni_{40}P_{14}B_6$ lie in the

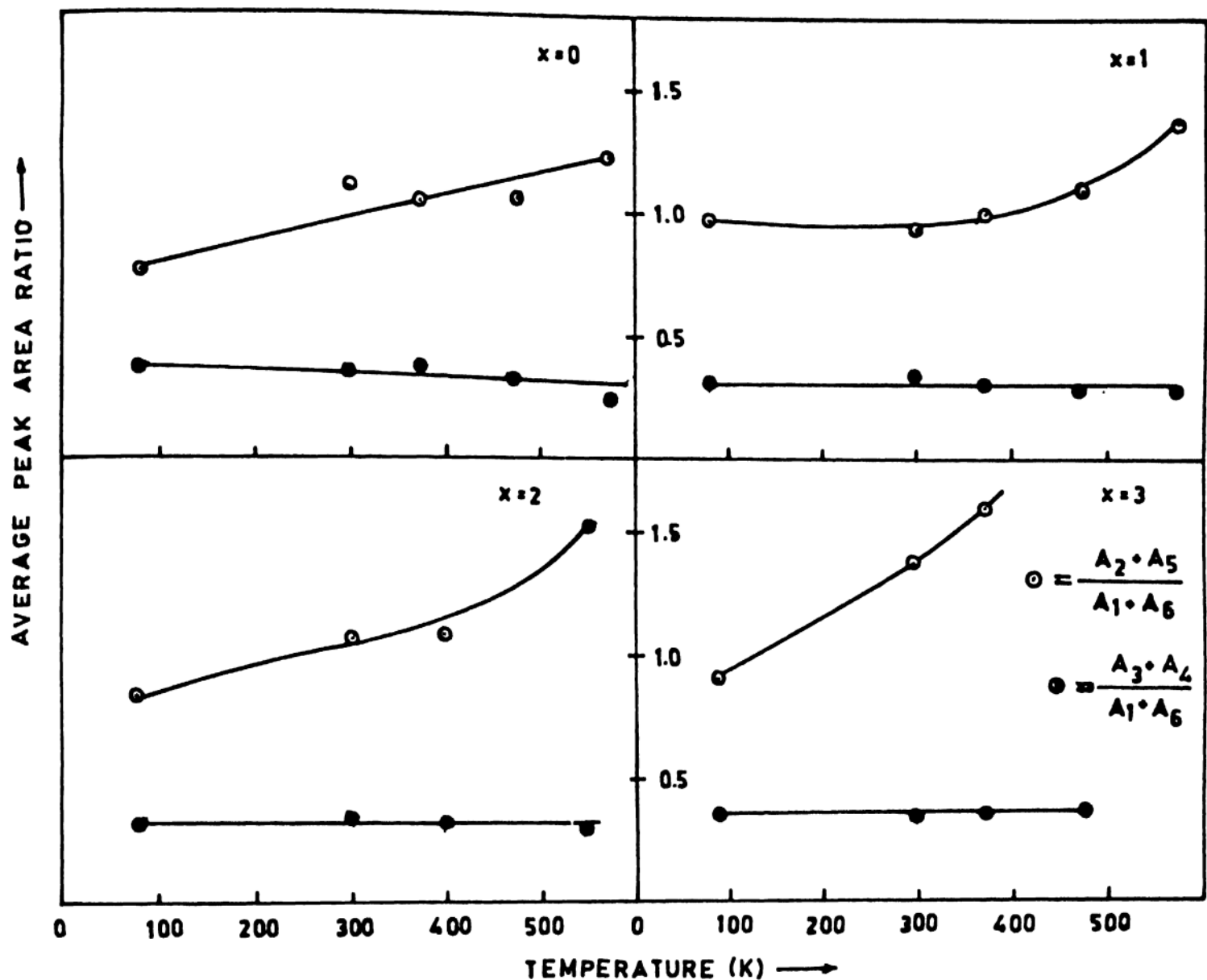


Fig. 5-7 : Average peak area ratios of spectral lines of amorphous $\text{Fe}_{70}\text{Ni}_{12-x}\text{Mo}_x\text{B}_{16}\text{Si}_2$ ($0 \leq x \leq 3$) alloys as a function of temperature where A_1 , A_2 , A_3 , A_4 , A_5 and A_6 are the areas of peaks 1, 2, 3, 4, 5, and 6 respectively.

Table 5-4: Area ratios of $\text{Fe}_{70}\text{Ni}_{12-x}\text{Mo}_x\text{B}_{16}\text{Si}_2$ ($0 \leq x \leq 3$) alloys at room temperature for the six peaks of Mössbauer spectrum. A_1 , A_2 , A_3 , A_4 , A_5 and A_6 represents the areas of six peaks in the Mössbauer spectrum.

x at. %	A_1 (10^5)	A_2 (10^5)	A_3 (10^5)	A_4 (10^5)	A_5 (10^5)	A_6 (10^5)	$\frac{(A_2+A_5)}{(A_1+A_6)}$	$\frac{(A_3+A_4)}{(A_1+A_6)}$
0	2.147	2.245	0.768	0.745	2.441	2.105	1.1021	0.356
1	3.908	3.262	1.119	1.325	3.678	3.445	0.9940	0.332
2	9.033	9.329	2.701	3.314	9.819	8.510	1.0915	0.343
3	7.305	9.156	2.121	2.728	10.099	6.617	1.3831	0.348

Table 5-5: Area ratios of $(\text{Fe}_{1-x}\text{Co}_x)_{75}\text{B}_{10}\text{Si}_{15}$ ($0.00 \leq x \leq 0.12$) alloys at room temperature for the six peaks of Mössbauer spectrum. A_1 , A_2 , A_3 , A_4 , A_5 and A_6 represents the areas of six peaks in the Mössbauer spectrum.

x at. %	A_1 (10^5)	A_2 (10^5)	A_3 (10^5)	A_4 (10^5)	A_5 (10^5)	A_6 (10^5)	$\frac{(A_2+A_5)}{(A_1+A_6)}$	$\frac{(A_3+A_4)}{(A_1+A_6)}$
0.00	10.298	7.777	3.325	3.317	8.750	10.495	0.795	0.319
0.02	3.586	3.137	1.072	1.021	3.460	3.429	0.940	0.298
0.04	2.709	3.259	0.603	0.820	3.360	2.696	1.225	0.263
0.06	5.850	6.166	1.662	1.904	6.530	6.145	1.058	0.297
0.08	7.131	6.866	2.029	2.120	7.460	6.771	1.031	0.299
0.10	5.330	5.464	1.745	1.611	6.050	5.393	1.074	0.313
0.12	13.855	13.755	4.168	4.352	14.792	13.794	1.033	0.308

plane of the ribbon, i.e., the value of $A_{2,5}/A_{1,6}$ ratio varies from 0.944 to 1.3831 depending upon the sample. This means that the magnetization axis is not in plane of the ribbon. This has also been reported for other samples like $Fe_{82}B_{12}Si_6$ (OK et al 1980) and $Fe_{81}B_{13.5}Si_{3.5}C_2$ (Saegusa et al 1982).

The room temperature area ratios for $(Fe_{1-x}Co_x)_{75}B_{10}Si_{15}$ ($0.00 \leq x \leq 0.12$) alloys are shown in Table 5-5. It is clear that the ratios of $A_{2,5}/A_{1,6}$ for all the alloys lie between 0.8 to 1.2 depending upon the sample. The similar observation in case of Fe-Ni-Mo-B-Si alloys reveals that as far as magnetization axis is concerned, there is not much change with respect to chemical composition in these metallic glasses. It is seen from the temperature dependence of area ratios for each sample as in Figure 5-7 that in each sample $A_{2,5}/A_{1,6}$ increases with temperature while the ratio $A_{3,4}/A_{1,6}$ remains essentially constant with temperature. A similar effect of temperature on the clamped sample was determined by a Saegusa et al (1982). OK et al (1980) have shown that the unclamped $Fe_{82}B_{12}Si_6$ sample does not show any temperature dependence of the magnetization axis. It is the stress induced in a clamped sample (due to differential thermal expansion) which is responsible for the observed temperature dependence of the magnetization axis. Hence the observed effect in our samples is obviously not an intrinsic effect. However, it is clear from RT measurements that the magnetization does not lie in the plane of the ribbon of any of the samples studied. Its direction is out of plane of the ribbon.

5.4.5 Thermal Scan Method :

Thermal scan method is used to detect Curie and crystallization temperatures at zero source velocity. The Curie temperature, T_c is the temperature above which the ferromagnetic order is destroyed, i.e., a ferromagnetic solid becomes paramagnetic. The crystallization temperature, T_x is the temperature at which the amorphous to crystalline transformation takes place. Experimentally, it is observed that the T_c for amorphous materials is always less than their crystalline counterparts. This implies that the T_c is decreased by amorphous nature although there are a few exceptions in rare-earth cobalt systems (Rhyne et al 1979).

Gubanov (1960b) has predicted that an increase or decrease of T_c can occur in amorphous magnetic alloys depending on the variation of J_{ij} , the exchange integral, with r_{ij} and on the shape of the radial distribution function (i and j refer to spin states i and j). Later, Kobe et al (1971 and 1972) showed that the structural fluctuations always lead to a decrease of T_c in agreement with experimental observations. A similar conclusion was drawn by Montgomery et al (1970) and Schreiber (1974) using temperature dependent Green functions. More recently, Slechta (1970) has shown that the structure fluctuations of the exchange can lead in principle to both a decrease or an increase of T_c as predicted by Gubanov (1960b).

The T_c of the iron-rich transition metal-metalloid glasses are always smaller than the ferromagnetic metal. The structural and chemical disorder affects T_c of glassy alloys tremendously. Substitution of the metals like Mo and Cr decreases the T_c of iron-rich metallic glasses by a large amount. We have measured the T_c of our samples using Mössbauer technique. The T_x also can be identified using this method. However, for T_x s this method may not be so accurate, as the change in slope of the counts versus temperature graph at T_x is sometimes not clearly traced. Also, it is very difficult to analyze the Mossbauer data near but below T_c , because of the overlap of lines resulting from the reduced H_{eff} and possibly line broadening due to relaxation effects. Therefore, T_c in this method is determined by an extrapolation of the $H_{eff}(T)$ vs. T curve to the value $H_{eff} = 0$ as shown in Fig. 5-8. So, the error in the determination of T_c in this method is usually large. This is the reason why we have concentrated on thermal scan method and DSC for conforming T_c s and T_x s of our metallic glasses.

In thermal scan method, the velocity of the transducer is set at zero which corresponds to the line position of the higher velocity component of the quadrupole doublet just above T_c . The counts are recorded for a fixed time of about 30 sec. while the temperature is raised at a fixed heating rate of approximately 5 K/min from 300 to 900 K. The results of the thermal scan for $Fe_{72}Co_3B_{10}Si_{15}$ and $Fe_{70}Ni_{10}Mo_2B_{16}Si_2$ alloys are as shown in Figures 5-9 and 5-10.

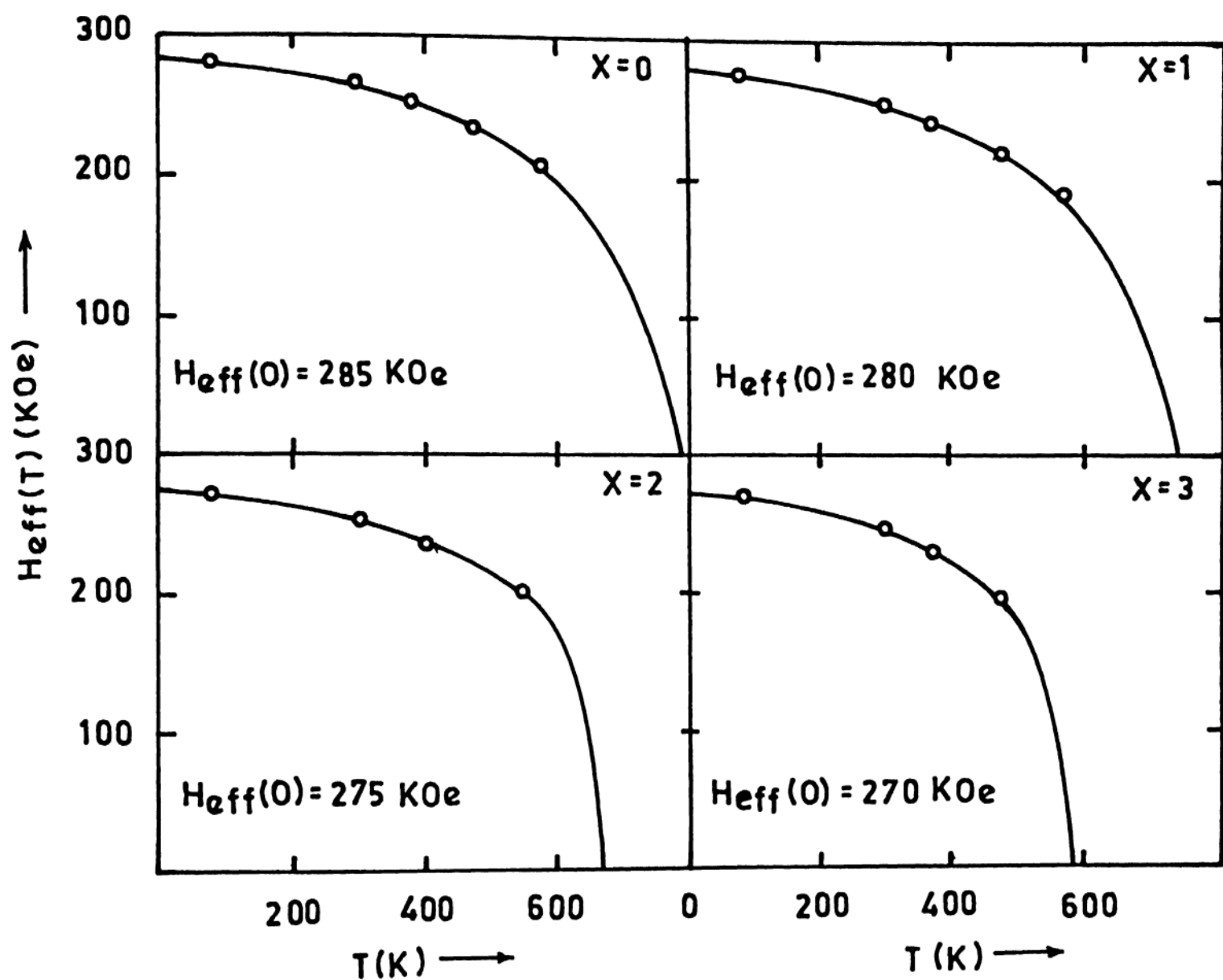


Fig. 5-8 : Temperature dependence of hyperfine field, H_{eff} of amorphous $\text{Fe}_{70}\text{Ni}_{12-x}\text{Mo}_x\text{B}_{16}\text{Si}_2$ alloy.

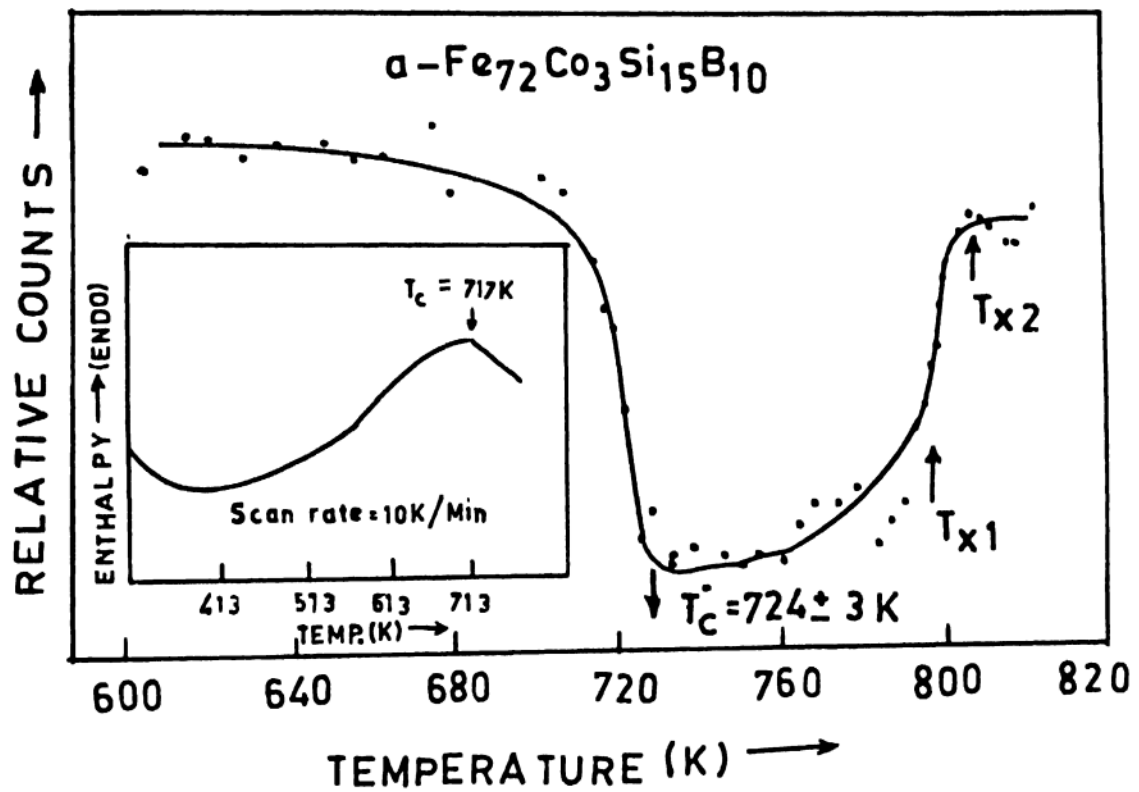


Fig. 5-9 : Counts measured for 30 sec. at zero Doppler velocity as a function of temperature of amorphous $\text{Fe}_{72}\text{Co}_3\text{B}_{10}\text{Si}_{15}$ alloy.

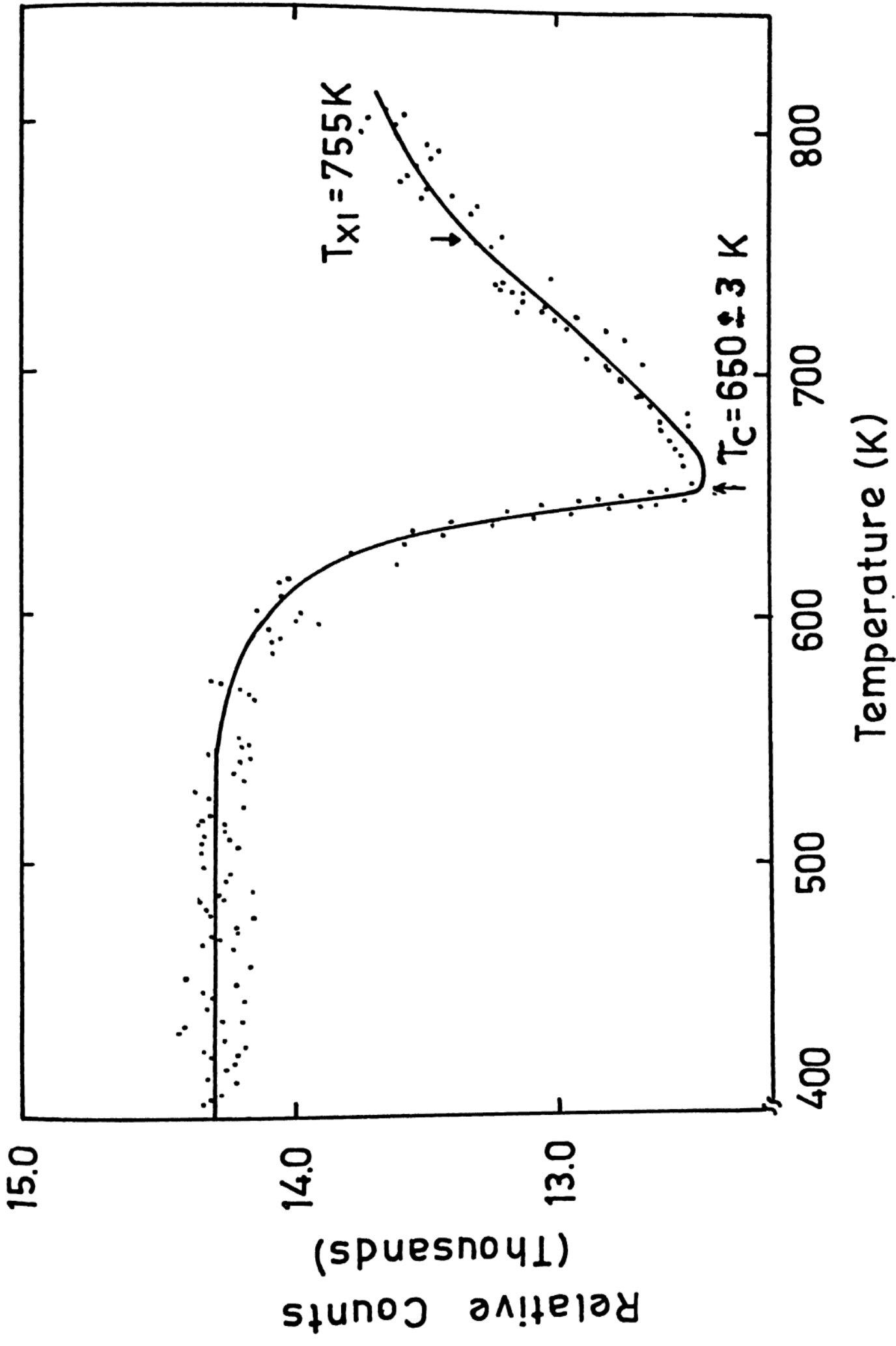


Fig. 5-10 : Counts measured for 30 sec. at zero Doppler velocity as a function of temperature of amorphous $\text{Fe}_{72}\text{Ni}_{10}\text{Mo}_2\text{B}_{16}\text{Si}_2$ alloy.

When the magnetic ordering starts disappearing the count rate starts falling, till then the count rate was almost constant. The T_c for $\text{Fe}_{72}\text{Co}_3\text{B}_{10}\text{Si}_{15}$ alloy is around 724 ± 3 K by this method. The insert in the Figure 5-9 shows the DSC scan at the heating rate of 10 K/min has the T_c around 717 ± 3 K for $\text{Fe}_{72}\text{Co}_3\text{B}_{10}\text{Si}_{15}$ metallic glass. The difference in T_c can be attributed to the difference in heating rates, the more the annealing the higher the T_c in these materials (Fig. 3-11). Hence, for lesser heating rates in Mössbauer measurements the T_c is showing higher values. The T_x s are identified as the temperature where the count vs. temperature graph starts changing its slope. The T_c s are in good agreement with in the experimental error with the T_c s obtained by DSC and resistivity measurements for the respective samples (chapter 3). For $\text{Fe}_{70}\text{Ni}_{10}\text{Mo}_2\text{B}_{16}\text{Si}_2$ alloy the T_c is around 650 ± 3 K and the T_{x1} is around 755 K by thermal scan method. Further details of T_c s and T_x of $(\text{Fe}_{1-x}\text{Co}_x)_{75}\text{B}_{10}\text{Si}_{15}$ ($0.00 \leq x \leq 0.12$) and $\text{Fe}_{70}\text{Ni}_{12-x}\text{Mo}_x\text{B}_{16}\text{Si}_2$ ($0 \leq x \leq 3$) alloys are discussed in the chapter 3.

5.4.6 Temperature dependence studies of Mössbauer spectra of Fe-Ni-Mo-B-Si alloys :

The Mössbauer studies on $\text{Fe}_{70}\text{Ni}_{12-x}\text{Mo}_x\text{B}_{16}\text{Si}_2$ ($0 \leq x \leq 3$) alloys in the temperature range 80 K to T_c (see Table 5-1 for T_c values) have been carried out and shown in Figures 5-11, 5-12, 5-13 and 5-14. As usual all the samples show six broad peaks which is a common observation for ferromagnetic metallic glasses.

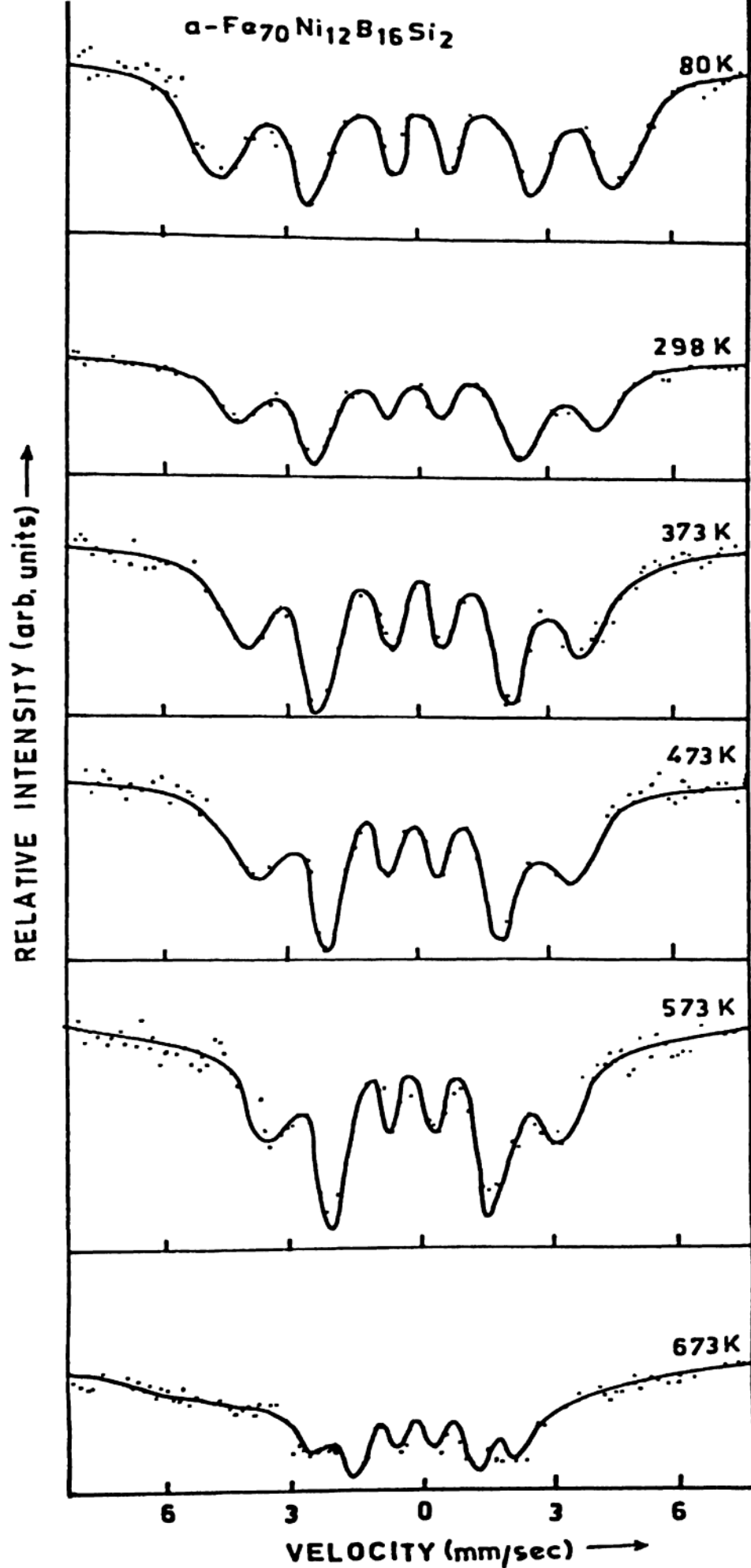


Fig. 5-11 : Mössbauer spectra of amorphous $\text{Fe}_{70}\text{Ni}_{12}\text{B}_{16}\text{Si}_2$ alloy at different temperatures.

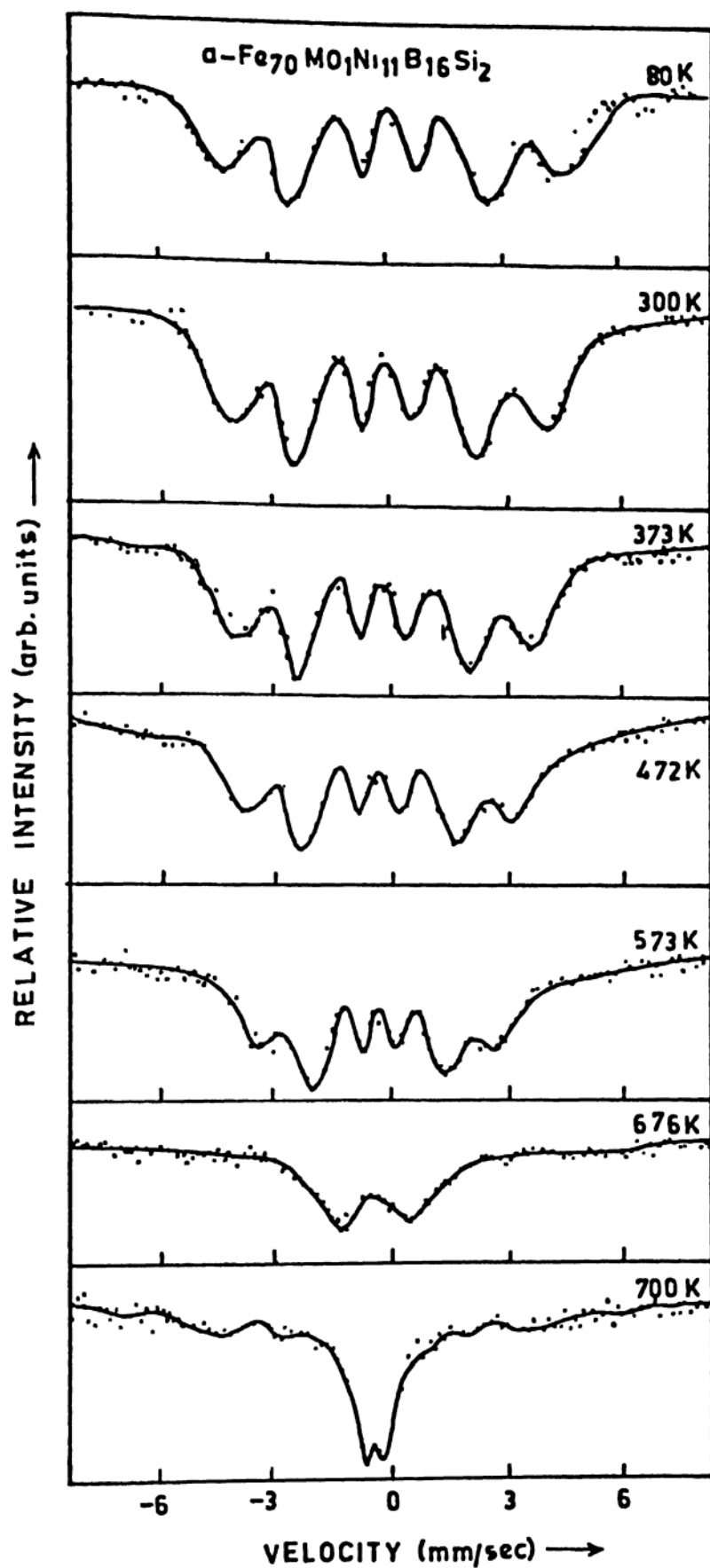


Fig. 5-12 : Mössbauer spectra of amorphous $\text{Fe}_{70}\text{Mo}_1\text{Ni}_{11}\text{B}_{16}\text{Si}_2$ alloy at different temperatures.

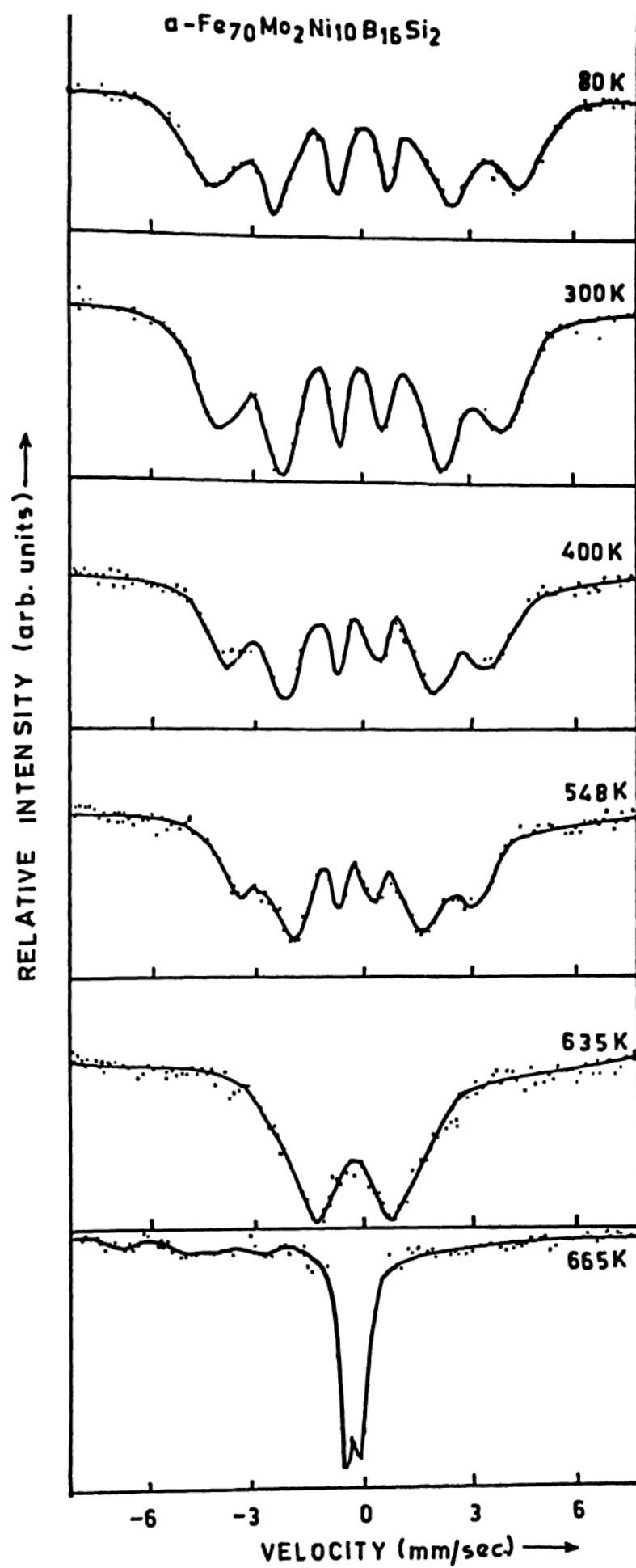


Fig. 5-13 : Mössbauer spectra of amorphous $\text{Fe}_{70}\text{Mo}_2\text{Ni}_{10}\text{B}_{16}\text{Si}_2$ alloy at different temperatures.

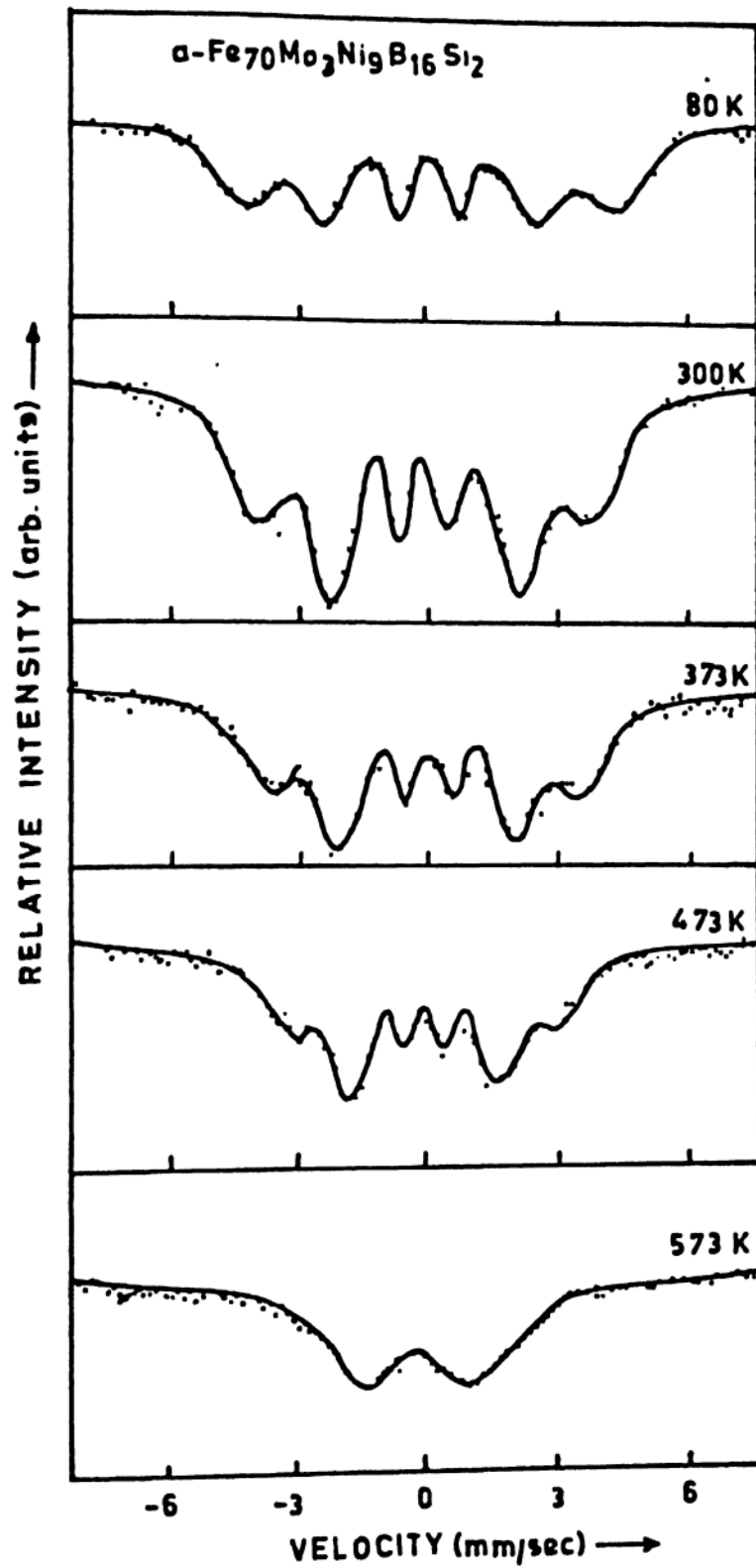


Fig. 5-14 : Mössbauer spectra of amorphous $\text{Fe}_{70}\text{Mo}_3\text{Ni}_9\text{B}_{16}\text{Si}_2$ alloy at different temperatures.

Here the line widths at room temperature for all the compositions from $x = 1$ to 3 are $\Gamma_1 > \Gamma_6$, $\Gamma_2 < \Gamma_5$, $\Gamma_3 < \Gamma_4$. The values of $1S$, T_c , $H_{eff}(RT)$, H_{mean} , H_p and H are tabulated in Table 5-3. In the following sections we discuss about the temperature dependence of magnetic hyperfine fields, isomer shifts and line widths of these metallic glasses.

5.4.6a Magnetic hyperfine interactions :

The temperature dependence of magnetic hyperfine interactions are calculated for $Fe_{70}Ni_{12-x}Mo_xB_{16}Si_2$ alloys for $x = 0, 1, 2$ and 3. The absence of long range crystalline order in metallic glasses is responsible for a distribution of hyperfine interaction parameters which broaden Mössbauer lines. We have analysed the data with $M = 9$ corresponding to the minimum x^2 . The results of the analysis carried out for the spectra of these amorphous alloys between 80 to 573 K are shown in Figures 5-15 and 5-16. The parameters evaluated like full width at half maximum (FWHM), mean field (H), peak field (H_p), effective hyperfine field ($H_{eff}(T)$) and the corresponding x^2 are tabulated in Tables 5-6, 5-7, 5-8 and 5-9 for $x = 0, 1, 2$ and 3 respectively. It is observed that H and H_p and FWHM decreases for $x = 0$ from 80 to 573 K continuously and for $x = 1, 2$ and 3, FWHM is almost a constant with temperature. However, the FWHM increases with increase in Mo concentration (Fig. 5-5). The $H_{eff}(T)$ values calculated directly from the spectra, coincides well with H_p values evaluated from $P(H)$ analysis within the

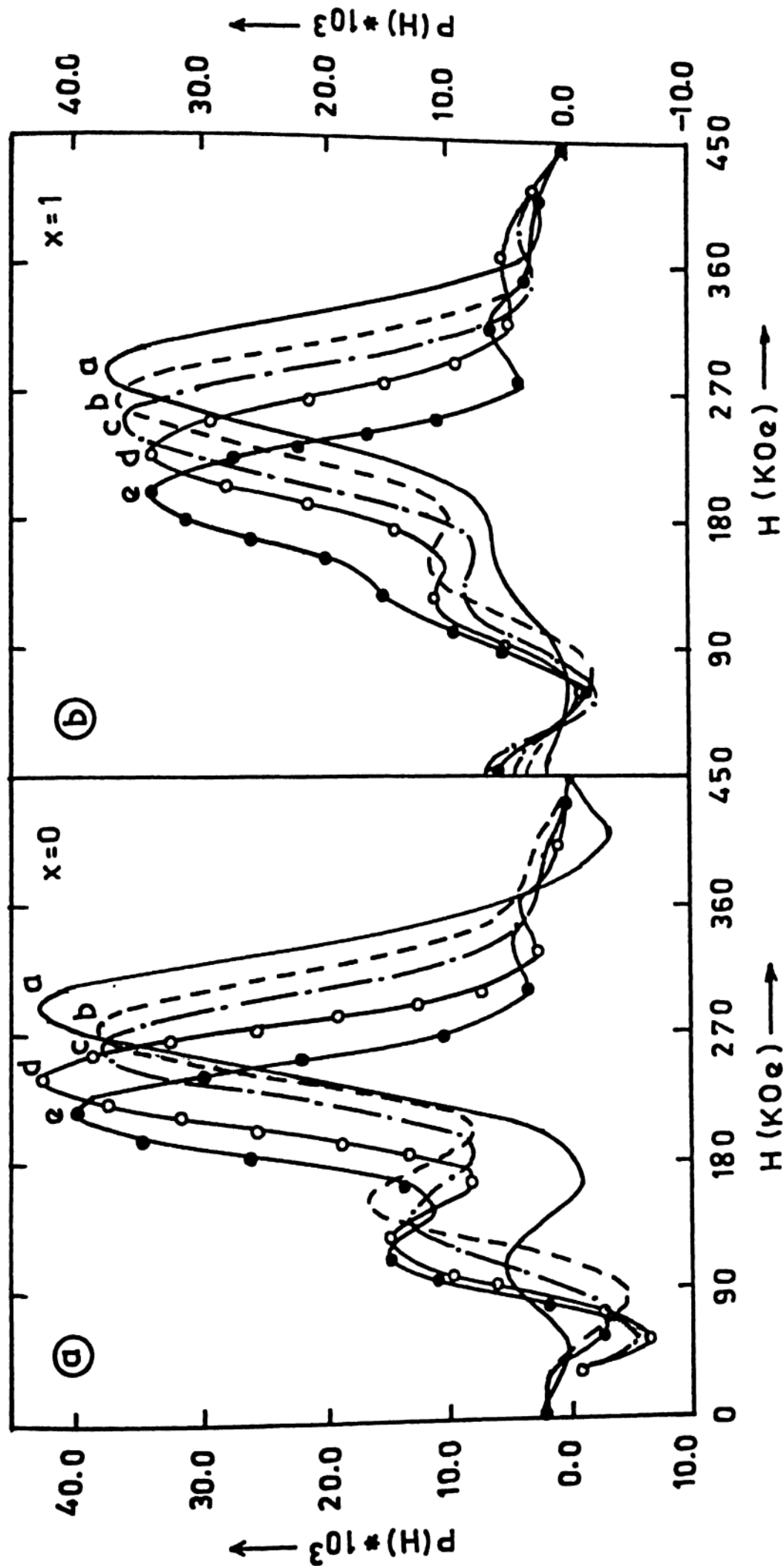


Fig. 5-15 : Hyperfine field distribution, $P(H)$ of amorphous $\text{Fe}_{70}\text{Ni}_{12-x}\text{B}_{16}\text{Si}_2$ alloys for $M = 9$.

- (a) For $x = 0$ at temperatures 80 K (a), 298 K (b), 373 K (c), 473 K (d) and 573 K (e)
 (b) For $x = 1$ at temperatures 80 K (a), 300 K (b), 373 K (c), 472 K (d) and 573 K (e)

Table 5-6: Temperature (T), most probable field (H_p), average field (\bar{H}), hyperfine field (H_{eff}) and full width at half maximum (ΔH) of $Fe_{70}Ni_{12-x}Mo_xB_{16}Si_2$ alloys.

Sample $x = 0$:

TEMP. (± 2 K)	H_p (± 3 KOe)	\bar{H} (± 3 KOe)	$H_{eff}(RT)$ (± 3 KOe)	ΔH (± 3 KOe)	x^2 (± 0.05)
80	288.0	266.4	280.0	92.3	1.22
298	272.0	252.0	267.0	87.8	1.25
373	261.0	238.7	253.2	85.5	1.14
473	240.8	213.4	232.5	78.8	1.31
573	216.0	208.5	209.4	76.5	1.70

Table 5-7: Temperature (T), most probable field (H_p), average field (\bar{H}), hyperfine field (H_{eff}) and full width at half maximum (ΔH) of $Fe_{70}Ni_{12-x}Mo_xB_{16}Si_2$ alloys.

Sample $x = 1$:

TEMP. (± 2 K)	H_p (± 3 KOe)	\bar{H} (± 3 KOe)	H_{eff} (RT) (± 3 kOe)	ΔH (± 3 kOe)	x^2 (± 0.05)
80	283.5	260.3	274.5	99.0	1.32
300	260.0	240.7	256.0	94.0	1.10
373	247.5	230.8	238.8	90.0	1.19
472	225.0	218.6	218.6	94.5	1.39
573	198.0	196.8	191.7	94.5	1.36

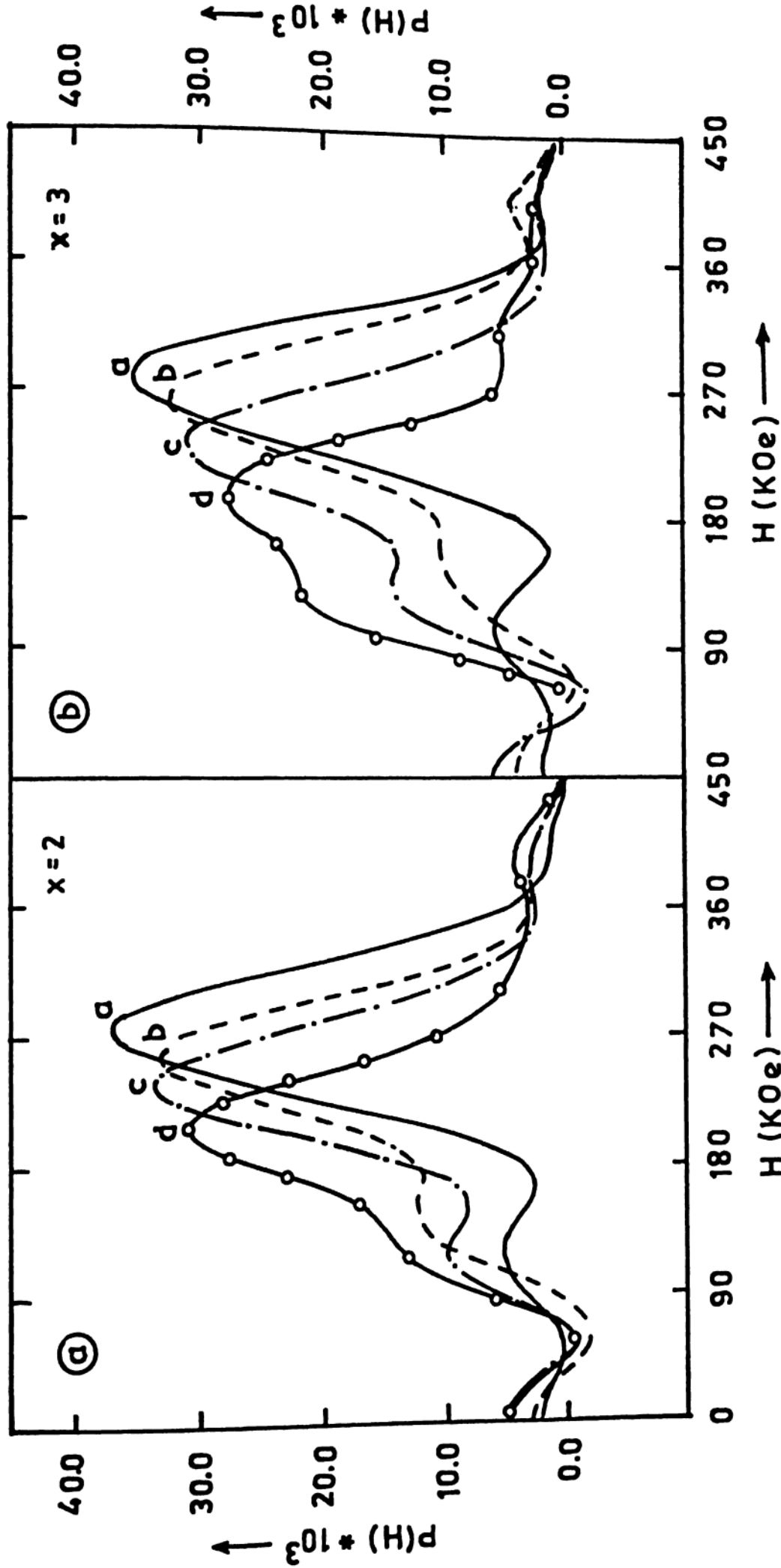


Fig. 5-16 : Hyperfine field distribution, $P(H)$ of amorphous $\text{Fe}_{70}\text{Ni}_{12-x}\text{MoB}_x\text{Si}_{16}\text{I}_2$ alloys for $M = 9$.

- (a) For $x = 2$ at temperatures, 80 K (a), 300 K (b), 400 K (c) and 548 K (d).
 (b) For $x = 3$ at temperatures, 80 K (a), 300 K (b), 373 K (c) and 473 K (d).

Table 5-8: Temperature (T), most probable field (H_p), average field (\bar{H}), hyperfine field (H_{eff}) and full width at half maximum (ΔH) of $Fe_{70}Ni_{12-x}Mo_xB_{16}Si_2$ alloys.

Sample $x = 2$:

TEMP. (± 2 K)	H_p (± 3 KOe)	\bar{H} (± 3 KOe)	$H_{eff}(RT)$ (± 3 kOe)	ΔH (± 3 kOe)	x^2 (± 0.05)
80	274.5	254.6	269.3	103.5	1.30
300	254.0	234.0	250.6	101.3	1.21
400	236.3	232.6	221.2	101.3	1.20
548	207.0	204.2	206.0	103.5	1.20

Table 5-9: Temperature (T), most probable field (H_p), average field (\bar{H}), hyperfine field (H_{eff}) and full width at half maximum (ΔH) of $Fe_{70}Ni_{12-x}Mo_xB_{16}Si_2$ alloys.

Sample $x = 3$:

TEMP. (± 2 K)	H_p (± 3 KOe)	\bar{H} (± 3 KOe)	H_{eff} (RT) (± 3 KOe)	ΔH (± 3 KOe)	χ^2 (± 0.05)
80	276.8	251.1	268.8	108.0	1.62
300	250.0	227.0	245.0	108.0	1.51
373	229.5	207.6	228.5	108.0	1.09
473	193.5	188.6	195.0	108.0	1.37

experimental accuracy. This suggests that the values of H_p evaluated from the analysis of the spectra are reasonably correct.

In the simple glasses like Fe_xB_{100-x} ($72 \leq x \leq 86$) the peak in $P(H)$ is usually symmetric, and shifts towards higher H_p as x increases (Chien et al 1979b). This is expected since the moment of Fe will scale with x . Since $\langle H_{eff} \rangle$ is approximately proportional to μ , it is clear that a distribution of H_{eff} values in the amorphous glasses refer to a distribution of magnetic moments. For example, the magnetic moments in amorphous $Fe_{80}P_{14}B_6$ have a range from $1.3 \mu_B$ to $2.4 \mu_B$ (Chien et al 1978b), the upper value of μ being greater than the moment of α -Fe ($2.2 \mu_B$). This distribution in μ has been derived from the hyperfine field distribution. The effect of adding other transition metals or different metalloids like Ni, P, B, Mo and Al etc., gave rise to different types of $P(H)$ distribution. For example, the $P(H)$ obtained for amorphous $Fe_{40}Ni_{40}P_yB_{20-y}$ (Chien et al 1978a) alloys show that in the absence of phosphorous the $P(H)$ curve is slightly assymmetric when compared to $Fe_{80}B_{20}$ amorphous alloy and the presence of P slightly increases the assymetry and shows very small shoulders at lower temperatures. Here the H_p does not seem to shift towards lower fields. But if we change Ni concentration in amorphous Fe-Ni-P-B alloys keeping P and B as constants, the H_p seems to shift towards lower fields (Chien et al 1978a).

The $P(H)$ distribution of Mo containing alloys seems to be quite different of all the above mentioned systems. For instance, in case of $(\text{Fe}_x\text{Mo}_{1-x})_{75}\text{P}_{16}\text{B}_6\text{Al}_3$ amorphous alloys (Chien et al 1979a) and for $x = 1$, a major peak is seen at 300 KOe and a insignificant structure at lower fields. As Mo concentration increases the amplitude of the smaller peak grows at the expense of the amplitude of the major peak. For $x = 0.7$, the lower field outgrows the high field peak. This peak at low field represents the fraction of Fe-atoms that do not experience a hyperfine field and this fraction increases as x decreases. In case of amorphous $\text{Fe}_{39}\text{Ni}_{39}\text{Mo}_4\text{B}_{16}\text{Si}_2$ alloy the lower peak (lower field side) seems to become prominent with increase in temperature (~ 451 KOe) and it has been attributed due to the iron sites containing Mo near neighbours giving rise to an antiferromagnetic interaction (Bhanu prasad et al 1987). Similarly in amorphous $\text{Fe}_{72}\text{Ni}_{10-x}\text{Mo}_x\text{B}_{16}\text{Si}_2$ alloys (Narendra Babu et al 1986) for $x = 2$ and 6, the ΔH is found to be 112 and 140 KOe respectively, which are significantly larger than the value of $\Delta H \approx 90$ KOe obtained for other metallic glasses containing no transition metal other than iron, cobalt and nickel, is definitely indicative of a bimodal distribution due to contribution to the hyperfine field from nearest and next nearest neighbours due to the presence of Mo which can give rise to an antiferromagnetic exchange interaction with the other transitional metal ions (Narendra Babu et al 1986).

It is quite interesting to see that in $\text{Fe}_{70}\text{Ni}_{12}\text{B}_{16}\text{Si}_2$ alloy

the ΔH decreases with increase in temperature indicating a common ordering temperature for all the ions. If the temperature dependence of the hyperfine field for ions is identical, then H should decrease and hence the ΔH decreases steadily as one goes from low temperatures to near T_c . This may be the reason for the decrease in ΔH in case of $x = 0$ in Fe-Ni-Mo-B-Si alloys. The dominant contribution to $P(H)$ arises mainly from the iron-iron and iron-nickel ferromagnetic interaction (Hatherly et al 1964). They derived the exchange integral between atom pairs in iron-nickel alloy from experiments on the spin-wave scattering of neutrons. They have determined the second moment of the exchange integral between atom pairs to be $J_{Fe-Fe}^{(2)} = -9$ meV, $J_{Fe-Ni}^{(2)} = 39$ meV and $J_{Ni-Ni}^{(2)} = 52$ meV. In addition to the large difference in the values of the exchange integral between atom pairs, the range of the exchange interaction is a very important factor in considering the fluctuation of the exchange field. If the exchange interaction is a very long-range one, the local fluctuation of the exchange field should be small even if the exchange interaction between different kinds of atom pairs has large differences, so that the magnetization and hence the internal field has no distribution at high temperatures. On the other hand, when the interaction is a very short-range one, i.e., if only the nearest neighbour interaction is dominant, the alloy should have a large local fluctuation of the exchange field according to the neighbouring atomic configuration. Thus the variations in the near-neighbour environment also causes a distribution in exchange fields throughout the material, and as a

result different ions may have hyperfine fields that show quite different temperature dependences (Tomiyoshi et al 1971 and Jaccarino et al 1964). In general this will have a tendency to cause ΔH to increase as the temperature increases.

In all other ($x = 1, 2$ and 3) cases the $P(H)$ distribution gave rise to two peaks, one major peak at higher field and one minor peak at lower field (around 90 to 100 KG). The minor peak has been suggested to be due to an artifact effect in the method of analysis (Moorjani et al 1984). The major peak is much more sensitive to temperature effect shifting to lower values with increase in temperature. This is to be expected as the hyperfine field decreases with increase in temperature. The minor peaks are fairly temperature sensitive. For $x = 0$, the major peak is quite symmetric, The FWHM decreases systematically with increase in temperature. For this observation we take those distributions, where the artifact effect will cause any error in determining FWHM. For $x = 1, 2$ and 3 samples, the major peak is significantly assymmetric even at the lowest temperature, where the artifact effect is far away from the major peak. This clearly shows that there is a bimodality in the distribution of hyperfine field. With increase in temperature, the line width for the $P(H)$ distribution remains more or less constant. Any small fluctuation may arise on account of the error in determining the line width in all assymmetric profile with bimodal distribution suggested. The sudden increase in FWHM for high temperature data arises due to overlap of the major peak with the minor peak attributed to

the artifact effect. This may therefore be omitted for discussion purposes. The bimodality in the major peak arises due to the presence of Mo. Molybdenum, which is a second row transition-metal like Cr and V in the first row can contribute to Fe-Mo antiferromagnetic exchange interactions and magnetic dilution effects contributing to the distribution in the lower field region and thereby giving rise to the bimodal distribution. The temperature dependence of the width of the distribution can be attributed to different fields having different temperature dependences. This is also suggested by the temperature dependence of line widths as discussed later wherein it is concluded that the long-range and short-range order interactions are important for those alloys in which Mo is present.

5.4.6b Temperature dependence of isomer shift :

The temperature dependence of isomer shift for amorphous $\text{Fe}_{70}\text{Ni}_{12-x}\text{Mo}_x\text{B}_{16}\text{Si}_2$ ($0 \leq x \leq 3$) alloys are studied and discussed in the following section. The details about the isomer shift has already been discussed in section 5.3. Briefly, this is a shift of the centroid of the spectrum of an absorber with respect to the source. This shift arises from the coulombic interaction of the nuclear charge density at the nucleus. As a result, the nuclear energy levels of the Mossbauer nucleus become shifted by a small but measurable amount ($\sim 10^{-4}$). The isomer shift, δ for a given Mossbauer nucleus is a measure of the relative s-electron density at the nucleus and hence provides information concerning

the valence state of the Mossbauer nuclei in the solid. The temperature dependence of IS can yield an estimate of the Debye temperature of the solid.

The IS of the samples ($x = 0, 1, 2$ and 3) at RT are 0.10, 0.18, 0.26 and 0.20 mm/sec, respectively. The temperature dependence of the isomer shift for these alloys are plotted in Fig. 5-17 and the values are listed in Table 5-10. This temperature dependent shift arises due to the thermal motion of the Mossbauer nuclei and is referred to as the second order Doppler effect. No doubt, there is a distribution in all the hyperfine parameters including isomer shift in an amorphous system. But, the simple LSF values should in principle correspond to isomer shift of maximum probability. So, analysis of temperature dependence of the IS data obtained should throw light on whether the amorphous solids can be approximated to a Debye model, an approximation of the harmonic force coupling between the atoms gives rise to a linear temperature dependence of IS (Wertheim 1964) given by $d(IS)/dT = -(3k_0/2MC^2)E_\gamma$, where k_0 is the Boltzmann constant, M is the atomic mass of the nucleus and E_γ is the energy of unperturbed gamma rays (Josephson 1960). For ^{57}Fe Mossbauer nucleus ($E_\gamma = 14.4$ KeV), the theoretical value of the slope is -7.3×10^{-4} mm/sec-K (Ok et al 1980). A computer fit to our experimental points for $\text{Fe}_{70}\text{Ni}_{12-x}\text{Mo}_x\text{B}_{16}\text{Si}_2$ ($x = 0, 1, 2$ and 3) alloys gives the slopes as $-(6.05, 6.10, 5.39$ and $6.45) \times 10^{-4}$ mm/sec-K, respectively, which within experimental accuracy is in the value quoted above. Thus one may

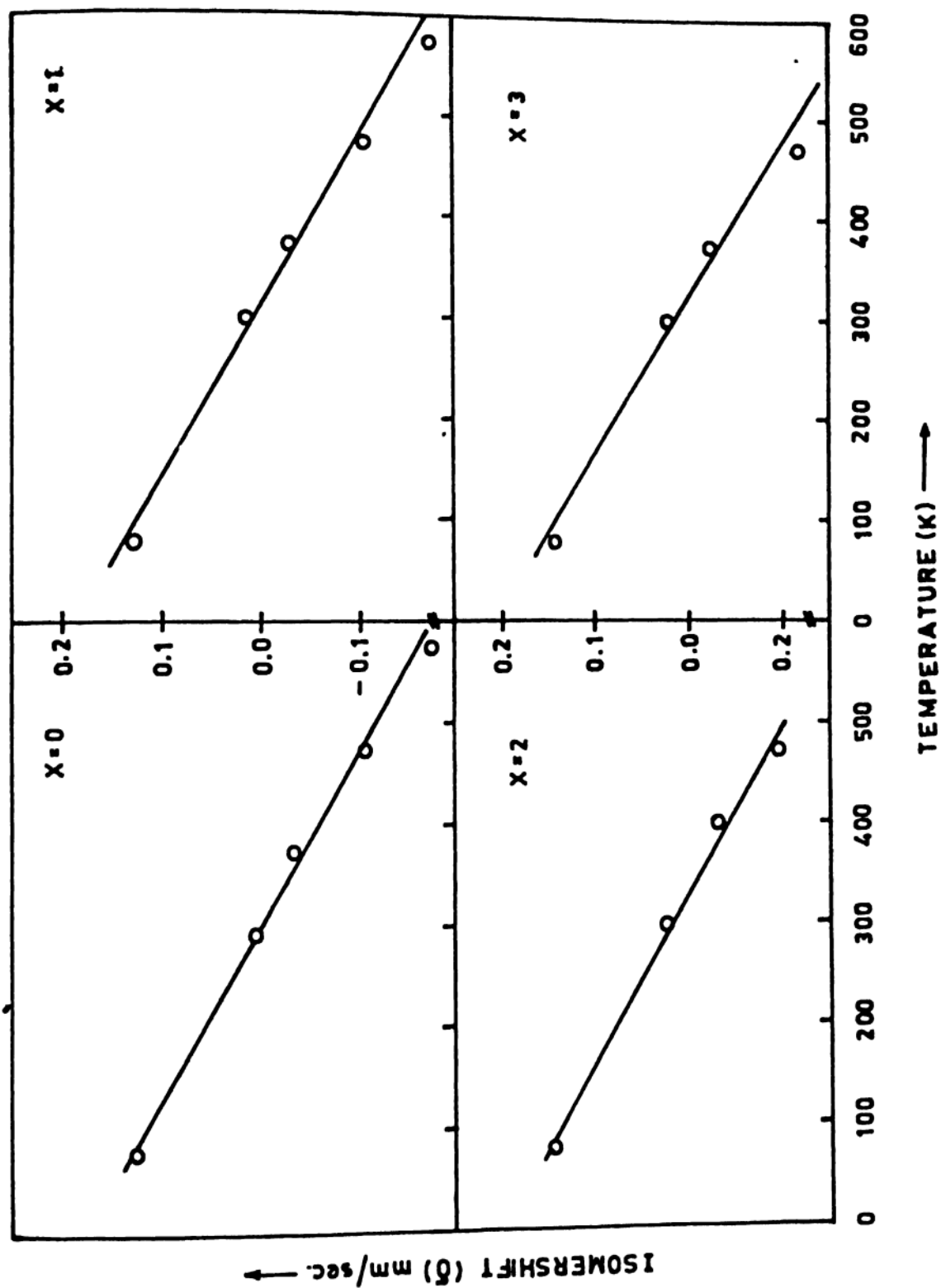


Fig. 5-17 : Temperature dependence of isomer shift of amorphous $\text{Fe}_{70}\text{Ni}_{12-x}\text{MoB}_x\text{Si}_2$ alloys ($x = 0, 1, 2$ and 3).

Table 5-10 : Temperature dependence of Isomershift of $\text{Fe}_{70}\text{Ni}_{12-x}\text{Mo}_x\text{B}_{16}\text{Si}_2$ ($0 \leq x \leq 3$) alloys.

x = 0		x = 1		x = 2		x = 3	
TEMP.	IS	TEMP.	IS	TEMP.	IS	TEMP.	IS
(+2)	(± 0.02)	(+2)	(± 0.02)	(+2)	(± 0.02)	(± 5)	(± 0.02)
(K)	(mm/s)	(K)	(mm/s)	(K)	(mm/s)	(K)	(mm/s)
80.0	0.13	80.0	0.13	80.0	0.15	80.0	0.14
298.0	0.01	300.0	0.02	300.0	0.03	300.0	0.02
373.0	-0.03	373.0	-0.03	400.0	-0.03	373.0	-0.03
473.0	-0.10	472.0	-0.10	548.0	-0.10	473.0	-0.12
573.0	-0.17	573.0	-0.17	----	-----	-----	-----

Infer that the coupling between atoms in these metallic glasses is harmonic to a good approximation.

5.4.6c Temperature dependence of line widths :

As per earlier discussions, it is well known that the first and sixth lines of a Mössbauer spectrum shows large line widths, which are due to a distribution in hyperfine fields present in the Mössbauer probe. Therefore, they are a measure of $P(H)$. A study of temperature dependence of the line width of the outermost lines can also provide information regarding IS, FWHM in $P(H)$ as well as the short-range or long-range magnetic interactions present in the sample. As the temperature is increased the line width of the outermost lines may vary in one of the following ways. (a) If $H_{\text{eff}}(T)/H_{\text{eff}}(0)$ has similar temperature dependence for all possible sites, then the line width will decrease monotonically. (b) The decrease of $H_{\text{eff}}(T)/H_{\text{eff}}(0)$ is faster for small values of H_{eff} . In this situation the line width will increase first and then decrease near T_c . (c) $H_{\text{eff}}(T)/H_{\text{eff}}(0)$ is slower for the small values of H_{eff} . This results in decrease of the line width first followed by an increase before another decrease as T tends to T_c .

Balogh (1978) has analyzed the behaviour of magnetic moment versus temperature. Case (a) is the narrow distribution of exchange interactions where the values fall monotonically, the distribution also fall monotonically and converges at T_c . This is the case where all the magnetic moments has the same temperature

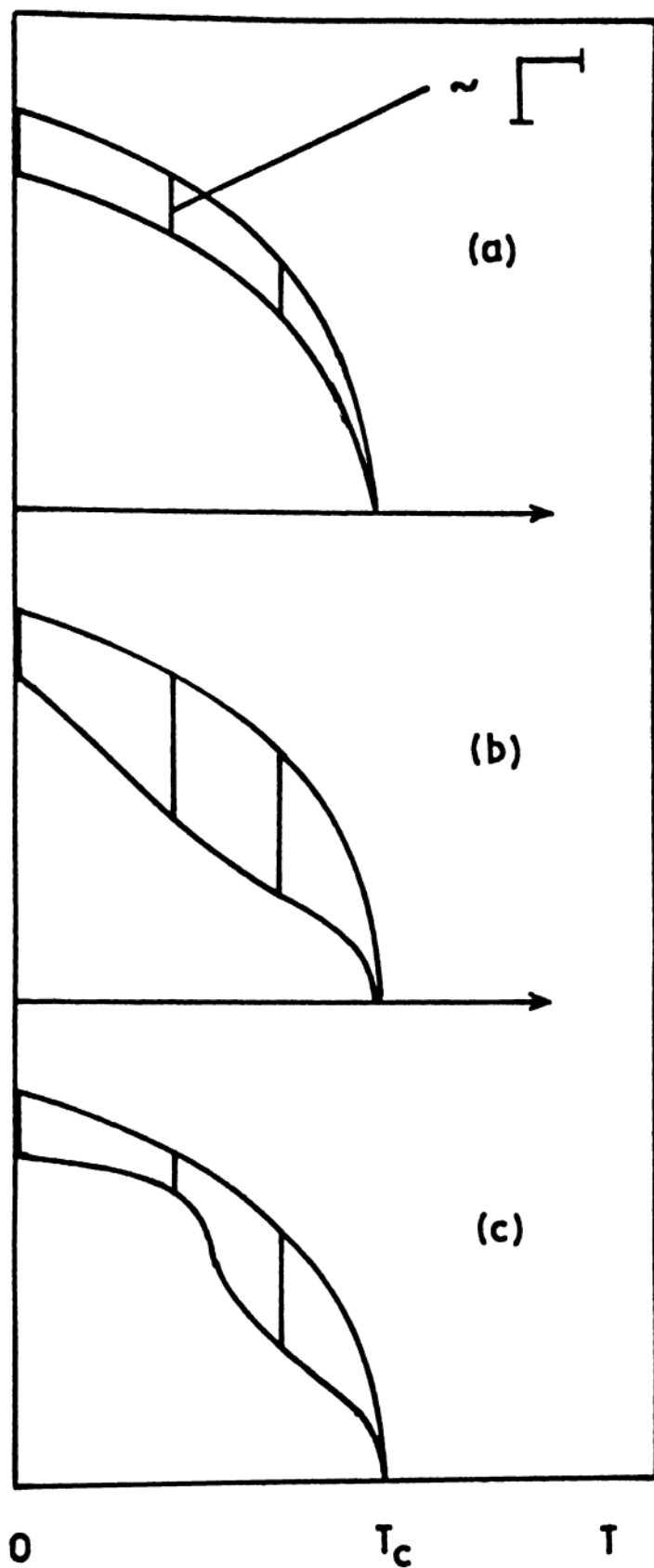


Fig. 5-18 : Schematic temperature behaviour of the magnetic moment distribution in the case of :
 (a) narrow exchange interaction distribution indicating predominant long-range interactions;
 (b) & (c) large exchange interaction distribution, characteristic of predominant short-range interactions.

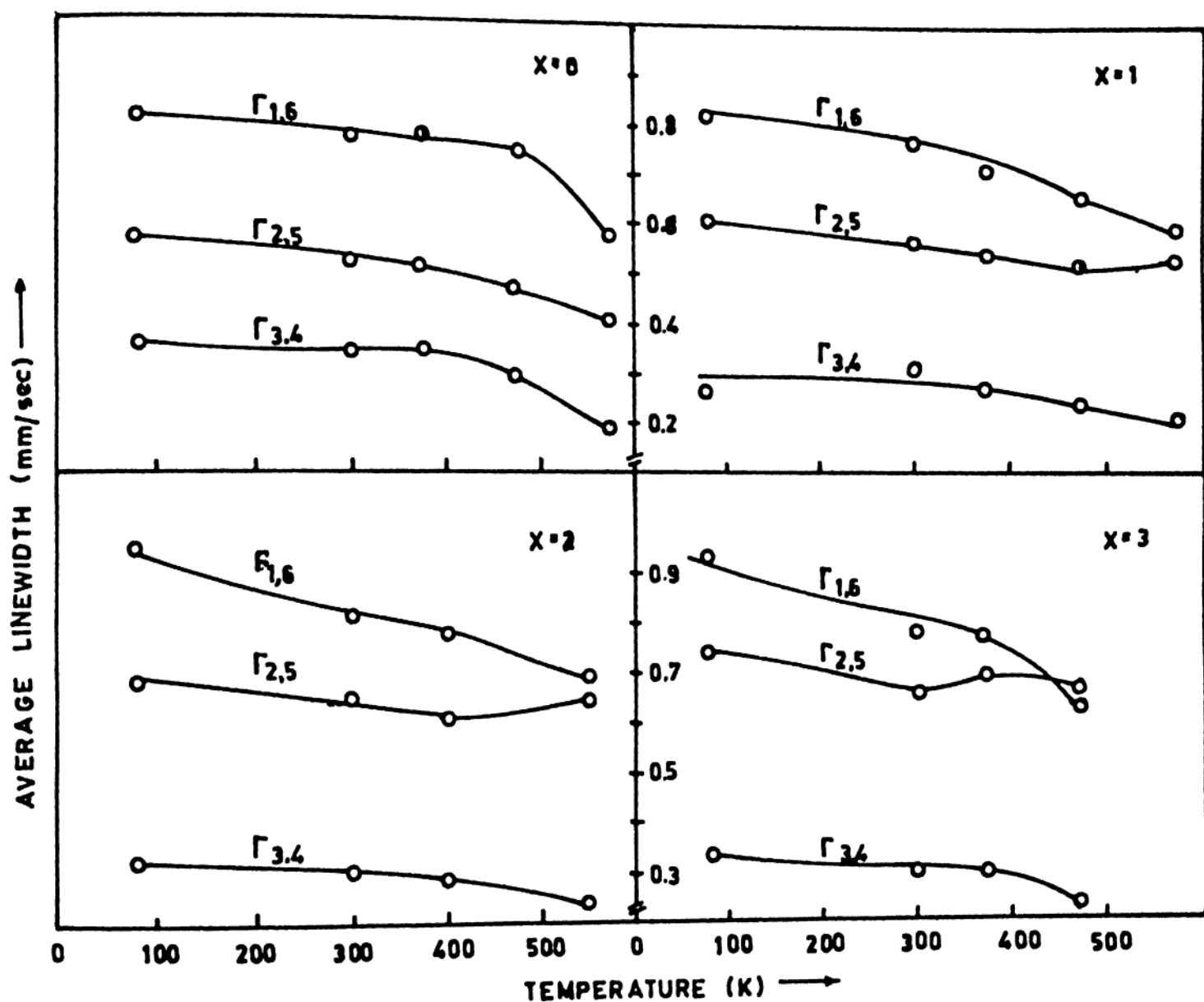


Fig. 5-19 : Average line widths of $\text{Fe}_{70}\text{Ni}_{12-x}\text{Mo}_x\text{B}_{16}\text{Si}_2$ ($0 \leq x \leq 3$) alloys. $\Gamma_{1,6} = (\Gamma_1 + \Gamma_6)/2$, similarly $\Gamma_{2,5}$ and $\Gamma_{3,4}$.

dependence. Cases (b) and (c) are similar. The field corresponding to long-range order follow the brillouin behaviour. The field corresponding to short-range order does not. Consequently, the systematic variation in the magnetic moment distribution is lost. The corresponding picture in Mössbauer spectroscopy will be dependent on the temperature effect of line width assuming that the line width corresponding to the distribution of the magnetic moment or a quantity proportional to it which is the hyperfine field in this case. This behaviour of magnetic moment vs. temperature is shown in Figure 5-18.

The systematic fall in line width due to temperature will imply case (a), any other behaviour will imply cases (b) and (c) indicating that the both short-range and long-range interactions are important.

Figure 5-19 shows the temperature dependence of average (HWHM) of lines 1 and 6, 2 and 5 and 3 and 4 of six-line Mössbauer spectra of amorphous $\text{Fe}_{70}\text{Ni}_{12-x}\text{Mo}_x\text{B}_{16}\text{Si}_2$ ($0 \leq x \leq 3$) alloys. In the present discussion the average line widths of lines 1 and 6, 2 and 5 and 3 and 4 (represented by $\Gamma_{1,6}$, $\Gamma_{2,5}$ and $\Gamma_{3,4}$) decreases monotonically as a function of temperature for $x = 0$ and falls in the category (a) indicating narrow distribution of exchange interactions, as expected for interactions of dominant long-range order. This is true for $x = 0$ in $\text{Fe}_{70}\text{Ni}_{12-x}\text{Mo}_x\text{B}_{16}\text{Si}_2$ alloys. On the otherhand for $x = 1, 2$ and 3, where the alloys contain 1, 2 and 3 at.% of Mo content, the temperature dependence of average line widths shows a

different kind of behaviour for different lines. i.e., $\Gamma_{1,6}$ and $\Gamma_{3,4}$ still follow the category (a) where the line widths decrease monotonically and $\Gamma_{2,5}$ shows a decrease in behaviour first and then increases before it decreases again. This behaviour is very clear in case of $x = 3$ as shown in Figure 5-19. This essentially means that the long-range order may be mixed with short-range order in Mo containing alloys, which is the cause for a complicated $P(H)$ as shown in hyperfine field distribution of these alloys in the earlier section.

5.5 SUMMARY :

Addition of 1.5 at.% of Co to $\text{Fe}_{75}\text{B}_{10}\text{Si}_{15}$ metallic glass decreases H from 242 to 239 KOe and increases T_c from 682 to 712 K. Further addition of Co at the steps of 1.5 at.% does not seem to affect H and T_c significantly, although there is a slight decrease in trend in Curie temperatures. On the other hand in Fe-Ni-Mo-B-Si alloys H and T_c decreases steadily till 3 at.% of Mo addition and for $x = 4$, not much change in these values are observed. The ratio of average hyperfine field to average magnetic moment of Fe-Ni-Mo-B-Si alloys at room temperature is around 1.6 ± 0.1 KOe-gm/emu. T_c s by thermal scan method is very well agreeing with that of DSC and resistivity measurements. H decreases with temperature in Mo containing alloys. The bimodality in the major peak arises due to the presence of Mo which can contribute to Fe-Mo antiferromagnetic exchange interactions and magnetic dilution effects contributing to the distribution in the lower field region.

CHAPTER VI

CRYSTALLIZATION STUDIES OF
AMORPHOUS $\text{Fe}_{40}\text{Ni}_{38}\text{Mo}_4\text{B}_{18}$ ALLOY

CHAPTER VI

This chapter gives the crystallization studies of amorphous $\text{Fe}_{40}\text{Ni}_{38}\text{Mo}_4\text{B}_{18}$ alloy and discusses the results. The differential scanning calorimetry (DSC) has been used for the experimental measurements. Isothermal and nonisothermal techniques are applied separately to cheque the extent of deviation of the crystallization parameters like activation energy, Avrami exponent etc.

6.1 INTRODUCTION :

During the last decade the theoretical as well as experimental studies on phase transformations in metallic glasses have been extensively studied (Henderson 1979, Scott 1983, Russew et al 1985 and Uwe Koster 1985). In all cases isothermal experimental analysis techniques are definitive (Calka and Stewart 1985 and Akhtar 1986), whereas the nonisothermal experimental analysis techniques are advantageous (Henderson 1979) for the following reasons. Firstly, certain industrial processes often depend on the kinetic behaviour of the systems undergoing phase transformations under nonisothermal conditions because of its simplicity in doing experiments and sensitivity towards rapid phase transformations. Secondly, nonisothermal experiments can be used to extend the temperature measurements beyond that accessible to isothermal experiments.

In the following investigations we have taken amorphous $\text{Fe}_{40}\text{Ni}_{38}\text{Mo}_4\text{B}_{18}$ (Metglas 2826 MB) alloy and studied its crista-

crystallization kinetics by isothermal and nonisothermal techniques. Isothermal analysis is carried out on the basis of Johnson-Mehl-Avrami (JMA) transformation (Johnson 1939) procedure and nonisothermal analysis by the Kissinger method (Kissinger 1956). The alloy of nominal composition $\text{Fe}_{40}\text{Ni}_{38}\text{Mo}_4\text{B}_{18}$ exhibited remarkable soft magnetic properties (Cumbrera et al 1979). The previous authors (Majumdar and Nigam 1980, Cumbrera et al 1982 and Raja et al 1987) have studied the crystallization process in the same alloy using DSC. The first two authors observed a three stage crystallization whereas the third one observed a two stage crystallization process. Hence, it may be of interest to see the crystallization process in detail in this metallic glass. Also nonisothermal method which is considered to be having several experimental conveniences (Henderson 1979) is yet to be considered for the fast data analysis. Because, isothermal method is mathematically more rigorous and definitive (Chen 1978 and Henderson 1979). Hence it may be a good idea to find out the extent of deviation of nonisothermal result from that of isothermal one.

6.2 ISOTHERMAL TRANSFORMATION :

The Johnson-Mehl-Avrami equation is usually written in the form (Johnson 1939)

$$x = 1 - \exp(-Kt^n) \quad 6-1$$

where x is the fraction of the transformation completed at

time t . K is a function of temperature and in general depends on both the nucleation rate and the growth rate and n is the 'Avrami exponent' which reflects the nucleation rate and/or the growth morphology. K is of the form

$$K = K_0 \exp(-E/RT) \quad 6-2$$

where E is the activation energy and R is gas constant. By logarithmic manipulation, Eqn. 6-1 can be written as

$$\ln[-\ln(1-x)] = \ln K + n \ln t \quad 6-3$$

which essentially means that the plot between $\ln[-\ln(1-x)]$ versus $\ln(t)$ is a straight line with a slope equal to n and intercept equal to $\ln K$.

The details of n can be evaluated following the procedure given by Christian (1975). The equation for n is given by

$$x = a + pd \quad 6-4$$

where $p = 1$ for linear growth, $p = 1/2$ for parabolic growth; $d = 1, 2$ or 3 for one, two or three-dimensional growth; $a = 0$ for no nucleation (i.e., zero nucleation rate), $a = 1$ for constant nucleation rate, $0 < a < 1$ for a decreasing nucleation rate and $a > 1$ for an increasing nucleation rate.

The activation energy, E , in isothermal transformation can be evaluated making use of Arrhenius relation (Akhtar 1986)

$$t_p = t_0 \exp(E/RT) \quad 6-5$$

where t_p is the time required to complete p percent of transformation at temperature T . Eq. 6-5 implies that $\ln(t_p)$ vs. $1/T$ plot gives rise to a slope equal to E/R , where R is gas constant.

6.3 NONISOTHERMAL TRANSFORMATION :

In metallic glasses and particularly in crystallization processes it is the enthalpy change with temperature variation which gives rise to exotherms. In the analysis of nonisothermal processes, Kissinger (1956) procedure is used to evaluate activation energy, E . The details of Kissinger procedure is as follows.

The basic equation that relates the rate of reaction to the fraction of the material decomposed may be written as (Murray et al 1949 and Vaughan 1955)

$$\left(\frac{\partial x}{\partial t}\right)_T = K_T(1-x) \quad 6-6$$

where x is the fraction of the material decomposed, K_T is the magnitude of the rate constant and is given by the Arrhenius equation

$$K_T = A e^{-E/RT} \quad 6-7$$

where A and E are the frequency factor and activation energy respectively. The former is a measure of the probability that a

molecule having energy E will participate in a reaction and the later is energy barrier opposing the reaction (Kissinger 1956).

By applying the condition that the reaction rate is maximum when its derivative with respect to time is zero and simultaneously applying a few mathematical manipulations one can obtain an equation of the form (Chen 1978 and 1981)

$$\frac{E}{k_B T_p} = \ln \left[\frac{T_p^2}{\phi} \right] + \text{constant} \quad 6-8$$

where T_p is the peak temperature, ϕ is the heating rate and k_B is the Boltzmann constant. In a $\ln (\phi/T_p^2)$ vs. $1/T_p$ plot the slope will give the E/k_B .

6.4 EXPERIMENTAL RESULTS AND DISCUSSION :

We have selected a single amorphous $\text{Fe}_{40}\text{Ni}_{38}\text{Mo}_4\text{B}_{18}$ alloy (Metglass 2826 MB) for which the isothermal and nonisothermal analyses are carried out. The nonisothermal run with the heating rate of 12.5 K/min shows two peaks having T_p at 706 and 807 K as shown in Fig.6-1(a) conforming two stage crystallization processes. This is a common observation for this alloy (Raja et al 1987). Using nonisothermal procedure, Antonione et al (1978) observed a two stage crystallization process at 703 and 777 K for the Metglas 2826 MB with activation energies 296 and 334 KJ/mole respectively for the first and second crystallization reactions. However, Majumdar and Nigam (1980) and Cumbrera et al

(1982) observed a three stage crystallization peaks at 728, 810 and 863 K for the first, second and third crystallization peaks, respectively. Cumbrera et al (1982) determined activation energies both from Kissinger (288 and 355 KJ/mole) and Isothermal (288 and 451 KJ/mole) methods using Differential Thermal Analysis (DTA), Differential Scanning Calorimetry (DSC) and resistivity measurements for the first two crystallization processes. It may be noted here that the activation energy deduced from Isothermal method for the second crystallization differs significantly from that obtained by Kissinger method (Cumbrera et al 1982). The two stage crystallization process formed in our case (Fig. 6-1a) is supported by the fact that for a variety of (Fe-Ni-Mo)B glasses a double crystallization is observed (Bhanuprasad 1987). Also, the resistivity measurements on the same alloy ($\text{Fe}_{40}\text{Ni}_{38}\text{Mo}_4\text{B}_{18}$) showed a double crystallization at temperatures 700 and 810 K which is supporting beyond doubt the two stage crystallization process in this alloy. The crystallization temperatures obtained by resistivity measurements are very well agreeing with the values obtained by DSC measurements as shown in Fig. 6-1d.

Isothermal annealing studies on the first peak at 717, 726 and 731.2 K and on the second peak at 763.3, 767.3 and 770.3 K are carried out. Figures 6-1(b) and (c) shows the typical Isothermal plots of metglas 2826 MB for the first and second crystallization processes respectively. These figures show the incubation time, τ , (time required to start the process) is 0.5 ± 0.05 min for the first crystallization process and nearly

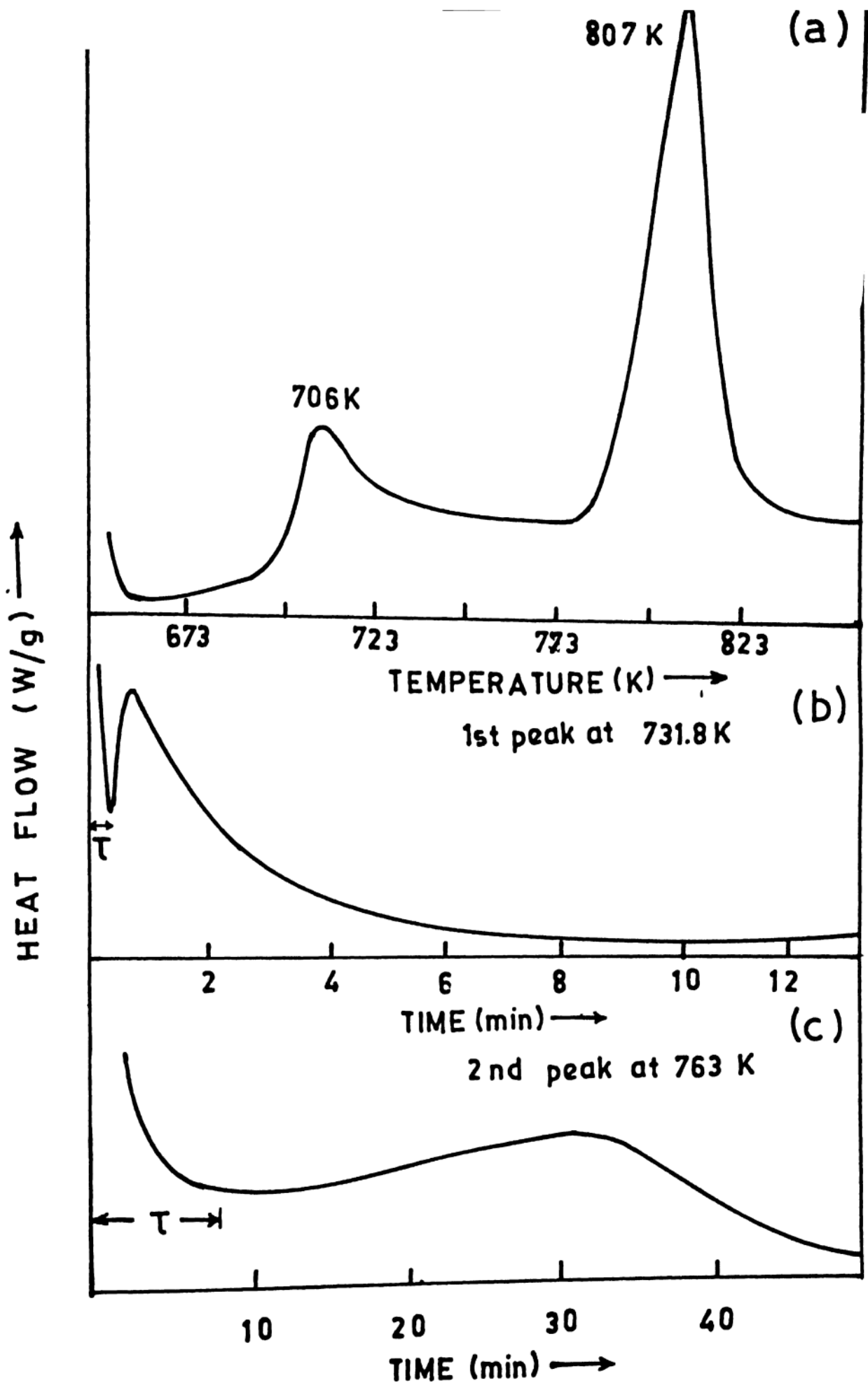


Fig. 6-1 : Isothermal annealing of amorphous $\text{Fe}_{40}\text{Ni}_{38}\text{Mo}_4\text{B}_{18}$ (2826 MB) alloy.
 (a) Nonisothermal run (heating rate 12.5 K/min).
 (b) Isothermal run of first peak at 731.8 K.
 (c) Isothermal run of second peak at 763 K.

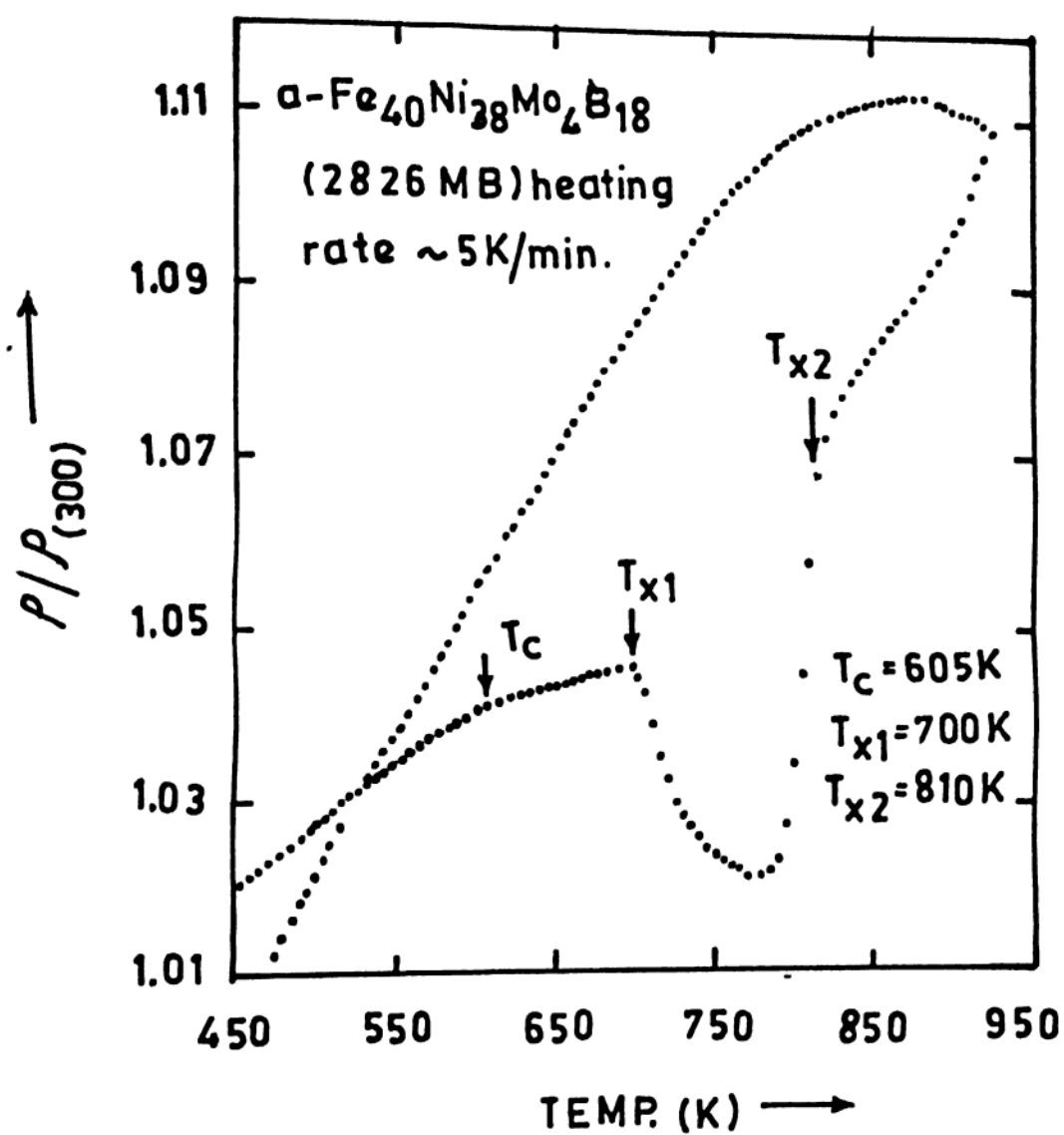


Fig. 6-1d : Resistivity ratio, $p(T)/p(300)$ vs. T of amorphous $\text{Fe}_{40}\text{Ni}_{38}\text{Mo}_4\text{B}_{18}$ alloy.

8.0 ± 0.5 min for the second crystallization process. The incubation period was taken as time interval between the specimen reaching the annealing temperature and the start of the transformation. The start of the transformation was taken as that instant at which the base line deviated from linearity. The nonisothermal runs are carried out with the heating rates 1.5, 4, 8, 12.5 and 20 K/min. In all the cases a two stage crystallization process is observed. The peak area in these plots increases with heating rates. This is expected because as the heating rate increases the rate of reaction and hence the dH/dt (H is enthalpy) changes rapidly with the temperature. The peak temperature, T_p moves towards higher temperatures with the increase in heating rates. Following Kissinger method and hence the Eqn.6-8, the activation energies for these two peaks are calculated. The graph between $\ln(\frac{1}{\sqrt{T_p}})$ versus $10^3/T_p$ is as shown in Figure 6-2. The activation energies for the first and second peaks are calculated to be 291 and 343 KJ/mole, respectively. These values are in good agreement with the values deduced by Antonione et al (1978) as shown in Table 6-1.

In isothermal analysis, the fraction of crystallization, x at any time t is calculated as the ratio $A(t)/A(\text{total})$ where $A(t)$ and $A(\text{total})$ are the areas under the isothermal exotherm at the time t and the total area of the exotherm, respectively. Plots of x versus time at different temperatures yielded sigmoidal curves and are shown in Figures 6-3(a) and 6-4(a). The activation energies of the crystallization processes are calculated from the

Table 6-1: Activation energies for the crystallization processes of amorphous $\text{Fe}_{40}\text{Ni}_{38}\text{Mo}_4\text{B}_{18}$ (Metglas 2826 MB) alloy.

S.No.	Peak 1 KJ/mole	Peak 2 KJ/mole	method	reference
1	284	374	Isothermal	present work
2	291	343	nonisothermal	present work
3	296	334	nonisothermal	Antonione et al (1978)
4	288	355	Kissinger	Cumbrera et al (1982)
5	270	375	Kissinger	Raja et al (1987)

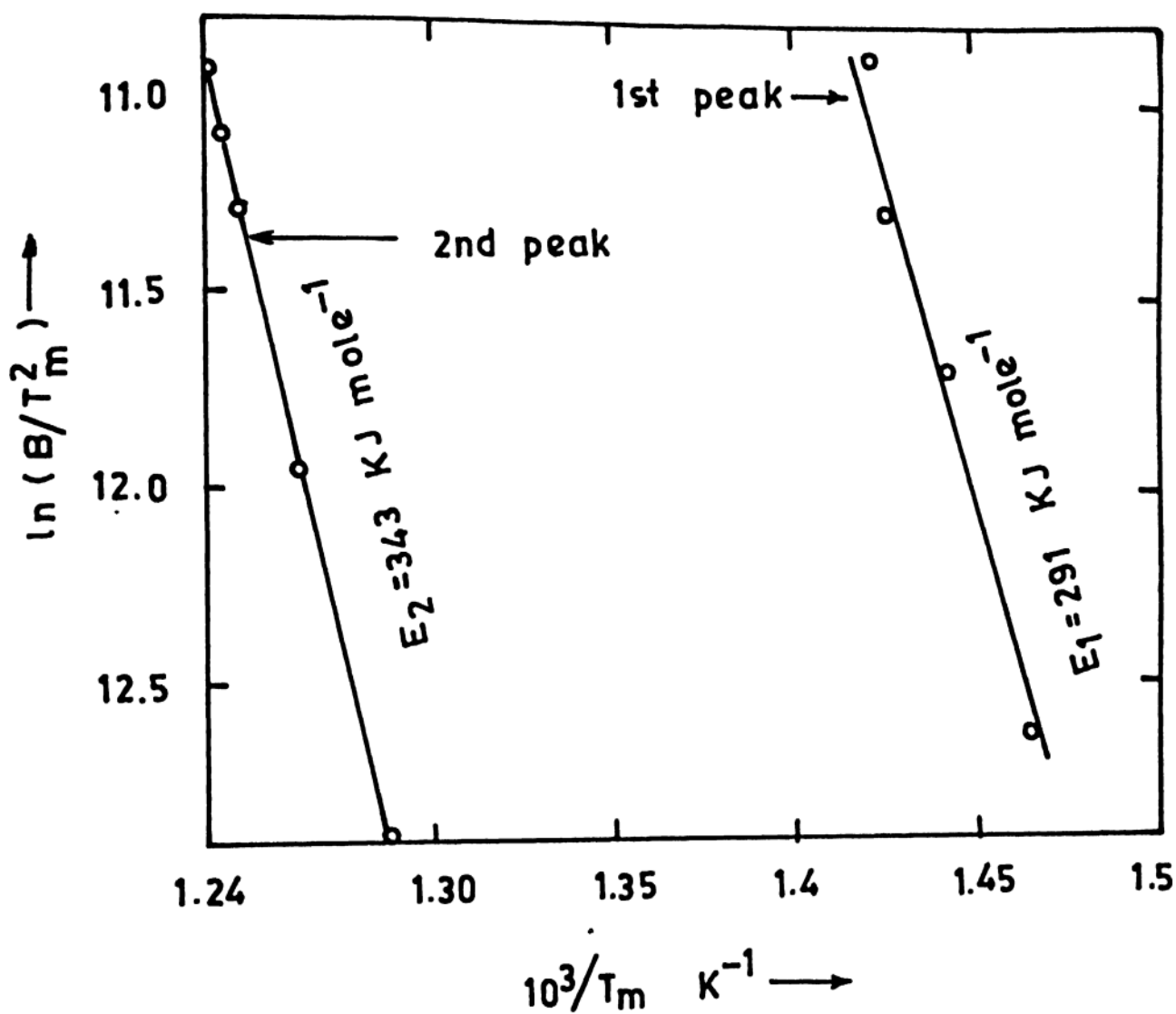
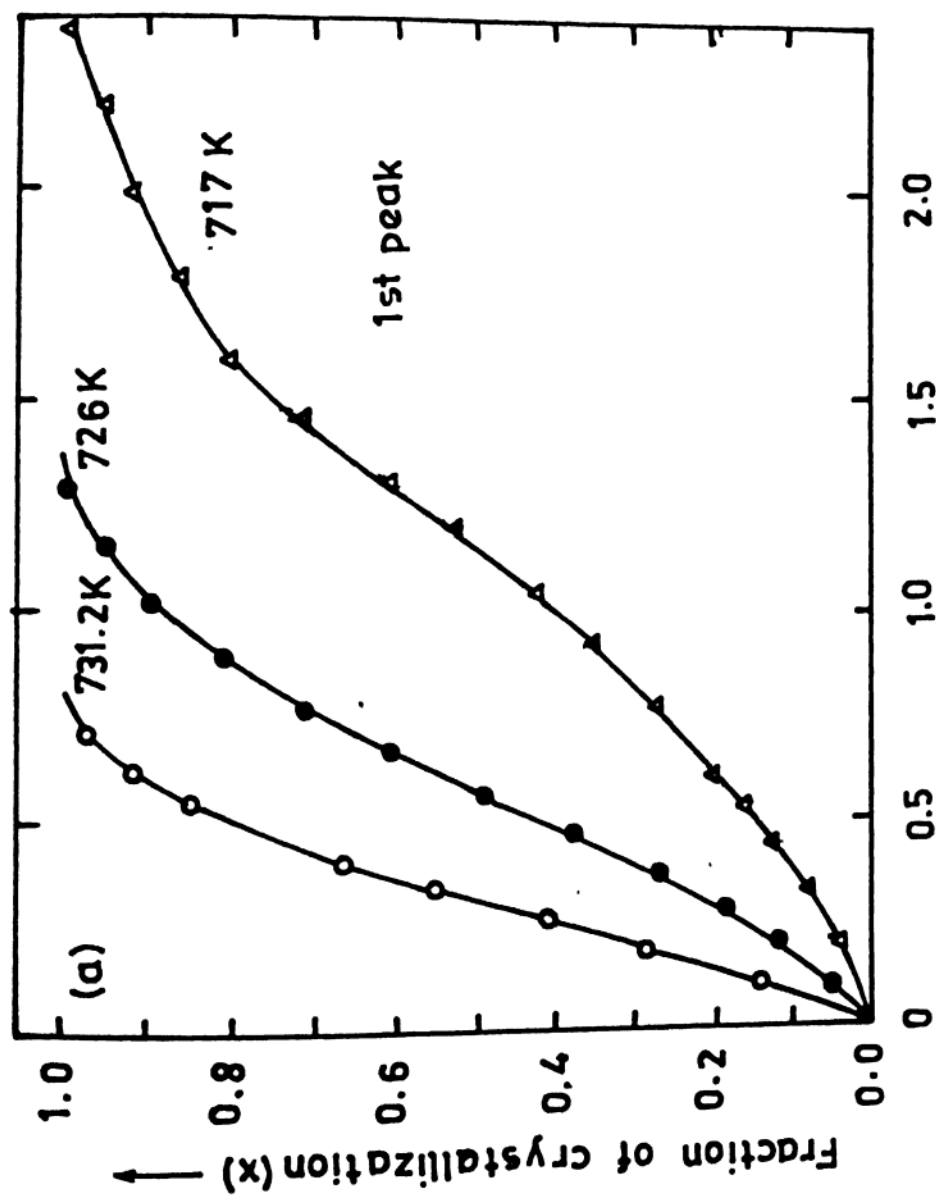


Fig. 6-2 : Kissinger plots for the first and second crystallization processes of amorphous $\text{Fe}_{40}\text{Ni}_{38}\text{Mo}_4\text{B}_{18}$ glass.

Isothermal exotherms making use of Eq. 6-5. The plots of $\ln(t)$ versus $10^3/T$ for the first and second crystallization peaks are as shown in Figures 6-3(b) and 6-4(b), respectively. In all the above plots the incubation time is subtracted before plotting the graphs. The activation energies found by isothermal studies are 298 and 401 KJ/mole at 60% fraction of crystallization and 284 and 374 KJ/mole for 80% fraction of crystallization for the first and second crystallization processes, respectively. The activation energies obtained agree very well with the activation energies deduced by other authors for the same alloy as shown in Table 6-1. The activation energies at 80% fraction of crystallization (284 and 374 KJ/mole) agree within experimental error with the nonisothermally deduced activation energies (291 and 343 KJ/mole) for the first and second crystallization processes.

The Avrami exponent, n is calculated using the Eqn. 6-3 by plotting $\ln[-\ln(1-x)]$ versus $\ln t$ and evaluating the slope of the straight line. The slope directly gives us the value of n . The plots are shown in Figures 6-5(a) and (b). The average value of n calculated is 1.72 ± 0.03 for the first peak and 3.06 ± 0.07 for the second peak. The interpretation of the nucleation and growth for these values is done by Equation 6-4 and is as follows.

For the first peak the value of n is 1.72 ± 0.03 . This allows us to select $d = 3$, $p = 1/2$ and $0 < a < 1$ and implies a three dimensional and parabolic growth with decreasing nucleation



$(t - \tau)$ min. \longrightarrow

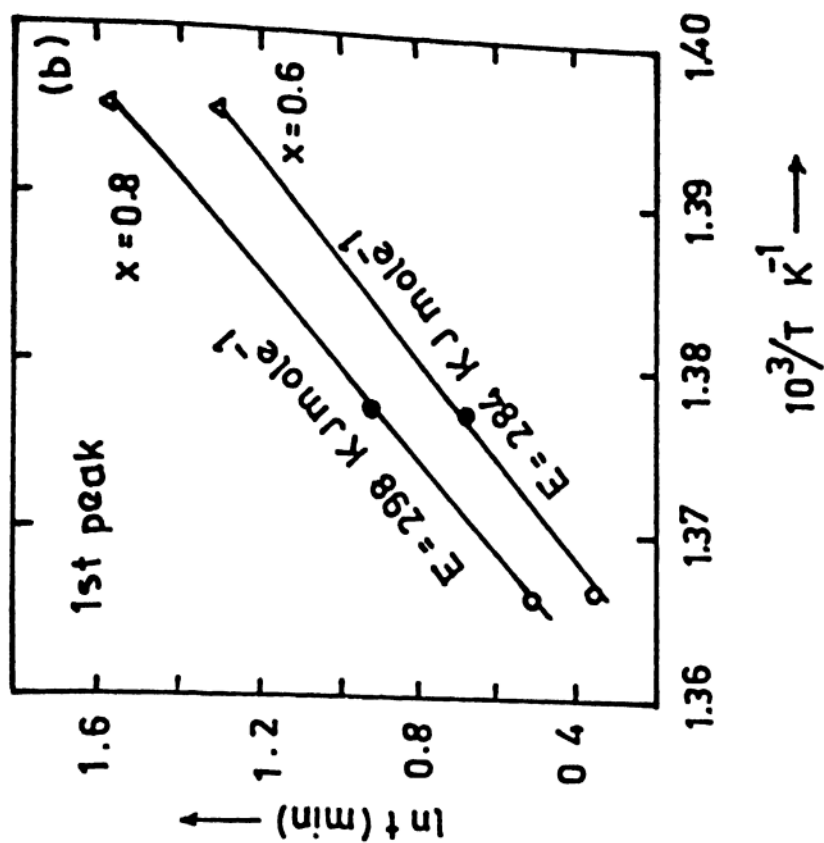


Fig. 6-3 : (a) Sigmoidal plots for the isothermal runs of amorphous $Fe_{40}Ni_{38}Mo_4B_{16}$ alloy for the first peak.
(b) $\ln t$ vs. $10^3/T$ at $x = 0.6$ and 0.8 (isothermal) for the first peak.

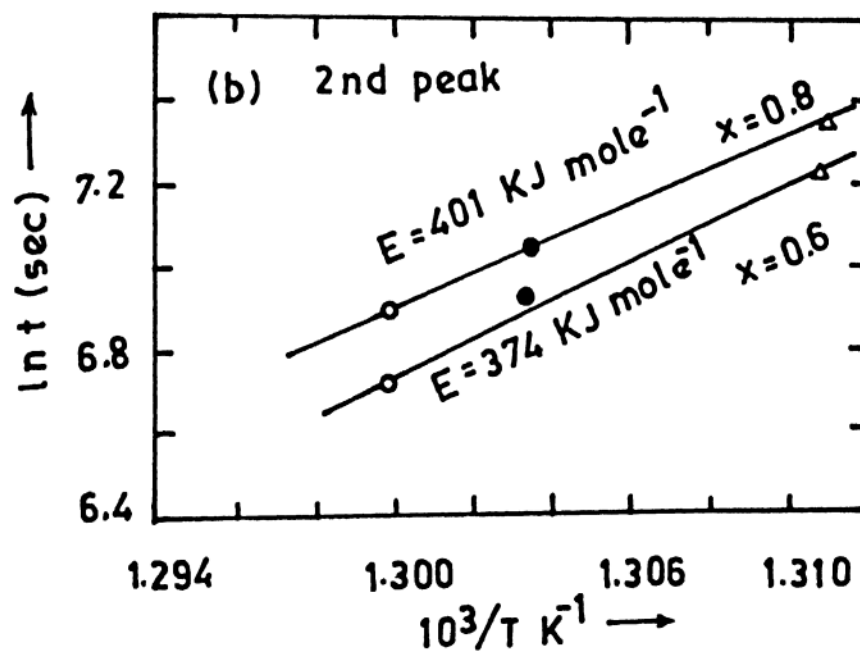
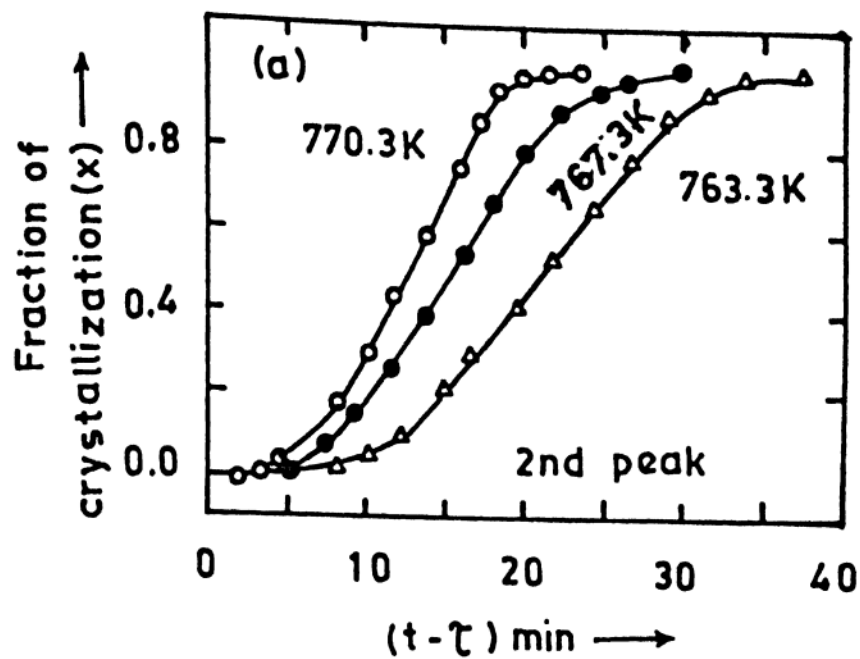


Fig. 6-4 : (a) Sigmoidal plots for the isothermal runs of amorphous $\text{Fe}_{40}\text{Ni}_{38}\text{Mo}_4\text{B}_{18}$ alloy for the second peak.
 (b) $\ln t$ vs. $10^3/T$ at $x = 0.6$ and 0.8 (isothermal) for the second peak.

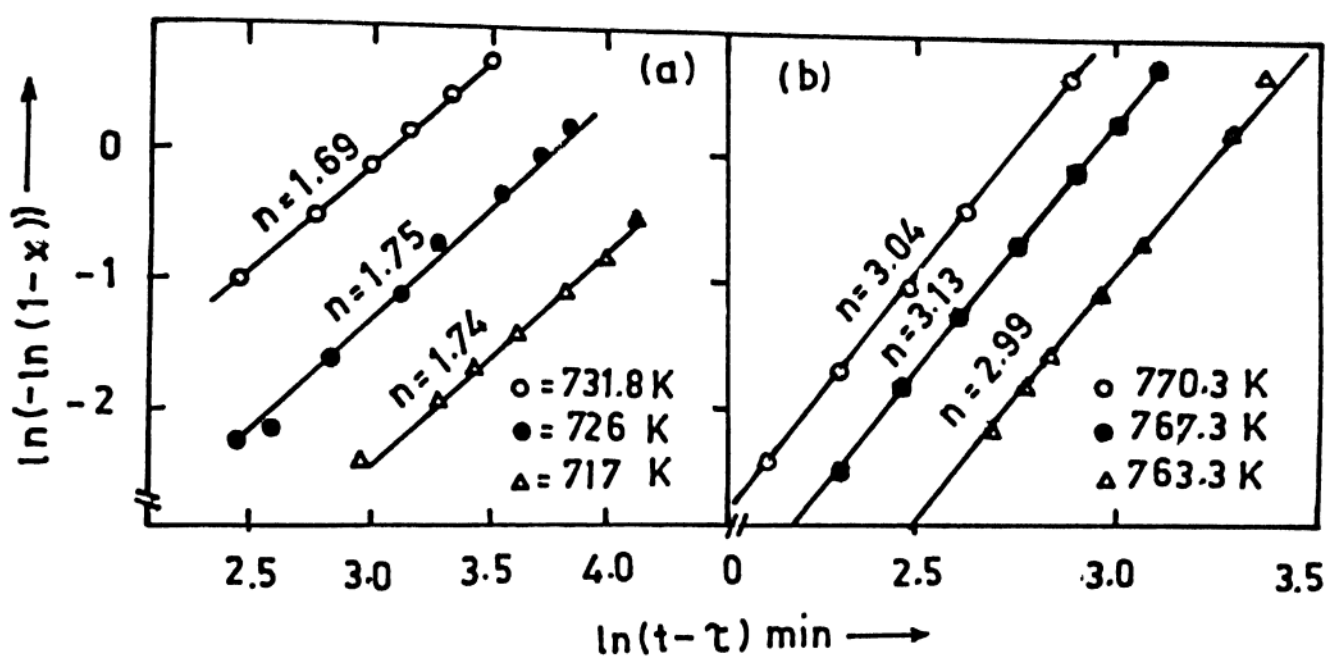


Fig. 6-5 : $\ln[-\ln(1-x)]$ vs. $\ln(t-\tau)$ of amorphous $\text{Fe}_{40}\text{Ni}_{38}\text{Mo}_4\text{B}_{18}$ alloy.

(a) First peak of crystallization (isothermal).

(b) Second peak of crystallization (isothermal).

rate (see section 6-2). In metallic glasses a three-dimensional growth is a common observation during crystallization (Mathur et al 1987). For the second peak, n is between 3.06 ± 0.07 , which implies $d = 3$, $p = 1/2$ and $a > 1$. This can also allow us to consider $d = 3$, $p = 1$ and $a < 1$. But Greer (1982) has suggested that the experimentally observed Avrami exponent falls short of the actual value because of certain instrumental and theoretical factors. It should be noted in Figure 6-4 that the value of E , increases with increase in the fraction transformed, x . Ranganathan et al (1981) have proposed a relationship

$$E = \left[\frac{n_n E_n + n_g E_g}{n} \right] \quad 6-9$$

Where subscripts n and g correspond to nucleation and growth, respectively. The activation energies for nucleation, E_n have been found to be considerably higher than the activation energies for growth, E_g in the same glass (Luborsky 1983). The increase of activation energy of the total process, E with transformed fraction (or time), thus implies that nucleation rate is increasing with time. Hence, $d = 3$, $p = 1/2$ and $a > 1$ is the suitable choice for the second crystallization process which suggested a three dimensional and parabolic growth with increasing nucleation rate.

Similar calculations of n have been tried in nonisothermal peaks adopting the same procedure as that of isothermal described above. Though the fraction of crystallization versus time plots

shown in Figures 6-6a and (b) shows similar sigmoidal plots as that of isothermal, n values differ drastically and yielded higher values. For example, the n value calculated from non-isothermal plots for the first peak is between 3.75 to 5.63. Surprisingly, for the second peak and for lower heating rates (1.5 and 4 K/min), the n value is 3.22 ± 0.07 and agree within experimental error with the isothermally deduced value (3.06). However, for higher heating rates, n increases towards higher values (3.6 to 4.7). The plots of $\ln[-\ln(1-x)]$ vs. $\ln(t)$ for the nonisothermal peaks are shown in Figures 6-7(a) and (b).

It has been stated that JMA transformation rate equation can only be applied to transformations involving nucleation and growth in a limited number of special cases under nonisothermal conditions and particularly when the rate of transformation, dx/dt depends only on fraction of crystallization, x and temperature, T (Henderson 1979). For a slow transformation and at lower heating rates, it is quite possible that the above condition may be satisfied. This may be the reason why the n value deduced by both isothermal and nonisothermal techniques in the present study are matching within experimental error for the heating rates below 4 K/min (for the second peak in our case). For the heating rates above 4 K/min the transformation depends on T as well as time and therefore violating one of the fundamental assumptions of JMA transformation (i.e., growth of a phase must depend on temperature and not on time). Hence, nonisothermal method can be safely used below the heating rates 4 K/min for the

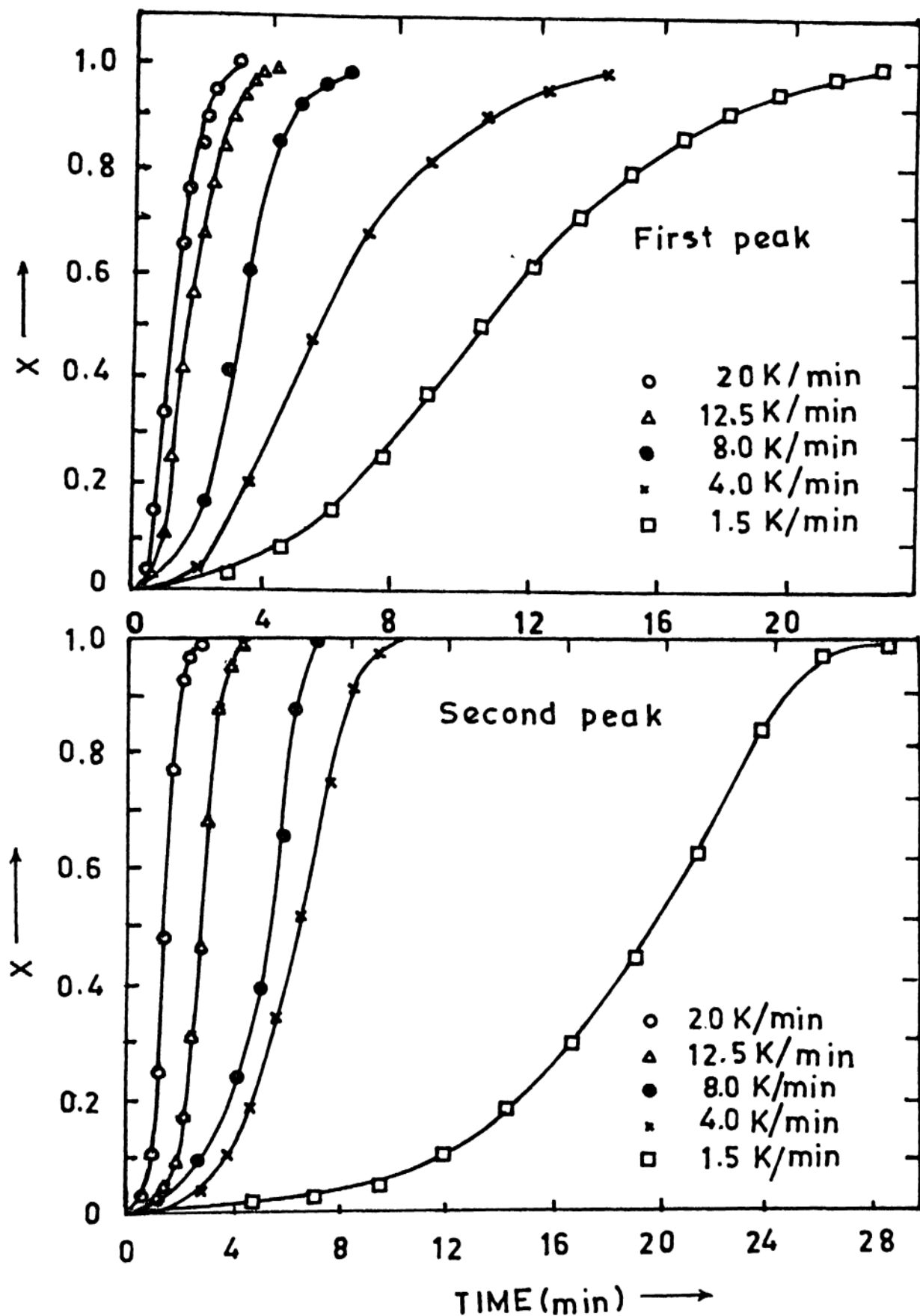


Fig. 6-6 : Fraction of crystallization, x vs. t for nonisothermal runs of amorphous $\text{Fe}_{40}\text{Ni}_{38}\text{Mo}_4\text{B}_{18}$ alloy.

(a) For the first peak (nonisothermal).

(b) For the second peak (nonisothermal).

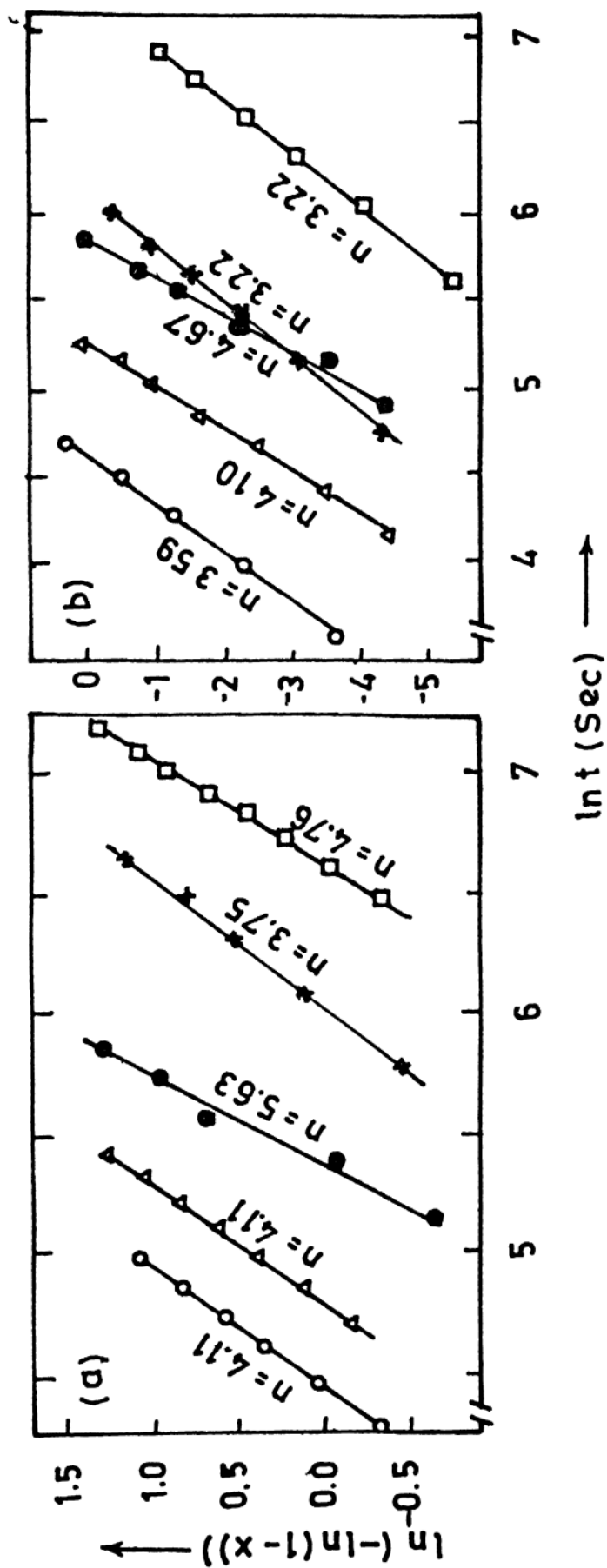


Fig. 6-7 : $\ln[\ln(1-x)]$ vs. $\ln(t-\tau)$ of amorphous $\text{Fe}_{40}\text{Ni}_{38}\text{Mo}_4\text{B}_{18}$ alloy.

(a) For the first peak (nonisothermal).
 (b) For the second peak (nonisothermal).

second stage of crystallization of $\text{Fe}_{40}\text{Ni}_{38}\text{Mo}_4\text{B}_{18}$ alloy. The first stage of crystallization is not a slow one. Therefore, only isothermal conditions have to be used to elucidate the crystallization kinetics.

G.5 SUMMARY :

The crystallization kinetics of amorphous $\text{Fe}_{40}\text{Ni}_{38}\text{Mo}_4\text{B}_{18}$ (Metglas 2826 MB) alloy has been studied by both isothermal and nonisothermal heating techniques using DSC. A two step crystallization process having peaks at 706 and 807 K is observed with a heating rate of 12.5 K/min. A similar crystallization process is obtained by resistivity measurements with a heating rate of 5 K/min. A slope change in resistivity vs. temperature is observed at 700 and 810 K, which is in good agreement with the values deduced by DSC measurements. The Avrami exponents calculated using isothermal technique (DSC) are 1.72 ± 0.03 for the first peak and 3.06 ± 0.07 for the second peak. The first stage of crystallization is suggested to be having three-dimensional and parabolic growth with decreasing nucleation rate. The second stage of crystallization is attributed to three-dimensional and parabolic growth with increasing nucleation rate. Similar calculations on nonisothermal runs yielded high values of n for the first ($3.75 \leq n \leq 5.3$) and second ($3.22 \leq n \leq 4.75$) stages of crystallization. In case of amorphous $\text{Fe}_{40}\text{Ni}_{38}\text{Mo}_4\text{B}_{18}$ alloy, it is suggested that the nonisothermal heating technique can be applied for the second peak at lower heating rates (≤ 4 K/min).

CHAPTER VII

CONCLUSIONS

CHAPTER VII

7.1 OVERALL CONCLUSIONS OF THE PRESENT WORK :

The iron-rich ferromagnetic metallic glasses of the type $(\text{Fe}_{1-x}\text{Co}_x)_{75}\text{B}_{10}\text{Si}_{15}$ ($0.00 \leq x \leq 0.12$), $\text{Fe}_{70}\text{Ni}_{12-x}\text{Mo}_x\text{B}_{16}\text{Si}_2$ ($0 \leq x \leq 3$) and $\text{Fe}_{40}\text{Ni}_{38}\text{Mo}_4\text{B}_{18}$ (Metglas 2826 MB) have been investigated in the temperature range 1.5 to 900 K by electrical resistivity, thermoelectric power, Mössbauer spectroscopy and DSC techniques, although, the whole temperature range and all the above mentioned techniques have not been necessarily used for all the sample measurements.

The electrical resistivity measurements of $(\text{Fe}_{1-x}\text{Co}_x)_{75}\text{B}_{10}\text{Si}_{15}$ alloys in the temperature range 1.5 to 300 K for compositions $x = 0.00$ to 0.08 and in the temperature range 80 to 900 K for compositions $0.00 \leq x \leq 0.12$ have been performed. Also, the resistivity measurements of $\text{Fe}_{70}\text{Ni}_{12-x}\text{Mo}_x\text{B}_{16}\text{Si}_2$ ($0 \leq x \leq 3$) alloys have been studied in the temperature range 1.2 to 900 K. The quantitative comparison of our results with theoretical predictions allows us to draw the following conclusions. Both the electron-ion potential scattering and electron-magnon scattering contribute to electrical resistivity. the structural contribution to resistivity dominates over the magnetic contribution in the entire temperature range for all the alloys studied and the $\rho_{\text{mag}}(T)$ is found to follow quadratic behaviour. All the glasses showed a minimum in resistivity (ρ_{min})

between 1.5 and 60 K. For all the Co containing alloys of the form Fe-Co-B-Si, the minimum in resistivity is around 20 K. Whereas for Fe-Ni-Mo-B-Si alloys, it varies drastically from 11 K for $x = 0$ to 60 K for $x = 3$. Logarithmic behaviour in T for $T < T_{min}$ and T^2 dependence for $T > T_{min} < 100$ K is observed for Fe-Co-B-Si alloys. Above 100 K the temperature dependence of resistivity is slightly parabolic with a small and positive T^2 coefficient ($\sim 10^{-7}$). At T_c a slight change in the slope of the resistivity ratio versus temperature graph is observed in case of Fe-Co-B-Si alloys. In Fe-Ni-Mo-B-Si alloys this slope change is not very clear. The temperature coefficient of resistivity, α , seems to be more or less same in Co containing alloys at least till 9 at.% of Co addition to $(Fe_{1-x}Co_x)_{75}B_{10}Si_{15}$ alloys. On the other hand the α for Fe-Ni-Mo-B-Si alloys seems to decrease fast with Mo addition. The absolute temperature resistivities for all the alloys lie below $150 \mu\Omega\text{-cm}$ and as α increases ρ decreases. Hence, it seems to follow the Mooij correlation.

The Curie temperature, T_c increases for even a small addition of cobalt (1.5 at.%) to $Fe_{75}B_{10}Si_{15}$ glass. Further addition of Co to these glasses changes T_c slightly. The T_c for Fe-Ni-Mo-B-Si alloys decreases drastically from 697 to 587 K with 3 at.% of Mo substitution. All the samples showed double crystallization indicating the two stage crystallization processes. The starting point of crystallization, T_{x1} increases from 715 to 795 K for 1.5 at.% of Co addition in Fe-Co-B-Si glasses. Similar to T_c , T_{x1} also does not seem to increase with

further cobalt substitution at the steps of 1.5 at.% each time atleast till 9 at.% of cobalt content. However, close observation of T_{x1} reveal that there is a slight but small decrease of T_{x1} for $x = 0.10$ onwards. The intensity of second crystallization peak diminishes with the addition of cobalt to Fe-Co-B-Si glasses. This is suggested due to the precipitation of (Fe-Co) alloy with (Fe-Co)B-Si amorphous matrix, which then crystallize further with higher concentration of cobalt, more (Fe-Co) alloy precipitates leaving to a sharper drop in resistivity. Similarly, in case of Fe-Ni-Mo-B-Si alloys the initial formation of (Fe-Ni-Mo) and Fe-Ni-B are expected and then these phases may dissociate to give more stable (Fe-Ni)B and Fe-Mo phases. The Debye temperature, θ_D of all the Co containing alloys are around 300 to 350 K. Whereas the θ_D for Fe-Ni-Mo-B-Si alloys are about 100 K less than the Fe-Co-B-Si metallic glasses. These values are obtained by subtracting an extra T^2 term at higher temperatures which has been attributed to the magnetic scattering. The Debye temperatures evaluated from these measurements which are in agreement with the θ_D values of other ferromagnetic glasses supports the magnetic contribution to electrical resistivity.

The thermoelectric power (TEP) of $(Fe_{1-x}Co_x)_{75}B_{10}Si_{15}$ ($0.00 \leq x \leq 0.12$) alloys in the temperature range 80 to 400 K has been studied. All the samples showed negative TEP through out the temperature range and it is linear below $T < T_{max}$ (T_{max} is the temperature at $|S_{max}|$). A broad maximum in $|S|$ around 300 to

400 K is observed at temperatures approximately equal to $T_c/2$. This maximum has the value of $|S|$ equal to $3.8 \mu\text{V/K}$ for $\text{Fe}_{75}\text{B}_{10}\text{Si}_{15}$ glass and with the addition of 1.5 at.% of cobalt to this glass it decreases to $2.8 \mu\text{V/K}$. The decrease in $|S_{\text{max}}|$ for further addition of Co content is feeble, if there is any. This implies that the parabolic behaviour between 80 K to crystallization temperature is decreasing with the addition of cobalt. There was no any correlation between the minimum in resistivity, ρ_{min} and the maximum in $|S|$. However, both the resistivity and TEP are not changing much with the addition of small quantities of cobalt. No theoretical model seems to explain completely the TEP behaviour of metallic glasses in the entire temperature range. i.e., $T \ll T_c$ to $T \geq T_c$.

Mössbauer spectroscopy measurements for Fe-Ni-Mo-B-Si alloys have been performed in the temperature range 80 to 900 K and for Fe-Co-B-Si alloys the room temperature spectra have been studied. Broad six-line spectra of the samples show that the sample is in the ferromagnetic state with random atomic arrangements and inequivalent Fe-sites. The absorption lines have large line widths which are about five to six times larger than the iron-foil line width at room temperature, which is a characteristic feature observed in all ferromagnetic metallic glasses. Major broadening in Mössbauer spectral lines is caused by the magnetic hyperfine field distribution. The thermal scan method shows that the T_c of the samples are very much in agreement with the values obtained by DSC. The T_c in thermal scan method is taken at a

place where the magnetic order completely collapses. The difference in the T_c determined by different methods like DSC, resistivity and Mössbauer has been attributed to the change in the heating rates which essentially increases T_c by annealing. Room temperature Mössbauer measurements show that the magnetization axis does not lie perfectly in the plane of the ribbon of any of the samples studied and its direction is out of plane of the ribbon.

Fourier analysis of the six-line Mössbauer spectra shows a well defined peak in $P(H)$ vs. H graph. With the addition of Mo, this peak shifts to lower fields in case of Fe-Ni-Mo-B-Si alloys. Whereas in Co containing alloys the shift in the peak field is zero or small. Since a large contribution (60 to 90%) is expected due to core polarization by the local moment on the Fe-atom, negligible effect of Co addition to Fe-B-Si system in the H and $P(H)$ indicates that the moments on Fe-atom are not substantially affected due to the presence of Co in the neighbourhood (Panissod et al 1982). However increase of T_c implies stronger exchange in terms of either J_{Fe-Co} or J_{Co-Co} , probably the former. Additional peaks (on the right side of $P(H)$) are observed at higher fields which have no physical meaning but arises due to the polynomial fitting.

For $x = 0$ sample, the major peak is quite symmetric, the FWHM decreases systematically with increase in temperature, whereas for $x = 1, 2$ and 3 samples the major peak is significantly assymmetric even at lowest temperatures where the

artifact effect is far away from the major peak. This clearly shows the bimodality in the distribution of hyperfine field. With increase in temperature, the line width (FWHM) for the P(H) distribution remains more or less constant. Any fluctuation may arise on account of the error in determining the line width in assymetric profile with bimodality suggested. The sudden increase in FWHM arises due to the overlap of major peak with the minor peak attributed to the artifact effect. The bimodality in the major peak arises due to the presence of Mo. Molybdenum, which is a second row transition-metal like Cr and V in the first row can contribute to Fe-Mo antiferromagnetic exchange interaction and magnetic dilution effects contributing to the distribution in the lower field region and thereby giving rise to the bimodal distribution. The temperature independence of the width of the distribution can be attributed to different fields having different temperature dependences. This also suggested by the temperature dependence of line widths.

The average line width, $\tau_{1,6}$ of the first and sixth peaks of the six-line Mössbauer spectra of $\text{Fe}_{70}\text{Ni}_{12-x}\text{Mo}_x\text{B}_{16}\text{Si}_2$ alloys decreases with increase in temperature indicating the narrow distribution of exchange interactions as expected for interactions of dominant long-range order. Addition of Mo to these glasses shows a different kind of behaviour. i.e., $\tau_{1,6}$ and $\tau_{3,4}$ decreases monotonically with temperature, whereas $\tau_{2,5}$ shows a decrease in behaviour first and then increases before it decreases again indicating the mixture of long-range and short-range order in Mo containing alloys.

Crystallization studies using DSC shows that the Isothermal method is the convenient and accurate method to elucidate crystallization kinetics. The activation energies and Avrami exponents (n) for the crystallization processes are 284 and 374 KJ/mole and 1.7 and 3.1 for the first and second peaks, respectively of $\text{Fe}_{40}\text{Ni}_{38}\text{Mo}_4\text{B}_{18}$ alloy. The n values deduced here suggests a three-dimensional and parabolic growth with decreasing nucleation rate and three-dimensional and parabolic growth with increasing nucleation rate for the first and second crystallization processes respectively. The activation energies determined by Kissinger method using nonisothermal technique are agreeing well (291 and 343 KJ/mole) with the Isothermal values. However, the Avrami exponents are not agreeing with the Isothermally deduced values. The nonisothermal runs to study the crystallization kinetics can be used only at very low heating rates and only for certain reactions where the thermal history dependence does not exist. In particular, in $\text{Fe}_{40}\text{Ni}_{38}\text{Mo}_4\text{B}_{18}$ alloy the nonisothermal kinetics can be used at lower heating rates (below 4 K/min) and for the second crystallization process only.

7.2 SUGGESTION FOR FUTURE WORK :

Due to the lack of experimental facilities and time factor the thesis has been presented with requisite experimental details and their analysis. This work can be extended into more details and many physical and chemical properties can be thoroughly understood.

Firstly, the magnetic contribution to electrical resistivity, $\rho_{\text{mag}}(T)$ has been suggested by taking into account the Debye temperature, Θ_D and its agreement with other similar iron-rich ferromagnetic materials in the literature. On the other hand $\rho_{\text{mag}}(T)$ can be proved theoretically by taking into account the diffraction model for the amorphous materials. Theoretical investigations of Bergmann et al (1978) and Richter et al (1979) showed that $\rho_{\text{mag}}(T)$ has two types of contributions, one going as T^2 , as in the case of crystalline ferromagnets, and the other going as $T^{3/2}$, which arises only in amorphous alloys. The $T^{3/2}$ contribution is at least two orders of magnitude greater than the T^2 term. Therefore, the theories mentioned above predicted a $T^{3/2}$ power law in contrast to the T^2 dependence found in our iron-rich ferromagnetic amorphous alloys. Our experimental investigations of T^2 dependence of $\rho_{\text{mag}}(T)$ is supported by Kaul et al (1986), where they found a dominant T^2 contribution to $\rho_{\text{mag}}(T)$. The $T^{3/2}$ in their ferromagnetic alloys is negligibly small compared to T^2 term. Therefore, it may be interesting to see the results by fitting the data nonlinearly to the theoretical Eqn. 3-8b (by guessing the parameters of a_1 , a_2 , $W(0)$ and Θ_D) and there by evaluating Θ_D . The equation (Eqn. 3-8b) from diffraction model does not take into account the $\rho_{\text{mag}}(T)$. ρ has linear temperature dependence for $T \geq \Theta_D$ and quadratic temperature dependence for $T \ll \Theta_D$. This quadratic temperature dependence has been shown to be due to structural as well as magnetic contributions to resistivity (Kaul et al 1986), although, structural contribution is dominated over the magnetic

contribution (chapter III). These physical parameters can be checked by nonlinearly fitting the theoretical Eqn. 3-8b with some additional parameter(s) such as T^m (m is the number) and then evaluating θ_D separately in each case. The evaluated values of θ_D are then compared with the experimentally deduced values. The method of evaluation of θ_D is as follows.

If we assume that the theoretical Eqn. 3-8b as $x_1(T)$ and magnetic contribution to electrical resistivity as T^2 and/or $T^{3/2}$, then the following equations can be formulated.

$$r(T) = x_1(T) + a_3 T^2 \equiv x_2(T) \quad 7-1$$

$$r(T) = x_1(T) + a_3 T^2 + a_4 T^{3/2} \equiv x_3(T) \quad 7-2$$

$$r(T) = x_1(T) + a_4 T^{3/2} \equiv x_4(T) \quad 7-3$$

where $\rho(T)$ is the normalized resistivity ratios. These three equations are simultaneously solved to get the θ_D theoretically and then compared with the experimentally deduced θ_D values, calculated in chapter III. The additional advantage of this procedure is that, it allows us to evaluate the structure factor, $S_0(2k_F)$ using Eqn. 3-10 with the help of the coefficients a_1 and a_2 . The five parameters, viz., a_1 , a_2 , $W(0)$, θ_D and $S_0(2k_F)$ can be used to recalculate the normalized resistivity ratios, $\rho(T)/\rho(T_0)$, (T_0 is the ice temperature) and temperature coefficient of resistivity, α , theoretically.

Secondly, in thermoelectric power (S) measurements, the boundaries for the temperature variation (80 to 400 K) have been fixed to our experimental investigations presented in the thesis

due to low temperature limitations. This can be extended from low (< 4.2 K) to high temperatures ($\geq T_x$). This enables us to find out the exact magnetic contribution to thermopower by the metallic glasses. This can be done experimentally by fitting the data between T_c and T_x , where the magnetic contribution to thermopower is nil and then subtracting this with the thermopower data below T_c , where the mixture of magnetic and other contributions are present. The theoretical analysis of this data together with the resistivity data might give us a clear understanding of the mechanisms present in the alloys.

Thirdly, we have limited our Mössbauer studies to only isomer shifts and hyperfine interactions. The detailed investigations can be further carried out using Handrich's model by fitting the data to an equation similar to the magnetization relation to temperature in crystalline ferromagnets, as the hyperfine fields in amorphous ferromagnets are proportional to the magnetization. Also, the spin-wave excitations and critical exponents can be studied using Mössbauer spectra.

Lastly, the crystallization process(es) of the metallic glasses can be clearly understood by systematic study of metallic glasses using x-ray, transmission electron microscopy (TEM) and DSC. All these techniques have to be extensively used to understand the growth, nucleation, stability and crystallized products. These techniques needs an accurate annealing and quenching of the samples prior to their experimentation.

Further work on the same lines can be carried out by preparing the glasses with higher compositions of cobalt in Fe-Co-B-Si (Iron-rich) alloys and also by replacing cobalt with Ni and Mo independently in the same series. This enables us to know the effects of these elements on the physical as well as chemical properties of metallic glasses.

REFERENCES

GENERAL REFERENCES

- GR 1973 **Amorphous Magnetism**, eds. H.O. Hooper and A.M. DeGraaf (Plenum Press, NY).
- GR 1976a **Rapidly Quenched Metals II**, eds. N.J. Grant and B.C. Glessen (MIT Press, USA).
- GR 1976b **"Structure and Properties of Glassy Metals"**, P. Duwez, Ann. Rev. Mater. Sci. 6, 83 (1976).
- GR 1977 **Amorphous Magnetism II**, eds. R.A. Levy and R. Hasegawa (Plenum press).
- GR 1978a **Metallic Glasses**, eds. J.J. Gilman and H. J. Leamy (Am. Soc. of Metals, USA)
- GR 1978b **Proc. of 3rd Int. Conf. on Rapidly Quenched Metals, (RQM3)**, Vol. 1 and 2, ed. B. Cantor (Metal Society, London).
- GR 1980a **Proc. of Int. Conf. on Liquid and Amorphous Metals (LAM3)**, eds. F. Cryot-Lackmann and P. Desre (J. Physique, 41 supplement 8, 1980).
- GR 1980b **Proc. of Int. Conf. on Metallic Glasses: Science and Technology**, Vol. 1 and 2, eds. C. Hargital, I. Bakonyi and T. Kemeny (Kultra, Budapest).
- GR 1980c **"Amorphous Magnetism"**, F. E. Luborsky In **Ferromagnetic Materials**, Vol. 1, ed. E.P. Wohlfarth (North-Holland).

- GR 1980d **"Glassy Metals"**, H.S. Chen, Rept. Prog. Phys. 43, 353 (1980).
- GR 1980e **"Metallic Glasses"**, R.W. Chan, Contemp. Phys. 21, 43 (1980).
- GR 1981a **Proc. Int. Conf. on Rapidly Quenched Metals IV (RQM1)**, Vol. 1 and 2, eds. T. Masumoto and K. Suzuki (Japan Soc. of Metals).
- GR 1981b **Glassy Metals I**, eds. H.J. Guntherodt and H. Beck (Springer-Verlag).
- GR 1981c **Proc. of Int. Conf. on Amorphous Systems Investigated by Nuclear Methods**, eds. Z. Kacjos, I. Deszl, D. Horvath, T. Kemeny, L. Marczis and D.L. Nagy (Balatonfured, Hungary).
- GR 1981d **Application of Nuclear Techniques to the Studies of Amorphous Metals**, ed. U. Gonser (IAEA, Vienna).
- GR 1982 **Rapidly Solidified Amorphous and Crystalline Alloys**, eds. K.H. Kear, B.C. Glessen and M. Cohen (North-Holland).
- GR 1983a **Glassy Metals II**, eds. H. Beck and H.-J. Guntherodt (Springer-Verlag).
- GR 1983b **"Electronic Structure of Metallic Glasses"**, U. Mizutani, Prog. Mater. Sci. 28, 97 (1983).

- GR 1983c **Glassy Metals: Magnetic, Chemical and Structural Properties**, ed. R. Hasegawa (CRC Press).
- GR 1983d **Amorphous Metallic Alloys**, ed. F. E. Luborsky (Butterworths).
- GR 1984a **Amorphous Glasses: Production, Properties and Applications**, ed. T.R. Anantharaman (Trans Tech, Switzerland).
- GR 1984b **Magnetic Glasses**, K. Moorjani and J.M.D. Coey (Elsevier).
- GR 1984c **"Magnetic Amorphous Alloys"**, T. Egami, Rept. Prog. Phys. 47, 1601 (1984).
- GR 1984d **Proc. of Int. Conf. on Liquid and Amorphous Metals (LAM5)**, eds. C.N.J. Wagner and W.L. Johnson, J. of Non-Cryst. Solids, 61 and 62, (1984).
- GR 1984e **"Electron Transport in Amorphous Metals"**, D.G. Naugle, J. Phys. Chem. Solids 45, 367 (1984).
- GR 1985 **Proc. of Int. Conf. on Rapidly Quenched Metals, RQM5**, eds. S. Steeb and H. Warlimont (North-Holland).
- GR 1986 **Rapidly Solidified Alloys and their Mechanical and Magnetic Properties**, eds. B.C. Giessen, D.E. Polk and A.I. Taub (Mater. Res. Soc., Pittsburgh).

- GR 1987a Rapidly Solidified Metals, T.R. Anantharaman and C. Suryanarayana (Trans Tech., Switzerland).**
- GR 1987b Amorphous and Liquid Materials, eds. E. Luscher, G. Fritsch and G. Jacucci (Martinus Nijhoff, Netherlands).**
- GR 1987c "Electron Transport In Metallic Glasses", J.S. Dugdale, Contemp. Phys. 28, 547 (1987).**
- GR 1987d Proc. of Int. Conf. on Metallic and Semiconducting Glasses, Vols. 1,2 and 3, ed. A.K. Bhatnagar (Trans Tech., Switzerland).**
- GR 1988 Proc. of Int. Conf. on Rapidly Solidified Metals, ROM6, eds. R. Cochrane and J.O. Strom-Olsen, Mater. Sci. and Engg. 99 (1988).**

REFERENCES

- Abrahams, E., Anderson, P.W., Licciardello, D.C. and Ramakrishnan, T.V. 1979 Phys. Rev. Lett. (42) 673
- Al'tshuler, B.L. and Aronov, A.G. 1979 Sov. Phys. JETP. (50) 968
- Akhtar, D. 1986 Scr. Metall. (20) 983
- Altounian, Z., Folles, C.L., Muir, W.B. and Strom-Olsen, J.O. 1983 Phys. Rev. B (27) 1955
- Anantharaman, T.R. and Suryanarayana, C. 1971 J. Mater. Sci. (6) 1111
- Anantharaman, T.R. 1984 Metallic Glasses : production, properties and applications (Trans Tech. Publs., Switzerland)
- Anderson, P.W., Halperin, B.I. and Varma, C.M. 1972 Phil. Mag. (25) 1
- Antonione, C., Battezzati, L., Lucci, A., Riontino, G. and Venturello, G. 1978 Scr. Metall. (12) 1011
- Asomoza, R., Fert, A., Campbell, I.A. and Mayer, R. 1977 J. Phys. F, (7) L327
- Babic, E., Marohnic, Z., Ocko, M., Hamzic, A., Saub, K. and Pivac, B. 1980 J. Mag. Magn. Mats. (15-18) 934

- Babu, T.G.N., Bhanuprasad, B., Jagannathan, R., Bhatnagar, Anil K. and Ramanan, V.R.V. 1984 Proc. Int. Chem. Congress of Pacific Basin Societies (Honolulu, Hawaii) Abstract No. 07F56
- Balbach, M.N., Muir, W.B., Altounian, Z. and Tu Guo-Hua 1982 Phys. Rev. B (26) 2963; Phys. Rev. B (27) 619
- Balanzat, M. 1980 Scr. Metall. (14) 173
- Balogh, J. and Vincze, I. 1978 Solid State Comm. (25) 695
- Barnard, R.D. 1972 In 'Thermoelectricity in Metals and Alloys' (Taylor and Francis Ltd., London) p.38
- Baro, M.D., Surinach, S., Clavaguera-Mora, M.T. and Clavaguera, N. 1984 J. Non-Cryst. Sol. (69) 105
- Basak, S., Nagel, S.R. and Glessen, B.C. 1980 Phys. Rev. B (21) 4049
- Bauminger, E.R., Diamant, A., Felner, I., Nowick, I., and Ofer, S. 1974 J. Phys. Lett. A (50) 321
- Beck, H. and Guntherodt, H.-J. 1981 In 'Glassy Metals I', eds. Guntherodt, H.-J. and Beck, H. (Springer-Verlag, New York) p.15
- Benerjee, N., Ratnamala Roy, Majumdar, A.K. and Hasegawa, R. 1981 Phys. Rev. B (24) 6801
- Bergmann, G. and Marquardt, P. 1978 Phys. Rev. B (17) 1355

- Bhanuprasad, B. and Bhatnagar, Anil K. 1982 Solid State Comm.
(41) 381
- Bhanuprasad, B. and Bhatnagar, Anil K. 1983 J. Mag. Magn. Mats.
(31) 1479
- Bhanuprasad, B. 1985 Ph.D thesis (University of Hyderabad, India)
- Bhanuprasad, B. and Bhatnagar, Anil K. 1987a Key Engg. Mats.
(14) 333
- Bhanuprasad, B., Bhatnagar, Anil K. 1987b Key Engg. Mats. (15)
579
- Bhatnagar, A.K. and Jagannathan, R. 1984a In 'Metallic Glasses:
production, properties and applications', ed. Anantharaman,
T.R. (Trans Tech Publications, Switzerland) p.89
- Bhatnagar, A.K., Bhanuprasad, B. and Munirathnam, N.R. 1984b
J. Non-Cryst. Sol. (61-62) 1201
- Bhatnagar, A.K., Prasad, B.B. and Jagannathan, R. 1984c
Phys. Rev. B (29) 4896
- Bhatnagar, A.K., Bhanuprasad, B. and Jagannathan, R. 1985a
J. Appl. Phys. (57) 3514
- Bhatnagar, Anil K. 1985b Hyperfine Interactions (24-26) 637
- Bhatnagar, A.K., Prasad, B.B., Muni Rathnam, N.R., Ravi, N.,
Rao, K.V. and Nielsen, O.V. 1985c Proc. 5th Int. Nat.
Con. on Rapidly Quenched Metals (1) 1055

- Bhide, V.G., ed. 1973 In 'Mössbauer effect and its Applications'
(Tata McGraw-Hill Publishing Co., Ltd., New Delhi, India)
- Blatt, F.J., Schroeder, P.A., Folies, C.L. and Grieg, D. 1976
In 'Thermoelectric Power of Metals' (Plenum, New York)
- Bohnke, G., Kaul, S.N., Kettler, W. and Rosenberg, M. 1983
Solid State Comm. (48) 743
- Boll, R. and Warlimont, H. 1981 IEEE Trans. Magnetics, (MAG-17)
3053
- Brodsky, M.H. 1979 'Amorphous Semiconductors' (Springer-Verlag,
New York)
- Brouers, F. and Brauwers, M. 1975 J. Phys. (Paris) Lett. (36) L17
- Brown, D., Fairbairn, S. and Morgan, G. J. 1979 Phys. Sta.
Solid. b (93) 617
- Cahn, R.W. 1980 Contemp. Phys. (21) 43
- Campbell, I.A., Fert, A. and Jaoul, O. 1970 J. Phys. C. Suppl.
(1) 595
- Campbell, C.C.M., Birchall, T., Suits, J.C. 1974 J. Phys. F (7)
727
- Cantor, B. 1978 'Rapidly Quenched Metals III' (Metals Society,
London)
- Carini, J.P., Nagel, S.R., Varga, L.K. and Schmidt, T. 1983
Phys. Rev. B (27) 7589

- Chen, H. S. 1978 J. Non-Cryst. Sol.(27) 257
- Chen, H.S. 1980 Rep. Prog. Phys. (43) 353
- Chen, H. S. 1981 J. Non-Cryst. Sol. (46) 289
- Chien, C.L. 1978a Phys. Rev. B (18) 1003
- Chien, C.L., Musser, D., Luborsky, F.E. and Walter, J.L. 1978b
J. Phys. F (8) 2407
- Chien, C.L., Musser, D., Luborsky, F.E. and Walter, J.L. 1978c
Solid State Comm. (28) 645
- Chien, C.L. and Chen, H.S. 1979a J. Appl. Phys. (50) 1574
- Chien, C.L., Musser, D., Gyorgy, E.M., Sherwood, R.C., Chen, H.
S., Luborsky, F.E. and Walter, J.L. 1979b Phys. Rev. B
(20) 283
- Chien, C.L. 1981 In 'Nuclear and Electron Resonance Spectro-
scopies Applied to Materials Science', eds. Kaufman, E.N.
and Shenoy, G.K. (North-Holland, Amsterdam) p.157
- Chien, C.L. and Unruch, K.M. 1982 Phys. Rev. B (25) 5790
- Christian, J.W. 1975 In 'The Theory of Transformation in Metals
and Alloys', 2nd ed. (Pergamon Press, Oxford)
- Cochrane, R.W., Harris, R., Strom-Olson, J.O. and Zuckerman,
M.J. 1975 Phys. Rev. Lett. (35) 676
- Cochrane, R.W. and Strom-Olson, J.O. 1977 J. Phys. F (7) 1799

- Coey, J.M.D. 1978 J. Appl. Phys. (49) 1208
- Cohen, R.L., ed. 1976 'Applications of Mössbauer spectroscopy' (Academic press, Inc., London)
- Cote, P.J. and Meisel, L.V. 1977 Phys. Rev. Lett. (39) 102
- Cumbrera, F. L., Millan, M., Conde, A., Marquez, R. and Vigier, P. 1982b J. Mater. Sci. (17) 861
- Cusack, N. and Kendall, P. 1958 Proc. of the Phys. Soc. (72) 898
- Czyzek, G. 1982 Phys. Rev. B (25)
- Davies, H.A. 1983 In 'Amorphous Metallic Alloys' ed. Luborsky, F.E. (Butterworths & Co., Ltd., London) p.8
- Delgado, R., Armbruster, H., Naugle, D.G., Tsai, C.L., Johnson, W.L. and Arthur Williams 1986 Phys. Rev. B (34) 8288
- Dey, S., Deppe, P., Rosenberg, M., Luborsky, F.E. and Walter, J.L. 1981 J. Appl. Phys. (52) 1805
- Dugdale, J.S., Pavuna, D. and Rhodes, P. 1985 Endeavour, New series (9) 62
- Dunlap, R.A. and Dini, K. 1985 J. Phys. F : Met. Phys. (15) 2289
- Durand, J. 1980 J. de Physique (41) C8-609
- Durand, J. and Pannisod, P. 1981 IEEE Trans. Magnetics (MAG-17) 2595

- Durand, J. 1983 In 'Glassy Metals : magnetic, chemical and structural properties'., ed. Ryusuke Hasegawa (CRC press, Inc., Boca Raton, Florida) p.135
- Duwez, P. and Lin, S.C.H. 1967 J. Appl. Phys. (38) 4096
- Egami, T. 1981 In ' Glassy Metals I', ed. Guntherodt, H.-J. and Beck, H. (Springer-Verlag, New York) 26
- Eibschutz, M. and Lines, I.E. 1973 Phys. Rev. B (7) 4907
- Evans, R., Greenwood, D.A. and Lloyd, P. 1971 Phys. Lett.(35A) 57
- Fahnle, M., Herzer, G., Kronmüller, H., Meyer, R., Sallé, M. and Egami, T., 1983 J. Mag. Magn. Mats. (38) 240
- Fritsch, G., Pollich, W., Dyckhoff, W., Schulte, A., Eckert, A. and Luscher, E. 1985 J. Non Cryst. sol. (74) 259
- Gallagher, B.L. 1981 J. Phys. F (11) L207
- Gallagher, B.L. and Grieg, D. 1982 J. Phys. F (12) 1721
- Gibson, M. A. and Delamore, G. W. 1987 J. Mater. Sci. (22) 4550
- Gilman, J.J. 1980 Science (208) 856
- Gonser, U., ed. 1975 In 'Mossbauer Spectroscopy' (Springer-Verlag, New York) p.1
- Gonser, U., Ghafari, M. and Wagner, H.G. 1978 J. Mag. Magn. Mats. (8) 175

- Grant, R.W. 1975 In 'Mössbauer Spectroscopy', ed. Gonser, U. (Springer-Verlag, New York) p.97
- Greenwood, N.N. and Gidd, T.C. 1971 In 'Mössbauer Spectroscopy' (Chapmann and Hall, London)
- Greer, A. L. 1982 Acta Metall. (30) 171
- Grieg, D. 1987 Key Engg. Mats. (14) 389
- Grest, G.S. and Nagel, S.R. 1979 Phys. Rev. B (19) 3571
- Gubanov, A.I. 1960a Fiz. Tverd. Tel. (2) 502
- Gubanov, A.I. 1960b Sov. Phys. Solid State (2) 468
- Guntherodt, H.-J. and Kunzi, H. U. 1978 In 'Metallic Glasses', ed. Parks, O. (American Society of Metals, New York) p.247
- Hanna, S.S., Heberle, J., Little John, C., Perlow, G.J., Preston, R.S. and Vincent, D.H. 1960a Phys. Rev. Lett.(4) 28
- Hanna, S.S., Heberle, J., Perlow, G.J., Preston, R.S. and Vincent, D.H. 1960b Phys. Rev. Lett. (4) 513
- Hansen. M. 1958 In 'Constitution of binary alloys' (McGraw-Hill, New York)
- Harris, R. and Strom-Olsen, J.O. 1983 In 'Glassy Metals II : Atomic structure and dynamics, Electronic structure, Magnetic properties', eds. Beck, H. and Guntherodt, H.-J. (Springer-Verlog, Berlin) p.325

- Hasegawa, R. and Tsuei, C.C. 1970 Phys. Rev.B (2) 1631; 1971 (3) 214
- Hatherly, M., Hirakawa, K., Lowde, R.D., Mallett, J.F., Stringfellow, M.W. and Torric, B.H. 1964 Proc. Phys. Soc. (84) 55
- Henderson, D.W. 1979 J. Non-Cryst. Sol. (30) 301
- Herzer, G. 1984 J. Mag. Magn. Mats. (45) 345
- Hesse, J. and Rubartsch, A. 1974 J. Phys, E (7) 526
- Hilzinger, H.R. and Kunz, W. 1984 IEEE Trans. Magnetics.(20) 1323
- Holden, A.J., Heine, V. and Samson, J.H. 1984 J. Phys. (14) 1005
- Hooper, H.O. and De Graff, A.M. (eds.) 1973 In 'Amorphous Magnetism I' (Plenum, New York)
- Imry, Y. 1980 Phys. Rev. Lett. (44) 469
- Jaccarino, J., Walker, L.R. and Wertheim. G.K. 1964 Phys. Rev. Lett. (13) 752
- Johnson, W.A. and Mehl, R.F. 1939 Trans. AIME (135) 416
- Johnson, W.L., Atzmon, M., Van Rossum, M., Dolgin, B.P. and Yeh, X.L. 1985 'Rapidly Quenched Metals V' (Elsevier, USA) 1515
- Jonson, M. and Girvin, S.M. 1979 Phys. Rev. Lett. (43) 1447
- Josephson, B.D. 1960 Phys. Rev. Lett.(4) 274

- Kadlecova, J., Handstein, A., Zemcik, T. and Zaveta, K. 1986
Phys. Sta. Soli. (a) (93) 213
- Kasuya, T. 1959 Prog. Phys. (22) 227
- Kaul, S.N. 1981 Phys. Rev. B (24) 6550
- Kaul, S.N. 1983 Phys. Rev. B (27) 5761
- Kaul, S.N., Kettler, W. and Rosenberg, M. 1986 Phys. Rev. B (33)
1987
- Kaul, S.N. and Rosenberg, M. 1987 Key Engg. Mats. (14) 475
- Kemeny, T., Fogarabsy, B., Vincze, I., Donald, I., Besnus, M.J.
and Davies, H.A. 1981 4th Int. Nat. Con. on Rapidly Quenched
Metals (Sendia) p.851
- Kettler, W., Wernhardt, R. and Rosenberg, M. 1982 J. Appl. Phys.
(53) 8248
- Kettler, W., Kaul, S.N. and Rosenberg, M. 1984 Phys. Rev. B (29)
6950
- Kettler, W.H., Kaul, S.N. and Rosenberg, M. 1989 Communicated
- Khein, H. -P., Ghafari, M., Ackermann, M. Gonser, U. and Wagner,
H.-G. 1982 Nucl. Inst. & Methods Phys. Res. (Netherlands)
(199) p.159
- Kissinger, H. E. 1956 J. Reas. of Nat. Bureau of Standards (57)
217

- Klement Jr., W., Willens, R.H. and Duwez, P. 1960 Nature (187) 869
- Kobe, S. and Handrich, K. 1971 Sov. Phys. Solid State (13) 734
- Kobe, S. and Handrich, K. 1972 Phys. Sta. Soli.(b) (54) 663
- Kondo, J. 1967 Solid State Physics (23), ed. Seltz, F.,
Turnbull, D. and Ehrenreich, W. (Academic Press, New York)
P.183
- Korenblit, I.Y. 1982 J. Phys. F (12) 1259
- Krishnan, R. 1984 In 'Recent Advances In Materials Research', ed.
Srivastava, C.M. (Oxford & IBM Publishing Co., New Delhi)
P.65
- Kuentzler, R. and Williams, D.E.G. 1985 J. Phys. F: Met. Phys.
(15) 2283
- Le Caer, G. and Dubois, J.M. 1979 J. phys. E (12) 1083
- Le Caer, G. and Dubois, J.M. 1981 Phys. Sta. Soli. (a) (64) 275
- Le Caer, G., Cadogan, J.M., Brand, R.A., Dubois, J.M. and
Guntherodt, H.-J. 1984 J. Phys. F: Met. Phys. (14) L73-L78
- Levy, R.A. and Hasegawa, R. (eds.) 1977 'Amorphous Magnetism II'
(Plenum, New York)
- Lin, S.C.H. 1969 J. Appl. Phys. (40) 2173
- Lin, H.C., Bevk, J. and Turnbull, D. 1979 Solid State Comm. (29)
641

- Lischer, E.J., Wilkinson, C., Ericsson, T., Haggstrom, G.,
Lundgren, I. and Wappling, R. 1974 J. Phys. C (7) 1344
- Logan, J. and Sun, E. 1976 J. Non-Cryst. Sol. (20) 285
- Luborsky, F.E., Fischer, J.J., Frischmann, P.G. and Johnson, I.A.
1978 J. Appl. Phys. (49) 1769
- Luborsky, F.E. 1980 In 'Ferromagnetic Materials (1) chap. 6 ed.
Wohlfarth, E.P. (North-Holland Publishing Company, Amsterdam)
- Luborsky, F.E. 1983 In 'Amorphous Metallic Alloys'
(Butterworths, London)
- Mader, S. and Nowick, A.S. 1965 Appl. Phys. Lett. (7) 57
- Madurga, V., Ascasibar, E., Gonzalez, J.M., Morala, M., Garcia-
Escorial, A., Peces, J.A. and Nielsen, O.V. 1983 Anales
de Fisica (79) 82
- Majumdar, A. K. and Nigam, A. K. 1980 J. Appl. Phys. (51) 4218
- Marc Oliver 1984 Ph.D thesis (McGill University, Montreal)
- Mathur, R. P. and Akhtar, D. 1987 Bull. Mater. Sci. (9) 269
- Matsuda, T. and Mizutani, U. 1982 J. Phys. F (12) 1877
- May, L., Druck, S.J. and Sellers, M. 1968 U.S. Atomic Energy
Comm. Rep. no. NYO 3798-2
- Meaden, G.T. 1965 'Electrical Resistance of Metals' (Plenum
Press, New York)

- Mizutani, U. 1983 Pro. Mats. Sci. (28) 97
- Mizutani, U. 1987 Key Engg. Mats. (14) 365
- Mogro-Campero, A. and Walter, J.L. 1980 J. Phys. Col. (41) C8 497
- Mogro-Campero, A., Walter, J.L. and Coan, T.E. 1981a Phys. Rev.B
(24) 3579
- Mogro-Campero, A. and Luborsky, F.E. 1981b J. Appl. Phys. (52)
515
- Montgomery, C.G., Krugler, J.I. and Stubbs, R.M. 1970 Phys. Rev.
Lett. (25) 669
- Mooji, J.H. 1973 Phys. Stat. Soli.(a) (17) 521
- Moorgan, G. J., Howson, M.A. and Paja, A. 1987 Key Engg. Mats.
(14) 377
- Moss, M., Smith, D.L. and Leferver, R.A. 1964 J. Appl. Phys.
Lett. (5) 120
- Mössbauer, R.L. 1958 Z. Physik (151) 124
- Mott, N.F. 1972 Phil. Mag. (26) 1249
- Murray, P. and White, J. 1949 Trans. Brit. Ceram. Soc. (48) 187
- Nagel, S.R. 1977 Phys. Rev. B (16) 1694
- Nagel, S.R. 1978 Phys. Rev. Lett. (41) 990

- Nagel, S.R., Vassilion, J., Horn, P.M. and Geissen, B.C. 1978
Phys. Rev. B (17) 462
- Nagel, S.R. 1982 In 'Advances In Chemical Physics', eds.
Prigogine, I. and Rice, S.A. (John Wiley and sons, New York)
p.227
- Narendra Babu, T.G., Jagannathan, R., Bhatnagar, Anil K. and
Ramanan, V.R.V. 1986 Hyperfine Interactions (27) 293
- Naugle, D.G. 1984 J. Phys. Chem. Sol. (45) 367
- Nguyen-manh, D., Mayou, D., Morgan, G.J. and Pasturel, A. 1987
J. Phys. F (17) 999
- OK, H.N. and Morrish, A.H. 1980 Phys. Rev. B (22) 4215
- Panissod, P., Durand, J. and Budnick, J.I. 1982 Nuclear Inst. and
Methods (199) 99
- Panissod, P. 1985 Hyperfine Interactions (1985) p.607
- Pekala, K. and Trykozko, R. 1981 Solid State Comm.(17) 101
- Pekala, K., Pekala, M. and Trykozko, R. 1983 Solid State Comm.
(46) 413
- Pekala, K. and Trykozko, R. 1984 J. Phys. F : Met. Phy.(14) 449
- Philippe Maltrepierre 1970 J. Appl. Phys. (41) 498
- Phillips, W.A. 1972 J. Low Temp. Phys. (7) 351

- Pietrokovsky, P. 1963 Rev. Sci. Inst. (34) 455
- Piotr Czernecki and Alojzy Wrzeclono 1985 Proc. 5th Int. Nat. Con. on Rapidly Quenched Metals (1) p.1067
- Pond Jr., R. and Maddin, R. 1969 Trans. Met. Soc. AIME (245) 2975
- Prince, D.C. 1976 The Australian National University, Australia, Research report No.5 (unpublished)
- Prince, D.C., Campbell, S.J. and Beck, P.J. , 1980 J. Phys. (Paris) (41) C1-263
- Raj, K., Durand, J., Budnick. J.I. and Shathsi, S. 1978 J. Appl. Phys. (49) 1676
- Raja, V.S. 1986 Ph.D thesis (I.I.Sc., Bangalore, India)
- Raja, V. S., Kishore and Ranganathan, S. 1987 Bull. Mater. Sci. (9) 207
- Ramakrishnan, S., Sundaram, S., Pandit, R.S. and Girish Chandra 1985 J. Phys. E: Sci. Instrum. (18) 650
- Ranganathan, S. and Von Helmendahl, M. 1981 J. Mater. Sci. (16) 2401
- Rao, K.V. 1983 In 'Amorphous Metallic Alloys', ed. Luborsky, F.E. (ButterWorths, London) p.401
- Rawson, H. 1967 Inorganic glass-forming systems (Academic press, London)

- Rhyne, J.J., Gschneider, K.A. and Leroy, E. 1979 In 'Hand Book of the Physics and chemistry of Rare-earths' (North-Holland, Amsterdam)
- Richter, R., Wolf, M. and Goedsche, F. 1979 Phys. Stat. Soli. b (95) 473
- Ryusuke Hasegawa 1982 In 'Glassy Metals : Magnetic, Chemical and structural properties' (CRC press, Inc., Florida, USA)
- Saegusa, N. and Morrish, A.H. 1982 Phys. rev. B (26) 10
- Sas, B., Toth, J., Lovas, A. and Konczos, G. 1983 Key Engg. Mats. (14) 493
- Schaafsma, A.S. 1981 Ph.D. thesis (University of Groningen, Groningen)
- Schreiber, J. 1974 Phys. Sta. Soli. (b) (52) K119; (61) K17
- Schurer, P.J. and Morrish, A.H. 1978 Sol. State Comm. (28) 81
- Scott, M. G. 1983 In 'Amorphous Metallic alloys' ed. Luborsky, F. E. (Butter worth & Co Ltd., London)
- Sharon, T.E. and Tsuei, C.C. 1971 Solid Sta. Comm, (9) 1923
- Sharon, T.E. and Tsuei, C.C. 1972 Phys. Rev. B (5) 1047
- Sinha, A.K. 1970 Phys. Rev. B (1) 4541
- Slechte, J. 1970 Phys. Sta. Soli.(b) (70) 531

- Slechte, J. 1975 Phys. Sta. Soli.(b) (67) 595
- Spano, M.L. and Bhagat, S.M. 1981 J. Mag. Magn. Mats. (24) 143
- Srinivas, V., Rajaram, G., Shiva prasad, Girish Chandra, Shringi, S.N. and Krishnan, R. 1987 Key Engg. Mats. (14) 481
- Suryanarayana, C. 1984 In 'Metallic Glasses : production, properties and applications' (Trans Tech Publications, Switzerland) p.249
- Takacs, L., Cadeville, M.C. and Vincze, I. 1975 J. Phys. F (5) 800
- Takacs, L. 1980 J. de Physique C1-265
- Tomiyoshi, S., Yamamoto, H. and Watanabe, H. 1971 J. Phys. Soc. Japan (30) 1605
- Toth, J., Sas, B. and Konczos, G. 1985 Proc. 5th Int. Nat. Con. on Rapidly Quenched Metals (1) p.1071
- Trammell, G.T. and Hannon, J.P. 1969 Phys. Rev. B (180) 337
- Tsuei, C.C. and Duwez, P. 1966a J. Appl. Phys. (37) 435
- Tsuei, C.C. and Duwez, P. 1966b J. Appl. Phys. (38) 4096
- Tsuei, C.C. and Hasegawa, R. 1969 Solid State Comm. (7) 1581
- Tsuei, C.C. 1977 Bull. Am. Phys. Soc. (22) 322
- Tsuei, C.C. 1978a Bull. Am. phys. Soc.(23) 359 and 406

- Tsuei, C.C. 1978b Solid State Comm. (27) 691
- Turnbull, D. and Cohen, M.H. 1961 J. Chem. Phys. (34) 120
- Uhlmann, D.R. and Hooper, R.W. 1978 'Metallic Glasses' eds. Leamy, H.J. and Gilman, J.J. (American Society for Metals, Ohio, USA) p.129
- Van der woude, F. 1966 Ph.D thesis (University of Groningen, Groningen)
- Van der woude, F. and Vincze, J. 1980 J. de Physique (41) C1-C51
- Vaughan, F. 1955 Clay Minerals Bull. (2) 265
- Vincze, I., Cadeville, M.C., Jesser, R. and Takacs, L. 1974 J. de Physique (35) C6-1676
- Vincze, I. 1978 Solid State Comm. (25) 689
- Uwe Koster and Herold, U. 1981 'Glassy Metals I' eds. Guntherodt, H. -J. and Beck, H. (Springer-Verlag, New York) p.225
- Uwe Koster 1987 Key Engg. Mats. (14) 281
- Waseda, Y. and Chen, H.S. 1978 Phys. Stat. Soli.(b) (87) 777
- Webb, D.J., Bhagat, S.M., Moorjani, K., Satkiewicz, F.G. and Poehler, T.O. and Manheimer, M.A. 1984 J. Non-Cryst. Sol. (61-62) 1377
- Weisman, I.D., Swartzendruber, L.J. and Bennett, L.H. 1969 Phys. Rev. B (117) 465

Wertheim, G.K., ed. 1964 In 'Mössbauer effect: principles and applications' (Academic press, New York)

Window, B. 1971 J. Phys. E (4) 401

Yu Mei and Luo, H.L. 1986 Phys. Rev. B (34) 509

Ziman, J.M. 1961 Phil. Mag. (6) 1013

Ziman, J.M. 1972 In 'Principles of The Theory of Solids
(Cambridge University, Cambridge, England)